STUDIES IN HETEROGENEOUS CATALYSIS: SUPPORTED HETEROPOLYACIDS CATALYZED ORGANIC REACTIONS

A THESIS SUBMITTED TO THE
UNIVERSITY OF PUNE

FOR THE DEGREE OF
DOCTOR OF PHILOSOPHY
(IN CHEMISTRY)

BY
DHANASHRI P. SAWANT

CATALYSIS DIVISION
NATIONAL CHEMICAL LABORATORY
PUNE - 411 008
INDIA

JUNE 2006

CERTIFICATE

Certified that the work incorporated in the thesis, “**Studies in Heterogeneous Catalysis: Supported heteropolyacids catalyzed organic reactions**” submitted by **Miss. Dhanashri. P. Sawant**, for the Degree of **Doctor of Philosophy**, was carried out by the candidate under my supervision in the Catalysis Division, National Chemical Laboratory, Pune - 411008, India. Materials obtained from other sources have been duly acknowledged in the thesis.

Dr. S.B.Halligudi

(Research Supervisor)

DECLARATION

I hereby declare that the work presented in this thesis entitled, "**STUDIES IN HETEROGENEOUS CATALYSIS: SUPPORTED HETEROPOLYACIDS CATALYZED ORGANIC REACTIONS**" submitted for Ph.D. degree in Chemistry is carried out by me under the supervision of Dr. S. B. Halligudi in Inorganic and Catalysis Division at National Chemical Laboratory, Pune. This work is entirely new and is not reported in full or by part in any thesis submitted by me. Any inadvertent omissions that might have occurred due to oversight or error in judgment are regretted.

(Dhanashri P. Sawant)

Date: 27/06/2006.
Division of Inorganic and Catalysis,
National Chemical Laboratory,
Pune-411 008.

Dedicated to My Family and Moral Supporters ….

ACKNOWLEDGEMENTS…

I express my deep sense of gratitude and indebtedness to my research guide, Dr. S. B. Halligudi, Scientist, National Chemical Laboratory, Pune, for his invaluable guidance, numerous discussions and constructive suggestions through out the course of this investigation.

Finally, my thanks are due to Dr. S. Sivaram, Director, NCL for allowing me to carryout the research work at NCL and CSIR, New Delhi, INDIA, for the financial support in the form of senior research fellowship. I am very much grateful to Dr. Rajiv Kumar, Head, Catalysis and Inorganic Chemistry Division, NCL for providing the facilities required for my work. I am grateful to Prof. F. Lefebvre, [France] for analyzing samples by Nuclear magnetic resonance spectroscopy. I thank Prof. Hartmann, Prof. Ernst and Dr.Vinu, [Germany] for their help during my visit.

I owe my special thanks to all scientific staff of our Division. I would like to thank Dr. Paul Ratnasamy, Dr. S. Sivasanker, Dr. A. V. Ramaswamy, Dr. Veda Ramaswamy, Dr. A. P. Singh, Dr. M. K. Dongare, Dr. C. V. V. Satyanarayana, Mrs. Nalini Jacob, Dr. S. P. Mirajkar, Dr. D. Srinivas, Dr. Murali Sastry, Dr. Selvaraj, Dr. S. Umbarkar, Dr. S. G. Hegde, Dr. C. S. Gopinath, Dr. A. J. Chandwadkar, Ms. Violet, Ms. Agashe, Ms. Nandini, Dr. Belhekar, Dr. Patil, Dr. Renu, Dr. Saguna, Dr. Pardhy, Dr. Deshpande, Dr. Awate, Dr. P. Manikandan, Dr. Raja, Mr. S. C. Jha and Mr. Purushothaman for their help and cooperation in completing my research work successfully. I would like to acknowledge the help received from Mr. Kashinathan and Mr. Madhu.

I take the opportunity to thank my friends Trissa (and family), Biju, Shanbhag, Ankur, Suman, Nevin, Suresh, Kala (and family), Sajani, Rajani, Surekha, Smita, Rohit, Sankar, Vasudev, Pallavi, Neelam, Rajendra, Reddy, Shiju, Thomas, Sebastian, and many others.

Words are not enough to express my love and gratitude to my family members. It is their love, blessings and prayers that helped me throughout my life. I am very much indebted to my family members, Aai, Baba, Mangesh, Preeti and Palak, from whom I have received invaluable help and moral support.

I would like to thank all my teachers and classmates for the encouragement that I received from them. Also, I would like to take an opportunity to thank all well-wishers and moral supporters who helped in smoothing my life journey and to show right path.

Above all, I thank God for his blessings, for leading me in the right path and for being there with me whenever I needed.

(Dhanashri P. Sawant)

CONTENTS

1. INTRODUCTION

2. SYNTHESIS AND CHARACTERIZATION TECHNIQUES

3. ZIRCONIA SUPPORTED HPAS

4. ZIRCONIA SUPPORTED TPA IN MCM-41

5. ZIRCONIA SUPPORTED TPA IN SBA-15

6. ZIRCONIA SUPPORTED STA IN MESOPOROUS SILICA

7. SUMMARY AND CONCLUSIONS

ABBREVIATIONS

AA	**Acetic acid**
Ac_2O	**Acetic anhydride**
AFM	**Atomic force microscopy**
BA	**Benzyl alcohol**
BC	**Benzoyl chloride**
BET	**Brunauer-Emmett-Teller**
BJH	**Barret−Joyner−Halenda**
BP	**Benzyl phenol**
CTABr	**Cetyltrimethyl ammonium bromide**
DBE	**Dibenzyl ether**
1-dd	**1-dodecene**
DPO	**Diphenyl oxide**
DRS	**Diffuse reflectance spectra**
EDAX	**Energy dispersive spectroscopy**
ESCA	**Electron spectroscopy for chemical analysis**
FT-IR	**Fourier-transform Infrared spectroscopy**
FT-RS	**Fourier-transform raman spectroscopy**
GADDS	**General area detector diffraction spectroscopy**
HPA	**Heteropoly acid**
IAA	**Isoamyl alcohol**
ICP-OES	**Inductively coupled plasma-optical emission spectroscopy**
LAB	**Linear alkyl benzene**
MAS	**Magic angle spinning**
2-MN	**2-Methoxynaphthalene**
MPA	**Molybdophosphoric acid**
MS	**Mesoporous silica materials**
MSA	**Molybdosilicic acid**
NMR	**Nuclear magnetic resonance**
PBE	**Phenyl benzyl ether**

PD	**Phenyl dodecane**
Pluronic P123	**Amphiphilic triblock copolymer (EO_{20}-PO_{70}-EO_{20})**
SAXS	**Small-angle X-ray scattering**
SEM	**Scanning electron microscopy**
STA	**Silicotungstic acid**
TEOS	**Tetraethyl orthosilicate**
TCD	**Thermal conductivity detector**
TEM	**Transmission electron microscopy**
TG-DTA	**Thermogravimetry-Differential Thermal Analysis**
TPA	**Tungstophosphoric acid**
TPD	**Temperature programmed desorption**
UV-Vis.	**Ultraviolet- Visible spectroscopy**
WO_3	**Tungsten oxide**
XPS	**X-ray photoelectron spectroscopy**
XRD	**X-ray diffraction**
XRF	**X-ray fluorescence spectroscopy**
ZrO_2	**Zirconia**

“Physics deals with clear body whereas physical chemistry deals with clear laws. But, catalysis deals with uncleared body and uncleared laws”.

CHAPTER – 1

INTRODUCTION

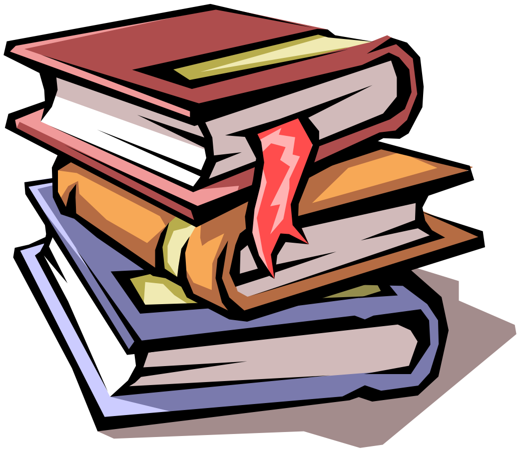

1. INTRODUCTION

1.1. GENERAL INTRODUCTION TO CATALYSIS

During the last four decades, there has been renewed interest in the use of heterogeneous catalysts in replacing the conventional homogeneous catalyst systems. Though homogeneous catalysts are well established individually optimized and commercially pronounced, based on statistical data, the future trend of R & D is on the development of new and potential catalyst systems practiced for industrial applications [1].

Some of the industrial processes approximately (127) (numbers are given in brackets) using solid acid-base catalysts are dehydration and condensation (18), isomerization (15), alkylation (13), etherification (10), amination (9), cracking (8), aromatization (7), hydration (7), oligomerization and polymerization (6), MTG/MTO-processes (5), hydrocracking (4), hydrogenation (4), esterification (3), disproportionation (2), MTBE→*i*-C'(4) and others (15) which mainly uses zeolites (74), oxides, complex oxides (54), ion-exchange resins (16), phosphates (16), solid acids (not specified) (7), clays (4), immobilized enzymes (3), sulfate, carbonate (3) and sulfonated polysiloxanes (3).

Badger process for the production of ethylbenzene (EB) from benzene and ethylene is a breakthrough technology in the field of aromatic alkylation reactions using solid acid catalysts [2]. Catalytic reforming, catalytic cracking, hydrocracking, alkylation, isomerization, and conversion of methanol into olefins are some of the most important industrial applications of heterogeneous catalysis. The green synthesis of organic compounds is an area of growing importance in industry and academic. Any modification in the existing organic process that removes environmentally harmful solvents and reagents, reduces waste, or involves recycling of materials can be considered a green adaptation.

1.2. HPAs IN CATALYSIS

Among the solid acid and base catalysts reported, heteropoly compounds provide a good candidature for the designing of mixed oxide catalysts and they have high capability in practical uses. The relationships among the following four levels of information can be established on the molecular basis: (i) catalytic performance; (ii) chemical and physical property; (iii) molecular, bulk composition and structure; and (iv) method of synthesis of catalyst [3-5]. The heteropoly compounds are used in solution as well as in the solid state as acid and redox catalysts. There are several industrial processes, which utilizes HPAs as catalysts [3,6]. Catalysis by HPAs and related polyoxometalate compounds is a field of increasing importance and the most of the pioneering work has been done since 1970s mainly by Japanese and Russian research groups [7-9]. HPAs have very strong acidities and exhibit fast reversible multielectron redox transformations under mild conditions. HPAs have high solubility in polar solvents and fairly high thermal stability in the solid state. These properties of HPAs render potentially promising acid, redox, and bifunctional catalysts in homogeneous as well as in heterogeneous systems.

1.2.1. Structure

HPAs are complex proton acids that incorporate polyoxometalate anions (heteropolyanions) having metal-oxygen octahedra as the basic structural units. This unique structure manifests itself to exhibit extremely high proton mobility and a "pseudoliquid phase" [5], while heteropolyanions can stabilize cationic organic intermediates. The first characterized and the best known of these is the Keggin heteropolyanion typically represented by the formula $XM_{12}O_{40}{}^{x-8}$, where X is the central atom (Si^{4+}, P^{5+}, etc.), x is its oxidation state, and M is the addenda metal ion (Mo^{6+}or W^{6+}). The M^{6+} ions can be substituted by other metal ions, e.g., V^{5+}, Co^{2+}, Zn^{2+}, etc. The Keggin anion is composed of a central tetrahedron XO_4 surrounded by 12 edge- and corner-sharing metal-oxygen octahedra MO_6 as shown in Fig. 1.1 (a). There are four types of oxygen atoms in the Keggin unit: four oxygen atoms of the central tetrahedron (O_a), twelve oxygen atoms that bridge addenda atoms not sharing a central oxygen atom (corner-sharing, O_b), twelve oxygen atoms that bridge two addenda atoms sharing the same central oxygen atom (edge-sharing, O_c), and twelve terminal oxygen atoms (O_d) associated with a single addendum atom as shown in Fig.1.1 (b). The octahedra are arranged in four M_3O_{13} groups. Each group is formed by three octahedra sharing edges and having a common oxygen atom, which is also shared with the central tetrahedron XO_4. Heteropoly compounds involve a large class of coordination-type salts and free acids, which are formed by the condensation of more than two different types of oxoanions as shown in Eq. (1.1).

$$12WO_4{}^{2-} + HPO_4{}^{2-} + 23H^+ \longrightarrow PW_{12}O_{40}{}^{3-} + 12H_2O$$ **....Eq. (1.1)**

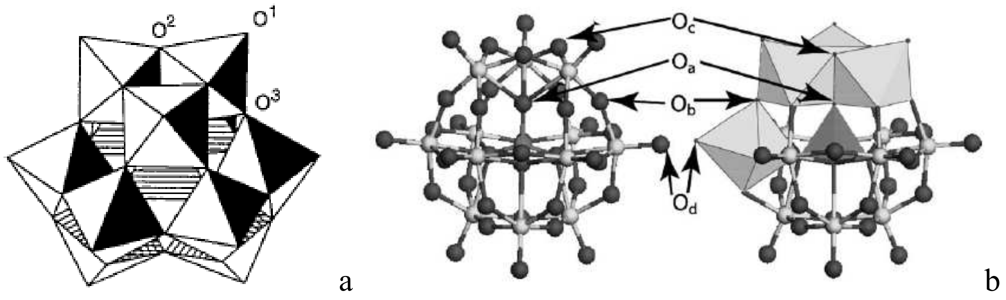

Fig. 1.1: *The Keggin structure of the $XM_{12}O_{40}^{x-8}$ anion (α-isomer)*[16]*: terminal (O^1), edge-bridging (O^2), and corner bridging (O^3) oxygen atom.*

1.2.1.1. Primary structure: The structure of the fundamental units is called the primary structure. Based on primary structure, different polyoxoanion structures exist. According to Pope and Müller [10], it is convenient to discuss the variety of polyoxometalate structure starting from a few highly symmetrical 'parent' polyanions; then many other polyoxometalate structures may be considered as their 'derivatives'. There are three such parent structures, with a tetrahedron (Keggin structure, T_d symmetry), an octahedron (Anderson- Evans, O_h symmetry), and an icosahedron (Dexter- Silverton structure, I_h symmetry) as their central polyhedron XO_n (n = 4, 6 or 12) that determines the symmetry of the whole polyanion.

a. Keggin structure: This is the first characterized [11] and the best-known structure, which is adopted by many polyoxometalates. In all types of heteropoly compounds, Keggin-type heteropoly compounds have been widely used in fundamental research and practical processes [12,13], which are considered to be fine catalysts.

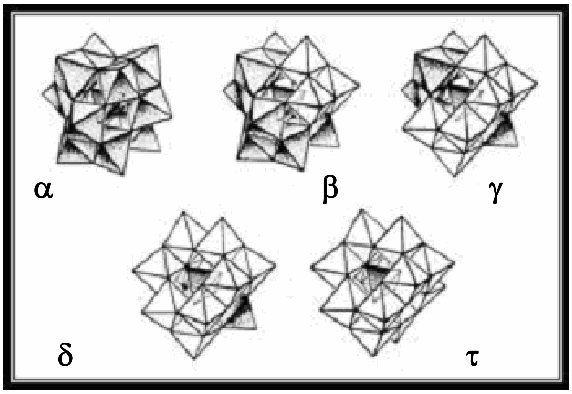

Fig. 1.2: *The Keggin structure of the $[XM_{12}O_{40}]^{x-8}$ anion: Baker-Figgis isomers.*

As previously mentioned in Keggin unit, the octahedra are arranged in four M_3O_{13} groups and each of the M_3O_{13} groups can be rotated 60° about its 3-fold axis, which leads to geometrical isomers as shown in Fig. 1.2 (Baker-Figgis isomers).

b. Lacunary-Keggin like structure: The lacunary structures are defined by Pope as having the molecular Keggin structure but missing one MoO_6 polyhedron [14,15] as shown in Fig. 1.3.

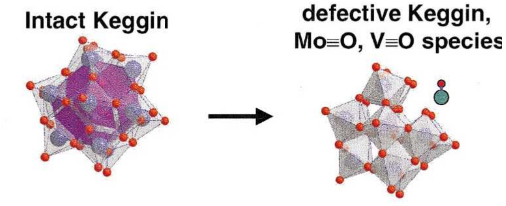

Fig. 1.3: *The structures of the α-Keggin anion* $[XM_{12}O_{40}]^{x-8}$ *and its lacunary derivative.*

c. Wells-Dawson structure: The Dawson structure dimeric (2:18) is formed by the fusion of two $PW_9O_{31}{}^{3-}$ units, "lacunary Keggin anions". Nowadays, much research is focused on Wells-Dawson type $[X_2M_{18}O_{62}]^{6-}$ anions [Fig. 1.4 (a)] due to their promising application as new catalyst materials [3,16].

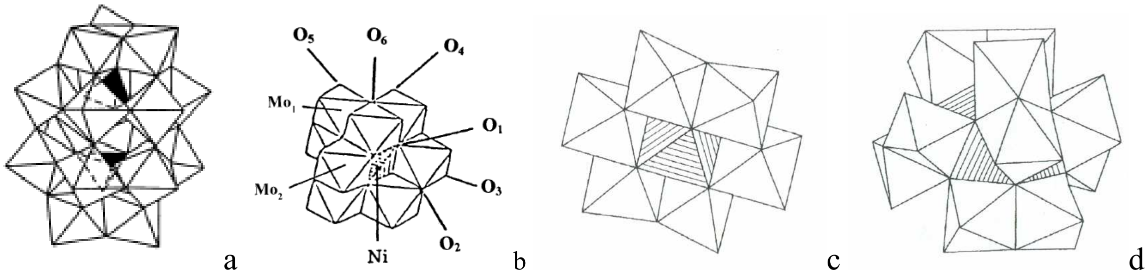

Fig. 1.4: *(a) Wells-Dawson structure of the* $[X_2M_{18}O_{62}]^{2x-16}$ *anion (α-isomer), (b) Waugh structure of* $(NiMo_9O_{32})^6$*, (c) Anderson-Evans structure of the* $[Te^{6+}Mo_6O_{24}]^{6-}$ *anion, (d) Dexter-Silverton structure of the* $[XM_{12}O_{42}]^{x-12}$ *anion.*

d. Waugh structure: The electronic structure of the typical Waugh-type heteropoly anion $(NiMo_9O_{32})^6$ has been calculated by the DV-Xα method and the structural data of $(NiMo_9O_{32})^6$ available in literature [17-19]. Its structure model is given in Fig. 1.4 (b).

e. Anderson-Evans structure: This example represents a different structural type with an octahedron as a central polyhedron [Fig. 1.4 (c)]. The Anderson-Evans structure is adopted by 6-heteropoly anions (e.g. $[Te^{6+}Mo_6O_{24}]^{6-}$) [10,20].

f. Dexter-Silverton structure: A less common type of 12-heteropoly anions $[XM_{12}O_{42}]^{x-12}$, where M is molybdenum (VI) and X is cerium (IV), uranium (IV), or thorium (IV), adopt this structure [Fig. 1.4 (d)]. In this anion, the central atom is surrounded by twelve oxygen atoms that form an icosahedron as a central polyhedron.

1.2.1.2. Secondary structure: Secondary structures are formed when the primary units are joined to form a solid. In this case, the secondary structure is formed by packing the polyanions into a body centered cubic (*bcc)* structure in which the protonated water dimer $(H_2O)_2H^+$ is connected to four anions by hydrogen bonding at the terminal oxygen atoms of the anions [Fig.1.5].

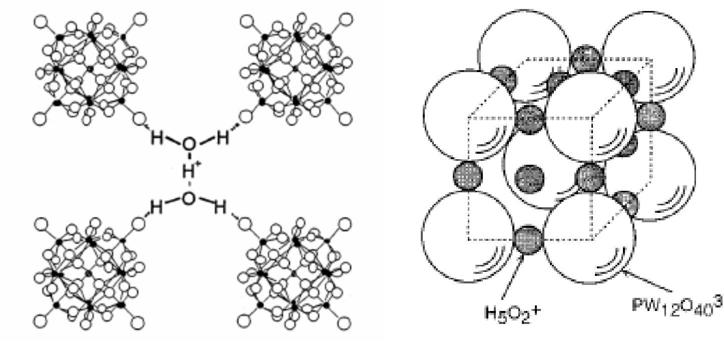

Fig. 1.5: *The Crystal packing and the secondary structure of* $H_3PW_{12}O_{40}.6H_2O$.

The fragment of the structure of the Keggin HPA, H_3 $[PW_{12}O_{40}]$. $6H_2O$ is determined by single-crystal X-ray analysis [21]. Generally, solid heteropoly compounds (HPAs and salts) form ionic crystals [22]. Then, depending on the amount of hydration water and on the counter-cation, several crystallographic arrangements exist and are presented in Table 1.1.

Table 1.1: Crystal structures of TPA hydrates

Formula (Hydrate)	Space group
$H_3PW_{12}O_{40}.29H_2O$	(cubic type B) *Fd3m*
$H_3PW_{12}O_{40}.24H_2O$	(rhombohedral type B) *R3m*
$H_3PW_{12}O_{40}.21H_2O$	(orthorhombic) *Pcca*
$H_3PW_{12}O_{40}.14H_2O$	(triclinic) *P1*
$H_3PW_{12}O_{40}.5H_2O$	(cubic type A) *Pn3m*

1.2.1.3. Tertiary structure: Recently, it was realized that, in addition to primary and secondary structures, the tertiary structure is very influential on the catalytic function of solid HPAs [3,4]. The tertiary structure is the structure of solid HPAs as assembled [Fig. 1.6]. The size of the particles, pore structure, distribution of protons in the particle is the features of the tertiary structure.

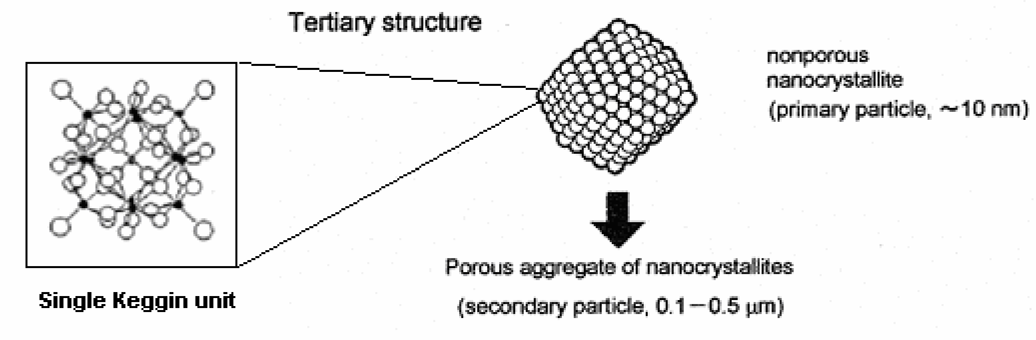

Fig. 1.6. *Tertiary structure of heteropoly anion.*

1.2.2. Synthesis

HPAs are synthesized as shown in eq. (1.2) and eq. (1.3) under acidic conditions by apparently simple inorganic reactions of the type:

$$[PO_4]^{3-} + 12[MoO_4]^{2-} + 24H^+ \longrightarrow [PMo_{12}O_{40}]^{3-} + 12H_2O \textbf{....Eq. (1.2)}$$

$$[SiO_4]^{4-} + 12[WO_4]^{2-} + 24H^+ \longrightarrow [SiW_{12}O_{40}]^{4-} + 12H_2O \textbf{....Eq. (1.3)}$$

Unwanted side reactions and the presence of complex equilibria are possible, so caution must be taken during preparation in order to avoid hydrolytic decomposition of polyanions and non-homogeneity of the metal cation to polyanion ratio in the solid. Details of the preparation procedures of HPAs and their salts in aqueous and non-aqueous solutions are given in a number of reviews and papers [23,24]. HPAs are prepared in solution by acidifying and heating in the appropriate pH range [25,26]. In case of eq. (1.2) and eq. (1.3), free acids are synthesized primarily by extraction with ether from acidified aqueous solutions and by ion exchange from salts of HPAs.

1.2.3. Textural properties

1.2.3.1. Stability

Along with the thermal stability, the stability of heteropolyanion in solution was also the subject of particular attention. Some solid HPAs are thermally stable and used in reactions with vapor-phase reactants conducted at high temperatures. The thermal stability is measured mainly by XRD, TG-DTA. Results from TG and DTA shows the presence of two types of water in heteropoly compounds, i.e., water of crystallization and "constitutional water molecules" [27]. Loss of the former usually occurs at temperatures below 473 K. At temperatures exceeding 543 K for $H_3PMo_{12}O_{40}$ or 623 K for $H_3PW_{12}O_{40}$, the constitutional water molecules (acidic protons bound to the oxygen of the polyanion) are lost. TG analysis of $H_3PW_{12}O_{40}$ and of $Cs_{2.5}H_{0.5}PW_{12}O_{40}$ showed that entire water molecules of crystallization are lost at temperatures as low as 573 K, and acidic groups are removed as water is formed from protons and lattice oxygens at temperatures exceeding 623 K. There are various kinds of stabilities, for example, thermal stability and hydrolytic stability in solution, and those stabilities change very much depending on the nature of HPAs [3-5].

The thermal stability of hydrogen forms of HPAs changes with heteroatom, polyatom, and polyanion structure in the order $H_3PW_{12}O_{40} > H_3PMo_{12}O_{40} > H_4SiMo_{12}O_{40}$, and $H_4SiW_{12}O_{40}$, which is much more stable than $H_6P_2W_{18}O_{62}$ [20,28,29]. The larger the central atom, the more stable is the heteropoly anion structure [30]. The thermal stability of $H_3PMo_{12}O_{40}$ and its salts changes with counter cations.

1.2.3.2. Acidity

I. Acidity in solution

Typical HPAs having the Keggin structure, such as $H_3PW_{12}O_{40}$ and $H_4SiW_{12}O_{40}$, are strong acids; protons are dissociated completely from the structures in aqueous solution [31]. The dissociation constants, pKa, of HPAs depend on the solvent. HPAs are much stronger acids than H_2SO_4, HBr, HCl, HNO_3, and $HClO_4$. For example, in AA, the acid strength of $H_3PW_{12}O_{40}$ is greater than that of H_2SO_4 by about 2 pK_a units. As for the acid strengths of HPAs, the following order has been reported for the compound in acetone [32]: $H_3PW_{12}O_{40} > H_4SiW_{12}O_{40} \approx H_3PMo_{12}O_{40} > H_4PMo_{11}VO_{40} > H_4SiMo_{12}O_{40}$. The acid strength decreases when W is replaced by Mo or V and when the central P atom is replaced by Si. So acidity increases in general with a decrease in the negative charge of the heteropolyanion, or an increase in the valency of the central atom (the valency of the central atom increases in the order Co< B< Si, Ge< P) [32]. The formation constants (in parentheses) of the complexes are as follows: $PW_{12}O_{40}^{3-}$ (1.30) < $PMo_{12}O_{40}^{3-}$ (3.11) < $SiMo_{12}O_{40}^{4-}$ (24.7). These values represent the capabilities of the heteropolyanion to form hydrogen bonds. Thus, the acid strength is in the order: $H_3PW_{12}O_{40} > H_3PMo_{12}O_{40} > H_4SiW_{12}O_{40} \approx H_4GeW_{12}O_{40} > H_4SiMo_{12}O_{40} > H_4GeMo_{12}O_{40}$. This is in general agreement with those obtained [33,34] with indicator tests.

In addition to the acidity, the softness of the heteropolyanion is an important characteristic relevant to catalysis [35]. The softness has been estimated by the equilibrium constant in aqueous solution of the following reaction [Eq. (1.4)] at 298 K.

$$Ag_nX + nNaI \rightleftharpoons nAgI + Na_nX \text{ (X = polyanion)} \quad \textbf{....Eq. (1.4)}$$

The order of softness was found to be: $SiW_{12}O_{40}^{4-} > GeW_{12}O_{40}^{4-} > PW_{12}O_{40}^{3-} > PMo_{12}O_{40}^{3-} > SiMo_{12}O_{40}^{4-} > SO_4^{2-}$.

II. Acidity in the solid state

There are three types of catalysis of solid HPAs; (1) surface, (2) bulk type I (= pseudoliquid), and (3) bulk type II catalysis, as shown in Fig.1.7. The acid catalysis of heteropoly compounds in the solid state is classified into “surface type” and “bulk type” catalysis.

1. Surface-Type Catalysis

The former occurs on those compounds, which are able to adsorb reactants only on the external surface. In this way, hydrocarbons are adsorbed in amounts lower than that corresponding to the monolayer.

2. Bulk-Type (I) and Bulk-Type (II) Catalysis

In the case of “bulk type” catalysis, the heteropoly compound can take up polar molecules in amounts corresponding to more than 100 surface layers [36,37]. In case the uptake of polar molecules such as alcohols, ethers, and amines gave integral multiples of the number of protons, and the rate of their adsorption is primarily determined by the polarity and by the molecular size [36]. The amount adsorbed can be controlled by changing the cation in the salts [38]. Considering the bulk adsorption properties, it turns out that catalytic reactions involving polar molecules occur not only at the surface but also in the bulk solid of certain HPAs.

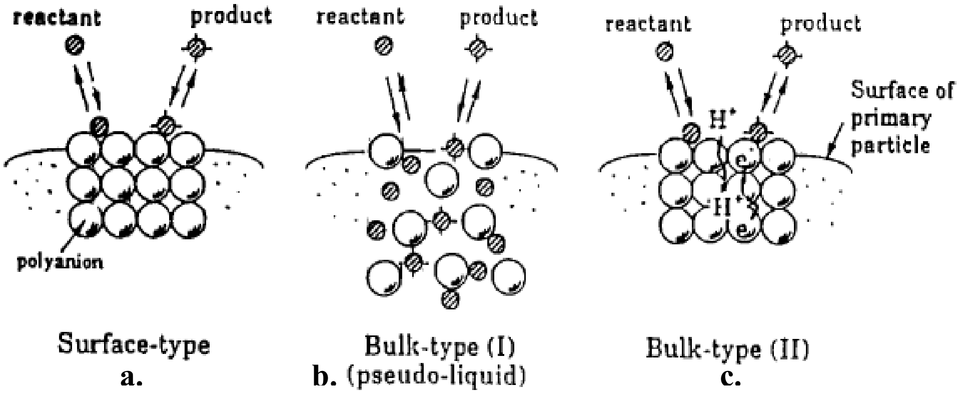

Fig. 1.7. *Three types of heterogeneous catalysis: (a) surface type, (b) Bulk-type (I)(pseudoliquid), (c) Bulk-type (II).*

Supporting HPAs on solids with high surface areas is a useful method for improving their catalytic performance. In general, strong interactions of HPAs with supports are observed at low loadings and the intrinsic properties of HPAs prevail at high loadings. The acid strength of $H_3PW_{12}O_{40}$ diminishes in the sequence of supports SiO_2>Al_2O_3>activated charcoal. The acid strengths of HPAs supported on SiO_2 [39] measured by NH_3 -TPD is in the following order: $H_3PW_{12}O_{40}$ (865 K) > $H_4SiW_{12}O_{40}$ (805 K) > $H_3PMo_{12}O_{40}$ (736 K) > $H_4SiMo_{12}O_{40}$ (696 K), where the figures in parentheses are the temperatures of desorption.

Supported HPA catalysts have much greater surface areas; hence they are more important for applications [1]. The acidity and catalytic activity of supported HPAs depends on the type of carrier, the HPA loading, conditions of pretreatment, etc. Acidic or neutral substances such as SiO_2 [39], active carbon [40,41], acidic ion-exchange resin [42], are suitable as supports, SiO_2 the most often used being. SiO_2 is relatively inert towards HPAs, at least above a certain loading level, although some chemical interaction takes place between HPAs and SiO_2. On the other hand, thermally decomposed Keggin structure of molybdenum acids on the silica surfaces may be reconstructed on exposure to water vapour [43,44]. Basic solids like Al_2O_3 and MgO tend to decompose HPAs [45,46]. Adsorption of HPAs onto silica, alumina and active carbon from aqueous and organic solutions has been studied [47-49]. Catalysts comprising TPA supported on titania [50], ZrO_2 [51,52] and H_3 $[PW_{12}O_{40}]$ encapsulated into mesoporous pure-silica molecular sieve MCM-41 has been prepared and characterized by different techniques [53,54]. H_3 $[PW_{12}O_{40}]$/MCM-41 has higher catalytic activity than H_2SO_4 or bulk H_3 $[PW_{12}O_{40}]$ and exhibits shape selectivity in liquid-phase alkylation of phenol [53]. H_3 $[PW_{12}O_{40}]$ supported on dealuminated zeolite Y has been characterized and tested in isomerization, disproportionation and dealkylation of m-xylene [55]. The Keggin-type HPAs, H_n $[XM_{12}O_{40}]$ (where n = 3, 4; X = Si, P; M = Mo, W) immobilized into a silica matrix by sol-gel technique and have been tested in Friedel-Crafts alkylations [56].

1.2.4. Application in catalysis

HPAs have several advantages as catalysts, which make them economically and environmentally attractive. Several new industrial processes based on HPA catalysis, such as oxidation of methacrolein, hydration of olefins (propene and butene), polymerization of tetrahydrofuran, have been developed and commercialized [1].

1.2.4.1. Homogeneous Reactions

HPAs catalyze a wide variety of reactions in homogeneous liquid phase offering strong options for more efficient and cleaner processing compared to conventional mineral acids [45,57].

Table 1.2: Homogeneous Reactions Catalyzed by HPA [45]

Reaction[a]	Rate ratio[b]	T (K)	Ref.
Hydration of isobutene[c]	2-4	313	11
Hydration of phenylacetylene	100	333	11
$PhC(CH_3)_2OOH \rightarrow PhOH + CH_3COCH_3$	1000	298	3
Olefin + HOAc $\rightarrow$ Ester	90	383	3
$THF + Ac_2O \rightarrow AcO(CH_2CH_2CH_2CH_2O)_nAc$	>1000	323	11
Styrene + HCHO $\rightarrow$ 1,3-dioxane	50	323	11

[a] *Unless otherwise stated, reactions were performed in organic media.* [b] *HPA/H_2SO_4 (per proton).* [c] *In aqueous solution.*

1.2.4.2. Biphasic Reactions

Polymerization of tetrahydrofuran (THF) is used for the preparation of polyoxytetramethylene glycol (PTMG), which is employed for manufacturing Spandex fibers and polyurethanes. Aoshima et al. [58] have developed a one-step process [Eq. (1.5)] for the THF polymerization to directly yield PTMG.

$$n\mathrm{THF} + H_2O \longrightarrow \mathrm{HO}\,[(CH_2)_4O]_n\mathrm{H}$$ **....Eq. (1.5)**

Esterification of *p*-nitrobenzoic acid is a step of the anesthetic synthesis. Ethyl *p*-nitrobenzoate is obtained in a 99% yield by esterification of *p*-nitrobenzoic acid with ethanol in the presence of TPA (3-7 wt.%) at 348 K [59].

1.2.4.3. Heterogeneous reactions

I. Acid catalyzed reactions

HPAs are more active catalysts for various reactions in solution than conventional inorganic and organic acids, and they are used as industrial catalysts for several liquid-phase reactions [4,60]. The paraffin alkylation is utilized in industry for obtaining higher octane paraffins which are blended into gasoline. H_2SO_4 or HF is used as homogeneous catalysts in this process. TPA supported (75%) on a series of carriers, such as mesoporous molecular sieve MCM-41, amorphous silica, and alumina, has been studied as the catalyst for the isobutane/2-butene alkylation in comparison with a MCM-22 zeolite [61]. HPAs and their salts are promising solid acid catalysts for Friedel-Crafts reactions, to replace the conventional homogeneous catalysts, such as $AlCl_3$, BF_3, and H_2SO_4, which causes serious environmental and operational problems-high toxicity, corrosion, spent acid disposal, difficulty of separation and recovery, etc.

Misono, Okuhara, et al. [62-64] demonstrated that the insoluble salt $Cs_{2.5}H_{0.5}PW$, which has a large surface area and strong acid sites, is a promising solid acid catalyst for Friedel-Crafts reactions. In the alkylation of 1,3,5-trimethylbenzene by cyclohexene, this salt was found to be more active than the parent acid TPA [65]. TPA supported (20-50 wt. %) on a mesoporous pure silica molecular sieve MCM-41, having 30 Å uniformly sized pores, exhibits a higher catalytic activity than H_2SO_4 or bulk TPA and shows shape selectivity in alkylation of 4-*tert*-butylphenol with olefins [66].

Active carbon strongly adsorbs certain amount of HPA, and carbon-supported HPAs thus obtained catalyze liquid-phase esterification and related reactions in polar media. The maximum HPA loading tightly retained on carbon in water or methanol is ~10 wt.%, slightly depending on the type of carbon and its pretreatment. Schwegler et al. [67] applied this catalyst for the esterification of phthalic anhydride with C_8-C_{10} alcohols at 373-393 K to yield dialkyl phthalates. Timofeeva et al. [68] found that the esterification of dipicolinic acid (DA) with butanol, which is a step of the synthesis of pharmaceutics, is catalyzed by TPA as well as by its insoluble salts.

II. Redox reactions

A general feature of heteropolymolybdates and heteropolytungstates is their high reducibility. Electrochemical investigations of Keggin-type heteropolyanions in aqueous or non-aqueous solutions have revealed sequences of reversible one- or two- electron ($1e^-$ or $2e^-$) reduction steps, which yield deeply colored mixed-valence species ("heteropoly blues"). In protic solvents, the Keggin anions exhibit electrochemical reduction by two electrons. The reduction potentials depend on pH as a result of protonation [69]. Misono et al. [70,71] have shown that the reduction of $H_3PM_{12}O_{40}$ (M=Mo,W) and its alkali-metal salts by H_2 consists of reoxidation and effects of constituent elements on redox properties in the solid state [72]. Generally reactions catalyzed by HPA-n proceed via a stepwise redox mechanism represented as shown below:

$$\text{HPA-}n + \text{Red} + m\text{H}^+ \rightarrow \text{H}_m(\text{HPA}-n) + \text{Ox} \quad \text{....Eq. (1.6)}$$

$$\text{H}_m(\text{HPA-}n) + (m/4)\text{O}_2 \rightarrow \text{HPA-}n + (m/2)\text{H}_2\text{O} \quad \text{....Eq. (1.7)}$$

This mechanism includes stoichiometric m-electron oxidation of the substrate, Red, by HPA-n to form the product, Ox, followed by reoxidation of the reduced form of the oxidant, H_m(HPA-n), with dioxygen, where H_m(HPA-n) = $H_m[PMo_{12-n}^{6+}V_{n-m}^{5+}V_m^{4+}]^{(3+n)-}$.

1.3. ZIRCONIA (ZrO_2)

Zirconium is in group IVB of the periodic table with a normal valency of 4. It displays no redox chemistry under normal circumstances, whilst its coordination number can reach up to 8. The aqueous chemistry of zirconium compounds is dominated by the desire to form zirconium-oxygen bonds [73,74]. This leads to the formation of the various types of polymeric compounds as shown in Fig.1.8. These structures provide the basis for the crystal structure in zirconium hydroxides and zirconium oxides derived from them.

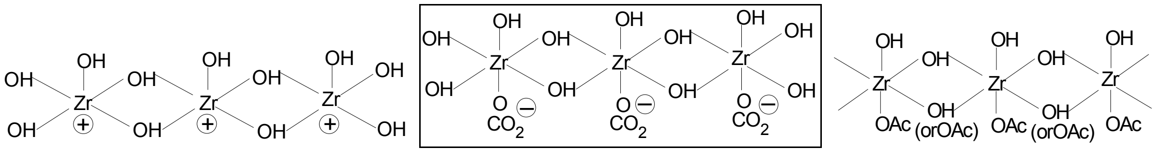

Cationic-Zirconium oxychloride
-Zirconium nitrate

Anionic- Ammonium zirconium carbonate
- Zirconium orthosulphate

Neutral- Zirconium acetate

Fig. 1.8. *Structural representations of polymeric zirconium species.*

ZrO_2 exhibits few key properties as: Usage temperature up to 2673 K, high density, low thermal conductivity (20% that of alumina), chemical inertness, resistance to molten metals, ionic electrical conduction, wear resistance, high fracture toughness, high hardness. It can exist in one of three phases, depending on the temperature [Fig 1.9]. The phases can be stabilized by the addition of dopants. At very high temperatures (>2643 K) the material has a cubic structure. At intermediate temperatures (1443 to 2643 K) it has a tetragonal structure. At low temperatures (below 1443 K) the material transforms to the monoclinic structure. However, tetragonal ZrO_2 can be prepared at low temperature (in the range of 823-1023 K) in the form of metastable phase. The transformation from tetragonal to monoclinic is rapid and is accompanied by a 3 to 5 percent volume increase that causes extensive cracking in the material.

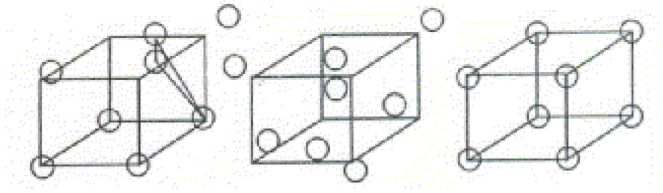

Monoclinic $\xrightarrow{\textbf{1373 K}}$ Tetragonal $\xrightarrow{\textbf{2573 K}}$ Cubic

Fig. 1.9. *Phase changes in ZrO_2.*

The cubic polymorph adopts the calcium difluoride (fluorite) structure in which the zirconium atoms are co-ordinated to eight oxygen atoms, while the tetragonal phase may be regarded as a slightly distorted fluorite structure whose difraction patterns can be indexed to a face centered tetragonal cell. The monoclinic polymorph, which is sometimes referred to as the Baddeleyite structure, contains zirconium atoms seven-coordinated to oxygen atoms [75]. Many divalent and trivalent cationic species such as Mg^{2+}, Ca^{2+}, and Y^{3+} have been incorporated into ZrO_2 to prepare cubic and tetragonal ZrO_2 that is stable at room temperature [76]. The band gap of ZrO_2 is 5.0 eV, much smaller than that of alumina and water, but the structure of the bands is expected to be similar. Because of this, ZrO_2 is a much softer acid-base than alumina or the oxide formations on Si_3N_4. The aqueous surface chemistry of ZrO_2 is well known [77,78] and it is considered to be weakly acidic in water.

1.3.1. Synthesis

ZrO_2 is usually obtained by the calcination of its hydroxide/oxyhydroxide, which is prepared by hydrolysis of zirconium salts like zirconyl oxychloride, zirconium nitrate with liquor ammonia. The influence of the pH of the reaction mixture on the nature of ZrO_2 formed from zirconium (IV) acetate solutions, processed either by boiling under reflux or by hydrothermal methods, has been investigated [79]. To develop particular catalytic properties such as high conversion and selectivity, the synthesis of ordered Nanostructured-mesoporous ZrO_2 with high specific surface area and narrow pore size distribution is of importance both in scientific and industrial application point of view. Knowles and Hudson [80] reported the synthesis of porous ZrO_2, using the alkyltrimethylammonium halide as surfactant and zirconyl chloride as zirconium source. Depending upon the surfactant/zirconium ratio (varying from 0.082 to 0.341), mesostructured ZrO_2 exhibit surface areas ranging from 238 to 329 m^2/g. Then either using amphoteric [81], anionic [82], or neutral templates [83] and, depending on the synthesis pathway, zirconyl chloride or zirconium propoxide as zirconium precursors, hexagonal, cubic or disordered mesoporous ZrO_2 were successfully obtained.

1.3.2. ZrO_2 as a support

I. Acidic property of ZrO_2

The catalytic activity and selectivity of ZrO_2 is greatly affected by the preparation methods, the activating treatments and the modifying agents. For instance, the addition of oxo-anions such as $[SO_4]^{2-}$, $[WO_4]^{2-}$, $[MoO_4]^{2-}$ and $[BO_3]^{3-}$ to freshly precipitated ZrO_2 has yielded solid materials with outstanding strong acid and catalytic properties, which are absent in each of the single components.

Sulphated zirconia (SO_4^{2-}/ZrO_2) shows the greatest acid strength ($H_o = -16.04$) among oxo-anion modified metal oxides [84]. SO_4^{2-}/ZrO_2 based catalysts are now being used for alkane isomerization; they can be operated at a lower reaction temperature than zeolite catalysts (353 vs. 533 K), and they do not need a chlorine supply as do the $AlCl_3$ based systems, which are additionally water sensitive [85,86]. The activity of SO_4^{2-}/ZrO_2 can be promoted by addition of Mn, Fe, or Ni cations. In proximity to the surface, an oxygen vacancy creates a surface metal cation site with a high degree of unsaturation, i.e., a strong Lewis acid site. It has attracted lot of attention due to its high catalytic activity for the conversion of small hydrocarbons especially n-butane isomerization [87]. It has been reported to possess high Lewis acidity and this has encouraged some studies on its use in liquid phase Friedel-Crafts benzoylation reactions [88]. The acylation requires very strong acids and except SO_4^{2-}/ZrO_2 and $AlCl_3$, the other acids were very ineffective. It is known that SO_4^{2-}/ZrO_2 is a superacid [89,90].

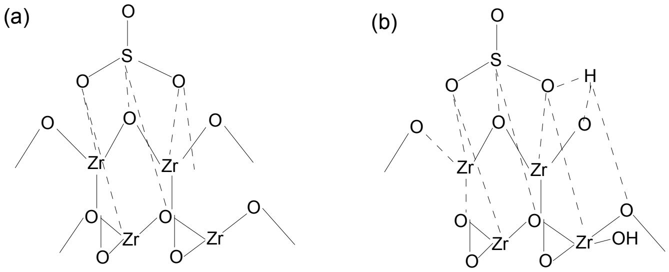

Fig 1.10. *Possible SO_4^{2-}/ZrO_2 acid site structures: (a) Lewis; (b) Brønsted.*

The main drawback of SO_4^{2-}/ZrO_2 is its limited thermal stability, since sulfate anions are partially removed as SO_x when calcined at high temperatures (>873 K) and the catalyst looses its acidity and activity [91,92].

Tungstated zirconia (WO_x–ZrO_2) provided a good alternative to SO_4^{2-}/ZrO_2 for some isomerization and alkylation reactions [93,94]. A microporous WO_x–ZrO_2 calcined at different temperatures (between 973 and 1073 K), was compared in a standard benzene alkylation with 1-dodedene. WO_x–ZrO_2 catalysts active for isomerization reactions at low temperature were prepared by impregnation of $ZrO_x(OH)_{4-2x}$ with a solution of ammonium metatungstate followed by oxidation treatments that sinter the ZrO_2 crystallites and increase the WO_x surface density. Surface area and XRD measurements show that dispersed WO_x species inhibit ZrO_2 crystallite sintering and stabilize tetragonal ZrO_2 crystallites during high-temperature oxidative treatments. The addition of a metal function (0.3 wt.% Pt) increases the turnover rate (based on W atoms) and selectivity for *n*-heptane isomerization [96]. WO_x–ZrO_2, which experiences rapidly increasing attention in isomerization catalysis, was also investigated by in situ UV-Vis. spectroscopy in a collaborative effort with Prof. Helmut Knozinger's group in Munich [97].

HPA and their salts are another class of compounds that may as well generate strong acidity once incorporated on ZrO_2 [98]. The addition of HPA on stabilized or hydrated ZrO_2 has been scarcely examined [99,100]. We have reported recently that the addition of a Keggin-type HPA, TPA, to freshly precipitated ZrO_2 yields strong solid acids ($H_o \geq -9.3$) which show high catalytic activity in the skeletal isomerization of 1-butene to isobutylene [100]. The chemical interactions between the HPA and the support are a matter of great interest because a strong interaction could fix the HPA to the carrier, avoiding the leaching of HPA in liquid-phase reactions [101] or maintaining a high HPA dispersion in gas-phase reactions. The thermal stability of the HPA's structure is also affected by the type of carrier. In silica supported TPA, ^{31}P MAS-NMR studies indicate that silanol (Si–OH) groups may participate in the HPA binding to form $(\equiv SiOH_2^+)(H_2PW_{12}O_{40}^-)$, though the mechanism is not yet clear [102]. Similar to the case of oxo-anion modified ZrO_2, it is very likely that bulky Keggin oxopolyanions on hydrated ZrO_2 may alter the structural transformation pathway upon different calcination conditions.

II. Oxidizing property of ZrO_2

One relevant example of the oxidizing character of ZrO_2 is the partial oxidation of methane on yttria-stabilised ZrO_2 yielding CO, CO_2, H_2O and H_2 [103]. Moreover, zirconium oxide gives high conversion of pyrolysis products with high hydrogen to carbon monoxide ratio in the product gas [104].

1.3.3. Applications of ZrO_2

ZrO_2 is a very interesting material for catalytic reactions, because it provides different functionalities [105]. ZrO_2 is a very important ceramic material and has found applications in a number of technologies, including fuel cell electrolytes [106], high-performance transformation-toughened structural engineering ceramic [107], catalysts [108], buffer layers for superconductor growth [109], oxygen sensor [110], damage resistant optical coatings [111], and gate dielectric [112,113]. Zirconium compounds have only recently been associated with catalysis, but it is now clear that the incorporation of zirconium can bring benefits to catalysts. As these benefits of zirconium are recognized, commercial products are becoming available.

Zirconium based catalysts can be used in hydrogenation [114,115], oxidation of methanol [115], amination [116], isomerization, esterification [117], electrocatalysis [118], DENOX [119], polymerization [120], refinery catalysts [121] and other catalytic reactions.

1.4. MESOPOROUS SILICA MATERIALS

Zeolites are crystalline alumino-silicates microporous silica based solids. Traditionally, zeolites are classified as crystalline materials in which Si and Al are tetrahedrally co-ordinated by oxygen atoms in a three-dimensional network. The main restriction of microporous zeolitic materials is the size constraints of *ca*. 0.75 nm and therefore not suitable for catalytic transformations involving organic molecules having kinetic diameters above 0.75 nm. The catalytic transformation of molecules with kinetic diameters larger than 0.75 nm, especially important for the preparation of fine chemicals, requires zeolitic materials with larger pore diameters. Hence, there has been an ever-growing interest in expanding the pore sizes of the zeolitic materials from micropore to mesopore region. According to IUPAC definition [122] porous materials may be divided into three types based on their pore dimensions like Microporous (< 20 Å), Mesoporous (20-500 Å) and Macroporous (> 500 Å). To overcome this difficulty, researchers had taken great efforts to synthesize mesoporous materials such as silicas [123], transitional aluminas [124] and pillard clays. However, the pores in these materials are generally irregularly spaced and broadly distributed in size. Thus, a gap has been bridged by the discovery of Mesoporous silica materials (MS) family, which have opened up new possibilities for preparing catalysts with uniform pores in the mesoporous region that can be easily accessed by bulky molecules that are present in crude oils and fine chemical productions.

MS has attracted much attention recently. The MS family is classified into MCM-41, MCM-48 and SBA-15 members which, are very interesting for their rich morphological transformations [125,126]. Very high surface areas (>700 $m^2 g^{-1}$) and the control of pore sizes are among the many desirable properties that have made such materials the focus of great interest. The synthesis of these materials opens definitive new possibilities for preparing catalysts with uniform pores in the mesoporous region, which will allow the ingress and egress of relatively large molecules in their mesopores for catalytic transformations. The most striking fact about the MS is that, although composed of amorphous silica, it displays an ordered structure with uniform mesopores arranged into a hexagonal (MCM-41 and SBA-15) and cubic (MCM-48) structures.

1.4.1. MCM-41, MCM-48 and SBA-15

In 1992 at Mobil Research and Development Corporation, Kresge et al. [125-131] reported the synthesis of a new family of silica/aluminosilicate mesoporous molecular sieves (like MCM-41, MCM-48) with large uniformly sized parallel channel pores. These materials are having pore sizes greater than 20 Å, large surface area usually greater than 1000 m^2g^{-1} and long range ordering. MCM-41, one of the members of this extensive family of mesoporous molecular sieves, possesses a hexagonal array of uniform mesopores. The main characteristics of MCM-41 materials are their high thermal stability, large surface area and narrow pore size distribution. MCM-41 is structurally stable towards thermal treatment, hydrothermal treatment with steam at mild conditions, mechanical grinding and also towards acid treatment at mild condition [132-134].

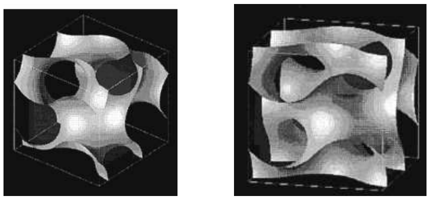

Fig. 1.11. *Minimal gyroid surface [135].*

MCM-48 silica was claimed to have the cubic space-group symmetry of *Ia*3*d* [136,137] that belonged to the same space group as the periodic minimal surface of gyroid (G) discovered by Schoen [136]. It shows high thermal stability up to 1023 K. All structural observations of the MCM-48 silica were explained well by assuming that the amorphous wall followed the G surface [137,138] and it has been found to possess a bi-continuous structure centered on the gyroid minimal surface [139] as shown in Fig. 1.11.

In 1998, the ordered mesoporous material, denoted SBA-15 mesoporous molecular sieves was first reported. It is silica with large, uniform mesopores arranged into a two-dimensional (2-D) hexagonal structure can readily be synthesized using triblock copolymer and oligomer templates with poly (ethylene oxide) (EO_n) blocks as organic structure-directing agents [140,141]. Further studies [142-144] revealed that this ordered SBA-15 mesoporous solids are actually connected through complementary pores (micropores and small mesopores) in the siliceous pore walls. With very large uniform pores (up to ~ 300

Å), thick pore walls, and superior hydrothermal stability, SBA-15 molecular sieves have the promising potential applications in many fields, such as the catalysis, separation, adsorption [145-147]. Large pore-size molecular sieves are much in demand for reactions or separations involving large molecules [148].

1.4.2. Formation Mechanism

MS can be synthesized in alkaline route [124,125], the acid route [126,149] or neutral route, by using amphiphiles as templates. In the acid route, the silica source is silicon alkoxides. The acid catalysis speeds up the hydrolysis versus the condensation rate and promotes mostly condensation at the ends of silica polymers to form linear silicate ions [150]. On the other hand, the alkaline catalysis favors both hydrolysis and condensation. Thus, the alkaline route leads to a highly condensed and compact structure, and the acid route leads to a more fuzzy and soft network [150]. The different routes for syn thesis of mesoporous molecular sieves are given in Table 1.3.

Table 1.3. Routes for synthesis of mesoporous molecular sieves

S	Example	pH	Resulting Phase
S^+I^-	Cetyltrimethyl ammonium ions + silicate species	10-13	Hexagonal, cubic and lamellar
$S^+X^-I^+$	Cetyltrimethyl ammonium ions + silicate species	< 2	Hexagonal
S^0I^0	$C_{12}H_{25}NH_2 + (C_2H_5O)_4Si$	< 7	Hexagonal

Where S = surfactant species ; I = inorganic species (Si); X = Cl, Br or OH

Most commonly used surfactant for synthesizing MCM-41 is cetyltrimethyl ammonium halide. These models for synthesizing MCM-41 are predicted upon the presence of a surfactant in solution to guide the formation of inorganic mesostructured form as the solubilized inorganic precursors.

1. Liquid-Crystal Templating Mechanism

Two mechanistic pathways have been proposed as per shown in Scheme 1.1 [132]. (A) The aluminosilicate precursor species occupied the space between a pre-existing hexagonal lyotropic liquid crystal (LC) phase and deposited on micellar rods of the LC phase. (B) The inorganics mediated, in some manner, the ordering into the hexagonal arrangement. In either case, the inorganic components (which were negatively charged at the high pH values used) preferentially interacted with the positively charged ammonium head groups of the surfactant and condensed into a solid, continuous framework.

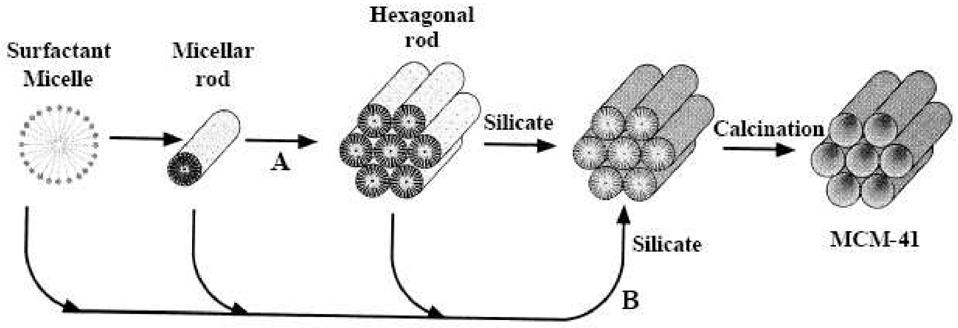

Scheme 1.1 *Liquid crystal templating mechanism proposed for the formation of MCM-41: (A) liquid crystal phase initiated and (B) silicate anion initated [132,133].*

The resulting organic inorganic mesostructure can be viewed alternatively as a hexagonal array of surfactant micellar rods embedded in a silica matrix; removal of the surfactants produced the open, mesoporous MCM-41 framework. The pathway (B) however, did not take place because the surfactant concentrations used were far below the critical micellar concentration (CMC) required for hexagonal LC formation. However, this is possible under different mechanistic conditions. A number of models have been proposed to explain the formation of mesoporous materials and to provide a rational basis to all the synthetic routes:

2. Silicate-Rod Assembly [151], 3. Silicate-Layer Puckering [152], 4. Charge-Density Matching [153], 5. Silicatropic-Liquid Crystals [154].

A generalized mechanism based on the specific type of electrostatic interaction between a given inorganic precursor I and surfactant head group S was proposed by Huo and co-workers [149]. Based on the nomenclature of the original LCT mechanism, which involve the anionic silicate species and cationic quaternary ammonium surfactant, could be categorized as the S^+I^- pathways. By extension other charge-interaction pathways are S^-I^+, $S^+X^-I^+$ (X is counter anion), and $S^-M^+I^-$ (M^+ is a metal cation). By operating below the isoelectronic point of silica (pH~2) under acidic conditions, the silicate species were cationic (I^+). The same ammonium surfactant S^+ could be used as a templating agent but the halide counteranion X^- became involved through this pathway as it serves to buffer the repulsion between I^+ and S^+ by means of weak hydrogen bonding interaction. mesoporous silica molecular sieves family has three well-defined mesophase MCM-41, MCM-48 and MCM-50. The surfactant to silica molar ratio is the key factor in obtaining the different mesophases. This is given in the following Table 1.4.

Table 1.4. Classification of Mesoporous Molecular sieves

Surfactant / silica	Phase
< 1.0	Hexagonal (MCM-41)
1.0-1.5	Cubic (MCM-48)
1.2-2.0	Thermally unstable materials
2.0	Cubic octamer $[(CTMA)SiO_{2.5}]_8$

All published syntheses for MCM-48 proceed via the hydrothermal reaction [131,155]. The reaction is a modification of Stöber's synthesis of non-porous silica spheres [156]. Compared with the hydrothermal pathway the new synthesis is faster than the traditional ones and produces MCM-48 spheres.

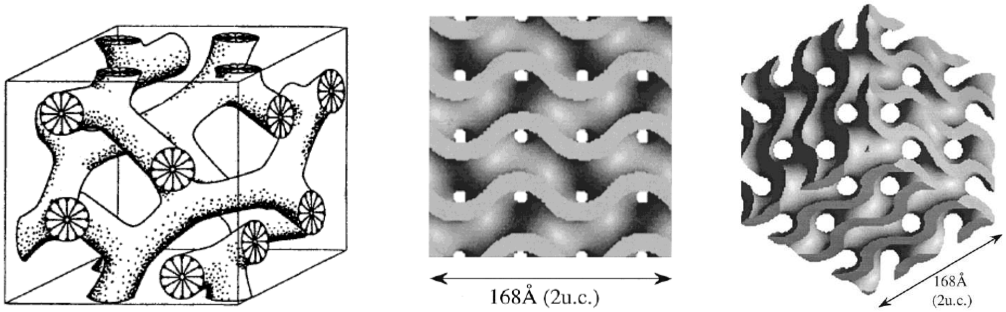

Fig. 1.12. *(a) Structure of MCM-48, 3D reconstructed structure models: (b) (100) section; (c) 3D-view along the [111] (two unit cells).*

It has been reported that, when MCM-48 is hydrothermally synthesized, a disordered surfactant-silica mesostructure is first formed within a short period of the reaction time (ca. 2 h) and then transforms to very small MCM-48 particles, less than 0.5 µm in diameter. The MCM-48 particles increase in size continuously with time, reaching a crystal size of about 1-3 µm (ca. 18 h). The reconstructed 3-D structure model for MCM-48 crystal is shown in Fig. 1.12. After the crystal morphologies are maintained until 30 h of the reaction time, the crystals are dissolved and transformed rapidly to a lamellar mesophase that exhibits clusters of randomly curved leaf-like morphologies [157,158].

The synthesis of SBA-15 can be accomplished using a cheap silica source, sodium silicate [159,160], which makes this synthesis commercially viable. Using aqueous acidic conditions ($pH\approx1$) and dilute triblock copolymer concentrations, SBA-15 has been synthesized with thick uniform silica walls (31 to 64 Å). At room temperature, the nonionic oligomeric surfactants frequently form cubic or 3-d hexagonal mesoporous silica structures, while the nonionic triblock copolymers tend to form hexagonal (*p6mm*) mesoporous silica structures. The assembly of the inorganic and organic periodic composite materials appears to take place by a hydrogen bonding $(S^0\,H^+)(X^-I^+)$ pathway. The assembly rate r increases with increasing concentration of $[H^+]$ and $[Cl^-]$, according to the kinetic expression $r = k\,[H^+]^{0.31}[Cl^-]^{0.31}$. With cationic surfactants and syntheses carried out in HCl media below the aqueous isoelectric point of silica, the key interactions are among the cationic surfactant, chloride anion, and the cationic silica species (designated as $S^+X^-I^+$, where S^+ is the cationic surfactant, X^- is the halide anion, and I^+ is a protonated Si-OH moiety, i.e., $[\mathrm{SiO}^{H}{}_{H}]^+$, and the overall charge balance is provided by association with an additional halide anion) [130,149].

1.4.3. Application of MCM-41, MCM-48 and SBA-15

The high surface area and large pore size of MCM-41 was used as catalyst, catalyst support, in sorption, for separations, in polymer chemistry etc. Soon after the discovery of MCM-41 and related materials in the late 80’s [124,161], the first uses of MCM-41 as catalyst support were reported [162,163]. The vast majority of studied MCM-41 as support was devoted to immobilization of homogeneous catalysts on the surface of MCM-41 [164]. Additionally, acids such as HPAs [165] or sulphonic acids [166] have been supported and evaluated in acid catalyzed reactions. Kozhevnikov et al. used 10-50% TPA loaded MCM-41 silicates [167]. These catalysts to be more efficient than H_2SO_4 or bulk TPA in liquid-phase alkylation of 4-*tert*-butylphenol by isobutene and styrene [168]. Using TPA loaded MCM-41 catalysts, Kresge et al. carried four test reactions, (i) *n*-butane conversion, (ii) *n*-hexane conversion, (iii) alkylation of isobutane with 2-butene, and (iv) alkylation of benzene with 1-tetradecene [169].

For vanadium, MCM-48 was used as support and loaded via a grafting process with VO (acac)$_2$ and subsequent mild oxidation [169]. MCM-48 seems to be a more interesting candidate as an adsorbent in separation techniques, e.g., supercritical fluid chromatography, or as a catalyst support than MCM-41. Several catalytic applications are described in the literature, e.g., *n*-decane conversion, carbon dioxide reduction [170,171], seems to be a promising candidate for applications in catalytic and separation technologies, e.g., supercritical fluid chromatography (SFC) [172].

Very few papers have appeared on supporting noble metal particles on ordered mesoporous oxides after the initial publications [173,174]. It was found that high surface area oxides prepared via these pathways could also be useful as catalysts and thus have a much wider range of applications. Both MCM-41 [175,176] and SBA-15 were loaded with rare earth oxides. Since phase transition temperatures depend, amongst others, on crystallite sizes for ZrO$_2$, investigations were initiated into supporting ZrO$_2$ on ordered mesoporous oxides (like MCM-41, SBA-15), because the pores could prevent the particles from growing larger than the pore sizes [177]. By anchoring a variety of functional groups on the internal surfaces, the sorption capacity and behavior of SBA-15 could be substantially altered. These properties have led SBA-15 to some intriguing applications, such as selective adsorption of heavy or noble metal [178,179], as controlled drug delivery matrixes [180,181], enzyme immobilization for biocatalysis [182-184], and immobilization of large chelating groups [185]. In light of its potential application in the area of drug delivery, there have been attempts recently to apply pure SBA-15 as a drug host [186,187].

1.5. PHYSICO-CHEMICAL CHARACTERIZATION

1.5.1. X-ray diffraction (XRD): Powder XRD is used to identify the structure, phase purity, degree of crystallinity, unit cell parameters and crystallite size. It helps in the study of the kinetics of crystallization of molecular sieves. XRD patterns of ZrO$_2$ exhibit peaks at $2\theta \sim 30$, 50 and 60°, characteristics of tetragonal zirconia (t-ZrO$_2$) phase, which could be indexed as (111), (202) and (131), respectively. XRD patterns of mesoporous phases exhibit peaks in the low angle region, the most intense peak being the (100) reflection. In the case of mesoporous silica materials (MCM-41, MCM-48 and SBA-15), the wall thickness is usually calculated by substraction of the inside pore diameters obtained by gas adsorption from the unit cell dimensions by XRD. Oxide like ZrO_2 shows characteristic peaks in the 2θ range 20-70 ° whereas ordered mesoporous materials exhibit characteristic peaks in the low angle region between 0.8 – 10°. The tetragonal crystallite size of the various samples was estimated from integral line width using the Debye-Scherrer relationship [188,189].

$$D_{hkl} = 0.9\ \lambda / B_{hkl} \cos\theta \quad \textbf{....Eq. (1.8)}$$

where, B_{hkl} is the effective line width of the X-ray reflection.

1.5.2. Sorption study: Molecular sieves have the ability to adsorb probe molecules of different sizes. Sorption capacities for probe molecules such as n-hexane, water, benzene, nitrogen etc. yield information about the hydrophilicity/hydrophobicity, pore dimensions and pore volume of the molecular sieves. Application of the Brunauer-Emmett-Teller (BET) equation is the standard method for the determination of surface areas of molecular sieves. The isotherm points are transformed with the linear version of BET equation:

$$p/V\,(p_0 - p) = 1/cVm + [(c-1)/cVm]\,(p/p_0) \quad \textbf{....Eq.(1.9)}$$

where, p is adsorption equilibrium pressure, p_0 is saturation vapor pressure of the adsorbate at the experimental temperature, V is volume of gas adsorbed at pressure p, V_m is volume of adsorbate required for monolayer coverage and c, a constant that is related to the heat of adsorption and liquefaction. The N_2-adsorption-desorption isotherms of MCM-41, MCM-48 and SBA-15 are of the type IV isotherm. The steep increase in N_2 adsorption (within the P/P_0 range between 0.2 to 0.4) corresponds to capillary condensation within uniform pores. The sharpness and the height of this step reflects the uniformity of the pore size and the pore volume respectively. The wall thickness of MS was determined as the difference between the repeat a_0 (from XRD) and the Horvath-Kawazoe pore diameter using N_2 adsorption [190].

1.5.3. Atomic force microscopy (AFM): The atomic force microscope was developed to overcome one of the main limitations of the STM, namely, the necessity of electrically conducting samples [191]. AFM is based on the interaction forces (short- or long-ranged, attractive or repulsive) that exist between atoms and molecules. The AFM is being applied to studies of phenomena such as abrasion, adhesion, cleaning, corrosion, etching, friction, lubrication, plating, and polishing. By using AFM one can not only image the surface in atomic resolution but also measure the force at nano-newton scale. The publications related to the AFM are growing speedily since its birth.

1.5.4. Scanning electron microscopy (SEM): The Scanning Electron Microscope (SEM) is one of the most versatile and widely used tools of modern science as it allows the study of both morphology and composition of biological and physical materials. By scanning an electron probe across a specimen, high-resolution images of the morphology or topography of a specimen, with great depth of field, at very low or very high magnifications can be obtained. Characterization of fine particulate matter in terms of size, shape, and distribution as well as statistical analyses of these parameters, may be performed. Non-agglomerated uniform spheres were obtained by the room temperature method while irregularly shaped particles were obtained by the hydrothermal synthesis i.e. is observed by SEM image of MCM-48 [192]. Scanning electron microscopy (SEM) images reveal that the as-synthesized SBA-15 sample consists of many rope-like domains with relatively uniform sizes of ~1 μm, which are aggregated into wheat-like macrostructures [135].

1.5.5. Transmission electron microscopy (TEM): TEM provide visualization of the pore structure and crystallite size of the material. In addition to structural characterization, it can also be used to detect the location of metal clusters and heavy cations in the framework [193]. In case of HPAs, a fairly regular periodic pattern is observed, which suggests that the individual heteropoly species were directly imaged. Individual anions of the Dawson-type cyclopentadienyl titanium (CpTi) heteropoly compound, $K_7\,(C_5H_5)TiP_2W_{17}O_{61}$, were observed by TEM [194]. TEM is used to elucidate the pore structure of mesoporous molecular sieves [193-197]. TEM images of calcined SBA-15 show well-ordered hexagonal arrays of mesopores (1D channels) and further confirm that SBA-15 has a 2D *p6mm* hexagonal structure [130,198]. From high-dark contrast in the TEM image of this sample, the distance between mesopores is estimated, in agreement with that determined from the XRD data.

1.5.6. FT-IR spectroscopy: FT-IR spectroscopy is a convenient and widely used method for the characterization of heteropolyanions. Keggin, Dawson, and lacunary heteropolyanions can be distinguished by their characteristic bands. In this way, IR spectroscopy can distinguish different types of oxygen atoms present in typical HPAs, oxygen connecting species [199-201]. Framework infrared spectroscopy provides additional information about the structural details of the molecular sieves. Maroni et al. [202] has been used different probe molecules to study the acidity of molecular sieves. The IR bands around 3600-3700 cm^{-1} confirm the presence of the silanol groups [203-204] or bridged hydroxyl groups in the molecular sieves and Brönsted acidities can be compared.

1.5.7. UV-Vis. spectroscopy: The electronic absorption spectra were recorded for structural and quantitative analysis and it gives information about the eletronic state of the heteropoly anions [205]. This technique is used to determine the coordination state of transition metal ions substituted in the matrix of the molecular, involving ligand-to-metal charge transfer spectrum. $PW_{12}O_{40}^{3-}$ shows absorption at about 38,000 cm^{-1}, due to ligand (oxygen) to metal (W) charge transfer (LMCT) [206]. The UV band positions of various HPAs are given in the literature [207]. This spectroscopic technique is used to determine the coordination state of transition metal ions substituted in the matrix of the molecular sieves, involving ligand-to-metal charge transfer transitions at ~ 200-220 nm.

1.5.8. NMR spectroscopy: NMR is used to characterize the acidity, the state of adsorbed molecules, reaction intermediates, in determining the nature with chemical environment of the atoms. This technique also has been found to be useful in understanding the structural, physicochemical properties of molecular sieves [208,209] and even the microporosity in case of HPAs [210-212]. The states of proton and crystallization water in the acid form were studied by high-resolution ^{31}P NMR and IR [213] and by ^{1}H [214] NMR. The resonance at 9.2 ppm, for anhydrous $H_3PW_{12}O_{40}$ was assigned to protons attached to the most basic bridging oxygen atoms, on the basis of IR results [213] and the basicity estimated by ^{17}O NMR spectroscopy. The ^{31}P chemical shift provides important information concerning the intactness of the structure in case of HPA. The ^{31}P-NMR chemical shift is greatly depends on water of hydration [215,216]. The ^{31}P NMR chemical shift is greatly dependant on n in $H_3PW_{12}O_{40}.nH_2O$ [216,217], the values being –15.1 to –15.6 ppm for n=6 and –11.1 to –10.5 ppm for n= 0.

The broad ^{29}Si NMR spectra of mesoporous samples closely resemble those of amorphous silica. The ^{29}Si MAS-NMR spectrum of the as-synthesized hexagonal SBA-15 shows three broad peaks at 92, 99, and 109 ppm. These peaks correspond to Q^2, Q^3, and Q^4 silica species, respectively, which are associated with progressively increased silica cross - linking. From the relative peak area, the ratios of these species are established to be

Q^2:Q^3:Q^4 = 0.07 : 0.78 :1. These results indicate that compared to MCM-41, SBA-15 has a somewhat less condensed, but similarly locally disordered, silica framework [218].

1.5.9. FT-Raman spectroscopy (FT-RS): Typical applications of FT-RS is in structure determination, multicomponent qualitative analysis, and quantitative analysis. Raman and IR spectra provide complementary information. FT-RS has also been used to study the structure of heteropoly compounds in solution [202,219-221] as well as in the form of solids, and supported form [222]. The details of Raman vibrational frequencies of Keggin anions (aqueous solutions) are listed in Table 1.5.

Table 1.5. Raman vibrational frequencies of Keggin anions, cm^{-1}

$PW_{12}O_{40}^{3-}$	$SiW_{12}O_{40}^{4-}$	$PMo_{12}O_{40}^{3-}$	$SiMo_{12}O_{40}^{4-}$	Modes of vibration
1011	998	997	982	$p\nu_{as}(M\text{-}O_d)^a$
996	981	981	962	$\nu_{as}(M\text{-}O_d)$

1.5.10. X-Ray Photoelectron Spectroscopy (XPS): XPS gives information about electron density of solid heteropoly compounds [223-225]. The binding energy of O1s electrons decreases with increasing negative charge of the heteropolyanion: $PW_{12}O_{40}^{3-}$ > $SiW_{12}O_{40}^{4-}$ ≥ $BW_{12}O_{40}^{5-}$ > $H_2W_{12}O_{40}^{6-}$ > $PW_{11}O_{39}^{7-}$ > $SiW_{11}O_{39}^{8-}$ > $H_2W_{12}O_{42}^{10-}$. For isostructral heteropolyanions, the O1s binding energy is higher for tungstates than for molybdates. A good correlation exists between the acid strength and the difference between O1s and W_{4f} binding energies of $H_3PW_{12}O_{40}$ and its salts. It also gives information on the elemental composition and the oxidation state of the elements. Mesoporous molecular sieves containing different heteroatoms such as Al, Ti, V, Nb and Zr have been analyzed by XPS technique to obtain information about the dispersion of the heteroatom in the structure [226-229].

1.5.11. Thermogravimetric and differential thermal analysis (TG-DTA): Thermal analysis is widely used to study the structural and thermal stability of HPAs and as-synthesized forms of molecular sieves. It provides information about the temperature required for the removal of adsorbed water, decomposition of the occluded organic cations in the pores and channels of molecular sieves and dehydroxylation at higher temperatures to produce Lewis acid sites. In case of mesoporous molecular sieves, the temperature at which an exotherm appears in the DTA after the loss of water molecules, gives helpful information about the temperature required to remove the template molecules from the pores during calcination. Phase transformations (if any) can also be understood from the exotherms obtained at higher temperatures.

The Keggin-type TPA, STA, MPA, and MSA decomposes at 738, 718, 648, and 623 K, respectively [230]. TG-DTG profile for H_3 $[PW_{12}O_{40}]$ hydrate shows three main peaks: (1) a peak at a temperature below 373 K corresponding to the loss of physisorbed water (a variable amount depending on the number of hydration waters in the sample); (2) a peak in the temperature range of 373-553 K accounted for the loss of $6H_2O$ molecules per Keggin unit, corresponding to the dehydration of a relatively stable hexahydrate H_3 $[PW_{12}O_{40}]$. $6H_2O$ in which the waters are hydrogen bonded to the acidic protons; and (3) a peak in the range of 643-873 K centered at about 743 K due to the loss of 1.5 H_2O molecules corresponding to the loss of all acidic protons and the beginning of decompositions of the Keggin structure. [230,231]. Generally, Keggin-type heteropoly compounds are the most stable among various polyoxometalates. The decomposition temperature (K) for the most typical Keggin HPAs, as estimated from TGA, decreases in the following series [230]:

$$\underset{738}{H_3\,[PW_{12}O_{40}]} < \underset{718}{H_3\,[SiW_{12}O_{40}]} < \underset{648}{H_3\,[PMo_{12}O_{40}]} < \underset{623}{H_3\,[SiMo_{12}O_{40}]}$$

1.6. OBJECTIVES AND SCOPE OF THE THESIS

It is evident from the literature survey that supported HPAs have opened new opportunities in the field of catalysis. The present study deals with the detailed and systematic study of the synthesis, characterization and catalytic applications of HPAs supported on ZrO_2 dispersed into mesoporous materials using wet-impregenation techniques. Considerable amount of literature is available on supported HPAs. However, the chemistry of HPAs supported on ZrO_2, its dispersion on mesoprous silica materials and their catalytic activity for various acid catalyzed reactions is less known. The interaction of the HPAs with supports and the reasons for the enhancement of the catalytic acitivity compared to the homogeneous counterpart is less discussed in the open literature. This motivated us to take up this investigation to find out the nature of interaction of HPAs with the support and what renders the HPA, the kind of stability, and enhanced catalytic activity. For this purpose we synthesized ZrO_2 supported HPAs (TPA and STA) and then finally dispersed it on mesoporous silica materials (MCM-41, MCM-48 and SBA-15) and used for various acid catalyzed reactions, with special emphasis on the synthesis of compounds used for the preparation of LABs, an opium-alkaloid antispasmodic, antioxidants, fine chemicals and perfumes. The large surface area, pore size and the stability of mesoporous materials attracted our attention hence, motivated us to disperse HPA/ZrO_2 on them inlui of synthesizing nano-composite material. To get more insight into the chemistry of the supported material we thoroughly characterized the material using different physico-chemical techniques. The type of interaction of HPA with the support and the reasons for its high thermal stability was established. These were tested for the Friedel-crafts alkylation [232-234], acetylation [235,236] and esterification [237]. Details such as optimization of reaction conditions so as to obtain higher TOF than their homogeneous analogues, kinetics and mechanistic studies were essential part of the present investigation.

1.7. OUTLINE OF THE THESIS

The thesis has been divided into seven chapters:

Chapter 1 gives a general introduction about HPAs, its structure, classification, and catalytic properties. It gives an introduction to supported-HPAs and the conventional supports used for the preparation of supported-HPAs. Further, this chapter gives an introduction to ZrO_2, its properties, and ZrO_2 based solid acids. It also gives an introduction to structure, classification, and application of mesoporous silica. Finally, the aim of the thesis is outlined briefly.

Chapter 2 describes the synthesis and techniques used for the characterization of ZrO_2-supported HPAs, mesoporous silica, and nano-sized composite material synthesized from mesoporous silica embedded oxide supported HPA.

Chapter 3 describes the characterization of ZrO_2 supported TPA and STA. The TPA/ZrO_2 catalysts were used in the liquid-phase benzoylation of DPO with BC. The effect of TPA loading, calcination temperature and reaction parameters on catalytic activity was studied and discussed. STA/ ZrO_2 catalyts were used for the detailed catalytic study of the liquid phase alkylation of benzene with α-olefin.

Chapter 4 describes the characterization of MCM-41 and MCM-48 supported TPA/ZrO_2 and its use in liquid-phase acetylation of veratrole with Ac_2O under flow conditions.

Chapter 5 describes the characterization results of TPA/ZrO_2 embedded inside SBA-15 and is used in the liquid-phase benzylation of phenol with BA and in liquid-phase acetylation of veratrole with Ac_2O.

Chapter 6 describes the characterization and catalytic activity of STA/ZrO_2 embedded inside SBA-15 for the liquid-phase esterification of IAA with AA.

Chapter 7 gives the summary and conclusions of the work carried out for this thesis.

1.8. REFERENCES

1. M. Misono, N. Nojiri, Appl. Catal.A: General, 64 (1990) 1.
2. J. N. Armor, Appl. Catal.A: General, 78 (1991) 141.
3. T. Okuhara, N. Mizuno, M. Misono, Adv. Catal., 41 (1996) 113.
4. M. Misono, In Proc. 10th Int. Congr. Catal., Budapest, 1992; Elsevier: Amsterdam, 1993; p 69.
5. M. Misono, Catal. Rev.-Sci. Eng., 29 (1987) 269.
6. N. Nojiri, M. Misono, Appl. Catal.A: General, 93 (1993) 103.
7. K. I. Matveev, Kinet. Katal., 18 (1977) 862.
8. Y. Ono, In Perspectives in Catalysis; J. M. Thomas, K. I. Zamaraev, Eds.; Blackwell: London, 1992; p 431.
9. I. V. Kozhevnikov, K. I. Matveev, Appl. Catal.A: General, 5 (1983) 135.
10. M. T. Pope, A. Müller, Angew. Chem. Int. Ed. Engl., 30 (1991) 34.
11. G. A.Tsigdinos, Top. Curr. Chem., 76 (1978) 1.
12. J. S. Anderson, Nature, 140 (1937) 850.
13. M. Misono, in Proceedings of 4th International Congress on Chemistry and Use of Molybdenum, Colorado, August, 1982.
14. G. Mestl, T. Ilkenhans , D. Spielbauer , M. Dieterle , O. Timpe , J. Kröhnert , F. Jentoft , H. Knözinger , R. Schlögl, Appl. Catal. A: General, 210 (2001) 13.
15. C. Rocchichioli-Deltcheff, R. Thouvenot, R. Franck, Spectrochimica Acta 32a, (1975) 587.
16. T. Ilkenhans, Ph.D. thesis, Johann Wolfgang Goethe- Universität, Frankfurt/M, 1996.
17. L. E. Briand, G. T. Baronetti, H. J.Thomas, Appl. Catal.A: General, 2003.
18. X. Shen-Xiu, Y. Sheng-Yong , C. Tian-Lang, International journal of quantum chemistry, 70(2),(1998),375.
19. A. Rosen, D. E. Ellis, Chem. Phys., 65 (1976) 3629.
20. P. Souchay, Polyanions et Polycations; Gauthier-Villars: Paris, 1963.
21. H. T. Evans, Jr. J. Am. Chem. Soc., 70 (1948) 1291.
22. G. M. Brown, M.-R. Noe-Spirlet, W.R.Bushing, H. A. Levy, Acta Cryst., B33 (1977) 1038.

23. Gmelin Handbuch der Anorganischen Chemie; Verlag Chemie: Berlin, 1933; System number 54 (Tungsten).
24. E. O. North, Inorganic Synthesis; H. S. Booth, Ed.; McGraw Hill: New York, 1939; Vol. 1, pp 127 and 129.
25. G. A.Tsigdinos, Ind. Eng. Chem. Prod. Res. Dev., 13 (1974) 267.
26. G.A.Tsigdinos, in "Heteropoly Compounds, Methodicum Chimicum" (K. Niedenzu and H. Zimmer, Eds.), Vol.8, Chap. 32. Academic Press, New York, 1976.
27. C. Rocchiccioli-Deltcheff, Inorg. Chem., 22 (1983) 207.
28. V. F.Chuvaev, K. I. Popov, V. I. Spitsyn, Dokl. Akad. Nauk SSSR, 255(1980) 892.
29. I. V. Kozhevnikov, A. Sinnema, R. J. J. Jansen, H.van Bekkum, Catal. Lett. , 27 (1994) 187.
30. D. H. J.Brown, Chem. Soc., (1962) 3189.
31. N. A. Polotebnova, A. A. Kozlenko, L. A. Furtune, Russ. Inorg. J. Chem., 21 (1976) 1511.
32. Y. Izumi, K. Matsuo, K. Urabe, J. Mol. Catal.A: Chem., 18 (1983) 299.
33. S. M. Kulikov, I. V. Kozhevnikov, Izv. Akad. Nauk SSSR, Ser. Khim., (1981) 498.
34. I. V. Kozhevnikov, K. I. Matveev, Usp. Khim., 51 (1982) 1985.
35. M. Furuta, K. Sakata, M. Misono, Y. Yoneda, Chem. Lett., 31(1979) 125.
36. A. Aoshima, S. Tonomura, S. Yamamatsu, Polymers for Adv. Technol., 2 (1990)127.
37. T. Okuhara, M. Misono, Dynamic Processes on Solid Surfaces; Tamarn, K., et al., Ed.; Plenum Press: New York, 1993; p 259.
38. X. L. C. Feng, F. Lefebvre, Catal. Lett., 22 (1993) 387.
39. A. Auroux, J. C.Vedrine, Stud. Surf. Sci. Catal., 20 (1985) 311.
40. M. A. Schwegler, H.van Bekkum, N. A. de Munck, Appl. Catal.A: General, 74 (1991) 191.
41. Y. Izumi, K. Urabe, Chem. Lett.,(1981) 663.
42. T. Baba, Y. Ono, Appl. Catal. A: General, 22 (1986) 321.
43. S. Kasztelan, E. Payen, J. B. Moffat, J. Catal., 125 (1990) 45.
44. F. Lefebvre, P. Dupont, A. Auroux, React. Kinet. Catal. Lett., 55 (1995) 3.

45. I. V. Kozhenikov, Chem. Rev., 98 (1998) 171.
46. T. Masuda, A. Igarashi, Y. Ogino, J. Jpn. Petrol. Inst., 23 (1980) 30.
47. S. M. Kulikov, M. N. Timofeeva, I. V. Kozhevnikov, V. I. Zaikovskii, L. M. Plyasova, I. A. Ovsyannikova, Izv. Akad. Nauk SSSR, Ser. Khim, (1989) 763.
48. L. R. Pizzio, C. V. Caceres, M. N. Blanco, J. Colloid Interface Sci, 190 (1997) 318.
49. P. G. Vazquez, M. N. Blanco, C. V. Caceres, Catal. Lett., 60 (1999) 205.
50. J. C. Edwards, C. Y. Thiel, B. Benac, J. F. Knifton, Catal. Lett., 51 (1998) 77.
51. E. Lopez-Salinas, J. G. Hernandez-Cortez, M. A. Cortes-Jacome, J. Navarrete, M. A. Llanos, A. Vazquez, H. Armendariz, T. Lopez, Appl. Catal. A: General, 175 (1998) 43.
52. E. Lopez-Salinas, J. G. Hernandez-Cortez, I. Schifter, E. Torres-Garcia, J. Navarrete, A. Gutierrez-Carrillo, T. Lopez, P. P. Lottici, D. Bersani, Appl. Catal. A: General, 193 (2000) 215.
53. I. V. Kozhevnikov, A. Sinnema, R. J. J. Jansen, K. Pamin, H.van Bekkum, Catal. Lett. , 30 (1995) 241.
54. C. T. Kresge, D. O. Marler, G. S. Rav, B.H.Rose, U.S.Patent 5,366,945, 1994.
55. K. Pamin, A. Kubacka, Z. Olejniczak, J. Haber, B. Sulikowski, Appl. Catal. A: General, 194-195 (2000) 137.
56. A. Molnar, C. Keresszegi, B. Torok, Appl. Catal. A: General, 189 (1999) 217.
57. J. B. Moffat, 'Metal-Oxygen Clusters. The surface and Catalytic properties of Heteropoly Oxometalates', Kluwer: New York, 2001.
58. Y. Izumi, K. Matsuo, K.Urabe, J. Mol. Catal., 84 (1983) 299.
59. I. V. Kozhevnikov, Catal. Rev. Sci. Eng., 37 (1995) 311.
60. K. Y. Lee, T. Arai, S. Nakata, S. Asaoka, T. Okuhara, M. Misono, J. Am. Chem. Soc., 114 (1992) 2836.
61. T. Okuhara, T. Nishimura, H. Watanabe, K. Na, M. Misono, in "Acid-Base Catalysis II.", Kodansha, Tokyo-Elsevier, Amsterdam (1994) 419.
62. Y. Izumi, M. Ogawa, W. Nohara, K. Urabe, Chem. Lett., (1992) 1201.
63. T. Okuhara, T. Nishimura, H. Watanabe, M. Misono, J. Mol. Catal. A: Chem., 74 (1992) 247.
64. M. Misono, T. Okuhara, Chemtech. (1993), November 23.

65. T. Okuhara, T. Nishimura, K. Ohashi, M. Misono, Chem. Lett., (1990) 1201.
66. A. Gutierrez, S. L. Soled, J. A. Paes, U.S. Patent 5,334,775, 1994.
67. I. V. Kozhevnikov, A. Sinnema, R. J. J. Jansen, K. Pamin, H.van Bekkum, Catal.Lett., 30 (1995) 241.
68. T. Okuhara, T. Nishimura, K. Ohashi, M. Misono, Chem. Lett., (1990) 1201.
69. G. J. Meuzelaar, L. Maat, R. A. Sheldon, I. V. Kozhevnikov, Catal. Lett., 45 (1997) 249.
70. J. N. Barrows, M. T. Pope, Adv. Chem. Ser., 226 (1990) 403.
71. M. Misono, K. Sakata, Y. Yoneda, W.Y. Lee, in " Proc. 7th Int. Congr. (40 Catal., Tokyo, 1980,"p.1047. Kodansha, Tokyo, Elsevier, Amsterdam, 1981.
72. N. Mizuno, T. Watanabe, M. Misono, J. Phys. Chem., 94 (1990) 890.
73. P. J. Moles, J. Aadhesion Sci. Technol., 6 (1992) 61.
74. F. Farnworth, S. L. Jones, I. McAlppine, Speciality Inorganic Chemicals, Special Publication No.40, Royal Society of Chemistry, London (1980).
75. D. K. Smith, H. W. Newkirk, Acta Crystallogr., 18 (1965) 983.
76. R. C. Garvie, J. Phys. Chem., 82 (1978) 218.
77. K. S. Ray, S. Kahn, Indian J. Chem., 13 (1975) 577.
78. A. E. Regazzoni, M. A. Blesa, A. G. J. Maroto, J. Colloid Interface Sci., 91 (1983) 560.
79. J. B. Frank, J. K. Stephen, I. M. Bell, R. J. H. Clark, C. B. Ponton, Journal of Solid State Chemistry, 145 (1999) 394.
80. J. A. Knowles, M. J. Hudson, Chem. Commun., (1995) 2083.
81. A. Kim, P. Bruinsma, Y. Chem, L. Q. Wang, J. Liu, Chem. Commun., (1997) 161.
82. G. Pacheco, E. Zhao, A. Garcia, A. Sklyarov, J. J. Fripiat, Chem. Commun., (1997) 491.
83. P. Yang, E. Zhao, D. I. Margolese, B. F. Chmelka, G. D. Stucky, Chem. Mater., 11 (1999) 2813.
84. G. L. Clark, D. H. Reynolds, Ind. Eng. Chem., 29 (1937) 711.
85. M. J. Hunter, Proceedings of DGMK-Conference "Chances for Innovative Processes at the Interface between Refining and Petrochemistry", Berlin, October (2002) 9.

86. F. Schmidt, Appl. Catal. A: General, 221 (2001) 15.
87. K. Arata, M. Hino, Mater. Chem. Phys., 26 (1990) 213.
88. G. D. Yadav, A. A. Pujari, Green Chemistry, 1 (1999) 69.
89. G. D. Yadav, M. S. Krishnan, O.P.R.D., 2 (1998) 86.
90. G. D.Yadav, N. Kirthivasan, J. Chem. Soc., Chem. Commun., (1995) 203.
91. T. Yamaguchi, K. Tanabe, Y. Kung, Mater. Chem. Phys., 16 (1986) 67.
92. K. Schumacher, M. Grün, K. K. Unger, Micropor. Mesopor. Mater., 27 (1999) 201.
93. M. Hino, K. Arata, Bull. Chem. Soc. Jpn., 67 (1994) 1472.
94. J. G. Santiesteban, J. C. Vartuli, S. Han, R. D. Bastian, C. D. Chang, J. Catal., 168 (1997) 431.
95. D. G. Barton, S. L. Soled, G. D. Meitzner, G. A. Fuentes, E. Iglesia, J. Catal., 181(1999) 57.
96. S. Kuba, P. Lukinskas, R. Ahmad, F.C. Jentoft, R.K. Grasselli, B.C. Gates, H. Knözinger, J. Catal., in press.
97. E. López-Salinas, J. G. Hernández-Cortéz, I. Schifter, E. Torres-García, J. Navarrete, A. Gutiérrez-Carrillo, T. López, P. P. Lottici, D. Bersani, Appl. Catal. A: General, 193 (2000) 215.
98. K. Saito, M. Nomura, S. Ohgoshi, Y. Akai, Prep. Symp. Am. Chem. Soc. Div. Petrol. Chem., 42 (1997) 712.
99. E. López-Salinas, J. G. Hernández-Córtez, M. Cortéz, J. Navarrete, M. Yanos, A. Vázquez, H. Armendaris, T. López, Appl. Catal. A: General, 175 (1998) 43.
100. Y. Izumi, K. Urabe, Chem. Lett., (1981) 663.
101. F. Lefebvre, J. Chem. Soc., Chem. Commun., (1992) 75.
102. A. G. Steghuis, J. G.van Ommen, J. A. Lercher, Catal. Toay, 46 (1998) 91.
103. D. Sutton, B. Kelleher, J. R. H. Ross, Biomass Bioenergy, 23 (2002) 209.
104. T. Yamaguchi, Catal.Today, 20 (1994) 199.
105. S. P. S. Badwal, Appl. Phys. A, 50 (1990) 449.
106. R. C. Garvie, R. H. Hannink, R. T. Pascoe, Nature, 258 (1975) 703.
107. J. F. Haw, J. Zhang, K. Shimizu, T. N.Venkatraman, D.-P. Luigi, W. Song, D. H. Barich, J. B. Nicholas, J. Am. Chem. Soc.,122 (2000)12561.
108. J. M. Phillips, J. Appl. Phys.,79 (1996)1829.

109. C. León, M. L. Lucía, Santamaría, J. Phys. Rev. B, 55 (1997) 882.
110. N. Mansour, K. Mansour, E. W. V. Stryland, M. J. Soileau, J. Appl. Phys., 67 (1990) 1475.
111. G. D. Wilk, R. M. Wallace, J. M. Anthony, J. Appl. Phys., 89 (2001) 5243.
112. V. V. Afanas'ev, M. Houssa, A. Stesmans, M. M. Heyns, Appl. Phys. Lett., 78, (2001) 3073.
113. L. Bruce, Appl. Catal. A: General, 4 (1982) 353.
114. J. G.van Ommen, Methane Conversion Ed. D. M.Bibby, Elsevier (1988) 213.
115. M. Shibagaki, Bull. Chem.Soc. Japan, 62 (1989) 1333.
116. B.-Q. Yu, Appl. Catal. A: General, 64 (1990) 41.
117. C. J. Wen, J. Appl. Electro. Chem., 8 (1978) 81.
118. Y. Murakami, G. Poncelet 'Prep Of Catal III Ed.', Elsevier 1983.
119. A. Andersoen, Angew Chemie Int. Ed. Engl., 15 (1976) 630.
120. K. C. Pratt, J. Catal., 124 (1990) 4216.
121. K. S. W. Sing, D. H. Everett, R. H. W. Haul, L. Moscou, R. A. Pierotti, J. Rouquerol, T. Siemienieiewska, Pure Appl. Chem., 57 (1985) 603.
122. R. K. Iler, "The Chemistry of silica", J. Wiley and Sons Inc., 1979.
123. K. Wefers, C. Misra, "Oxides and Hydroxides of Alumina"; Alcoa Technical Paper No. 19, Revised, Alcoa Laboratories, 1987.
124. C. T. Kresge, M. E. Leonowicz, W. J. Roth, J. C. Vartuli, J. S. Beck., Nature, 359 (1992) 710.
125. J. S. Beck, J. C. Vartuli, W. J. Roth, M. E. Leonowicz, C. T. Kresge, K. D. Schmitt, C. T.-W. Chu, D. H. Olson, E. W. Sheppard, S. B. Higgins, J. L. Schlenker. J. Am. Chem. Soc., 114 (1992) 10834.
126. Q. Huo, S. I. Margoleses, U. Ciesla, D. G. Demuth, P. Feng, D. E. Gier, P. Sieger, B. F. Chmelka, F. Schüth, G. D. Stucky. Chem. Mater., 6, 1176 (1994).
127. C. T. Kresge, M. E. Leonowicz, W. J. Roth, J. C. Vartuli, U.S. Patent, 5,098,684 (1992).
128. P. T. Tanev, T. J. Pinnavaia, Science, 267 (1995) 865.
129. J. S. Beck, C. T. Chu, I. D. Johnson, C. T. Kresge, M. E. Leonowicz, W. J. Roth, J. C. Vartuli, U.S.Patent, 5,108,725 (1992).

130. A. Monnier, F. Schüth, Q. Huo, D. Kumar, D. Margolese, R. S. Maxwell, G. D. Stucky, M. Krishnamurty, P. Petroff, A. Firouzi, M. Janicke, B. F. Chmelka, Science, 261 (1993) 1299.
131. Q. Huo, D. I. Margolese, G. D. Stucky, Chem. Mater., 8 (1996) 1147.
132. Z. Luan, H. He, W. Zhou, C-F. Cheng, J. Klinowski, J. Chem. Soc., Faraday Trans., 91 (1995) 2955.
133. M. V. Landau, S. P. Varkey, M. Herkowitz, O. Regev, S. Pevzner, T. Sen, Z. Luz, Micropor. Mesopor. Mater., 33 (1999) 149.
134. C. N. Perez, E. Moreno, C. A. Henriques, S. Valange, Z. Gabelica, J. L. F. Montero, Micropor. Mesopor. Mater., 41 (2000) 137.
135. K. Schumacher, P. I. Ravikovitch, A. D. Chesne, A. V. Neimark, K. K. Unger, Langmuir, 16 (2000) 4648 .
136. A. H. Schoen, NASA Technical Note D-5541; NASA: Washington, DC, 1970.
137. R. Schmidt, M. Stöcker, D. Akporiaye, E. H. Torstad, A. Olsen, Micropor. Mater., 5 (1995) 1.
138. V. Alfredsson, M.W. Anderson, Chem. Mater., 8 (1996) 1141.
139. A. H. Schoen, Infinite Periodic Minimal Surfaces without Intersections; NASA Technical Note TD-5541, 1970.
140. D. Zhao, J. Feng, Q. Huo, N. Melosh, G. H. Fredrickson, B. F. Chmelka, G. D. Stucky. Science, 279 (1998) 548.
141. H. J. Shin, C. H. Ko, R. Ryoo, J. Mater. Chem., 11 (2001) 260.
142. S. A. Bagshaw, E. Prouzet, T. J. Pinnavaia, Science, 269 (1995) 1242.
143. R. Ryoo, C. H. Ko, M. Kruk, V. Antochshuk, M. Jaroniec, J. Phys. Chem. B, 104 (2000) 11465.
144. S. Jun, S. H. Joo, R. Ryoo, M. Kruk, M. Jaroniec, Z. Liu, T. Ohsuna, O. Terasaki, J. Am. Chem. Soc., 122 (2000) 10712.
145. Y. S. Cho, J. C. Park, B. Lee, Y. Kim, J. Yi, Catal. Lett., 81 (2002) 89.
146. Z. Zhang, S. Dai, D.A. Blom, J. Shen, Chem. Mater., 14 (2002) 965.
147. J. M. Kim, G. D. Stucky, Chem. Commun., (2000) 1159.
148. M. Antonietti, C. Göltner, Angew. Chem. Int. Ed. Engl., 36 (1997) 910.

149. Q. Huo, S. I. Margoleses, U. Ciesla, P. Feng, D. E. Gier, P. Sieger, B. F. R. Leon, P. M. Petroff, F. Schüth, G. D. Stucky, Nature, 368 (1994) 317.
150. C. Sanchez, F. Ribot, New J. Chem., 18 (1994) 1007.
151. C.-Y. Chen, S. L. Burkett, H.-X. Li, M. E. Davis, Micropor. Mater.,2 (1993) 27.
152. A. Steel, S. W. Carr, M. W.Anderson, J. Chem. Soc. Chem. Commun., (1994) 1571.
153. G. D. Stucky, Q. Huo, A. Firouzi, B. F. Chemlka, S. Schacht, I. G. Voigt-Martin, F. Schüth, Stud. Surf. Sci. Catal., 105A (1997) 3.
154. A. Firouzi, D. Kumar, L. M. Bull, T. Besier, P. Sieger, Q. Huo, S. A. Walker, J. A. Zasadzinski, C. Glinka, J. Nicol, D. Margolesse, G. D. Stucky, B. F.Chmelka, Science, 267 (1995) 1138.
155. D. Zhao, D. Goldfarb, J. Chem. Soc., Chem. Commun., 8 (1995) 875.
156. W. Stöber, A. Fink, E. Bohn, J. Coll. Interf. Sci., 26 (1968) 62.
157. R. Ryoo, J. M. Kim, In Proceedings of the 12th International Zeolite Conference, Baltimore, MD, July 5-10, 1998.
158. M. M. J. Treacy, B. K. Marcus, M. E. Bisher, J. B. Higgins, Eds.; Materials Research Society: Warrendale, Pennsylvania, 1999; Vol. I, p. 689.
159. S. S. Kim, A. Karkamkar, T. J. Pinnavaia, M. Kruk, M. Jaroniec, J. Phys. Chem. B, 105 (2001) 7663.
160. M. E. Davis, Chem. Ind. 4, 137 (1992).
161. A. Corma, A. Martinez, V. Martinez-Soria, J. B. Monton, J. Catal., 153 (1995) 25.
162. U. Junges, W. Jacobs, I. Voigt-Martin, B. Krutzsch, F. Schüth, J. Chem. Soc. Chem. Commun., (1995) 2283.
163. T. Yanagisawa, T. Shimizu, K. Kuroda, C. Kato, Bull. Chem. Soc. Jpn., 63 (1990) 988.
164. D. Brunel, Micropor. Mesopor. Mater., 27 (1999) 329.
165. M. J. Verhoef, P. J. Kooyman, J. A. Peters, H.van Bekkum, Micropor. Mesopor. Mater., 27 (1999) 365.
166. W. van Rhijn, D. De Vos, W. Bossaert, J. Bullen, B. Wouters, P. Grobet, P. A. Jacobs, Stud. Surf. Sci.Catal., 17 (1998) 183.

167. I. V. Kozhevnikov, A. Sinnema, R. J. J. Jansen, K. Parmin, H. van Bekkum, Catal. Lett., 30 (1995) 241.
168. C. T. Kresge, D. O. Marler, J. S. Rav, B. H. Rose, U.S. Patent 5,366,945, 1994.
169. P. Van Der Voort, M. Mathieu, E. F. Vansant, S. N. R. Rao, M.G. White, J. Porous Mater., 5 (1998) 305.
170. J. Carrazza, F. Gonzalez, R. Adrian, D. Djaouadi, J.G. Moore, D.Y. Shahriari, C.C. Landry, J. Lujano, In Proceedings of 12th International Zeolite Conference; Baltimore, 1998.
171. S. Zhang, Y. Fujii, H. Yamashita, K. Koyano, T. Tatsumi, M. Anpo, Chem. Lett., 7 (1997) 659.
172. K. Schumacher, Diploma thesis, Universität Mainz, 1997.
173. U. Junges, W. Jacobs, I. Voigt-Martin, B. Krutzsch, F. Schüth, J. Chem. Soc. Chem. Commun., (1995) 2283.
174. C. A. Koh, R. Nooney, S. Tahir, Catal. Lett.,47 (1997) 199.
175. B. Marler, U. Oberhagemann, S. Vortmann, H. Gies, Micropor. Mater., 6 (1996) 375.
176. W. Hammond, E. Prouzet, S. D. Mahanti, T. J. Pinnavaia, Micropor. Mesopor. Mater., 27 (1999) 19.
177. W. Stichert, F. Schüth, Chem. Mater., 10 (1998) 2020.
178. A. M. Liu, K. Hidajat, S. Kawi, D. Y. Zhao, Chem. Commun., (2000) 1145.
179. T. Kang, Y. Park, Yi, J. Ind. Eng. Chem. Res., 43 (2004) 1478.
180. M. Vallet-Regi, A. Ra´mila, R. P. del Real, J. Pe´rez-Pariente, J. Chem. Mater., 13 (2001) 308.
181. B. Muñoz, A. Ra´mila, J. Pe´rez-Pariente, I. Dı´za, M. Vallet-Regi, Chem. Mater., 15 (2003) 500.
182. J. Lei, J. Fan, C. Z.Yu, L. Y. Zhang, S. Y. Jiang, B. Tu, D. Y. Zhao, Micropor. Mesopor. Mater., 73 (2004) 121.
183. J. Deere, E. Magner, J. G. Wall, B. K. Hodnett, Catal. Lett., 85 (2003) 19.
184. A. Vinu, V. Murugesan, M. Hartmann, J. Phys. Chem. B, 108 (2004) 7323.
185. R. J. P. Corriu, A. Mehdi, C. Reye, C. Thieuleux, Chem.Commun., (2002) 1382.

186. A. L. Doadrio, E. M. B. Sousa, J. C. Doadrio, J. Pe´rez-Pariente, I. Izquierdo-Barba, M. J. Vallet-Regi, Controlled Release, 97 (2004) 125.
187. G. Cavallaro, P. Pierro, F. S. Palumbo, F. Testa, L. Pasqua, R. Aiello, Drug Delivery, 11 (2004) 41.
188. J. He, X. Duan, C. Li, Materials Chem. and Phys., 71 (2001) 221.
189. L. R. Pizzio, P. G. Vázquez, C. V. Cáceres, M. N. Blanco, Appl. Catal. A: General 256 (2003) 125.
190. G. Hovarth, K. J. Kawazoe, J. Chem. Eng. Jpn., 16 (1983) 470.
191. G. Binnig, H. Rohrer, Ch. Gerber, E. Weibel, Phys. Rev. Lett.,49 (1982) 57.
192. K. Schumacher, M. Grün, K. K. Unger, Micropor. Mesopor. Mater., 27 (1999) 201.
193. A. Chenite, Y. L. Page, Sayari, Chem. Mater., 7(1995) 1015.
194. J. F. Keana, M. D. Ogan, Y. Lu, M. Beer, J. Varkey, J. Am. Chem. Soc., 108 (1986) 7957.
195. C. F. Cheng, H. He, W. Zhou, J. Klinowski, Chem. Phys. Lett., 244 (1995) 117.
196. J. S. Beck, J. C. Vartuli, G. J. Kennedy, W. J. Roth, S. E. Schramm, Chem. Mater., 6 (1994) 1816.
197. V. Alfredsson, M. Keung, A. Monnier, G. D. Stucky, K. K. Unger, F. Schüth, J. Chem. Soc., Chem. Commun., (1994) 921.
198. C. T. Kresge, M. E. Leonowicz, W. J. Roth, J. C. Vartuli, J. S. Beck, ibid., 359 (1992) 710.
199. Y. Izumi, R. Hasebe, K. J. Urabe, Catal., 84 (1983) 402.
200. P. Jun, Q. Lun-Yu, Ya-guang, Ch. Inorg. Chim. Acta, 183 (1991) 157.
201. M. Misono, Kagaku no Ryoiki, 35 (1981) 519.
202. V. A. Maroni, K. A. Martin, S. A. Johnson, ACS Sym. Ser., 368 (1988) 85.
203. P. A. Topsoe, R. Pederson, E. G. Derouance, J. Catal., 70 (1984) 369.
204. P. A. Jacobs, W.Y. Martier, Zeolites, 2 (1982) 226.
205. T. J. R.Weakley, Structure and Bonding , 18 (1974) 131.
206. G. M. Varga, E. Papaconstantiou, M. T. Pope, Inorg. Chem., 9 (1970) 667.
207. S. L. Alternau, M. T. Pope, R. A. Prados, H. So, Inorg. Chem., 2 (1975) 417.
208. X. Chen, L. Huang, Q. Li, J. Phys. Chem. B., 101 (1997) 8460.
209. A. Steel, S. W. Carr, M. W.Anderson, Chem. Mater., 7 (1995) 1829.

210. M. Misono, T. Okuhara, CHEMTECH, 23 (1993) 23.
211. J. Bank, Z. Schwenk, Phys. B, (1976) 75.
212. M. T. Pope, S. E. O'Donnell, R. A. Prados, J. Chem. Soc., Chem. Commun., (1975) 22.
213. Y. Jeannin, G. Herve, A. Proust, Inorg.Chim. Acta, 189 (1992) 319.
214. G. Chidichimo, A. Golemme, D. Imbardelli, E. Santoro, J. Phys. Chem., 94 (1990) 6826.
215. S. Uchida, K. Inumaru, M. Misono, J. Phy. Chem. B, 104 (2000) 8108.
216. Y. Kanada, Y. Lee, S. Nakata, S. Asaoka, M. Misono, Chem. Lett., (1988) 139.
217. T. Okuhara, T. Nishimura, H. Watanabe, K. Na, M. Misono, in “Acid-Base Catalysis II,” p.419. Kodansha, Tokyo-Elsevier, Amsterdam, 1994.
218. Q. Huo, R. Leon, P. M. Petroff, G. D. Stucky, Science, 268 (1995) 1324.
219. L. Jonsson, Acta Chem. Scand., B 37 (1983) 761.
220. M. S. Giprazak, G. E. Leroi, S. R. Crouch, Appl. Spectros.,36 (1982) 285.
221. T. Fukumoto, K. Murata, S. Ikeda, Anal. Chem., 56(1984) 929.
222. Y. Zuolong, L. Shufang, H. Furong, W. Shunli, Z. Guilin, Z. Suxian., Kexue Tongbao,32 (1987)1540.
223. M. Akimoto, K. Shima, E. Echigoya, J. Chem. Soc., Faraday Trans., 179, (1983) 2467.
224. M. Akimoto, K. Shima, H. Ikeda, E. Echigoya, J. Catal., 86 (1984) 173.
225. A. Aboukaïs, D. Ghoussoub, E. B.-Crusson, M. Rigole, M. Guelton, Appl. Catal. A: General, 111 (1994) 109.
226. R. Mokaya, W. Jones, J. Mater. Chem., 9 (1999) 555.
227. R. Mokaya, J. Catal., 186 (1999) 470.
228. A. Sayari, K. M. Reddy, I. Moudrakovski, Stud. Surf. Sci. Catal., 98 (1995) 19.
229. V. F. Chuvaev, K. I. Popov, V. I. Spitsyn, Dokl. Akad. Nauk. SSSR, 255 (1980) 892.
230. C. Hu, M. Hashimoto, T. Okuhara, M. Misono, J. Catal., 143 (1993) 437.
231. G. M. Maksimov, Russ. Chem. Rev., 64 (1995) 445.
232. D. P. Sawant, B. M. Devassy, S.B. Halligudi, J. Mol. Catal. A: Chem., 217 (2004) 211.

233. D. P. Sawant, S. B. Halligudi, J. Mol. Catal. A: Chem., 237 (2005) 137.
234. D. P. Sawant, A. Vinu, Nalini E. Jacob, F. Lefebvre, S. B. Halligudi, J. Catal., 235 (2005) 341.
235. D. P. Sawant, Vinu A., F. Lefebvre, S. B. Halligudi, J. Mol. Catal. A: Chem. (special edition), (accepted).
236. D. P. Sawant, M. Hartmann, S. B. Halligudi, Micropor. Mesopor. Mater., 2006 (communicated).
237. D. P. Sawant, M. Hartmann, S. P. Mirajkar, F. Lefebvre, S. B. Halligudi , J. Catal., 2006 (communicated).

CHAPTER – 2

SYNTHESIS AND CHARACTERIZATION

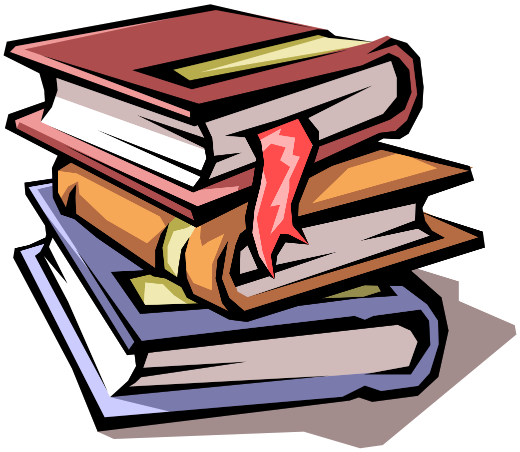

2. SYNTHESIS AND CHARACTERIZATION TECHNIQUES

2.1. INTRODUCTION

There is no doubt that catalysis is very rewarding research field. The fact that in solid acid catalysts, it is possible to modify the acid properties of the material in a predetermined direction through synthesis and post-synthesis treatment and furthermore it is possible to "confirm" those modifications by available characterization techniques. This chapter deals with the synthesis of supported HPAs catalysts by wet-impregenation method and different techniques used for its characterization.

2.2. CHEMICALS AND REAGENTS

The chemicals utilized for the entire research work is listed below with their purity in parenthesis.

Cetyltrimethylammonium bromide (CTABr) (>99 %), tetraethyl orthosilicate (TEOS) (>99 %), triblock copolymer of ethylene oxide (EO) and propylene oxide (PO), $EO_{20}PO_{70}EO_{20}$ (Pluronic P123) ($M_{\text{avg}} = 5800$), sodium silicate (>99 %), veratrole (>99 %), phenol (>99 %), benzyl alcohol (BA) (>99 %), anisole (~99.7 %), thioanisole (>99 %), veratrole (>99 %), 2-methoxynaphthalene (>99 %), isobutyl benzene (>99 %), isoamyl alcohol (≥ 99 %) and acetic acid (AA) (>99 %) were received from Aldrich. Liquor ammonia (25 %), acetic anhydride (>99 %) and benzoyl chloride (>99%) were received from s.d. Fine Chem. Ltd., Mumbai. DPO (>99%) was obtained from Loba Chemie Ltd., Mumbai. Methanol (99.9 %), benzene (>99 %) and 1-dodecene (>99 %) were purchased from E-Merck India Ltd., Mumbai. K-10 montmorillonite purchased from Fluka. Zirconium oxychloride $ZrOCl_2.8H_2O$ (>99.5%), TPA (>99 %) and STA (> 99 %) were received from Merck. Zeolites H-beta, H-ZSM-5 and H-Y recovered by calcining NH_4-Y were obtained from Catalysis Pilot Plant (CPP-NCL, Pune). H-Mordenite was obtained from PQ Zeolites BV, Netherlands. All the chemicals were used without purification.

2.3. CATALYST SYNTHESIS

2.3.1. ZrO_2 supported HPA

The ZrO_2 supported HPA catalyst was prepared by wet impregenation of a methanolic solution of HPA (TPA, STA etc.) over zirconium oxyhydroxide. Zirconium oxyhydroxide was obtained by the hydrolysis of aqueous 0.5 M zirconium oxychloride solution with the drop wise addition of aqueous ammonia (10 M) to a final pH of 10. The precipitate is filtered and washed with ammoniacal water (pH=8) till free from chloride ions and tested by silver nitrate test. Zirconium oxyhydroxide thus obtained was dried at 393 K for 12 h, powdered well and dried again for another 12 h. Each time, 4 ml of methanol per gram of solid support was used and the mixture was stirred in a rotary evaporator for 8-10 h. After stirring, the excess of methanol was removed by evaporation at 323 K on a rota-evaporator under vacuum. The resulting solid materials were dried at 393 K for 24 h and ground well.

A series of catalysts were prepared by suspending a known amount of dried ZrO_2 in a methanolic solution of HPA (4 ml methanol for 1 g of dried ZrO_2). This mixture was stirred in a rotary evaporator for 8–10 h followed by evaporation to dryness. The resulting samples were dried at 393 K for 24 h, powdered. All samples were calcined in shallow quartz tube placed in a tubular furnace 1023 K in air for 4 h. The samples were heated at the rate of 5 °C min^{-1} to the specified temperature and held for 4 h under static conditions, and then cooled at the rate of 5 °C min^{-1} to room temperature. A series of catalysts with different HPA loadings were prepared by changing the HPA concentration in methanol and calcined at 1123 K. The 15 wt.%HPA/ZrO_2 was prepared and calcined at different calcination temperature.

2.3.2. Silica supported HPA

HPA supported on silica was prepared from an aqueous solution of HPA and SiO_2 by incipient wetness impregenation as per given in literature [1]. The aqueous solution of HPA at a concentration of 15 wt.% of support was added drop-wise to SiO_2 at room temperature while stirring vigorously. The wet sample was then dried at 373 K in an oven. After impregenation, the sample was dried in an oven at 373 K overnight and then calcined at 573 K in air for 5 h. The silica gel support was prepared by the hydrolysis of TEOS in presence of HNO_3 followed by drying at 393 K for 12 h, powdering and further drying for another 12 h.

2.3.3. Mesoporous silica

2.3.3.1. MCM-41

The pure siliceous MCM-41 material was prepared as described in the literature [2]. The gel composition used for preparing Si-MCM-41 material was 10 SiO_2: 5.4 $C_nH_{2n+1}(CH_3)_3NBr$: 4.25 Na_2O: 1.3 H_2SO_4: 480 H_2O. C_{16}-MCM-41 is prepared using CTABr (32.0 g) and 115 g of water and this mixture was stirred for 30 min at room temperature. Sodium silicate solution (37.4 g) was added drop wise to the surfactant solution under vigorous stirring for another 30 min. Then 2.4 g of H_2SO_4 in 10 g of water was added to the above mixture and the stirring was continued for another 30 min. The resulting gel was transferred into a polypropylene bottle and kept in an oven at 373 K for 24 h. After cooling to room temperature, the resultant solid was recovered by filtration, washed with distilled water and dried in an oven at 373 K for 6 h. Finally the material was calcined in a muffle furnace at 813 K for 10 h to give MCM-41.

2.3.3.2. MCM-48:

MCM-48 was synthesized by the conventional hydrothermal pathway by following the procedure described in literature [3,4]. The molar composition of the gel was 1 TEOS: 0.25 Na_2O: 0.65 $C_{16}H_{33}(CH_3)_3NBr$: 0.62 H_2O. CTABr (31.2 g) was dissolved in (93.6 g) deionized water at 318 K and stirred for 40 min. Then TEOS (30 g) followed by sodium hydroxide (69 g, 1 M) solution were added to the above mixture and the stirring was continued for another 1 h at room temperature. The resulting gel was transferred into a polypropylene bottle and kept in an oven at 373 K for 72 h under static condition. After cooling to room temperature, the solid was recovered by filtration, washed with ethanol followed by distilled water and dried in an air oven at 373 K for 6 h. Finally, the material was calcined in a muffle furnace at 813 K for 10 h to give MCM-48.

2.3.3.3. SBA-15

SBA-15 was synthesised with a gel composition of 4 g Polymer: 0.041 TEOS: 0.24 HCl: 6.67 H_2O as per literature procedure [5,6]. A typical synthesis consisting of amphiphilic triblock copolymer (EO_{20}-PO_{70}-EO_{20}) (4 g) was dispersed in 30 g of water and stirred for 4 h. Then, 120 g of 2 M HCl solution was added and stirred for 2 h. To this homogeneous solution, 8.54 g of TEOS was added under stirring. The resulting gel was aged at 313 K for 24 h and finally heated to 373 K for 48 h. After synthesis, the solid was filtered, washed with distilled water and dried in an air oven at 373 K for 5 h followed by calcination at 813 K to remove the triblock- copolymer.

2.3.3.4. Mesoporous silica embedded ZrO_2 supported HPA

Mesoporous silica supports (MS i.e. MCM-41, MCM-48 and SBA-15 etc.) embedded ZrO_2 supported HPA i.e. HPA/ZrO_2/MS composite materials were prepared by impregenating pure siliceous MS with an aqueous solution of $ZrOCl_2.8H_2O$ with a predetermined ZrO_2: MS weight ratio and the same amount of ZrO_2 loading was used over MS, which corresponded to monolayer coverage [7]. The resulting mixture was stirred in a rotary evaporator for 2-3 h followed by evaporation to dryness and dried at 373 K for 12 h and powdered well for further use. A series of catalysts with different HPA loadings were prepared by suspending a known amount of an aqueous solution of HPA (10-12 ml distilled water) per g of dried ZrO_2/MS support. This mixture was stirred in a rotary evaporator for 2-3 h followed by evaporation to dryness and the samples were dried at 373 K for 12 h, powdered and calcined at 1123 K in air for 4 h.

A series of catalysts with different (%) HPA were synthesized and calcined at 1123 K. The 15 wt.%HPA/22.4 wt.%ZrO_2/MS catalyst was calcined at different calcination temperatures. While catalyst with different (%) ZrO_2 over 15 wt.% HPA/ZrO_2/MS were prepared and calcined at 1123 K. For studying the effect of ZrO_2 addition, a catalyst sample without ZrO_2 was synthesized by impregnating an aqueous solution of 3.36 wt.% TPA over SBA-15 following the same procedure described above. The effect of adding TPA was studied by preparing a catalyst without TPA, which was prepared by impregnating 22.4 wt.% ZrO_2 over SBA-15. Neat 15 wt.% TPA/ZrO_2 was prepared by mixing aqueous solution of TPA with zirconium oxychloride. All the catalysts were calcined at 1123 K for 4 h.

For comparison, the catalysts like TPA/MS and TPA/MS-F were synthesized. The functionalized support (SF) was prepared by addition of 3-aminopropyltriethoxysilane to a suspension of silica (S) in refluxing toluene, then stirred for 5 h as per given in literature [8]. The solid was filtered, washed in a soxhlet apparatus with diethylether and dichloromethane and then dried at 393 K. Then S and SF were impregnated by means of the equilibrium adsorption technique at 293 K, by contacting 1 g of support with 4 cm^3 of TPA solution in ethanol/water as solvent, under constant stirring for 72 h. The solids were separated from the solutions by centrifugation and dried at 343 K for 24 h (named TPA/S and TPA/SF). Solids were then leached with toluene at 293 K under continuous stirring, for two periods of 24 h. The obtained catalysts were denoted as TPA/S-T and TPA/SF-T. Functionalized MS (MS-F) was obtained and then impregnated, using the techniques described in the previous item. Besides, MS was also impregnated by the same method. After solution was separated by centrifugation, the solids were dried at room temperature, thus obtained samples of TPA/MS and TPA/MS-F. In order to evaluate the HPA retention in the mesoporous structure, these samples were leached in ethanol/water for two periods of 24 h at 293 K, in a stirring device (hereinafter named TPA/MS-L and TPA/MS-F-L). For comparison purpose Zn^{2+} montmorillonite catalyst was prepared as per literature procedure [9]. To a 1 M solution of zinc chloride, 80 g of K-10 montmorillonite was added. Stirring was maintained for 16-30 h in order to saturate the exchange capacity of montmorrilonite K-10. The clay suspension was centrifuged and the supernatant solution was discarded. The clay catalyst was washed each time with fresh distilled water and centrifuged till the disappearance of Cl^- ions from the discarded water. The clay was dried overnight in an oven at 393 K and finely ground in a mortar. H^+ montmorillonite was prepared according to the literature procedure [10].

2.4. PHYSICO-CHEMICAL CHARACTERIZATION

2.4.1. Elemental analysis

ICP-OES analysis was done on Perkin-Elmer Optima 2000 DV with Winlab software instrument. Standard solutions were used for calibration. This instrument can analyze aqueous solutions for metals with either a Radial or an Axial plasma configuration. In Axial mode, you can generally achieve a 5-10 ppb detection limit, depending upon the element.

The other technique for chemical analysis was XRF, which was carried out on a sequential wavelength dispersive X-ray spectrometer (WD-XRF), Rigaku 3070 E Model with Rh target. WD-XRF was an excellent method for the qualitative and quantitative determination of the major and important trace elements.

For microstructural analyses a modern Leica Stereoscan-440 SEM equipped with Phoenix EDAX, is used. A high stability of the electron beam was achieved by a Schottky field emission gun. The producer indicates a resolution of 1 nm (at 20 kV).

2.4.2. XRD

For XRD measurement of the sample at low angle region, Bruker SAXS instrument was used with GADDS using Cu-Kα radiation at steps of 0.01°. XRD pattern of the samples at wide-angle region was measured on Rigaku Model D/MAXIII VC, Japan, λ=1.5418 Å with Ni filtered Cu-Kα radiation

2.4.3. Sorption study

The BET surface area of samples were measured with an Omnisorb 100CX (Coulter, USA) system under liquid N_2 temperature, using N_2 as an adsorbent. Sample was outgassed at 523 K for 2-3 h under helium before subjecting the sample for N_2-adsorption. The isotherms were analyzed in a conventional manner in the region of the relative pressure, p/p_0 = 0.05 to 0.3. The BJH method was used to determine the area of the pore walls and uses the Kelvin equation to correlate the partial pressure of nitrogen in equilibrium with the porous solid to the size of the pores where capillary condensation takes place. The pore size distribution is obtained by analysis of the desorption isotherm.

2.4.4. AFM

The agglomerate-like morphology of the material was studied by AFM in the contact mode on a VEECO Digital instruments multimode scanning probe microscope equipped with a nanoscope IV controller. According to the interaction of the tip and the sample surface, the AFM can be classified as repulsive or Contact mode and attractive or Non-contact mode.

2.4.5. SEM

The morphology of the catalytic material was determined by JEOL-JSM-5200 SEM with a resolution of 5.5 nm.

2.4.6. TEM

Formation of nanoparticles was detected by TEM (JEOL Model 1200 EX instrument operated at an accelerating voltage at 120 kV). Samples were prepared by placing droplets of a suspension in isopropanol on a polymer microgrid supported on a Cu grid for TEM measurements.

2.4.7. FT-IR spectroscopy

Shimadzu FTIR-8201PC equipment, in diffuse reflectance spectra (DRIFT) mode and a measuring range of 600-1200 cm^{-1} was used to obtain the FT-IR spectra of solid samples.

2.4.8. UV-Vis. spectroscopy

DRS for solid samples were recorded in the range of 200-600 nm using Shimadzu UV-2101PC Spectrophotometer, fitted with a diffuse reflectance chamber with inner surface of $BaSO_4$. Diffuse Reflectance UV-Visible spectroscopic technique measures the scattered light reflected from the surface of samples in the UV-Visible range (200-800 nm).

2.4.9. NMR spectroscopy

The state of TPA in the catalyst and retention of mesoporosity of silica support were elucidated by ^{31}P CP-MAS, ^{1}H MAS NMR on Bruker DSX-300 MHz spectrometer and ^{29}Si-MAS NMR on Bruker DRX-500 MHz spectrometer, respectively. ^{31}P CP-MAS NMR was recorded at 121.5 MHz with high power decoupling with a Bruker 4 mm probehead. The spinning rate was 10 kHz and the delay between two pulses was varied between 1 and 30 s to ensure that a complete relaxation of the ^{31}P nuclei occurred. The chemical shifts are given relative to external 85% H_3PO_4.

2.4.10. FT-RS

The Raman spectrometer (The Brücker FRA106) is equipped with a Nd: YAG (Neodymium: Yttrium Aluminium Garnet) Laser that is frequency doubled to 532 nm. The laser was operated at a power level of 20 mW measured at the sample with a power meter. The spectra have been collected at room temperature in the wavelength range from 0 to 4000 cm^{-1}. The spectral resolution of the spectrometer is 5 cm^{-1}. Sampling times were between 20 to 25 min. The electrons are generated by thermionic emission from a metal filament, and accelerated to ~25 keV. A system of electrical and magnetic field 'optics' is used to focus the beam to a spot ~10 nm in diameter on the sample surface.

2.4.11. XPS

XPS spectra were recorded on a VG Microtech Multilab-ESCA 3000 spectrometer equipped with a twin anode of Al and Mg. All measurements were made on as received powder samples using Mg-Kα X-ray at room temperature. Base pressure in the analysis chamber was 4 × 10^{-10} Torr. Multichannel detection system with nine channels was employed to collect the data. The overall energy resolution of the instrument was better than 0.7 eV, determined from the full width at half maximum of the $4f_{7/2}$ core level of gold surface. The errors in all the B.E. values were within ±0.1 eV. The binding energy correction was performed using the C_{1S} peak of carbon at 284.9 eV as reference.

2.4.12. TG-DTA

TG-DTA measurements were performed on Setaram TG-DTA 92 apparatus from room temperature to 1273 K in flowing dry air (ca. 50 ml min^{-1}), using α-Al_2O_3 as reference. For each experiment 25-30 mg of the sample was used with a heating rate of 10 °C min^{-1}. TGA curves are depicted as first derivative DTG of the direct weight loss traces.

2.4.13. TPD of NH_3

The total amount of acidity of the catalyst was estimated by TPD of NH_3 on Micromeritics AutoChem 2910 instrument. It was carried out after 0.1 g of the catalyst sample was dehydrated at 773 K in dry air for 1 h, purged with helium for 0.5 h. The temperature was decreased to 398 K under the flow of helium and then 0.5 ml NH_3 pulses were supplied to the samples until no more uptake of NH_3 is observed. NH_3 was desorbed in helium flow by increasing the temperature to 813 K with a heating rate of 10°C min^{-1} measuring NH_3 desorbed by TCD.

2.4.14. FT-IR of pyridine adsorption

The nature of acid sites (Brønsted and Lewis) of the catalyst samples with different loadings were characterized by in-situ FT-IR spectroscopy with chemisorbed pyridine in drift mode on FTIR-8300 Shimadzu SSU-8000 instrument with 4 cm^{-1} resolution and averaged over 500 scans. These studies were performed by heating pre-calcined powder samples in-situ from room temperature to 673 K with heating rate of 5 °C min^{-1} in a flowing stream (40 ml min^{-1}) of pure N_2. The samples were kept at 673 K for 3 h and then cooled to 373 K and then pyridine vapors (20 μl) were introduced under N_2 flow and the IR spectra were recorded at different temperatures up to 673 K. A resolution of 4 cm^{-1} was attained after averaging over 500 scans for all the IR spectra recorded here.

2.5. REFERENCES

1. A. Miyaji, T. Echizen, K. Nagata, Y. Yoshinaga, T. Okuhara, J. Mol. Catal A: Chem., 201 (2003) 145.
2. M. Hartmann, S. Racouchot, C. Bischof, Micropor. Mesopor. Mater., 27 (1999) 309.
3. K. Schumacher, M. Grün, K. K. Unger, Micropor. Mesopor. Mater., 27 (1999) 201.
4. A. Monnier, F. Schüth, Q. Huo, D. Kumar, D. Margolese, R. S. Maxwell, G. D. Stucky, P. Petroff, A. Firouzi, M. Janicke, B. F. Chmelka, Science, 261 (1993) 1299.
5. D. Zhao, J. Feng, Q. Huo, N. Melosh, G. H. Fredrickson, B. F. Chmelka, G. D. Stucky, Science, 279 (1998) 548.
6. D. Zhao, J. Sun, Q. Li, G. D. Stucky, Chem. Mater., 12 (2000) 275.
7. J. He, X. Duan, C. Li, Materials Chem. and Phys., 71 (2001) 221.
8. L. R. Pizzio, P.G. Vázquez, C.V. Cáceres, M. N. Blanco, Appl. Catal. A: General 256 (2003) 125.
9. B. M. Choudary, M. Sateesh, M. Lakshmi Kantam, K. V. R. Prasad, Appl. Catal. A: General, 171 (1998) 155.
10. B. M. Choudary, M. R. Sarma, K. V. Kumar, J. Mol. Catal. A: Chem., 87 (1994) 33.

CHAPTER – 3

ZIRCONIA SUPPORTED HPAs

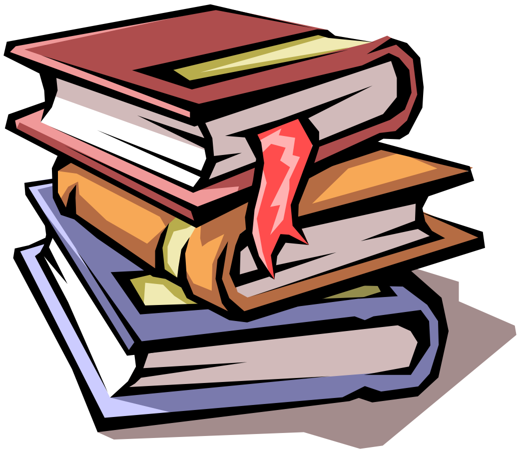

3. ZIRCONIA SUPPORTED HPAs

3.1. INTRODUCTION

This section represents the characterization of ZrO_2-supported TPA and STA catalysts by different characterization techniques and their catalytic performances in the liquid phase alkylation of DPO with BC and acetylation of veratrole with Ac_2O.

3.2. CHARACTERIZATION- RESULTS AND DISCUSSION

3.2.1. XRD

ZrO_2 calcined at 1023 K mainly exists in monoclinic form with small amount of tetragonal form. The XRD pattern of the catalysts with different TPA loadings (Fig. 3.1) shows that the tetragonal form of ZrO_2 increases with increase in loading and is fully tetragonal for the catalyst containing 30 wt.% of TPA. When the loading exceeds 15 wt.%, the formation of WO_3 crystallites was also observed [1]. Thus, the added TPA stabilizes the tetragonal phase of ZrO_2 and such stabilization of tetragonal phase in case of ZrO_2 and other oxides has been reported in literature [2,3]. When TPA loading exceeded monolayer coverage, the excess TPA that does not interact with ZrO_2 decomposed and the X-ray diffractogram showed the presence of bulk crystalline WO_3.

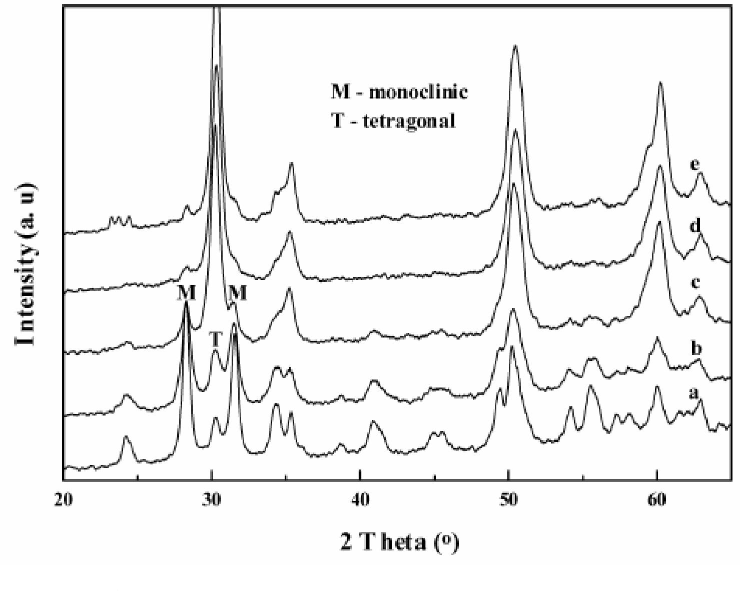

Fig. 3.1: *XRD patterns of (a) ZrO_2, (b) 5, (c) 10, (d) 15, and (e) 20 wt.% TPA/ZrO_2 calcined at 1023 K.*

Wide angle XRD pattern for different STA (%) loadings over ZrO_2 and calcined at 1023 K is shown in Fig. 3.2 (A). Similar trend was observed for STA/ZrO_2 as discussed in case of TPA/ZrO_2. Fig. 3.2 (B) XRD pattern shows the effect of different calcination temperatures over 15 wt.% STA/ZrO_2. At calcination temperature of 1123 K, it shows fully tetragonal form of zirconia and on further increase in temperatureWO$_3$ crystallites are observed.

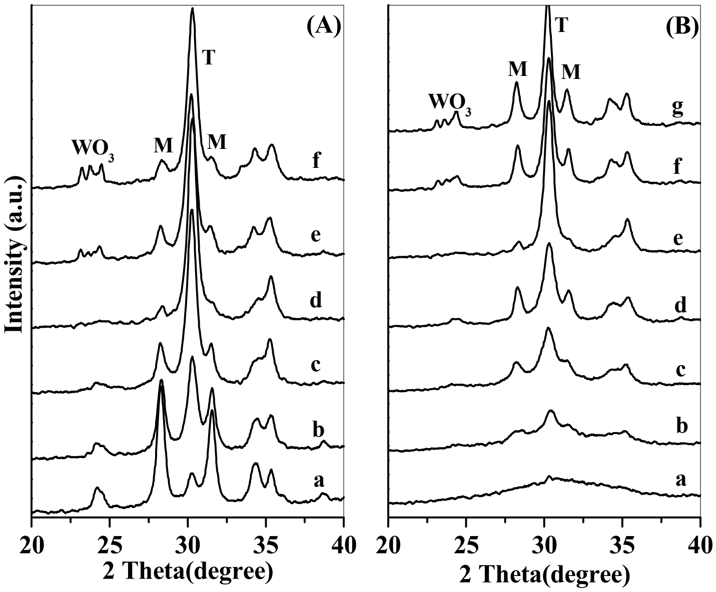

Fig. 3.2: *XRD patterns of (A) (a) ZrO_2, (b) 5, (c) 10, (d) 15, (e) 20, and (f) 25 wt.% STA/ZrO_2 catalysts calcined at 1023 K and (B) 15 wt.% STA/ZrO_2 catalyst calcined at (a) 623 K, (b) 723 K, (c) 823 K, (d) 923 K, (e) 1023 K, (f) 1073 K, and (g) 1123 K.*

3.2.2. Sorption Study

After calcination at 1023 K, the surface area of pure zirconium oxyhydroxide dried at 393 K showed decrease in surface area from 331.6 m^2g^{-1} to 16 m^2g^{-1}. Addition of TPA to the support resulted in surface area increase, which became maximum i.e. 53.2 m^2g^{-1} for 15 wt.%TPA/ZrO_2 calcined at 1023 K (Table 3.1). There is an increase in surface area with increase in (%) TPA loading which could be because of the strong interaction of TPA with the support reducing the surface diffusion of ZrO_2 and inhibits sintering and stabilizes the tetragonal phase of ZrO_2. N_2 adsorption measurements show that surface area increases with TPA loadings up to 15 wt.% and decreases with further increase in loading. For a fixed TPA loading, surface area was found to decrease with increase in calcination temperature.

Table 3.1: Characteristics of TPA/ZrO_2 catalysts calcined at 1023 K

TPA (wt.%)	Surface area (m^2 g^{-1})	Total Acidity (mmol/g)
5	40.2	0.23
10	46.3	0.36
15	53.2	0.46
20	52.3	0.23
30	44.9	0.16

3.2.3. NMR spectroscopy

For studying the state of phosphorous in HPA, NMR is one of the important characterization techniques. The chemical shift depends upon the phosphorous environment and on factors such as hydration number, addenda metal ion, and support, etc. [4-8]. For higher loadings, the acid site density decreases due to the decomposition of TPA into its constituent oxides as indicated by the formation of WO_3 crystallites as evident from XRD and phosphorous (V) oxide detected by NMR [9]. ^{31}P CP-MAS NMR spectra (Fig. 3.3) of 15 wt.%TPA/ZrO_2 calcined at 1023 K indicated that at monolayer coverage, the heteropolyanion was well dispersed on ZrO_2 surface and retained its integrity.

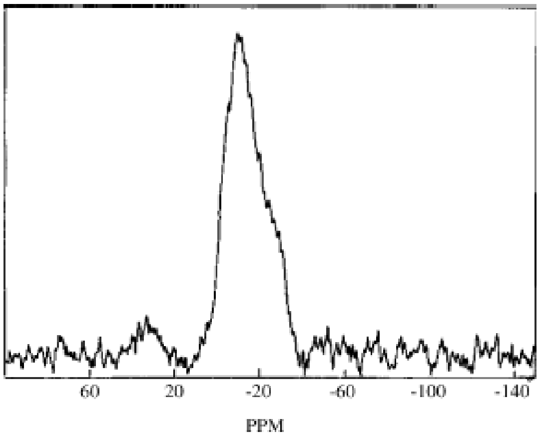

Fig. 3.3: *^{31}P CP-MAS NMR spectra of 15 wt.% TPA/ZrO_2 calcined at 1023 K.*

3.2.4. TPD of NH_3

The adsorption-desorption of ammonia technique was used to determine the total acidity. The amount of sorbed NH_3 (mmol/g) of the catalysts with different TPA loadings are listed in Table 3.1. Acidity measurements by TPD of ammonia shows that the density of acid sites increases with TPA loading and reaches its maximum for the catalyst containing 15 wt.% TPA, while it shows decrease in acidity with further increase in TPA loading. This could be explained as, the highest acidity corresponds to a monolayer of polyoxometalate on ZrO_2 support

Similar observation was noticed in case of STA/ZrO_2 catalyst system (Fig. 3.6 and 3.7). It is seen that with increase in STA loading up to 15 wt.%, it shows increase in acidity and so catalytic activity. But on further increase in STA loading, the acidity decreases due to decomposition of STA into WO_3 crystallites. As calcination temperature of 15 wt.% STA/ZrO_2 increased up to 1023 K, it shows high acidity with maximum catalytic activity due to monolayer coverage of STA over ZrO_2. But on exceeding calcination temperature above 1023 K, it shows decrease in acidity due to the decomposition of STA forming.

3.3. BENZOYLATION OF DPO WITH BC

3.3.1. Introduction

Friedel–Crafts alkylation and acylation of aromatic hydrocarbons have been studied extensively using Lewis acid catalysts, such as, BF_3, $AlCl_3$, $FeCl_3$, $TiCl_4$ and protonic acids like HF, H_2SO_4 [10-12]. The use of conventional Lewis and mineral acid catalysts has lead to environmental problems, especially in large-scale production sites. Hence, there is a need to find newer catalyst systems to replace conventional catalysts for the Friedel–Crafts reactions preferably solid acid catalysts.

Among the solid acids reported, SO_4^{2-}/ZrO_2 has been found to be highly active catalysts in much acid catalyzed reactions [13,14]. In recent years, alternate to existing solid acid catalysts, development of metal oxide supported catalysts, such as, ZrO_2 supported HPA catalysts have gained importance, since these provide advantages over others like higher thermal stability, cost effective and eco-friendly systems for applications in large-scale production [9,15]. Acylation of an aromatic substrates has been carried out using solid acid catalysts such as SO_4^{2-}/ZrO_2 [14,16], HPA [17,18] and acid activated clays [16-18]. Friedel–Crafts acylation of aromatic compounds is pioneered by Izumi et al. [19]. Silica supported TPA catalyst was used for the acylation of *p*-xylene with BC and anisole with Ac_2O [20] and have reported that TPA was unchanged on silica surface after the reaction. Recently, TPA supported over hexagonal mesoporous silica was used as a solid acid catalyst in the synthesis of acetoveratrone via acylation of veratrole by Ac_2O [21]. Alkylation of DPO with long chain olefins using smectite clay [22] and benzylation with benzyl chloride using sulfated ZrO_2 as a catalyst [23] have also been reported. Alkylation of DPO with olefins, alcohols and BC give commercially important alkylated products, for instance, heat transfer fluids and perfumery compounds. In view of the importance of the reaction products, the catalytic performance of TPA/ZrO_2 catalyst in benzoylation of DPO using BC to give selectively monoalkylated product was studied.

3.3.2. Experimental procedure

The liquid phase benzoylation of DPO by BC was carried out in a 50ml round bottom flask equipped with heating arrangement to the required reaction temperature (constant temperature-oil bath), water condenser and a magnetic stirrer for agitation. In a typical run, DPO and BC were mixed in required mole ratio and added to the pre-activated catalyst. Excess DPO are taken in most of the runs and the catalytic activity with respect to the conversion of limiting reagent BC is monitored as a function of time under the pre-decided reaction conditions. The reaction mixture was magnetically stirred and heated to the required temperature at atmospheric pressure. As soon as the catalyst comes in contact with the reaction mixture, the color of the catalyst changed from white to faint brown and with time changed to dark wine red, which indicated the progress of the reaction. Samples of the reaction mixture withdrawn at regular intervals of time were analyzed by a gas chromatograph (Shimadzu 14B GC) equipped with a SE-52 packed column, coupled with FID detector. Authenticity of the products was confirmed by GCMS (Shimadzu QP-5000). From the GC analysis, percentage conversion of BC and selectivity for products were calculated and used in the interpretation of data.

The experimental procedure is same for all the reactions mentioned in Chapters 4, 5, and 6.

3.3.3. Results and discussion

Liquid phase benzoylation of DPO with BC catalyzed by 15 wt.% TPA/ZrO_2 calcined at 1023 K under optimized reaction conditions gave *para*- (benzoyl) DPO (A) and *ortho*- (benzoyl) DPO (B) as shown in the reaction scheme 3.1:

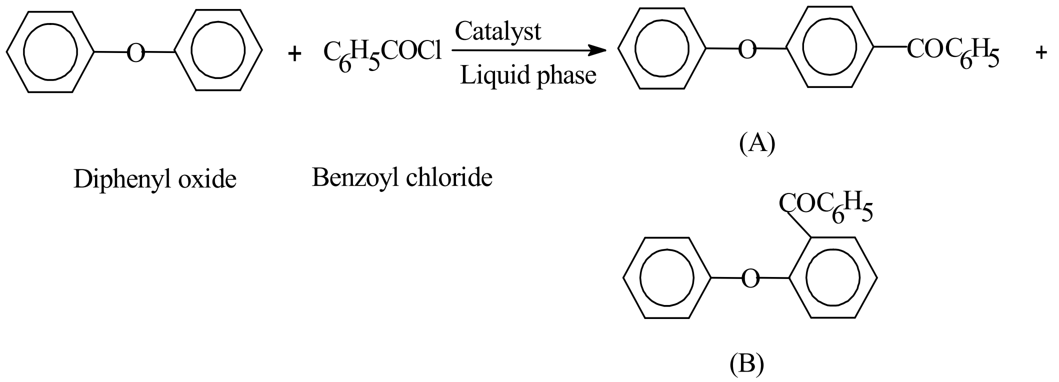

where, (A)= *p*-(benzoyl)diphenyl oxide, (B)= o-(benzoyl)diphenyl oxide

Scheme 3.1: *Benzoylation of DPO with BC.*

In the benzoylation of DPO, BC gets protonated in presence of a catalyst and electrophilic substitution of carbocation in *ortho*- or *para*- positions of phenyl ring of DPO results in the formation of benzoylated products. In the above reaction, the substitution of carbocation in *para* position was found to be more facile and hence higher selectivity to *para*-(benzoyl) DPO.

3.3.3.1. Catalytic activities of different catalysts

The activities of different catalysts, such as, H-beta, H-Y, H-ZSM-5, H-Mordenite, neat TPA and 15 wt.% TPA/SiO_2-calcined at 1023 K were tested in the benzoylation of DPO under identical reaction conditions and the results are summarized in Table 3.2.

Table 3.2: Comparison of the catalytic activities of different catalysts

Catalyst	SAR [a] (molar ratio)	Surface area [b] (m^2/g)	Acidity [c] (mmol/g)	BC Conv. (%)	Product distribution [d] (%)	
					2-BDPO	4-BDPO
Neat TPA*	-	7	-	48.6	23.0	77.0
15wt.%TPA/ZrO_2 calcined at 1023 K	-	53.2	0.46	39.3	2.6	97.4
15wt.%TPA/SiO_2 calcined at 1023 K	-	16	nil	9.8	1.9	98.1
H-beta	30	540	0.94	40.4	3.3	96.7
H-Y	13.5	530	2.25	22.5	11.0	89.0
H-Mordenite	20	490	0.72	8.7	-	100
H-ZSM-5	60	364	0.82	3.5	-	100

Reaction conditions: Catalyst/ BC (wt./wt.) = 0.28; Temperature = 393 K; DPO/ BC (molar ratio) = 7;DPO = 0.026 mol; Time =3h.

[a] *SAR (SiO_2/Al_2O_3) measured by atomic absorption*

[b] *measured by nitrogen BET method using an area meter*

[c] *measured by TPD of ammonia*

[d] *2-BDPO = 2-(benzoyl)DPO; 4-BDPO = 4- (benzoyl)DPO*

* *Amount of catalyst is taken as per TPA content.*

It is seen that TPA (homogeneous) catalyst gave the highest conversion of BC (48.6%), followed by H-beta, 15 wt.%TPA/ZrO_2, H-Y and the rest. It is also observed that 15 wt.%TPA/SiO_2 has the lowest activity in the reaction, because it has no acidity required for acid catalyzed reactions. The absence of acidity in 15 wt.%TPA/SiO_2 calcined at 1023 K confirmed that TPA decomposed on SiO_2 support and lost its acidity. Among the zeolite catalysts, H-beta is found to be more active since it has more strong and medium acid sites and gave higher conversion of BC followed by H-Y (highest acidity and large pore but weaker acid sites). Similarly, lowest activity of H-ZSM-5 might be explained on the basis of its smaller pore size compared with the larger size of the products. While, H-Mordenite has one-dimensional pore with elliptical channels, 6.5Å×7.0Å also has low activity. Therefore, we took up 15 wt.%TPA/ZrO_2 calcined at 1023 K as the catalyst for further investigations on its catalytic performance in the benzoylation of DPO with BC.

3.3.3.2. Effect of TPA loading

Benzoylation experiments were conducted using different TPA loaded (5–30 wt.%) catalysts and the results are presented in Table 3.3.

Table 3.3: Catalytic data on benzoylation of DPO by BC[a]

Catalyst	BC, conv. (%)	Product distribution[b] (%)		4-BDPO/2-BDPO ratio
		2-BDPO	4-BDPO	
Effect of TPA loading (wt.%) on ZrO_2 calcined at 1023 K				
5 wt.%TPA/ZrO_2	7.5	1.6	98.4	62.3
10 wt.%TPA/ZrO_2	17.9	2.1	97.9	47.1
15 wt.%TPA/ZrO_2	39.3	2.6	97.4	37.3
20 wt.%TPA/ZrO_2	36.8	2.4	97.6	41.5
30 wt.%TPA/ZrO_2	21.7	2.3	97.7	44.2
Effect of calcination temperature (K) on 15 wt.%TPA/ZrO_2				
923	21.8	3.5	96.5	27.6
1023	39.3	2.6	97.4	37.3
1123	10.0	1.9	98.1	52.2
Catalyst recycling				
Fresh	39.3	2.6	97.4	37.3
Ist recycle	39.0	3.2	96.8	30.1
IIst recycle	37.7	4.3	95.7	22.7

[a] *Reaction conditions: Catalyst/BC (wt./wt.) = 0.28; Temperature = 393 K; DPO/ BC (molar ratio) = 7;DPO = 0.026 mol; Time =3h*

[b] *2-BDPO = 2-(benzoyl) DPO ; 4-BDPO = 4- (benzoyl) DPO.*

It is seen that BC conversion increased with increase in TPA loading up to 15 wt.% and decreased further with increase in loading. Since, 15 wt.% catalyst is more acidic than others (Table 3.1), it gave highest BC conversion (39.3%) under the optimized reaction conditions. However, it is evident from the results presented in Table 3.3 that the selectivity for *p*- (benzoyl) DPO is highest and almost remaining the same at all conversions of BC.

In order to check the leaching of TPA into the reaction mixture, alkylation of DPO with BC was carried out for 2 h under optimized reaction conditions using fresh 15%

TPA/ZrO_2 calcined at 1023 K. The reaction was stopped and catalyst was separated by filteration and then same reaction mixture was stirred further for 2 h under same reaction conditions. It was found that in the absence of the catalyst, there was no further increase in the conversion of BC, which indicated the absence of leaching of TPA into the reaction mixture. This observation confirmed that the reaction was catalyzed heterogeneously. In addition to this, leaching of TPA (dissolution of P or W) into the filtrate was tested by ICP-OES. This showed that the filtrate did not contain P or W and were completely absent in solution, which confirmed that alkylation reaction occurred heterogeneously by surface mechanism. For testing catalytic activity of regenerated catalyst, the catalyst used in the first cycle of the reaction was separated by filteration, washed two to three times with 1,2-dichloromethane and then dried in an oven for overnight at 373 K. Then catalyst is activated at 773 K for 4 h in airflow. This activated catalyst is further used for alkylation of DPO with BC under optimized reaction conditions. The above procedure was repeated in one more cycle and the catalytic activity (conversion of BC) is presented in Table 3.3. From the results it is concluded that even after 2nd cycle there was no appreciable loss in the catalytic activity indicated by the conversion of BC.

This procedure for leaching and recyability study was used further in all reactions and no leaching was observed and the reactions were found to be truly heterogeneous. Then all the catalysts were recyclable and their recyclability was given in tabular form for all reactions in Chapters 4, 5 and 6.

3.3.3.3. Effect of calcination temperature

Benzoylation of DPO by BC was conducted with 15 wt.% TPA/ZrO_2 catalysts calcined at different temperatures under selected conditions and the results are presented in Table 3.3. From the data, it is seen that the conversion of BC increased up to the calcination temperature 1023 K and then decreased on further increase in calcination temperature. This observation supports the fact that 15 wt.% TPA/ZrO_2 calcined at 1023 K has the maximum concentration of acid sites (surface density of 7.2 Wnm^{-2}) because of a TPA monolayer covered over the support and gave high activity.

3.3.3.4. Effect of reaction parameters

Benzoylation of DPO was carried out in the range of temperatures 373–413 K to know the effect of temperature on the conversion of BC and the product selectivities using

15 wt.%TPA/ZrO_2/SBA-15 catalyst calcined at 1023 K. The effect of temperature on the conversion of BC is shown in Fig. 3.4 (a) along with the reaction conditions (legend). It is seen from the graph that as the temperature is increased from 373 to 413 K, conversion of BC increased without appreciable change in the selectivity for products. The highest conversion of BC (39.3%) was at 393 K in 3 h with o- and p-selectivities 2.6 and 97.4%, respectively. Hence, 393 K was selected as the optimized temperature for further studying the benzoylation reaction.

The influence of DPO: BC molar ratio on the conversion of BC and products distribution are presented in Fig. 3.4 (b). The DPO/BC mole ratio was varied from 1 to 15, keeping other conditions the same. As DPO/BC molar ratio is increased from 1 to 15, conversion of BC increased linearly with no change in the product distribution and gave highest selectivity for *p*-benzoyl DPO.

To know the effect of 15 wt.% TPA/ZrO_2 catalyst concentration on the conversion of BC and products selectivity, the reaction was conducted by varying the catalyst concentration in the range 1–5 wt.% of total reaction mixture (5 g). The results are shown in Fig. 3.5 (a) as a conversion of BC as a function of catalyst concentration. It is seen from the graph that the conversion of BC increased from 26 to 45% linearly in 3 h, giving highest selectivity for *p*-benzoyl DPO (>97%).

In order to study the effect of time on stream, benzoylation reaction was studied as a function of time under optimized conditions and the results are shown in Fig. 3.5 (b). Conversion of BC was almost linearly increased with increase in time, while *o*- and *p*-selectivities with highest selectivity for *para* product in the benzoylation reaction remains the same through out.

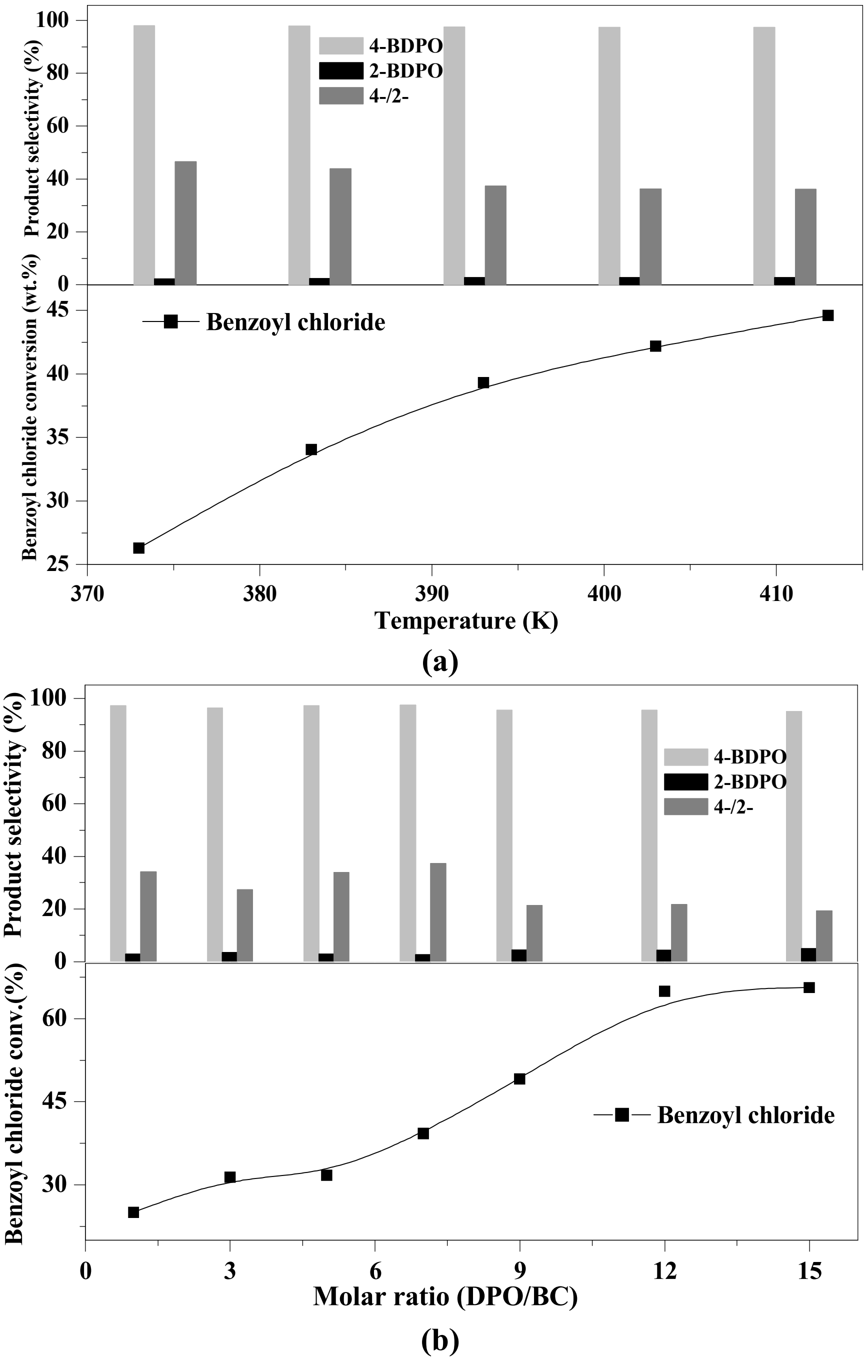

Fig. 3.4: *(a) Effect of reaction temperature. (Reaction conditions: catalyst = 15 wt.% TPA/ZrO$_2$, catalyst wt. = 0.15 g (3 wt.% of the total reaction mixture), wt. of reaction mixture = 5 g, (DPO/BC) molar ratio = 7:1, time = 3 h).*

(b) Effect of DPO to BC molar ratio. (Reaction conditions: catalyst = 15 wt.% TPA/ZrO$_2$, catalyst wt. = 0.15 g (3 wt.% of the total reaction mixture), wt. of reaction mixture = 5 g, temperature = 393 K, time = 3 h).

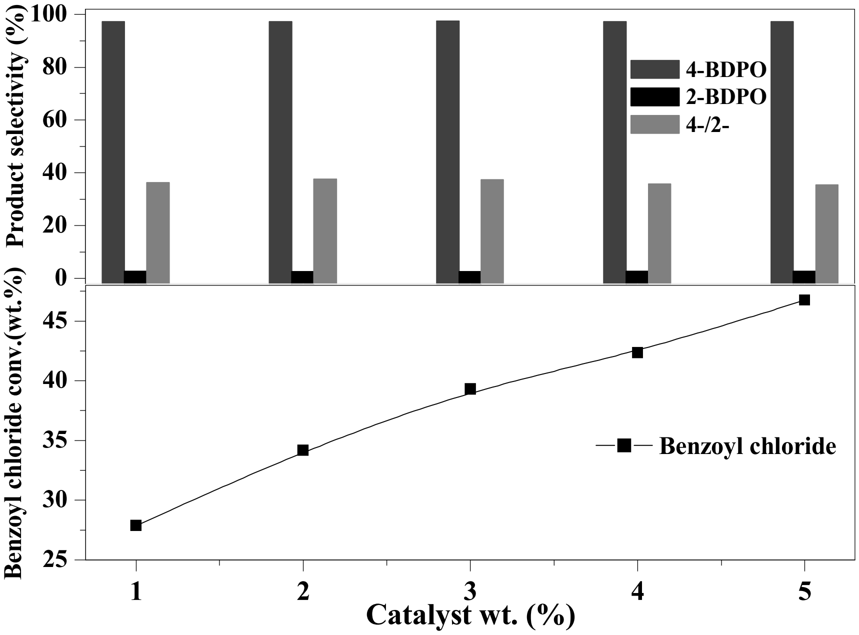

(a)

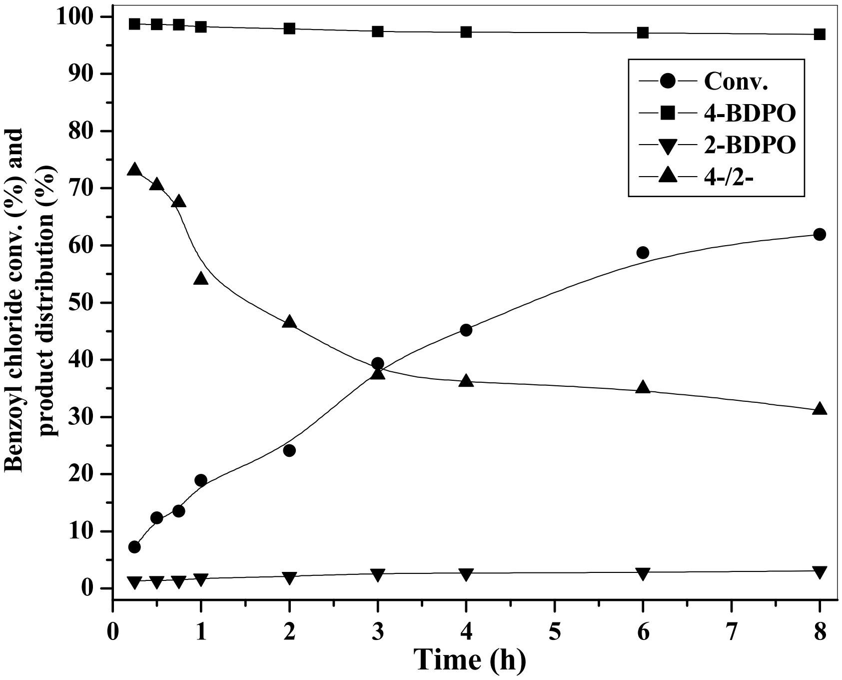

(b)

Fig. 3.5: *(a) Effect of catalyst concentration. (Reaction conditions: Catalyst = 15 wt.% TPA/ZrO2, wt. of the reaction mixture = 5 g, temperature = 393 K, (DPO/BC) molar ratio = 7:1, time = 3 h).*

(b) Study of time on stream. (Reaction conditions: catalyst = 15 wt.% TPA/ZrO2, catalyst wt. = 0.15 g (3 wt.% of the total reaction mixture), wt. of reaction mixture = 5 g, temperature = 393 K, (DPO/BC) molar ratio = 7:1).

3.3.4. Conclusions

Benzoylation of DPO with BC was carried out over 15 wt.% TPA/ZrO_2 catalyst calcined at 1023 K in liquid phase conditions. The catalyst with 15 wt.% loading gave highest catalytic activity at 393 K with DPO: BC molar ratio 7 and 3 wt.% catalyst concentration (of the total reaction mixture). The above catalyst was recyclable, cost effective and environmental friendly and could be used in similar reactions.

3.4. ALKYLATION OF BENZENE WITH α-OLEFIN

3.4.1. Introduction

LABs are important intermediates for synthetic detergents and these are traditionally manufactured in using $AlCl_3$ or HF acid catalysts. Because of the hazardous nature of conventional systems, there is a need to develop solid acid catalysts to replace the existing production methods. Solid acid catalysts such as zeolites [24-30], clays [31,32], HPA [33-37], fluorided silica-alumina [38], ionic liquids [39-41], H-ZSM-5, H-ZSM-12, H-Y [42-44], La-doped Y zeolite [45] and high silica mordenite (HSM) [46] have been widely investigated for the above transformations. Immobilized $AlCl_3$ over MCM-41 has been used for benzene alkylation with α-olefins [47]. Already UOP/Petresa has industrialized a process with Al–Mg silicate catalyst for alkylation of benzene with α-olefins [48,49].

A new catalytic distillation technology for benzene alkylation with α-olefins with suspended catalytic distillation (SCD) column has been developed [50]. Recently, supported TPA catalyst was used for synthesizing LAB with high activities and selectivities to 2-LAB [51,52]. The present work deals with the alkylation of benzene with 1-dd using ZrO_2 supported STA as the catalyst. The reaction was carried out with an aim to maximize 1-dd conversion together with the selectivity to 2-PD as compared to other isomers like 3-, 4-, (5 + 6)-LAB.

3.4.2. Experimental procedure

Experiments on alkylation of benzene were conducted in a 50 ml Parr autoclave under nitrogen pressure. The catalysts were activated at 500 °C for 4 h and cooled to room temperature prior to their use in the reaction. In a typical run, a weighted amount of 15 wt.% STA/ZrO_2 mixed with known amount of benzene and 1-dd was placed in the reactor. The reactor was pressurized with nitrogen (6–7 bar) and heated to the desired temperature with stirring at 500 rpm. After a fixed interval of time, the reactor was cooled to room temperature and a sample of the reaction mixture was withdrawn and centrifuged to get a clear solution and analyzed for products. The products of alkylation of benzene were analyzed by Shimadzu 14B gas chromatograph fitted with a SE-52 capillary column coupled with FID. Since, benzene was in excess, conversions were estimated based on the limiting alkylating reagent. The products were also identified by GC–MS analysis.

3.4.3. Results and discussion

Alkylation of benzene with 1-dd catalyzed by 15 wt.% STA/ZrO_2 calcined at 1023 K under optimized reaction conditions gave 2-, 3-, 4- and (5 + 6)-PD as shown in the Scheme 3.2.

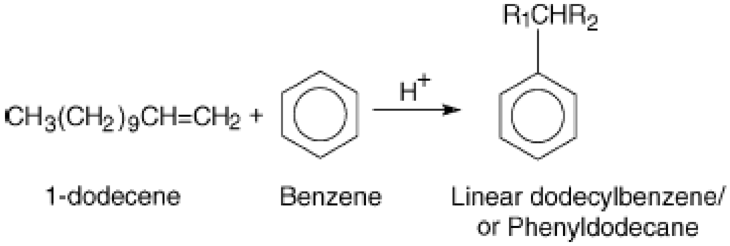

Scheme 3.2: *Alkylation of benzene with 1-dd.*

The formation of isomers of PD are likely by the electrophilic substitution of carbenium ion, which is formed upon chemisorption of 1-dd on the catalyst surface as shown in Scheme 3.3.

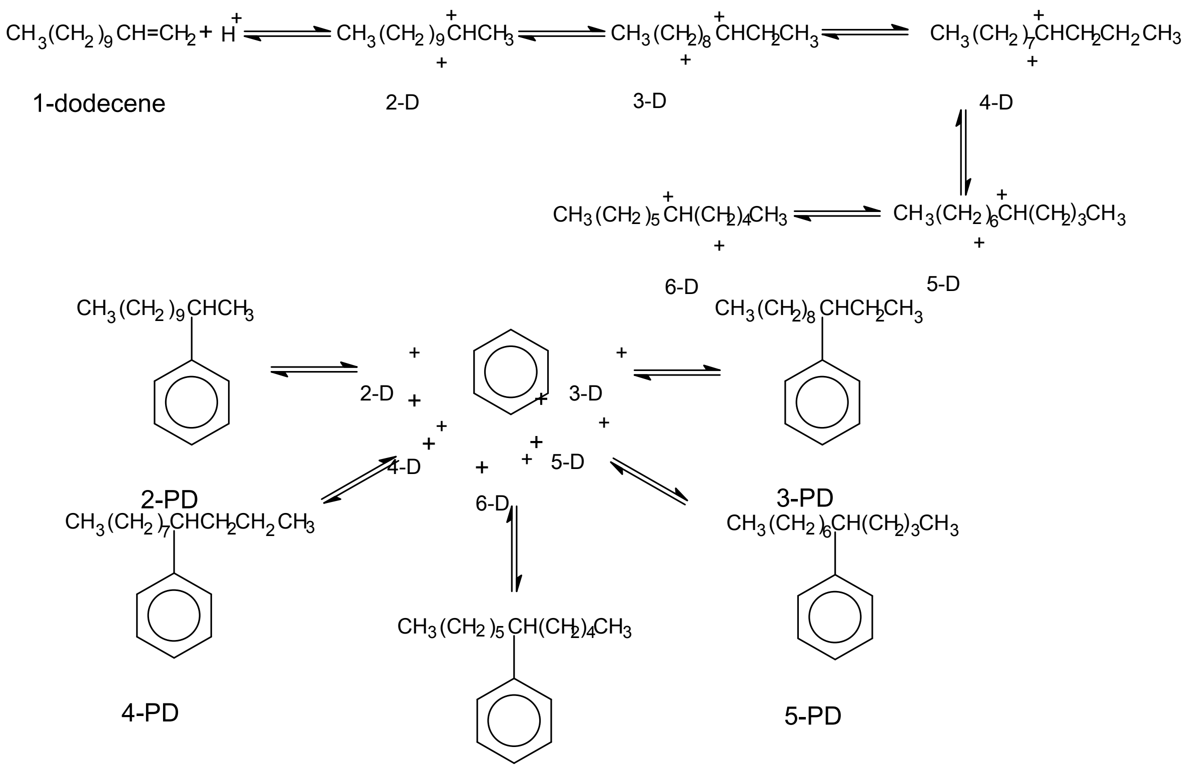

Scheme 3.3: *Mechanism of formation of PD.*

3.4.3.1. Catalytic activities of different catalysts

The catalytic activities of different catalysts in the alkylation of benzene with 1-dd under identical reaction conditions and the results are summarized in Table 3.4. It is seen from the results that STA (neat) gave the lowest conversion, which was due to its low surface area. It was also observed that 15 wt.% STA/SiO_2 calcined at 1023 K showed less catalytic activity in the reaction, since it had no acidity required for acid catalyzed reactions. Among the zeolite catalysts, H-Y was more active than others due to its highest acidity with large pores gave higher conversion of 1-dd followed by H-beta (strong and medium acid sites), H-Mordenites and H-ZSM-5.Therefore, we chose 15 wt.% STA/ZrO_2 calcined at 1023 K as the catalyst for further investigations on its catalytic performance in the benzene alkylation with 1- dd.

Table 3.4: Activities of different catalysts in alkylation of benzene with 1-dd

Catalyst	1-dd conversion (Wt.%)	Acidity (mmol/g)	%Selectivity			
			2-PD	3-PD	4-PD	(5+6)-PD
Neat STA	0.7	-	75.9	15.3	4.5	4.3
15%STA/ZrO$_2$$^{1023\ K}$	50.8	0.25	47.1	17.4	10.9	24.6
15%STA/SiO$_2$$^{1023\ K}$	6.6	Nil	59.2	16.2	8.5	16.1
H-ß (30)	39.0	0.94	62.4	19.6	7.1	10.9
H-Y (13.5)	44.9	2.25	36.4	22.1	14.4	27.1
H-Mordenite (20)	4.7	0.72	89.5	10.5	-	-
H-ZSM-5 (60)	0.1	0.82	100	-	-	-

Reaction conditions: Benzene: 1-dd.=10:1 (molar ratio), Pressure = 6-7 bars, Amount of catalyst =600 mg (3 wt.% of total reaction mixture), Reaction Time= 4h.
In bracket, (Si/Al) ratio of respective zeolites are given.
PD= Phenyldodecane.

3.4.3.2. Effect of STA loading

Alkylation experiments were conducted using different STA loaded (5–25 wt.%) catalysts to know the effect on the conversion of 1-dd and the results are shown in Fig. 3.8.

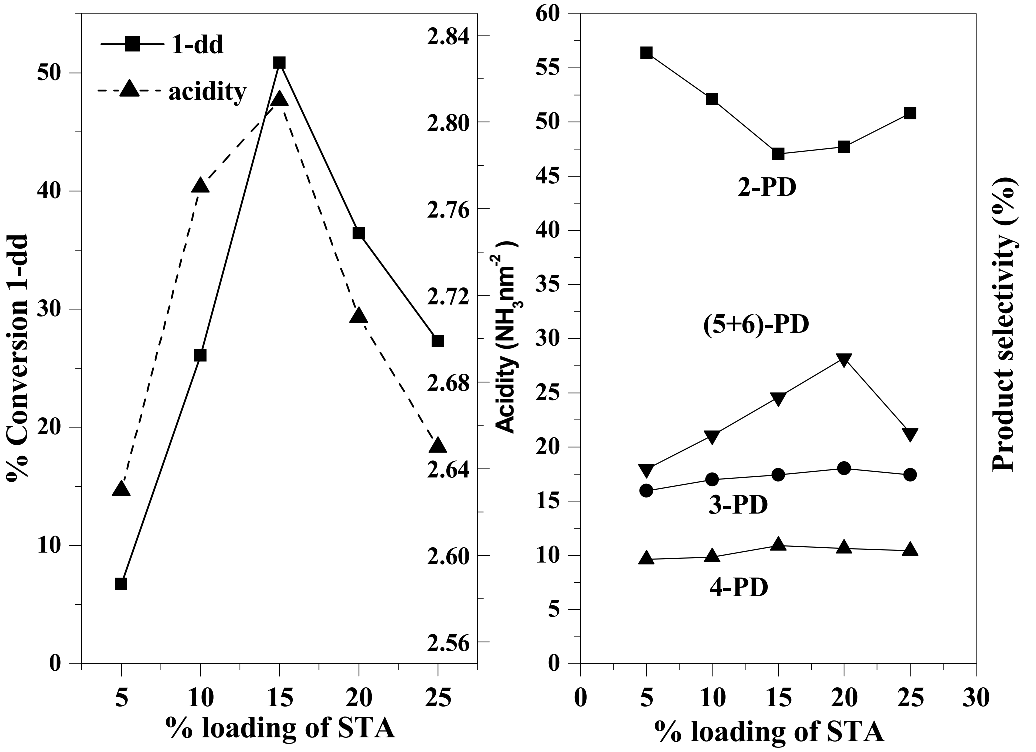

Fig. 3.6: *Effect of STA loadings and acidity on 1-dd conversion and product selectivity. (Reaction conditions: temperature = 403 K, benzene/1-dd molar ratio = 10, catalyst weight = 0.6 g (3 wt.% of total reaction mixture), N_2 pressure = 6–7 bar, time=4h).*

It is seen that conversion of 1-dd increased with increase in STA loading up to 15 wt.% and decreased with further increase in loading. As shown in Fig. 3.6, 15 wt.% catalyst is more acidic than others, hence it gave highest 1-dd conversion (50.8%) under the optimized reaction conditions. From the results presented in Fig. 3.6, it is evident that the selectivity for 2-PD is higher than the other isomers of LAB.

3.4.3.3. Effect of calcination temperature

For studying the effect of calcination temperatures on 15 wt.% STA/ZrO_2 catalyst, alkylation of benzene with 1-dd was conducted and the results are shown in Fig. 3.7. From the results, it is seen that the conversion of 1-dd increased up to 1023 K calcination temperature and then on further increase in calcination temperature, the conversion of 1-dd decreased.

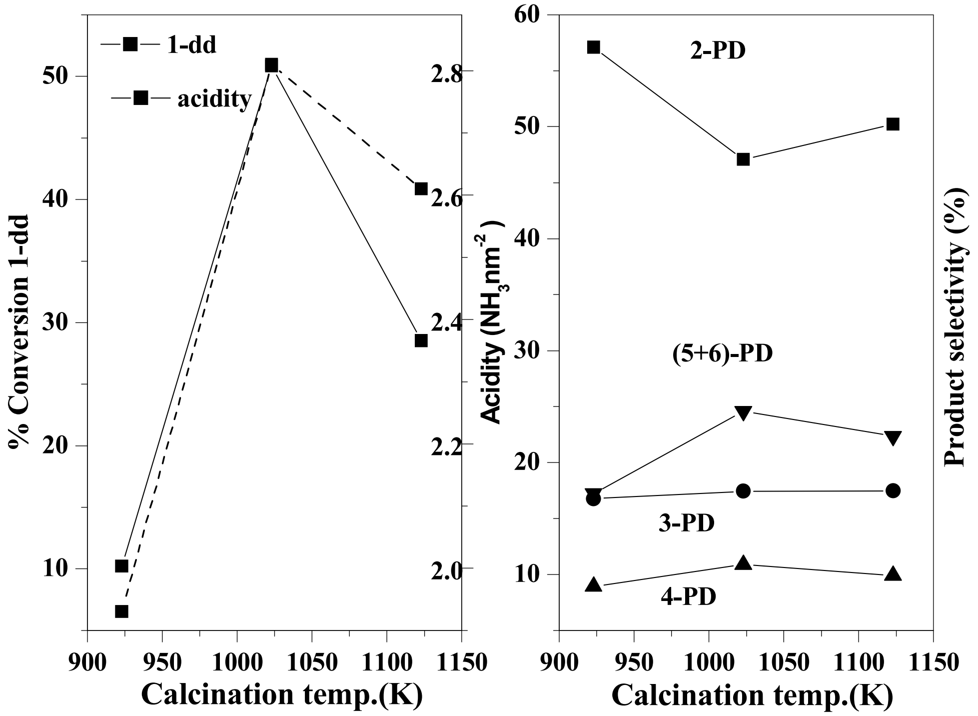

Fig. 3.7: *Effect of calcination temperature and acidity on 1-dd conversion and product selectivity. (Reaction conditions: temperature = 403 K, benzene/1-dd molar ratio = 10, catalyst weight = 0.6 g (3 wt.% of total reaction mixture), N_2 pressure = 6–7 bar, time=4h).*

3.4.4.4. Effect of reaction parameters

To know the effect of 15 wt.% STA/ZrO_2 catalyst concentrations on the conversion of 1-dd and the product selectivity, the alkylation reaction was conducted by changing the catalyst concentration in the range of 1–5 wt.% of total reaction mixture (20 g), keeping constant molar ratio of benzene: 1-dd as 10, 403 K and 4 h.

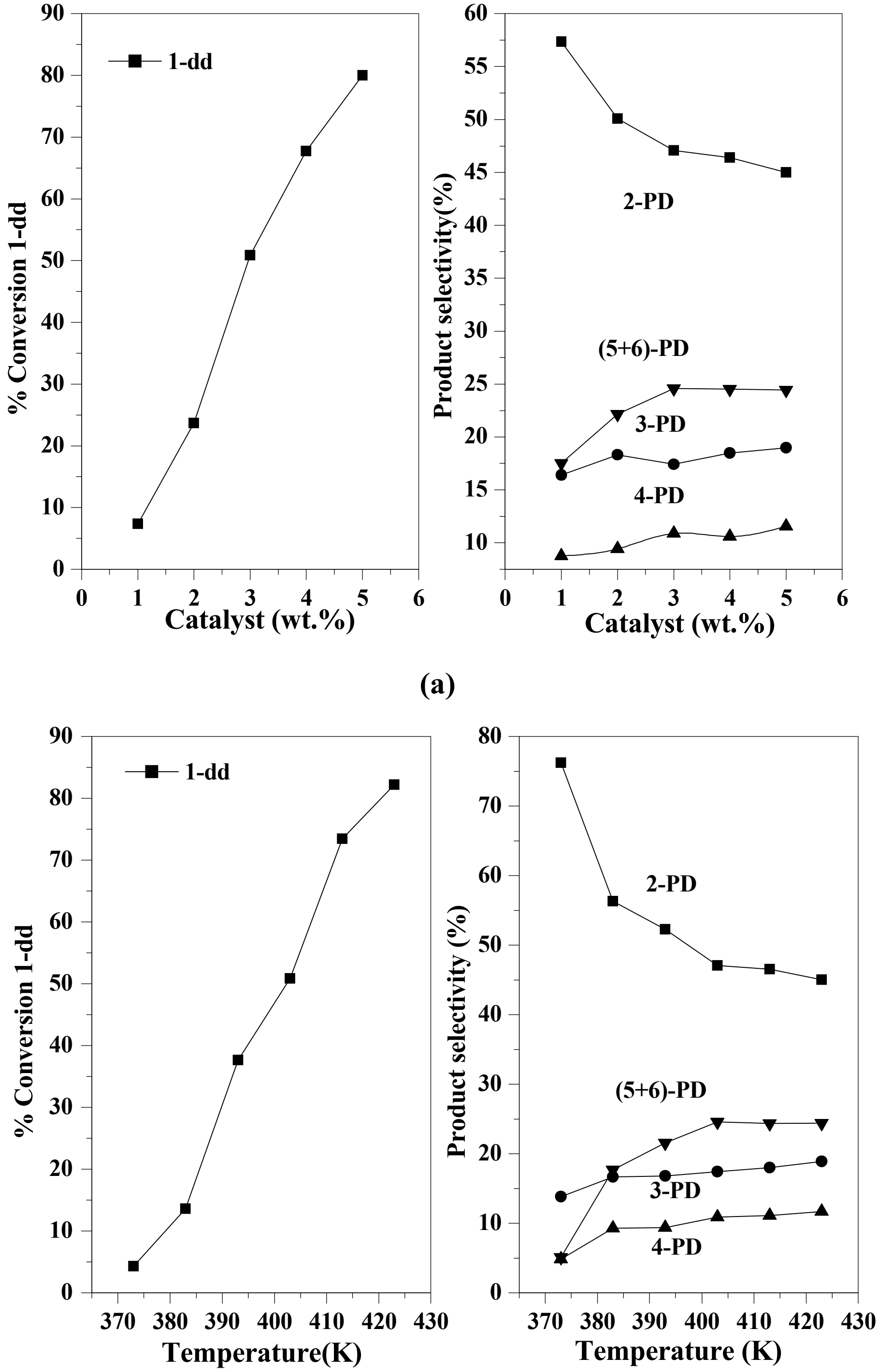

(a)

(b)

Fig. 3.8: *(a) Effect of catalyst weight on 1-dd conversion and product selectivity. (Reaction conditions: temperature = 403 K, benzene/1-dd molar ratio = 10, N_2 pressure = 6–7 bar, time=4h).*

(b) Effect of temperature on 1-dd conversion and product selectivity. (Reaction conditions: benzene/1-dd molar ratio = 10, catalyst weight = 0.6 g (3 wt.% of total reaction mixture), N_2 pressure = 6–7 bar, time=4h).

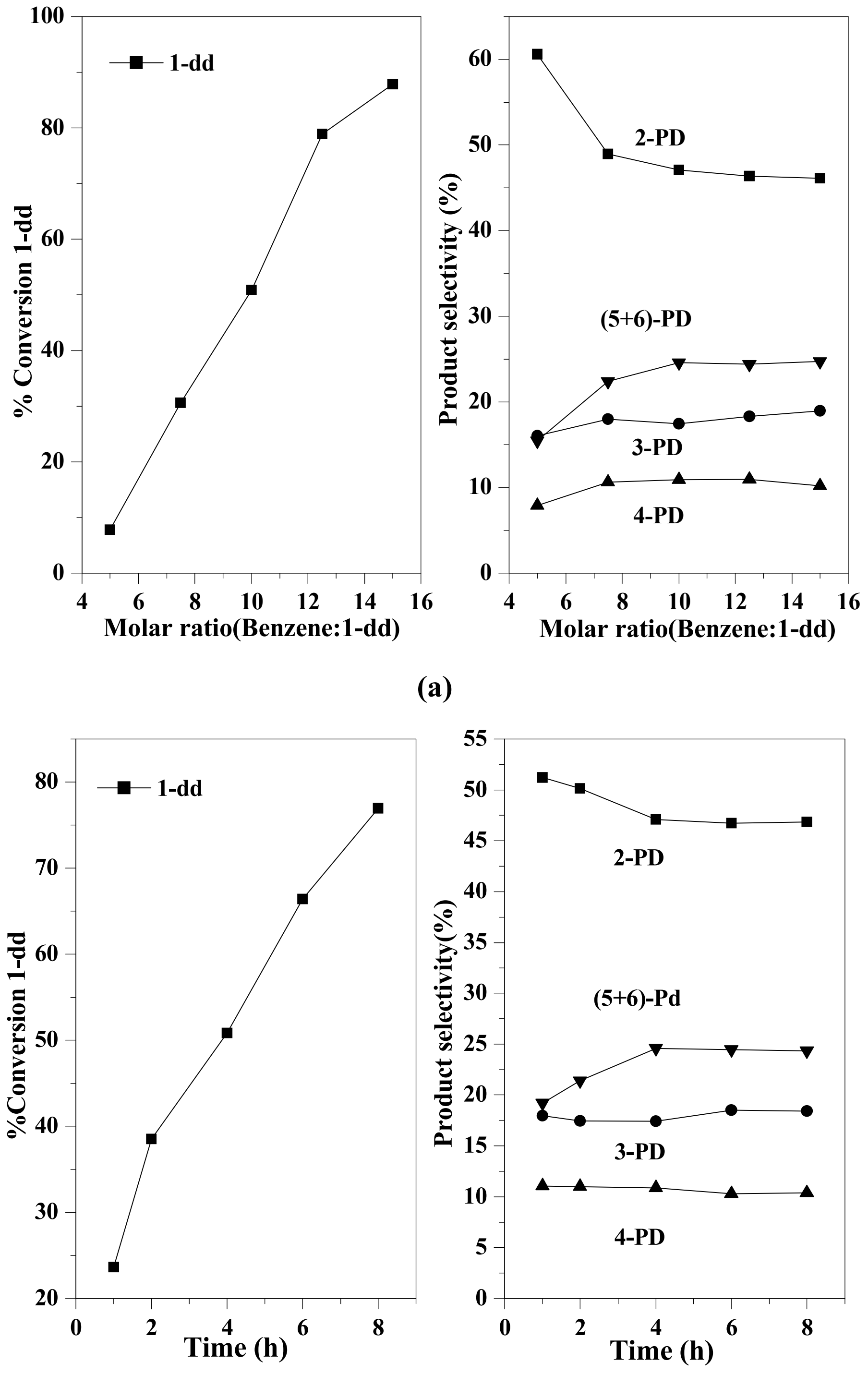

(a)

(b)

Fig. 3.9: *(a) Effect of molar ratio on 1-dd conversion and product selectivity. (Reaction conditions: temperature = 403 K, catalyst weight = 0.6 g (3 wt.% of total reaction mixture), N_2 pressure = 6–7 bar, time=4h).*

(b) Effect of reaction time on 1-dd conversion and product selectivity. (Reaction conditions: temperature = 403 K, benzene/1-dd molar ratio = 10, catalyst weight = 0.6 g (3 wt.% of total reaction mixture), N_2 pressure = 6–7 bar).

The results are shown in Fig. 3.8 (a) as conversion of 1-dd as a function of catalyst concentration. It is seen from the Fig. 3.8 (a) that the conversion of 1-dd increased from 7.4 to 80% linearly in 4 h, giving highest selectivity for 2-PD. The alkylation of benzene was carried out in the temperature range 373–423 K to know the effect of temperature on the conversion of 1-dd and the product selectivities as shown in Fig. 3.8 (b). It is seen from the Fig. 3.8 (b) that the conversion of 1-dd is increased from 4.3 to 82.2% with increase in temperature from 373 to 423 K. The optimum conversion of 1- dd (50.8%) was obtained at 403 K with product selectivites 2-LAB (47.1%), 3-LAB (17.4%), 4-LAB (10.9%) and (5 + 6)-LAB (24.6%), respectively.

Activation energy evaluated from the graph -ln rate versus $1/T$ was found to be 34.7 kcal mol^{-1}. The effect of benzene: 1-dd molar ratio on the conversion of 1-dd and product distribution are presented in Fig. 3.9 (a). The mole ratio of benzene: 1-dd was changed from 5 to 15, keeping other conditions the same. As benzene: 1-dd molar ratio is increased from 5 to 15, conversion of 1-dd increased linearly from 7.8 to 87.8 with high selectivity for 2-PD. In order to study the effect of time on stream, alkylation reaction was studied as a function of time under optimized conditions and the results are shown in Fig. 3.9 (b). Conversion of 1-dd was almost linearly increased with increase in time from 23.6 to 76.9%, while 2-PD has the highest selectivity.

3.4.4.5. Alkylation of benzene with other olefins

To investigate the effect of chain length of α-olefins, the alkylation of benzene was carried out with 1-octene and 1-decene under similar optimized reaction conditions using 15% STA/ZrO_2 calcined at 1023 K. It was found that the conversion of 1-olefins in general was decreased with increase in chain length of α-olefin as presented in Table 3.5. It is also seen that with increase in chain length, selectivity to respective 2-LAB products were decreased.

Table 3.5: Alkylation of benzene by using different α-olefins

Alkylating agent	1-Olefin Conversion (Wt.%)	% Selectivity			
		2-LAB	3-LAB	4-LAB	(5+6)-LAB
1-Dodecene	50.8	47.1	17.4	10.9	24.6
1-Decene	52.2	57.9	18.9	23.2(4-+5-)	-
1-Octene	54.5	63.6	21.9	14.5	

LAB = Linear alkyl benzene.
Reaction conditions: Benzene: 1-dd.=10:1 (molar ratio), N_2 Pressure = 6-7 bars, Catalyst =15 wt.% STA/ZrO_2 calcined at 1023 K (600 mg, 3 wt .% of total reaction mixture), Temperature = 403 K, Reaction Time= 4h.

The recyclability of the catalyst is given in Table 3.6.

Table 3.6: Recyclability of catalyst

Cycle	1-dd conversion (Wt.%)	%Selectivity			
		2-PD	3-PD	4-PD	(5+6)-PD
Fresh	50.8	47.1	17.4	10.9	24.6
Ist Run	50.7	47.8	17.3	10.7	24.2
IInd Run	48.7	48.0	17.3	10.7	24.0

Reaction conditions: Benzene: 1-dd.=10:1 (molar ratio), Pressure = 6-7 bars, Catalyst=15wt.% STA/$ZrO_2^{1023\ K}$, Catalyst =15 wt.% STA/ZrO_2 calcined at 1023 K (600 mg, 3 wt. % of total reaction mixture), time= 4h, temperature=403 K.
PD = Phenyldodecane.

3.4.5. Conclusions

Alkylation of benzene with 1-dd was carried out over 15 wt.% STA/ZrO_2 catalyst calcined at 1023 K in liquid phase conditions under N_2 atmosphere. The catalyst with 15 wt.% loading showed highest catalytic activity at 403 K with benzene: 1-dd molar ratio 10 and 3 wt.% catalyst concentration (of the total reaction mixture). Under the optimized reaction conditions, STA/ZrO_2 showed good catalytic activity with a maximum conversion of 1-dd (50.8%) and the selectivity to 2-PD was the highest (47.1%) as compared with other isomers like 3-, 4-, 5- and 6-PD at 403 K. The above catalyst was recyclable, cost effective and environmental friendly and could be used in similar reactions.

3.5. REFERENCES

1. JCPDS-International Center for diffraction data, 1990, Card 43-1035.
2. E. Lopez-Salinas, J. G. Hermandez-Cortez, I. Schifter, E. Torres-Garcia, J. Navarrete, A. Gutierrez-Carrillo, T. Lopez, P. P. Lottici, D. Bersani, Appl. Catal. A: General, 193 (2000) 215.
3. A. Khodakov, J. Yang, S. Su, E. Iglesia, J. Catal., 177 (1998) 343.
4. M. Misono, Chem. Commun., (2001) 1141.
5. C. J. Dillon, J. H. Holles, R. J. Davis, J. A. Labinger, M. E. Davis, J. Catal., 218 (2003) 54.
6. A. Ghanbari-Siahkali, A. Philippou, J. Dwyer, M. W.Anderson, Appl. Catal. A: General, 192 (2000) 57.
7. A. Molnar, T. Beregszaszi, A. Fudala, P. Lentz, J. B. Nagy, Z. Konya, I. Kiricsi, J. Catal., 202 (2001) 379.
8. S. Uchida, K. Inumaru, M. Misono, J. Phys. Chem. B, 104 (2000) 8188.
9. B. M. Devassy, S. B. Halligudi, S. G. Hegde, A. B. Halgeri, F. Lefebvre, Chem. Commun., 10 (2002) 1074.
10. G. A. Olah, Friedel–Crafts and Related Reactions, vols. 1–4, Wiley-Interscience, New York, London, 1963–1964.
11. G. A. Olah, Friedel–Crafts and Related Reactions, vols. 1–4, Wiley- Interscience, New York, London, Sydney, Toronto, 197.
12. G. A. Olah, G. K. S. Prakash, J. Sommer, Superacids, Wiley- Interscience, Brisbane, Toronto, 1985.
13. X. Song, A. Sayari, Catal. Rev. Sci., 38 (1996) 329.
14. G. D. Yadav, J. J. Nair, Micropor. Mesopor. Mater., 33 (1999) 1.
15. B. M. Devassy, G. V. Shanbhag, S.B. Halligudi, J. Mol. Catal. A: Chemical, 210 (2004) 125.
16. G. D. Yadav, M. S. Krishnana, Chem. Eng. Sci., 54 (19) (1999) 4189.
17. G. D. Yadav, A. A. Pujari, Green Chem., 1 (2) (1999) 69.
18. G. D. Yadav, N. S. Asthana, Ind. Eng. Chem. Res., 41 (2002) 5565.
19. Y. Izumi, K. Urabe, M. Onaka, ‘Zeolite, Clay and HPA in Organic Reactions’, Kodansha/VCH, Tokyo, 1992.

20. J. Kaur, K. Griffin, B. Harrison, I. V. Kozhevnikov, J. Catal., 208 (2002) 448.
21. G. D. Yadav, H. G. Manyar, Micropor. Mesopor. Mater., 63 (2003) 85.
22. H. Asakura, H. Tomioka, J. Chem. Soc. Jpn., Chem. Ind. Chem., 1 (2002) 37.
23. G. D. Yadav, S. Sengupta, Org. Proc. Res. Develop., 6 (2002) 256.
24. Y. Xu, R. X. Huang, P. C. Wu, Chinese Patent 1072353A (1993).
25. W. Cheng, W.G. Liang, Y. Jin, Petrochem. Technol., 3 (1996) 164.
26. J. L.G. Almeida, M. Dufanux, Y. B. Taarit, Appl. Catal. A: General, 114 (1994) 141.
27. Y. Cao, R. Kessas, C. Naccache, Appl. Catal. A: General, 184 (1999) 231.
28. S. Sivasanker, A. Thangara, J. Catal., 138 (1992) 386.
29. P. M´eriaudeau, Y. B. Taarit, A. Thangaraj, J. L. G. Almeida, C. Naccache, Catal. Today, 38 (1997) 243.
30. Z. L. Bo, Y. H. Fu, S. Z. Chen, J. East, Chin. Inst. Chem. Technol., 6 (1993) 696.
31. J. A. Kocal, US Patent 5034564 (1991).
32. R. E. Marinangeli, J. S. Holmgren, US Patent 5491271 (1996).
33. R. T. Sebusky, A. M. Henke, Ind. Eng. Chem. Process Des. Dev., 2 (1971) 272.
34. M. Misono, Catal. Rev. Sci. Eng., 29 (1987) 269.
35. M. Misono, T. Okuhara, CHEMTECH, 11 (1993) 23.
36. Y. Izumi, M. Ono, M. Ogawa, K. Urabe, Chem. Lett., 5 (1993) 825.
37. J. Zhang, Z. Zhu, C. Li, L. Wen, E. Min, J. Mol. Catal. A: Chem., 198 (2003) 359.
38. C. D. Chang, S. Han, J. G. Santiesteban, US Patent 5516954 (1996).
39. K. Srirattnai, S. Damronglerd, S. Omi, S. Roengsumran, A. Petsom, G.-H. Ma, Tetrahedron Lett., 43 (2002) 4555.
40. K. Qiao, Y. Deng, J. Mol. Catal. A: Chem., 171 (2002) 81.
41. C. DeCastro, E. Sauvage, M. H. Valkenberg, W. F. Holderich, J. Catal., 196 (2000) 86.
42. J. L. G. Almeida, M. Dufaux, Y. B. Taarit, JAOCS, 71 (7) (1994) 675.
43. B. Vora, P. Pujado, I. Imai, Chem. Eng., 19 (1990) 187.
44. W. Liang, Y. Jin, Z. Yu, Z. Wang, B. Han, M. He, E. Min, Zeolites, 17 (1996) 297.
45. L. B. Zinner, K. Zinner, M. Ishige, A. S. Araujo, J. Alloys Compd., 193 (1993) 65.

46. S. Samanta, N. K. Mal, P. Kumar, A. Bhaumik, J. Mol. Catal. A: Chem., 215 (2004) 169.
47. X. Hu, M. L. Foo, G. K. Chuah, S. Jaenicke, J. Catal., 195 (2000) 412.
48. J. L. B. Tejero, A. M. Danvila, US Patent 5146026 (1993).
49. J. L. B. Tejero, A. M. D. Algeciras, US Patent 5157158 (1992).
50. L. Y. Wen, E. Z. Min, G. X. Pang, W.Y. Yu, J. Chem. Ind. Eng., 1 (2000) 115.
51. L. Y. Wen, The new technology developement of suspending catalytic distillation (SCD), Doctoral Thesis, Research Institute of Petroleum Process, Beijing, 1998.
52. B. M. Devassy, F. Lefebvre, S. B. Halligudi, J. Catal., 229 (2005) 576.

CHAPTER – 4

ZIRCONIA SUPPORTED TPA IN MCM-41

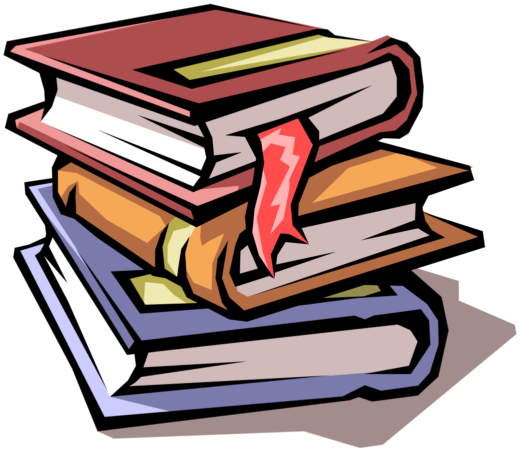

4. ZIRCONIA SUPPORTED TPA IN MCM-41

4.1. INTRODUCTION

This chapter represents the characterization of TPA over ZrO_2 dispersed uniformly in mesoporous silica (MS) channels of MCM-41 and MCM-48. Catalysts with different TPA loadings (5 to 50 wt.%) on 22.4 wt.%ZrO_2/MCM-41 and 15 wt.%TPA on different ZrO_2 loadings (10-70 wt.%)/MCM-41 were prepared and calcined at 1123 K. These catalyst systems were screened for their performances in the liquid phase acetylation of veratrole with Ac_2O and the reaction conditions for higher substrate conversions and product selectivities have been evaluated.

4.2. CHARACTERIZATION-RESULTS AND DISCUSSION

4.2.1. Elemental analysis

The ratio of P: W (1: 12) in 15 wt.%TPA/22.4 wt.%ZrO_2/MCM-41 corresponding per Keggin unit was estimated by XRF (1: 12.13) and ICP-OES (1:12.07).

4.2.2. XRD

Fig. 4.1(A) shows the XRD patterns of 15 wt.%TPA/different wt.%ZrO_2 over MCM-41 and the main diffraction peak corresponding to (100) reflection of MCM-41 in the mesoporous region was intact up to 22.4 wt.% ZrO_2 loading. At 30 wt.% ZrO_2 loading, intensity of (100) reflection decreased drastically. Wide-angle XRD patterns showed well-defined peaks characteristics of tetragonal ZrO_2 (t-ZrO_2) phase and monoclinic ZrO_2 (m-ZrO_2, $2\theta \sim 28°$) phase also appeared when the ZrO_2/MCM-41 wt. ratio was higher than 0.5.

Fig. 4.2 (A) and 4.2 (B) illustrates the XRD patterns of the catalysts with different TPA loadings over 22.4 wt.%ZrO_2/MCM-41. It showed that the peaks corresponding to MCM-41 appeared up to 30 wt.%TPA loading indicating intact mesoporous structure. On further increase in TPA loading, the mesoporous structure of MCM-41 was collapsed. From wide angle XRD, it was seen that up to 15 wt.%TPA loading, TPA/ZrO_2 dispersed uniformly and formed monolayer coverage. With further increase in TPA loading showed a peak corresponding to WO_3 crystallites of decomposed TPA. The XRD pattern (Fig. 4.3) indicated that even after modification, MCM-48 by TPA/ZrO_2, its mesoporosity was intact, which exhibited peaks indexed as (211) and (220).

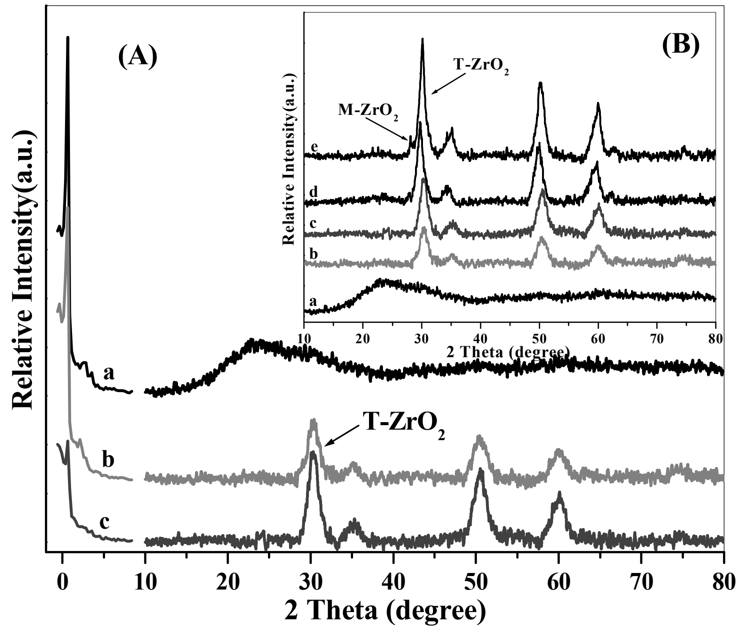

Fig. 4.1: *XRD patterns of (A) a) 15 wt.%TPA/10 wt.%ZrO$_2$/MCM-41, b) 15 wt.%TPA/22.4 wt.%ZrO$_2$/MCM-41, c) 15 wt.%TPA/30 wt.%ZrO$_2$/MCM-41 and (B) wide angle XRD of a) 15 wt.%TPA/10 wt.%ZrO$_2$/MCM-41, b) 15 wt.%TPA/22.4 wt.%ZrO$_2$/MCM-41, c) 15 wt.%TPA/30 wt.%ZrO$_2$/MCM-41, d) 15 wt.%TPA/50 wt.%ZrO$_2$/MCM-41 and e) 15 wt.%TPA/70 wt.%ZrO$_2$/MCM-41 calcined at 1123 K.*

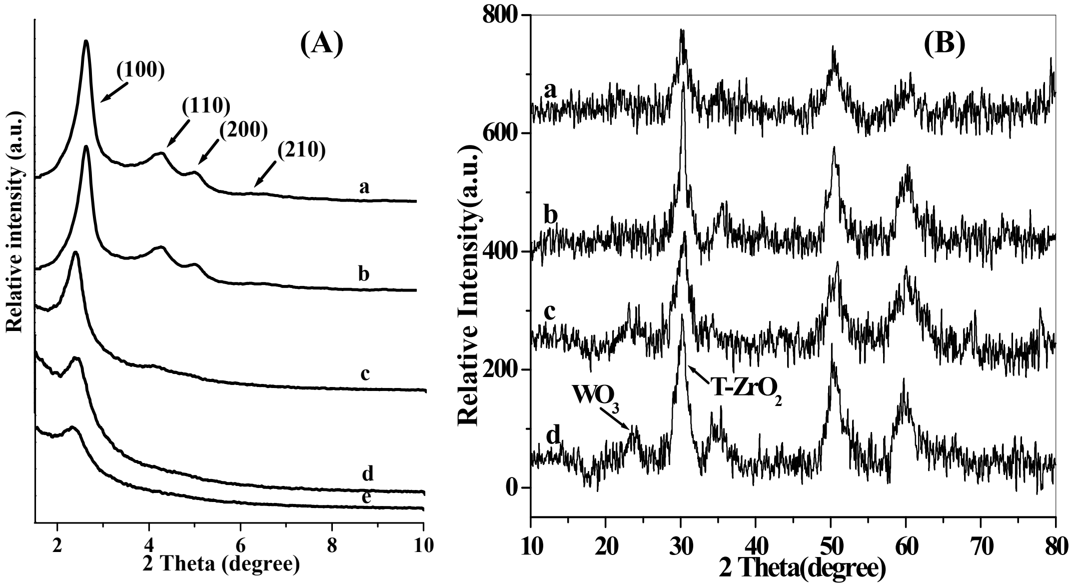

Fig. 4.2: *XRD patterns of (A) a) MCM-41, b) 5, c) 15, d) 30, and f) 50 wt.% TPA/22.4 wt.%ZrO$_2$/MCM-41 and (B) wide angle XRD of a) 50, b) 30, c) 15, and d) 5 wt.% TPA/22.4 wt.%ZrO$_2$/MCM-41 calcined at 1123 K.*

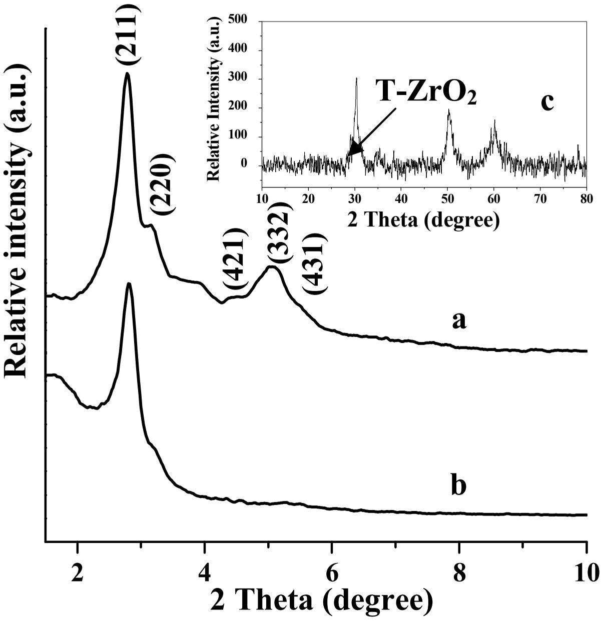

Fig. 4.3: *XRD patterns of a) MCM-48, b) 15 wt.%TPA/22.4 wt.%ZrO_2/MCM-48 and c) (Inset figure) wide angle XRD of 15 wt.%TPA/22.4 wt.%ZrO_2/MCM-48.*

While inset Fig. 4.3 (c) showed ZrO_2 was present only in tetragonal phase with monolayer coverage of TPA over ZrO_2 in MCM-48 channels.

4.2.3. Sorption study

The surface area, pore volume and pore diameter of the catalysts are presented in Table 4.1. It is seen (Table 4.1) that with increase in ZrO_2 loading, marginal decrease in surface area, pore volume and pore diameter were observed as compared to parent MCM-41. It is also seen that a gradual decrease in the above values have been observed with increase in TPA loadings as well. With these observations, it could be presumed that TPA/ZrO_2 was finely dispersed inside mesoporous channels of MCM-41 and MCM-48. The N_2 adsorption-desorption isotherms of 15 wt.%TPA/22.4 wt.%ZrO_2/MCM-41 and 15 wt.%TPA/22.4 wt.%ZrO_2/MCM-48 catalysts are typical of type IV with an unslope but without hysteresis loop at $p/p_0 = 0.2$-0.4 as shown in Fig. 4.4, similar to the one observed for pure MCM-41 and MCM-48.

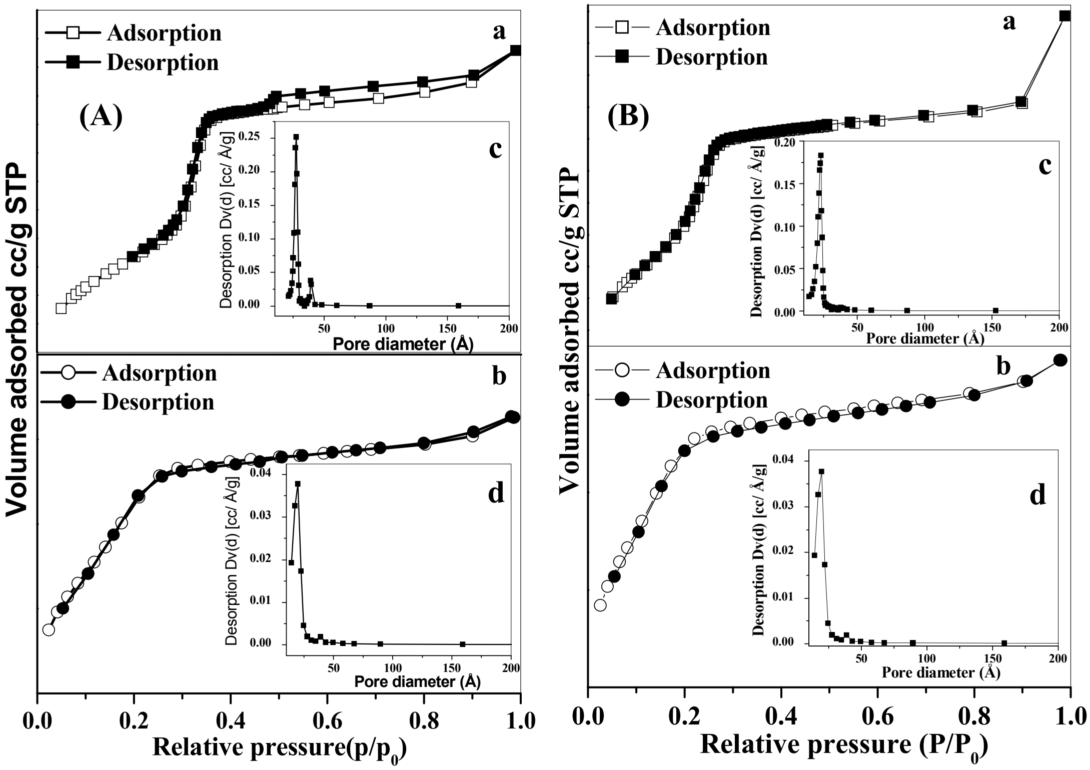

Fig. 4.4: *BET isotherm (A) a) MCM-41, b) 15 wt.%TPA/22.4 wt.%ZrO_2/MCM-41, B) a) MCM-48, b) 15 wt.%TPA/22.4 wt.%ZrO_2/MCM-48 and pore size distribution (Insight figure) c) MCM-41, d) 15 wt.%TPA/22.4 wt.%ZrO_2/MCM-41, B) c) MCM-48, d) 15 wt.%TPA/22.4 wt.%ZrO_2/MCM-48.*

BJH pore size distribution for 15 wt.%TPA/22.4 wt.%ZrO_2/MCM-41 and 15 wt.%TPA/22.4 wt.%ZrO_2/MCM-48 showed a mean value at 1.97 nm and 1.72 nm, respectively.

4.2.4. TEM

A Typical morphology of 15 wt.%TPA/22.4 wt.%ZrO_2/MCM-41 and 15 wt.%TPA/22.4 wt.%ZrO_2/MCM-48 with their parent MCM-41 and MCM-48 were observed through TEM as shown in Fig. 4.5. TEM of MCM-41 and 15 wt.%TPA/22.4 wt.%ZrO_2/MCM-41 [Fig. 4.5 (a-c)] showed a well-defined hexagonal array of unidirectional pore (space group *p6mm*) [1]. The 15 wt.%TPA/22.4 wt.%ZrO_2/MCM-48 sample retained the morphology and cubic-type ordering structure on the (110) cubic phase similar to those of pure MCM-48 [2] as shown in Fig. 4.5(d-e). TEM analysis also revealed that no obvious extra phases of TPA/ZrO_2 species were present outside the mesoporous channels.

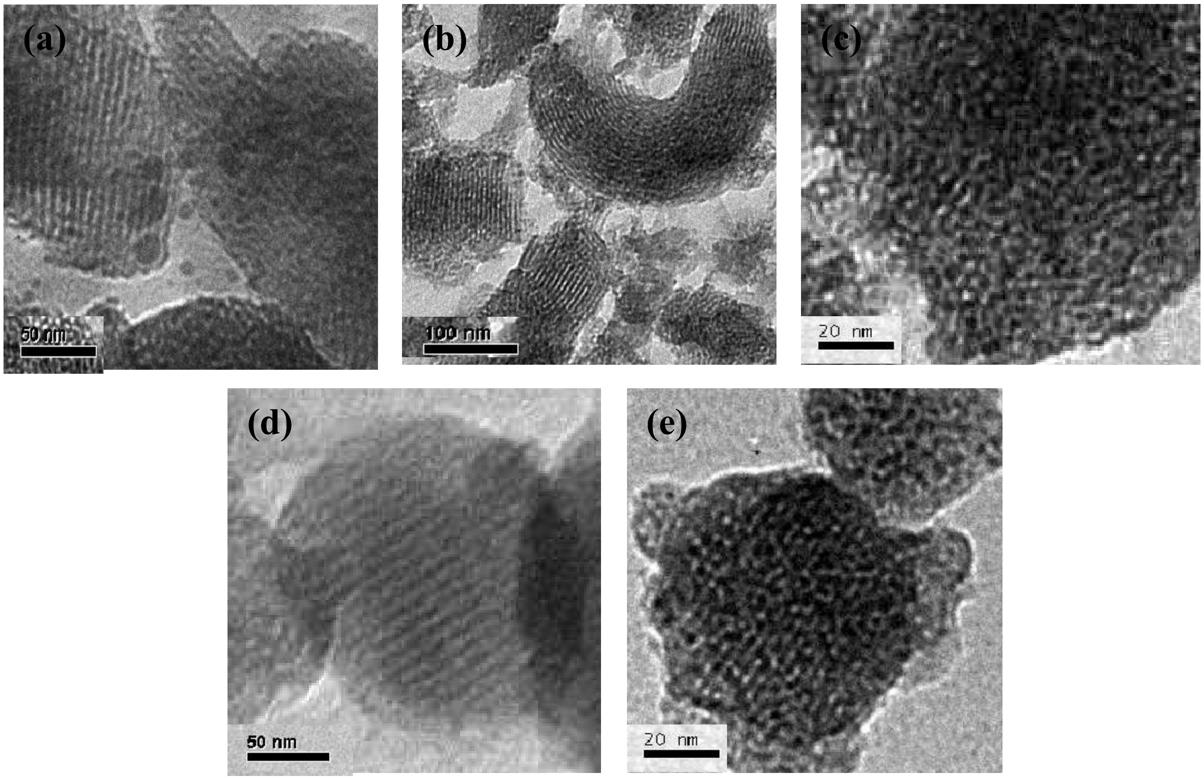

Fig. 4.5: *TEM of a) MCM-41, b) and c) 15 wt.%TPA/22.4 wt.%ZrO_2/MCM-41, d) MCM-48, e) 15 wt.%TPA/22.4 wt.%ZrO_2/MCM-48.*

4.2.5. FT-IR Spectroscopy

Pure silica exhibited IR bands at 1100 and 806 cm^{-1} and weak shoulder band at 974 cm^{-1} related to surface OH groups. While pure TPA showed characteristic peaks at 1079 cm^{-1} (P-O), 983 cm^{-1} ($W=O_t$), 893 cm^{-1} ($W-O_c-W$) and 810 cm^{-1} ($W-O_e-W$) [3]. The spectra of 15 wt.%TPA/22.4 wt.%ZrO_2/MCM-41, 15 wt.%TPA/22.4 wt.%ZrO_2/MCM-48 and 22.4 wt.%ZrO_2/MCM-41 catalysts are presented in Fig. 4.6. For TPA/ZrO_2/MS samples, two bands of TPA appeared around 983 and 888 cm^{-1}, while the bands around 1079 and 810 cm^{-1} overlapped with the strong bands of SiO_2. The spectra of ZrO_2 exhibit a wide band in the range 400-700 cm^{-1} extending up to 1150 cm^{-1} [4]. For samples containing lower TPA loading showed bands with low intensity as compared to bulk TPA spectra, which was due to masking of bands by wide bands of the support.

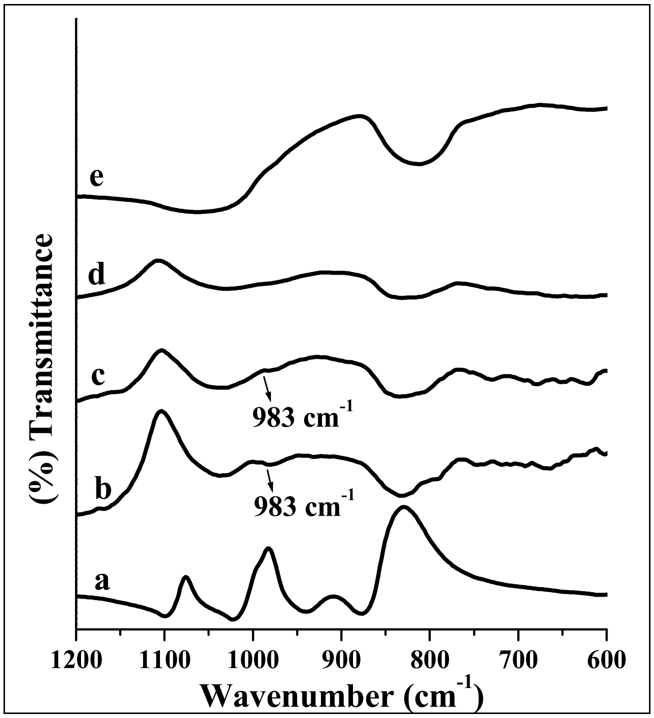

Fig. 4.6: *FT-IR DRS spectra of a) Pure TPA, b) 15 wt.%TPA/22.4 wt.%ZrO_2/MCM-41, c) 15 wt.%TPA/22.4 wt.%ZrO_2/MCM-48, d) 22.4 wt.%ZrO_2/MCM-41and e) Pure silica calcined at 1123 K.*

4.2.6. UV-Vis. spectroscopy

In case of the TPA/ZrO_2 modified mesoporous silica i.e. MCM-41 and MCM-48 samples, the ZrO_2 and $PW_{12}O_{40}{}^{3-}$ anion are the detectable species present. The UV-Vis. spectra of ZrO_2 showed a band at 275 nm [5], while HPA showed a band at 265 nm for TPA [6]. TPA modified samples showed only one band, as ZrO_2 band was overlapped with strong band of TPA (Fig. 4.7). Due to the oxygen-metal charge-transfer, the tungstophosphate anion $[PW_{12}O_{40}]^{3-}$ species showed TPA characteristic band at 263-265 nm (Fig. 4.7) in both 15 wt.%TPA/22.4 wt.%ZrO_2/MCM-41 and 15 wt.%TPA/22.4 wt.%ZrO_2/MCM-48 catalysts samples.

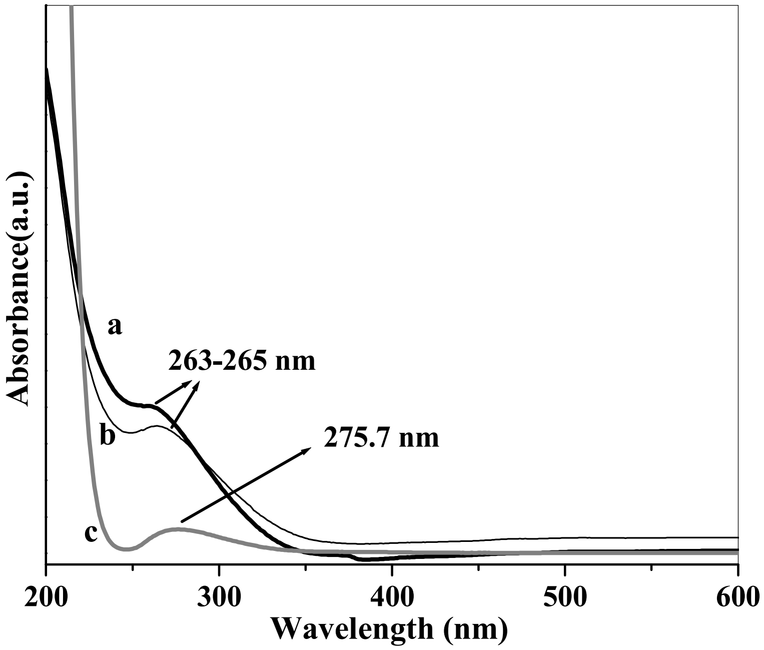

Fig. 4.7: *UV-Vis. spectra of a) 15 wt.%TPA/22.4 wt.%ZrO_2/MCM-41 and b) 15 wt.%TPA/22.4 wt.%ZrO_2/MCM-48 calcined at 1123 K and c) 22.4 wt.%ZrO_2/MCM-41.*

4.2.7. NMR spectroscopy

^{31}P CP-MAS NMR spectra for different loadings of TPA showed in Fig. 4.8 were consistent with XRD observations. Neat TPA showed ^{31}P peak at –12 ppm indicating intact Keggin structure according to literature [7]. Cross-polarization technique has been used because of the low concentration of 'P' in the catalyst systems since TPA/ZrO_2 was embedded inside the mesoporous channels. Hence, very broad spectrum with noisy signal were observed with all the catalysts, where the peak with maximum height was considered as major signal (Fig. 4.8). It was found that up to 15 wt.%TPA loading, peak at –12.2 ppm was observed as a major one. But on further increase in TPA loading i.e. for 30 wt.%TPA, it showed two peaks 50-50 % peak at –12.2 ppm and –24.8 ppm indicated that TPA decomposed partially into WO_3 crystallites. At 50 wt.%TPA, a new peak appeared at –30 ppm, typical of P-O-P linkages [8], which was associated with phosphorous oxide a by-product of decomposed TPA. These peak positions corresponded to the center of the maximum of the broad peaks. The broad line at –12 ppm was probably related to species formed by linking the Keggin unit to ZrO_2 support. Indeed, the first part of the interaction between TPA and ZrO_2 would be a protonation of surface hydroxyl groups of ZrO_2, leading to $(\equiv Zr\text{-}OH_2)_n^+[H_{3-n}W_{12}PO_{40}]^{n-3}$ species [9].

Upon heating water was removed, leading to a direct linkage between the polyanion (which has probably retained a structure similar to that of Keggin ion) and the support. Since our system deals with high temperature (1123 K), so extensive dehydroxylation of TPA was possible to give above species. When the polyanion decomposed, a new signal appeared at –30 ppm. As the support is heterogeneous, a distribution of surface species will be obtained. Since TPA/ZrO_2 dispersed uniformly in the MCM-41 channels, instead of sharp peak like bulk TPA, line broadening has been observed in our system. From literature reference [10], it was to be noted that the broadening and lowfield shift of ^{31}P NMR peak upon thermal dehydration is consistent with reported studies [11-14]. This was consistent with the fact that P was geometrically at the center of the Keggin anion, i.e. far away from the proton, and that the Keggin anion remained intact, even though some local distortions has occurred.

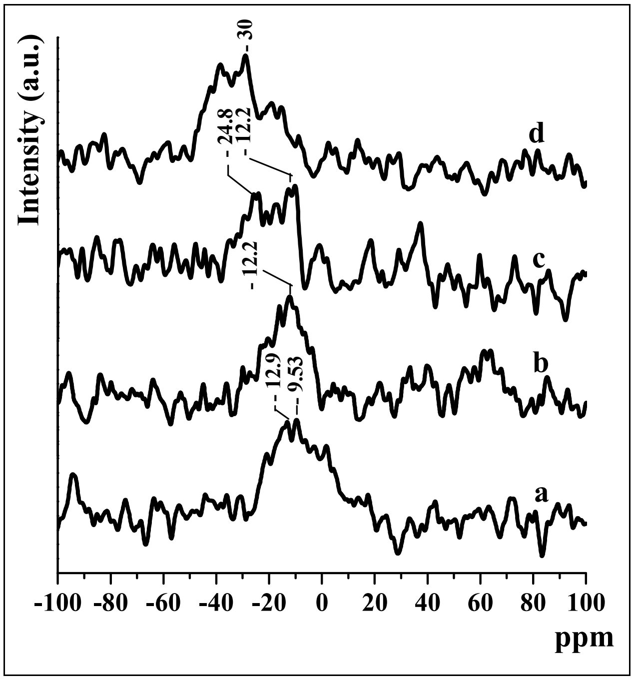

Fig. 4.8: *^{31}P CP-MAS NMR spectra of a) 5, b) 15, c) 30 and d) 50 wt.% TPA/22.4 wt.%ZrO_2/MCM-41 calcined at 1123 K.*

4.2.8. TPD of NH_3

TPD of NH_3 was performed to determine the total amount of acidity of the catalysts. TPD profiles of the 15 wt.%TPA with different wt.% of ZrO_2 over MCM-41 and different TPA loadings over 22.4 wt.%ZrO_2/MCM-41 are shown in Fig. 4.9 (A) and (B), respectively. All samples showed a broad desorption pattern indicating the surface acid strength was widely distributed.

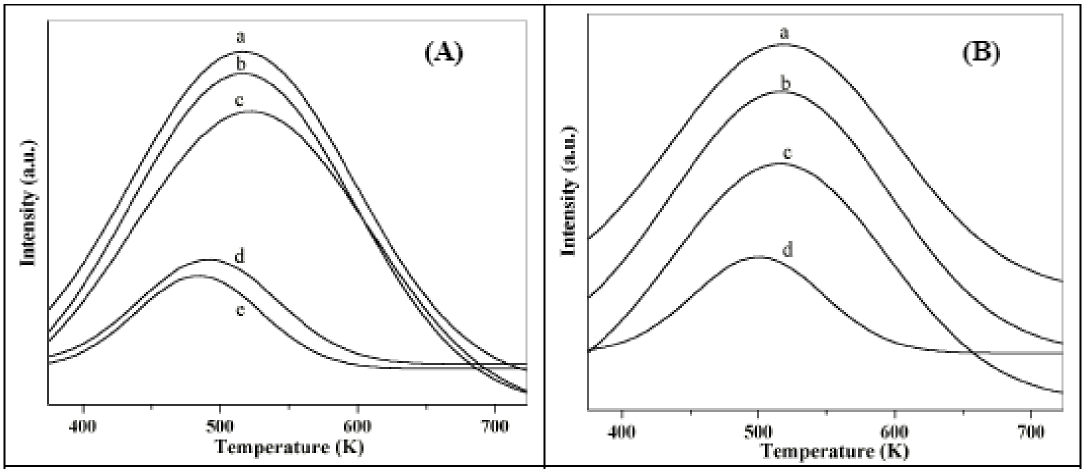

Fig. 4.9: *NH_3-TPD of (A) a) 15 wt.%TPA/10 wt.%ZrO_2/MCM-41, b) 15 wt.%TPA/22.4 wt.%ZrO_2/MCM-41, c) 15 wt.%TPA/30 wt.%ZrO_2/MCM-41, d) 15 wt.%TPA/50 wt.%ZrO_2/MCM-41, e) 15 wt.%TPA/70 wt.%ZrO_2/MCM-41 and (B) TPD of NH_3 of a) 5, b) 15, c) 30 and d) 50 wt.% 15 wt.%TPA/22.4 wt.%ZrO_2/MCM-41 calcined at 1123 K.*

4.2.9. FT-IR pyridine adsorption

Brønsted and Lewis acidity of the catalysts were distinguished by pyridine adsorption in situ FTIR spectroscopy. FTIR spectra of pyridine adsorbed on all of the catalysts were recorded from 373–673 K under a flow of N_2. At 373 K, important pyridine ring modes occurred at approximately 1609, 1575, 1489, and 1442 cm^{-1}. In addition to these vibrations, spectra showed two more peaks, around 1640 and at 1539 cm^{-1}. Pyridine molecules bonded to Lewis acid site absorbed at 1609 and 1442 cm^{-1}, whereas those responsible for Brønsted acid sites (pyridinium ion) showed absorbance at 1539 and 1640 cm^{-1}. Brønsted and Lewis acidity of the catalysts were distinguished by the technique of pyridine adsorption in-situ FT-IR spectroscopy and represented in Fig. 4.10.

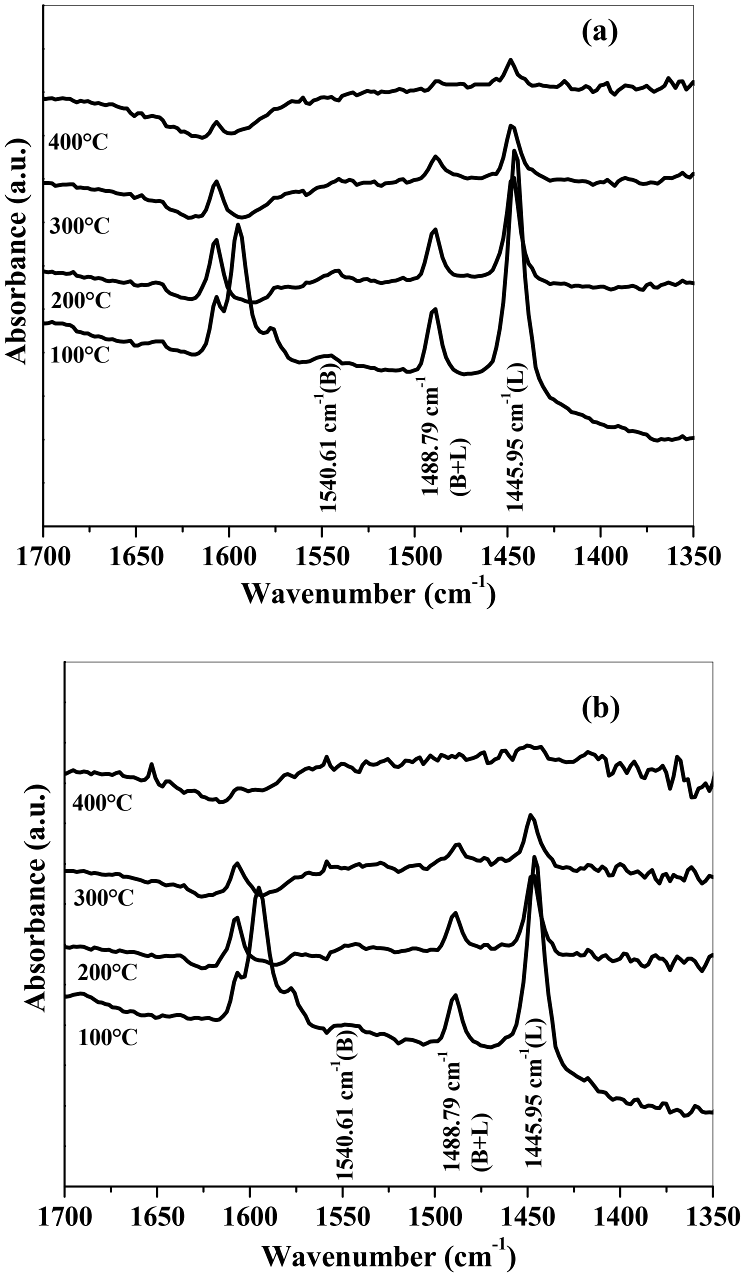

Fig. 4.10: *FT-IR Pyridine adsorption isotherms of a) 15 wt.%TPA/22.4 wt.%ZrO*$_2$*/MCM-41 and b) 15 wt.%TPA/22.4 wt.%ZrO*$_2$*/MCM-48 calcined at 1123 K.*

The Brønsted /Lewis (B/L) ratio was calculated from the IR absorbance intensities [15] of bands at 1539 (B) and 1442 (L) cm^{-1} of 15 wt.%TPA/22.4 wt.%ZrO$_2$/MCM-41 catalyst calcined at 1123 K and plotted against ZrO_2 (wt.%) and TPA (wt.%) loading as shown in Fig. 4.11 (A) and (B), respectively.

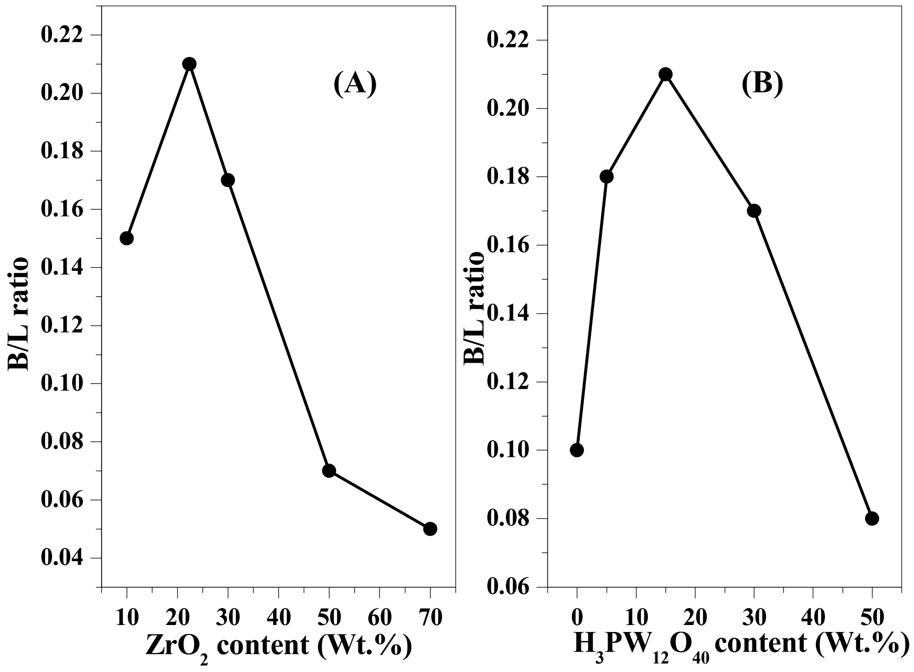

Fig. 4.11: *(A) B/L ratio Vs ZrO_2 content (wt.%) for 15 wt.%TPA/different wt.%ZrO_2/MCM-41 and (B) B/L ratio Vs $H_3PW_{12}O_{40}$ content (wt.%) for different wt.%TPA/22.4 wt.%ZrO_2/MCM-41 calcined at 1123 K.*

It was found that with increase in ZrO_2 content upto 22.4 wt.%, B/L ratio increased and on further increase in ZrO_2 it decreased. As reported [16], the threshold value for monolayer dispersion of ZrO_2 over MCM-41 was 22.4 %, which was determined according to the method reported earlier [17]. XPS analysis has been used to investigate the interaction between the guest (ZrO_2) and the host (MCM-41) and was found that ZrO_2 was more likely to interact with MCM-41 by hydrogen bonds involving Si-O-H groups of the MCM-41 with zirconium atoms in ZrO_2. Due to such interaction at monolayer coverage free hydrogen was available from MCM-41 support. While below and above 22.4 wt.%ZrO_2 loading, this interaction was not that predominant due to less ZrO_2 content and also due to multilayer formation in both the mesoporous supports. Similarly, B/L ratio increased with TPA (wt.%) loading upto 15 wt.% and on further increase it decreased. Thus, the sample with 15 wt.%TPA/22.4 wt.%ZrO_2/MCM-41 has the highest acidity, which was due to the monolayer coverage of TPA on ZrO_2 finely dispersed in mesopores of MCM-41. The decrease in B/L ratio and the loss in catalytic activity were due to the decomposition of TPA, which exceeds monolayer coverage at higher TPA loading.

The genesis of Brønsted acidity of 15 wt.%TPA/22.4 wt.%ZrO_2/MCM-41 calcined at 1123 K could be explained as, during calcination dehydroxylation of support takes place and in this process interaction of TPA with support would be partially weakened to give free H^+ ions (Brønsted acid sites). Assuming that some TPA protons react with (OH) groups in hydrated ZrO_2, it would be reasonable to expect that some terminal W=O bonds of TPA might react with partially dehydroxylated $(Zr\ (\text{-}O)_3)^+$ species to form anchored TPA species, e.g. the formation of Zr-O-W bonds. These TPA species would exert an electron withdrawing effect on surface Zr^{4+} cations, making them to behave as strong Lewis acid sites. Keeping in view of all the above facts, we hypothesize that the interaction between TPA and ZrO_2 might be weakened till monolayer coverage (15 wt.% and 1123 K) so that TPA protons are free for reactions to proceed and thereby increasing Brønsted acidity and the total acidity (due to ZrO_2 Lewis acidity increases). While on further increase in TPA loading, might be due to multilayer formation, bulk properties of TPA would be more predominant, causing destruction of TPA to give WO_3 crystallites (partially proved by NMR). The interaction between TPA and ZrO_2 within the allowed phase transformation was responsible for the high acidity.

4.3. ACETYLATION OF VERATROLE

4.3.1. Introduction

Acetoveratrone (3’, 4’-dimethoxyacetophenone) is produced from veratrole using mineral acid catalysts, which is used in the synthesis of papaverine (1-(3,4-dimethoxybenzyl)-6,7-dimethoxyisoquinoline), an opium-alkaloid antispasmodic. Acetoveratrone is also synthesized by using hafnium (IV) triflate [18], scandium triflate [19] and hafnium triflate as catalysts in presence of lithium perchlorate nitromethane system [20] and carboxylic acid or trisubstituted silyl carboxylates in presence of trifluoromethyl benzoic acid anhydride [21]. Zeolite HY was found to be more active than Hß [22-25] in the above reaction. Cation-exchanged clays were also tested for this reaction [26]. HPA supported over hexagonal mesoporous silica (HMS) in presence of 1,2-dichloroethane as a solvent is used for the synthesis of acetoveratrone [27]. However, there is no report on the use of supported HPA catalysts for acetylation of veratrole in solvent free conditions. TPA/ZrO_2/MS are the new catalyst systems, which provides high surface area, large pore volume, higher acidity and high thermal stability. Hence, it is the purpose of our study to develop such catalyst system, needed for acetylation of veratrole under solvent free conditions.

4.3.2. Results and discussion

Acetylation of veratrole with Ac_2O catalyzed by 15 wt.%TPA/22.4 wt.%ZrO_2/MCM-41 calcined at 1123 K under reaction conditions studied gave Acetoveratrone (3', 4'-dimethoxyacetophenone) as shown in the Scheme-4.1.

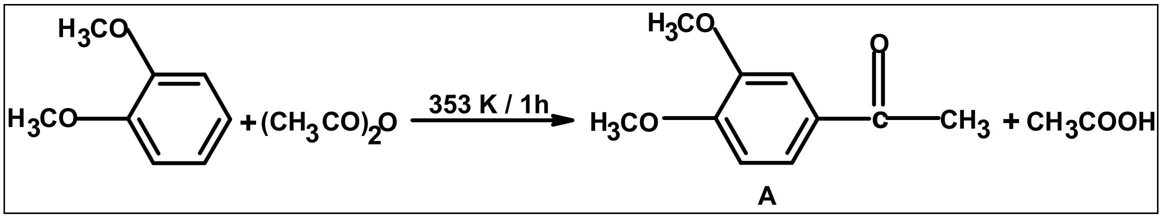

Scheme 4.1: *Acetylation of Veratrole by Ac_2O*

It is known that the acetylation reaction proceeds through an acylium intermediate H_3CCO^+, generated from the adsorption of the acylating agent onto the Brønsted acidic sites of the catalyst, which adds to aromatic ring via electrophilic substitution to give the acetylated product.

4.3.2.1. Catalytic activitivities of different catalysts

Acetylation of veratrole by Ac_2O was conducted using different TPA loaded (5-50 wt.%) catalysts to know the effect of TPA loading on the conversion of Ac_2O and the results are presented in Table 4.1. Also, turnover frequencies (TOF) and rate constants have been given for the catalysts with different TPA (%), ZrO_2 (%) loadings and as well as for different supports (Table 4.1). It is seen that MCM-41 is better than MCM-48 support. As, 15 wt.%TPA/22.4 wt.%ZrO_2/MCM-48 has large surface area with less pore volume and pore diameter as compared to 15 wt.%TPA/22.4 wt.%ZrO_2/MCM-41 calcined at 1123 K showed less activity and this could be due to the difference in their pore structures and preferred blocking of pores in case of MCM-48. MCM-41 has a hexagonal array of unidirectional pores (space group *p6mm*), while MCM-48 has cubic pore system (space group *Ia3d*). In addition to this, MCM-48 material possess a bicontinuous structure centered on the gyroid minimal surface that divided available pore space into two nonintersecting subvolumes. Hence, TPA/ZrO_2 might get dispersed in MCM-41 channels more uniformly as compared to MCM-48. From Table 4.1, it shows that 15 wt.%TPA/22.4 wt.%ZrO_2/MCM-41 shows highest Ac_2O (%) conversion and maximum rate constant as compared to other catalyst systems. Similarly, 22.4 wt.%ZrO_2 gave maximum Ac_2O conversion among different ZrO_2 (%) loaded catalysts. However, the neat 15 wt.%TPA/ZrO_2 gave low catalytic activity in acetylation of veratrole with a conversion of Ac_2O (10.9 %), which is at least four times less than 15 wt.%TPA/22.4 wt.%ZrO_2/MCM-41 calcined at 1123 K under the same reaction conditions. While 3.36 wt.%TPA/ZrO_2 shows 2.5 times less catalytic activity as compared to 15 wt.%TPA/22.4 wt.%ZrO_2/MCM-41. The presence of TPA has significant effect on the catalytic activities. 15 wt.%TPA loaded on 22.4 wt.%ZrO_2/MCM-41 has shown two-fold increase in catalytic activity as compared to 22.4 wt.%ZrO_2/MCM-41 (Table 4.1). While, Table 4.1 also shows the total acidity of TPA/ZrO_2 with different supports including unsupported catalysts. Among these, 15 wt.%TPA/22.4 wt.%ZrO_2/MCM-41 was found to have the highest acidity and thereby highest catalytic activity in acetylation of veratrole by Ac_2O. The NH_3-TPD data for different TPA (%) loaded catalysts suggested that the total acidity of the catalysts increased up to 15 wt.%TPA loading and decreased with further increase.

The catalytic activities of H-Y and Zn (II)-exchanged clay catalysts were evaluated in the acetylation of veratrole with Ac_2O under identical reaction conditions for comparison with the catalytic activity of 15 wt.%TPA/22.4 wt.%ZrO_2/MCM-41 catalyst.

Table 4.1: Physicochemical properties of the catalysts and their catalytic activities in acetylation of veratrole

Catalyst	S_{BET} (m^2/g)	Pore volume (cm^3/g)	Pore diameter (Å)	Total Acidity (mmol g^{-1})	Ac_2O ,%Conv. (TOF)**	Rate constant x $10^{-5}(s^{-1})$
MCM-41*	1155	0.88	30.5	nil	nil	nil
22.4 wt.%ZrO_2/MCM-41	589	0.38	27.7	0.24	20.5	6.4
15wt.%TPA/10 wt.%ZrO_2/MCM-41	573	0.33	23.2	0.26	28.4(0.09)	9.3
15wt.%TPA/22.4 wt.%ZrO_2/MCM-41	516	0.28	19.7	0.33	43.9(0.15)	16.1
15wt.%TPA/30 wt.%ZrO_2/MCM-41	491	0.24	18.7	0.26	31.7(0.11)	10.6
15wt.%TPA/50 wt.%ZrO_2/MCM-41	479	0.20	17.8	0.18	10.6(0.04)	3.1
15wt.%TPA/70 wt.%ZrO_2/MCM-41	402	0.13	15.8	0.15	5.1(0.02)	1.5
5wt.%TPA/22.4 wt.%ZrO_2/MCM-41	533	0.32	21.7	0.27	32.4(0.32)	10.9
30wt.%TPA/22.4 wt.%ZrO_2/MCM-41	499	0.22	17.9	0.24	30.5(0.05)	10.1
50wt.%TPA/22.4 wt.%ZrO_2/MCM-41	481	0.20	17.2	0.19	19.2(0.02)	5.9
MCM-48*	1096	0.71	26.1	nil	nil	nil
22.4 wt.%ZrO_2/MCM-48	612	0.62	24.8	0.10	11.1	3.3
15wt.%TPA/22.4 wt.%ZrO_2/MCM-48	540	0.22	17.2	0.25	27.1(0.09)	8.8
15wt.%TPA/ZrO_2	11	-	-	0.02	10.9(0.01)	3.2
3.36 wt.%TPA/MCM-41	479	0.19	27.1	0.18	17.5(0.06)	5.3

**Except these entries all other catalysts were calcined at 1123 K in air.*

***TOF is calculated by considering three protons per Keggin unit (mol. $mol^{-1}H^{+}.s^{-1}$)(Reaction conditions: temp. = 353 K, veratrole/Ac_2O molar ratio = 5, catalyst wt.=0.09g (3 wt.% of total reaction mixture), time = 1 h).*

The total acidity (mmol/g) and activities expressed in terms of Ac_2O conversion (wt. %) are presented in Table 4.2.

Table 4.2: Acetylation of veratrole with Ac_2O: A comparison study

Catalyst	Total Acidity (mmol g^{-1})	Ac_2O conversion (mol. %)	TOF (mol. $mol^{-1}H^{+}{}_{or}$ $Zn^{2+}.s^{-1}$)
H-Y	2.25	40.0	0.064
Zn^{2+}-montmorillonite K-10 clay	0.67	20.3	0.0039
15 wt.%TPA/22.4 wt.%ZrO_2/SBA-15	0.33	43.9	0.15

Reaction conditions: temperature = 353 K, veratrole/Ac_2O molar ratio = 5, catalyst =15 wt.%TPA/22.4 wt.%ZrO_2/MCM-41 (0.09g, 3 wt.% of total reaction mixture), time = 1 h.

Among the catalysts, H-Y showed comparable catalytic activity with 15 wt.%TPA/22.4 wt.%ZrO_2/MCM-41 due to highest acidity with large pores tri-dimensional zeolite network with supercages. For zeolite, the number of active protons was taken to be equivalent to the Al content [28]. Zn^{2+}- exchanged clay showed lowest TOF (which is expressed per active metal center i.e. Zn^{2+}) under these reaction conditions, which may be due to the diffusion limitations. But, 15 wt.%TPA/22.4 wt.%ZrO_2/MCM-41 catalyst calcined at 1123 K, shows highest catalytic activity in terms of TOF as 0.15 s^{-1}, with three accessible H^+ per Keggin anion [29] was chosen for further investigations on its catalytic performance in the veratrole acetylation with Ac_2O.

4.3.2.2. Effect of reaction parameters

The effect of catalyst concentration on the conversion of Ac_2O in veratrole acetylation was studied with 15 wt.%TPA/22.4 wt.%ZrO_2/MCM-41 calcined at 1123 K by varying catalyst concentration from 1 to 5 (wt.%) of total reaction mixture. Conversion of Ac_2O increased from 20.8 to 56.7 % with increase in catalyst concentration as shown in Fig. 4.12 (a).

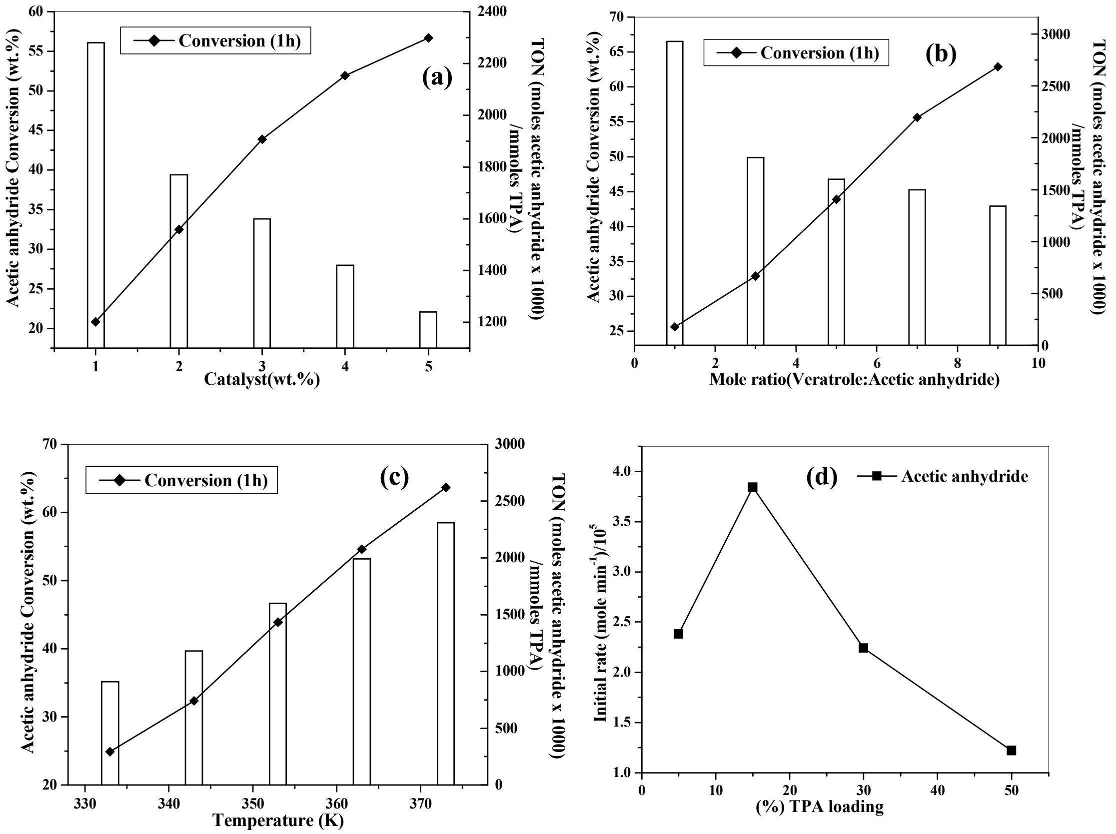

Fig. 4.12: *(a) Effect of catalyst weight on veratrole acetylation. (Reaction conditions: temperature = 353 K; veratrole/Ac_2O molar ratio = 5 and time = 1 h).*
(b) Effect of molar ratio on veratrole acetylation. (Reaction conditions: temperature = 353K, catalyst wt.=0.09g (3 wt.% of total reaction mixture), time = 1 h).
(c)Effect of reaction temperature on veratrole acetylation. (Reaction conditions: veratrole/Ac_2O molar ratio = 5, catalyst wt.=0.09g (3 wt.% of total reaction mixture), time= 1 h).
(d) Initial rate Vs different TPA (%) loading over 22.4 wt.%ZrO_2/MCM-41 calcined at 1123 K. (Reaction conditions: temperature = 353 K; veratrole/Ac_2O molar ratio = 5, catalyst wt.=0.09g (3 wt.% of total reaction mixture), t = 20 min.)

The effect of veratrole to Ac_2O mole ratio on Ac_2O conversion was studied with 15 wt.%TPA/22.4 wt.%ZrO_2/MCM-41 catalyst calcined at 1123 K by varying veratrole/Ac_2O molar ratio in the range 1-9, by keeping other conditions same as shown in Fig. 4.12 (b). The conversion of Ac_2O increased from 25.6 to 62.9 % with increase in veratrole/Ac_2O molar ratio up to 9.

The effect of temperature on conversion of Ac_2O was studied in the temperature range 333-373 K and the results are shown in Fig. 4.12 (c). The turn over number (TON) and conversion of Ac_2O increased substantially from 24.9 to 63.7 with increase in temperature.

Here, initial rates w.r.t. conversion of Ac_2O for different TPA (%) loaded over 22.4 wt.%ZrO_2/MCM-41 catalysts are shown in Fig. 4.12 (d). It is seen that initial rates (expressed in mole min^{-1}) increased with increase in TPA loading up to 15 wt.% and decreased with further increase. Among the catalysts, 15 wt.%TPA/22.4 wt.%ZrO_2/MCM-41 has the highest acidity and hence gave the highest activity.

4.3.2.3. Kinetic study

The rate data for the acetylation of veratrole by Ac_2O in excess of veratrole over 15 wt.%TPA/22.4 wt.%ZrO_2/MCM-41 catalysts could be fitted well to a pseudo-first order rate law. Hence, the standard equations for a first-order series reaction $C_A/C_{Ao} = e^{-K}{}_1t$ has been used for the determination of rate constant, where C_A and C_{Ao} are the concentration of Ac_2O at initial time and at time t, respectively. The rate constants calculated for different catalysts are presented in Table 4.1. At one particular temperature, first-order rate constants were calculated at different reaction time and then the constant values of 'k_1' showed that the acetylation of veratrole is a first-order reaction. Energy of activation of the reaction was evaluated graphically. The activation energy (E_a) was obtained from a plot of –ln k_1 against 1/T (Fig. 4.13). A linear plot with negative slope equivalent to (Ea/R), which gave an activation energy of 7.89 k cal mol^{-1}.

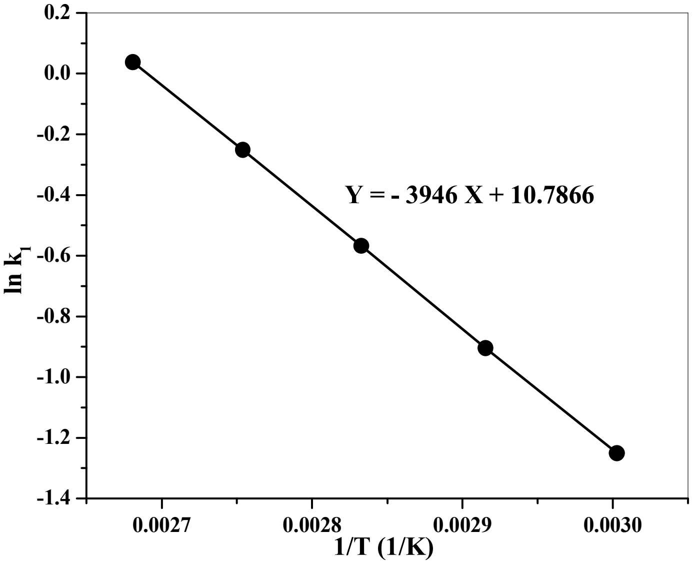

Fig. 4.13: *Arrhenius plot of ln k_1 Vs 1/T.*

The recyclability of the catalyst is given in Table no. 4.3

Table 4.3: Recycling of catalysts in acetylation of veratrole

Cycle	Ac_2O conv. (wt.%)	Acetoveratrone selectivity (%)	TON
Fresh	43.9	100	1596
I^{st}	43.6	100	1584
II^{nd}	43.0	100	1566

Reaction conditions: temperature = 353 K, veratrole/Ac_2O molar ratio = 5, catalyst wt.=0.09g (3wt.% of total reaction mixture), time = 1 h.
TON (Turnover number) = (mole Ac_2O converted/ mmole TPA) x 1000.

4.3.3. Conclusions

Acetylation of veratrole with Ac_2O was carried out over 15 wt.%TPA/22.4 wt.%ZrO_2/MCM-41 catalyst calcined at 1123 K in liquid phase conditions under N_2 atmosphere. The catalyst was fully characterized and the stability of TPA on the support has been established satisfactorily. The 15 wt.%TPA/22.4 wt.%ZrO_2/MCM-41 catalyst gave highest catalytic activity expressed in terms of conversion of Ac_2O at 353 K with veratrole: Ac_2O molar ratio 5 and 3 wt.% catalyst concentration (of the total reaction mixture) was maximum (43.9 %) and 100% selectivity for acetoveratrone (3’, 4’-dimethoxyacetophenone). The rate constant and the activation energy for intrinsic kinetics on the surfaces for the above reaction have been evaluated.

4.4. REFERENCES

1. C. Cong-Yan, L. Hong-Xin, M. E. Davis, Micropor. Mater., 2 (1993) 17.
2. R. Schmidt, M. Stöcker, M. D. Akporiaye, E. H. Tørstad, A. Olsen, Micropor. Mater., 5 (1995) 1.
3. W. Kuang, A. Rives, M. Fournier, R. Hubaut, Appl. Catal. A: General, 250 (2003) 221.
4. L. Pizzio, P. Vázquez, C. Cáceres, M. Blanco, Catal. Lett., 4 (2001) 77
5. A. V. Emeline, G. V. Kataeva, A. S. Litke, A. V. Rudakova, V. K. Ryabchuk, N. Serpone, Langmuir, 14 (1998) 5011.
6. L. Pizzio, P. Vázquez, C. Cáceres, M. Blanco, Catal. Lett., 4 (2001) 77.
7. M. Misono, Chem. Commun., 2001,1141.
8. E. Lopez-Salinas, J. G. Hernandez-Corez, I. Schifter, E. Torres-Garcia, J. Navarrete, A. Gutierrez-Carillo, T. Lopez, P. Lottici, D. Bersani, Appl. Catal. A-General, 193 (2000) 215.
9. Y. Wu, X. Ye, X. Yang, X. Wang, W. Chu, Y. Hu, Ind. Eng. Chem. Res., 35 (1996) 2546.
10. N. Essayem, Y. Y. Tong1, H. Jobic, J. C. Vedrine, Appl. Catal. A: General, 194 – 195 (2000) 109.
11. R. I. Maksimovskaya, Kinet. Katal., 36 (1995) 836.
12. Y. Kand, K.Y. Lee, S. Nakata, S. Asaoka, M. Misono, Chem. Lett., (1988) 139.
13. Y. Hirano, K. Inumaru, T. Okuhara, M. Misono, Chem. Lett., (1996) 1111.
14. S. Uchida, K. Inumaru, J. M. Dereppe, M. Misono, Chem. Lett., (1998) 643.
15. B. H. Davis, R. A. Keogh, S. Alerasool, D. J. Zalewski, D. E. Day, P. K. Doolin, J. Catal., 183 (1999) 45.
16. J. He, X. Duan, C. Li, Materials Chem. and Phys., 71 (2001) 221.
17. Y. Zong, X. M. Pan, L. Y. Duan, Y.C. Xie, Chinese J. Catal., 18 (1997) 321.
18. A. Kawada, S. Mitamura, S. Kobayashi, Syn. Lett.,7 (1994) 545.
19. I. Hachiya, M. Moriwaki, S. Kobayashi, Tet. Lett., 36 (1995) 409.
20. I. Hachiya, M. Moriwaki, S. Kobayashi, Bull. Chem. Soc. Jpn., 68 (1995) 2053.
21. K. Suzuki, M. Mukoyama, Jpn. Pat. , 06 145 092, 1994.
22. M. Spagnol, L. Gilbert, D. Alby, Ind. Chem. Libr., 8 (1996) 29.

23. T. Raja, A. P. Singh, A. V. Ramaswamy, A. Finiels, P. Moreau, Appl. Catal. A: General, 211 (2001) 31.
24. C. Guignard, V. Pédron, F. Richard, R. Jacquat, M. Spagnol, J. M. Coustard, G. Pérot, Appl. Catal. A: General, 234 (2002) 79.
25. P. Moreau, A. Finiels, P. Meric, J. Mol. Catal. A: Chem., 154 (2000) 185.
26. B. M. Choudary, M. Sateesh, M. L. Kantam, K.V. Ram Prasad, Appl. Catal. A: General, 171 (1998) 155.
27. G. D.Yadav, H. G. Manyar, Micropor. Mesopor. Mater., 63 (2003) 85.
28. J. Kaur, K. Griffin, B. Harrison, I. V. Kozhevnikov, J. Catal., 208 (2002) 448.
29. D. G. Barton, S. L. Soled, G. D. Meitzner, G. A. Fuentes, E. Iglesia, J. Catal., 181 (1999) 57.

CHAPTER – 5

ZIRCONIA SUPPORTED TPA IN SBA-15

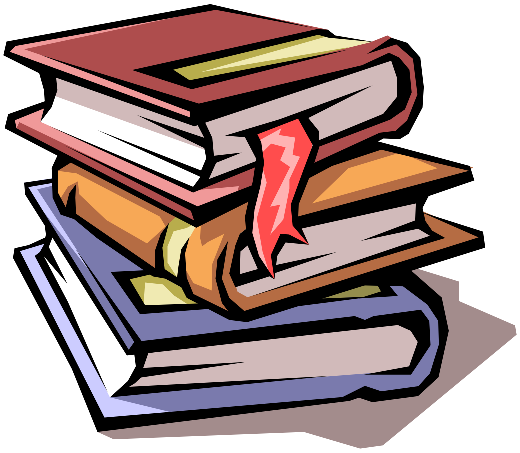

5. ZIRCONIA SUPPORTED TPA IN SBA-15

5.1. INTRODUCTION

This section presents the characterization of TPA over ZrO_2 dispersed uniformly in mesoporous silica (MS) channels of MCM-41, MCM-48 and SBA-15. Catalysts with different TPA loadings (5 to 90 wt.%) on 22.4 wt.%ZrO_2/MCM-41 and 15 wt.%TPA on different ZrO_2 loadings (10-70 wt.%)/MCM-41 were prepared and calcined at 1123 K. Also, 15 wt.%TPA/22.4 wt.%ZrO_2/ SBA-15 catalysts calcined in the range 923 to 1273 K were prepared. These catalysts were screened for their catalytic activities in the liquid phase benzylation of phenol with BA and acetylation of veratrole and other aromatic substates with Ac_2O.

5.2. CHARACTERIZATION-RESULTS AND DISCUSSION

5.2.1. Elemental analysis

The ratio of P: W (1: 12) in 15 wt.%TPA/22.4 wt.%ZrO_2/MCM-41 corresponding to a Keggin unit was estimated by XRF analysis as (1: 12.13) and by ICP-OES analysis as (1:12.07).

5.2.2. XRD

The X-ray powder diffraction patterns of the catalysts with different (%) TPA loadings calcined at 1123 K are shown in Fig. 5.1 (a), and those of 15 wt.% TPA/22.4 wt.% ZrO_2/SBA-15 calcined at different calcination temperatures are shown in Fig. 5.1 (b). The small angle XRD patterns of TPA/ZrO_2 modified samples were typical of hexagonally ordered mesoporous materials, with one sharp peak indexed as (100) and two smaller peaks indexed as (110) and (200), typical of hexagonal (*p6mm*) of parent SBA-15.

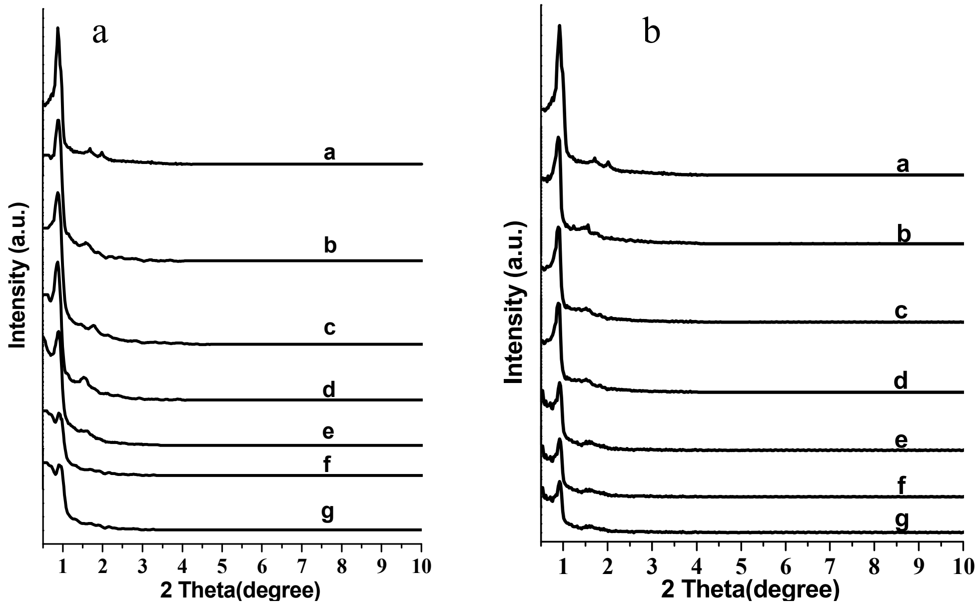

Fig. 5.1: *(a) Low angle XRD: a, SBA-15, TPA/22.4 wt% ZrO_2/SBA-15 with: b, 5; c, 15; d, 30; e, 50; f, 70; and g, 90 wt% TPA loading and calcined at 1123 K, including insight wide-angle XRD, respectively. (b) Low angle XRD: a, SBA-15, 15 wt% TPA/22.4 wt% ZrO_2/SBA-15 calcined at: b, 923; c, 1023; d, 1123; e, 1173; f, 1223; and g, 1273 K; including insight wide-angle XRD, respectively.*

Fig. 5.1 (a) shows that the mesoporous structure remained intact up to 50 wt.% TPA loading and after this it started loosing mesoporosity. In addition, the 15 wt.% TPA-loaded sample showed intact mesoporosity even after calcination up to 1273 K. Further the added TPA stabilized the tetragonal phase of ZrO_2. Such stabilization of the phase composition desired for specific applications in the presence of other mesoporous oxides prevented the particles from growing larger than the pore sizes. XRD patterns displayed three well-defined peaks characteristic of tetragonal ZrO_2; these can be indexed as (111), (202), and (131). Fig.5.2 (a) shows the wide-angle XRD patterns of the catalysts with different (%) TPA loadings calcined at 1123 K, wherein XRD patterns of pure TPA is compared with all modified samples. Wide-angle XRD patterns show three well-defined peaks characteristics of tetragonal ZrO_2 (t-ZrO_2) i.e. $2\theta \sim 30$, 50 and 60° phase, which could be indexed as (111), (202) and (131). Wide-angle XRD of TPA over 22.4 wt.% ZrO_2/SBA-15 shows monolayer coverage up to 15 wt.% loading and above this, it started decomposing into WO_3 ($2\theta \sim 23.12$, 23.59, and 24.38°) crystalline peaks as seen in Fig. 5.2(a). Similarly, 15 wt.% TPA/22.4 wt.% ZrO_2/SBA-15 showed monolayer coverage up to 1123 K calcination temperature. However, above 1123 K, it showed decomposition of TPA into WO_3 crystallites [Fig. 5.2 (b)]. As for bulk ZrO_2, crystallization of the amorphous phase to the metastable tetragonal phase typically occurred in the range 673–773 K, but after impregnating over SBA-15, the stabilization of transition of phases shifted to 923 K.

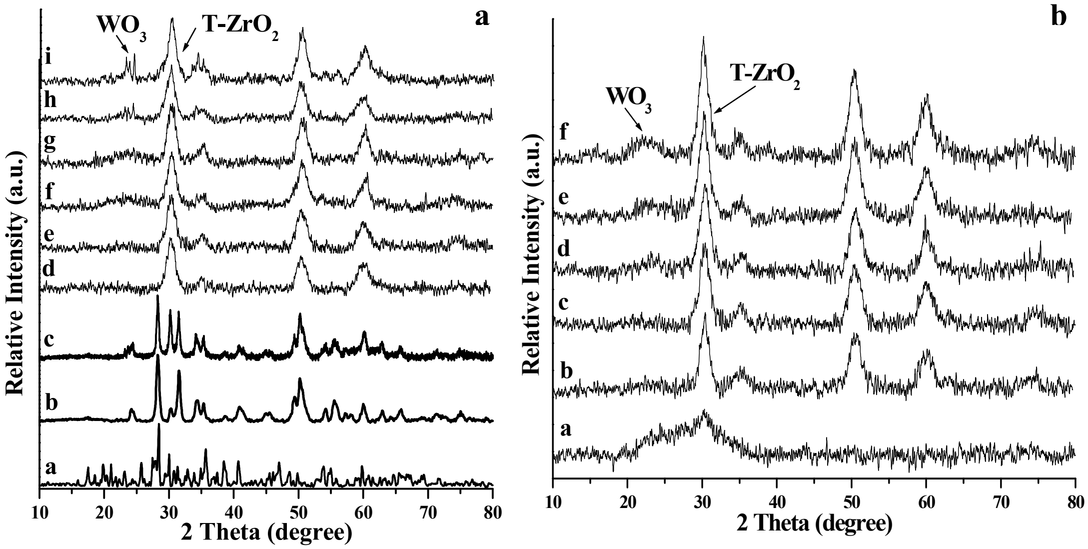

Fig. 5.2: *XRD patterns of (a) a) neat TPA, b) ZrO_2, c) 15 wt.%TPA/ZrO_2, d) 5, e) 15, f) 30, g) 50, h) 70 and i) 90 wt.% catalysts calcined at 1123 K and (b) 15 wt.% catalyst calcined at a) 923, b) 1023, c) 1123, d) 1173, e) 1223, and f) 1273 K.*

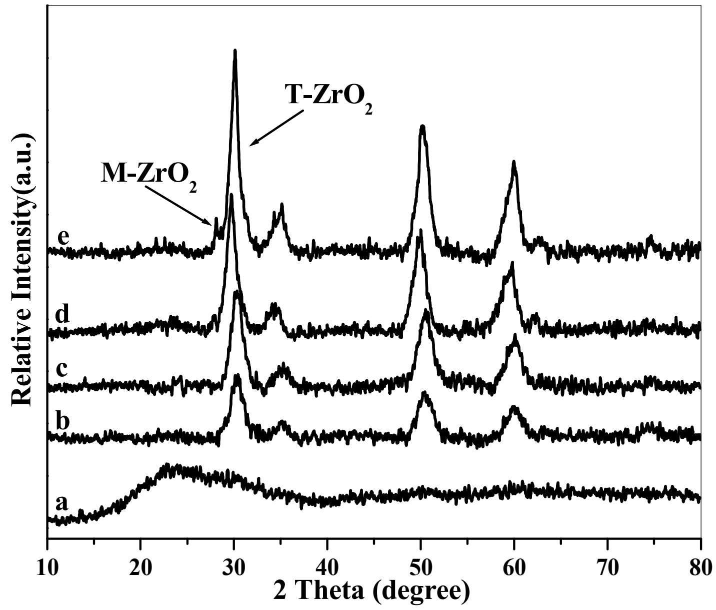

Fig. 5.3: *XRD patterns of 15 wt.% TPA over a) 10, b) 22.4, c) 30, d) 50, and e) 70 wt.% ZrO$_2$/SBA-15 catalysts calcined at 1123 K.*

The XRD patterns of 15 wt.%TPA/ 22.4 wt.%ZrO$_2$/SBA-15 with different ZrO$_2$ (%) loading over SBA-15 shows that, monoclinic ZrO$_2$ (m-ZrO$_2$, 2θ ~ 28°) phase also appeared when the ZrO$_2$/SBA-15 wt. ratio was higher than 0.5.

5.2.3. Sorption study

The textural properties of plain and modified SBA-15 with different loadings of TPA (wt.%)/22.4 wt.% ZrO$_2$ are presented in Table 5.1. It is seen that the surface area, pore size, and pore volume of modified SBA-15 decreased when compared with parent SBA-15. This indicates that TPA/ZrO$_2$ was well dispersed inside the pores of mesoporous channels. The adsorption isotherms and BJH pore size distributions of 15 wt.% TPA/22.4 wt.% ZrO$_2$/SBA-15 and parent SBA-15 are shown in Fig. 5.4.

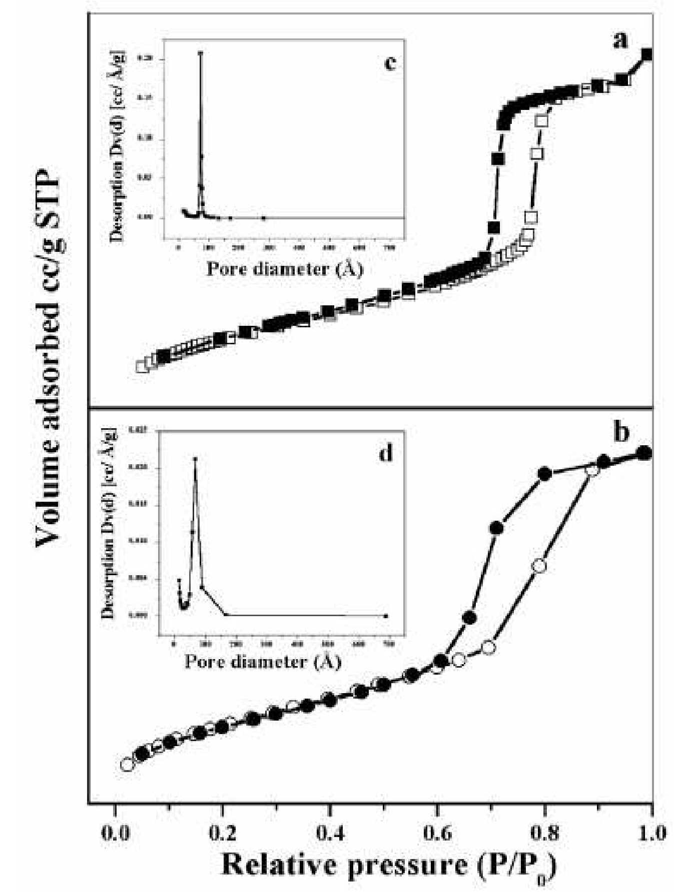

Fig. 5.4: *Nitrogen adsorption isotherms with insight figure of (pore size distribution) of (a) calcined SBA-15 (c) and (b) 15 wt.% TPA/22.4 wt.% ZrO$_2$/SBA-15 (d) calcined at 1123 K.*

It is seen from Fig. 5.4 that the mesostructure was retained after loading of 15 wt.% TPA/22.4 wt.% ZrO$_2$ into SBA-15 even after calcination up to 1123 K. However, the surface area of the samples up to 50 wt.% TPA loading were still >300 m^2 g^{-1}, and pore volume was in the range of 0.53– 0.63 cm^3 g^{-1} (Table 5.1), which are sufficient for catalytic functions. Though the surface areas of modified MCM-41 and MCM-48 were greater than those of corresponding modified SBA-15 samples, their catalytic activities were lower compared with those of 15 wt.% TPA/22.4 wt.% ZrO$_2$/SBA-15 (Table 5.1) due to narrow pore diameters. Also, the surface area and pore size of 15 wt.% TPA/22.4 wt.% ZrO$_2$/SBA-15 decreased with increasing calcinations temperature (Table 5.1). The neat 15 wt.% TPA/ZrO$_2$ calcined at 1123 K had low surface area due to sintering of ZrO$_2$ support, resulting in the formation of larger particles and low acidity due to the decomposition of TPA into WO_3 and other corresponding oxides.

Table 5.1: Physicochemical properties of the catalysts and their catalytic activities

Sample	Surface area (m^2g^{-1})	Pore volume (cm^3g^{-1})	Pore diameter (Å)	Total Acidity ($mmolg^{-1}$)	B/L	BA Conv., (%)
SBA-15	929	1.36	73.3	-	-	-
MCM-41	1155	0.88	30.5	-	-	-
MCM-48	1096	0.71	26.1	-	-	-
22.4% ZrO_2/SBA-15	426	0.69	71.3	0.30	0.92	27
3.36%TPA/SBA-15	341	0.60	70.4	0.29	0.88	21
5%TPA/ZrO_2/SBA-15	398	0.63	67.9	0.30	1.01	29
15%TPA/ZrO_2/SBA-15	372	0.59	67.7	0.42	1.45	56
30%TPA/ZrO_2/SBA-15	329	0.57	67.4	0.35	1.16	43
50%TPA/ZrO_2/SBA-15	328	0.53	67.0	0.33	1.12	31
70%TPA/ZrO_2/SBA-15	199	0.33	66.7	0.28	0.85	21
90%TPA/ZrO_2/SBA-15	199	0.31	66.0	0.26	0.58	15
15%TPA/22.4%ZrO_2/MCM-41	516	0.28	19.7	0.33	0.21	44
15%TPA/22.4%ZrO_2/MCM-48	540	0.34	17.2	0.25	0.17	10
15%TPA/ZrO_2 (Neat)	11	-	-	0.02	1.09	5
Effect of calcinations temperature (K) on 15 wt.% TPA/22.4 wt.%ZrO_2/SBA-15						
923	481	0.63	68.4	0.26	0.58	15
1023	410	0.61	68.1	0.33	1.12	32
1123	372	0.59	67.7	0.42	1.45	56
1173	326	0.47	67.3	0.34	1.19	38
1223	249	0.42	66.8	0.26	0.69	29
1273	212	0.33	66.1	0.24	0.42	13
Effect of ZrO_2(%) loading on 15 wt.%TPA/wt.%ZrO_2/SBA-15 calcined at 1123 K						
10	416.8	0.67	68.6	0.30	0.92	30
30	297.3	0.48	67.1	0.32	1.15	33
50	190.9	0.34	66.6	0.23	1.09	24
70	167.9	0.25	66.0	0.21	0.76	14

All catalysts were calcined at 1123 K except entries 1, 2 and 3. Entries from 6–11 were with 22.4% ZrO_2*. Entry 1, crystal size (by TEM) = 7.1 nm; entry 4,* ZrO_2 *phase (tetragonal), crystal size (by TEM) = 5.5–6.5 nm and (by XRD) = 6.1 nm; entry 7,* ZrO_2 *phase (tetragonal), crystal size (by TEM) = 3–4 nm and (by XRD) = 3.4 nm.*

Reaction Conditions: phenol, 2.52 g (0.026 mol); $PhCH_2OH$*, 0.48 g (0.0044 mol); catalyst, 0.15 g; temperature 363 K; time, 3 h.*

The nitrogen adsorption-desorption isotherms and pore size distribution at 77 K shown in Fig. 5.5 are of type IV for SBA-15 and for different TPA (%) loadings over 22.4 wt.%ZrO_2/SBA-15 calcined at 1123 K.

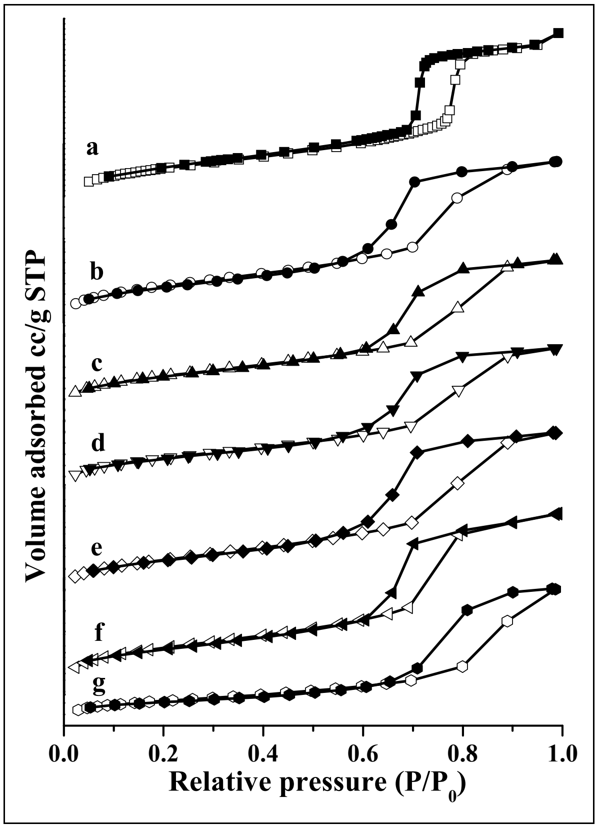

Fig. 5.5: *BET isotherm a) SBA-15, b) 5, c) 15, d) 30, e) 50, f) 70 and g) 90wt.%TPA/22.4 wt.%ZrO_2/SBA-15 calcined at 1123 K.*

A well-defined step associated with the filling of the mesopores due to capillary condensation occurs approximately at P/P_0 = 0.54 to 0.59-1.00 for 5-90 wt.% of TPA over 22.4 wt.%ZrO_2/SBA-15 catalyst calcined at 1123 K and at P/P_0 = 0.69-1.00 in SBA-15. These phenomena can be attributed to the encapsulation of TPA inside the channels of SBA-15, and furthermore, the higher loading above 50 wt.% lead to a partial blocking of the pores. The textural properties of 22.4 wt.%ZrO_2/SBA-15 with different (%) TPA loadings, 15 wt.%TPA/22.4 wt.%ZrO_2/SBA-15 calcined at different calcination temperatures and 15 wt.%TPA/wt.%ZrO_2/SBA-15 with different (%) ZrO_2 loadings are presented in Table 5.1. It is seen that the surface area, pore size and pore volume of modified SBA-15 decreased as compared with parent SBA-15. As TPA/ZrO_2 was well dispersed inside the pores of mesoporous channels so with increase in TPA and ZrO_2 loadings catalysts shows decrease in surface area, pore volume and pore diameter. Similarly, in case of 15 wt.%TPA/22.4 wt.%ZrO_2/SBA-15 surface area and pore size decreases with increase in calcination temperature.

5.2.4. AFM

The agglomerate-like morphology of the layer was studied by atomic force microscopy (AFM) method. The reactive particles of zirconium oxide formed are of 5.5-6.5 nm size, while size of TPA is about 3-4.5 nm and this combination of sizes appears to prevent a dense uniform packing of the particles.

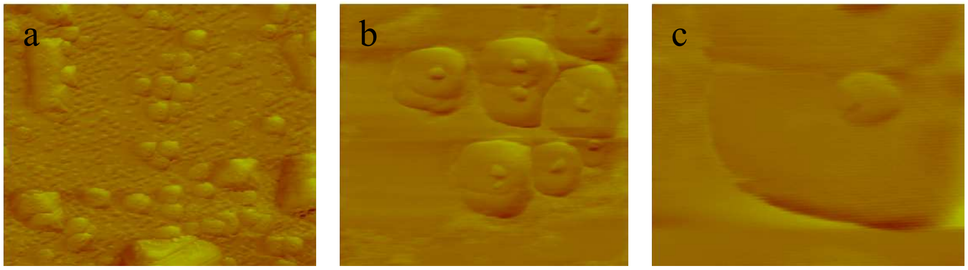

Fig. 5.6: AFM contact mode friction images of 15 wt.%TPA/22.4wt.%ZrO_2/SBA-15 on mica surface a) 5µm x 5µm, b) 1µm x 1µm, c) 266 nm x 266 nm.

5.2.5. SEM

The morphology of the supported and unsupported SBA-15 catalyst is shown in Fig. 5.7. The micromorphology of the supported catalyst remained the same, which was wheat-like even after modification of SBA-15 [1].

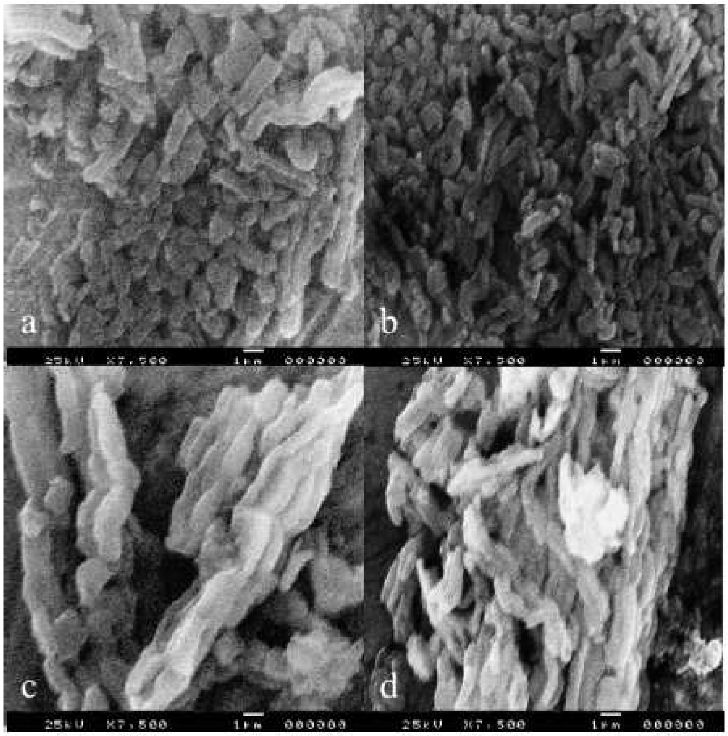

Fig. 5.7: *Scanning electron micrograph of (a) calcined SBA-15 at 813 K, and (b) SBA-15, (c) 22.4 wt.% ZrO_2/SBA-15, (d) 15 wt.% TPA/22.4 wt.% ZrO_2/SBA-15 calcined at 1123K.*

5.2.6. TEM

TEM measurements were carried out to study the morphology of the parent SBA-15 and TPA/22.4 wt.% ZrO_2 modified SBA-15 samples. TEM images of 15 wt.% TPA/22.4 wt.% ZrO_2/SBA-15 show the retention of the periodic structure of SBA-15 precursor even after calcining at 1123 K. TEM images of 15 wt.% TPA/22.4 wt.% ZrO_2/SBA-15 [Figs. 5.8 (a–d)] confirm that the hexagonally arranged mesopores of SBA-15 are retained and TPA/ZrO_2 mainly dispersed inside the pores. Fig. 5.8(a) clearly shows the uniform dispersion of TPA/ZrO_2 inside the SBA-15 channels. Figs. 5.8(b) and (d) show the periodic structure of SBA-15 precursor in different beam directions with pore size of 7.1 nm. After supporting SBA-15 with 15 wt.% TPA/22.4 wt.% ZrO_2, small particles of TPA/ZrO_2 formed inside nanochannels of SBA-15 (Figs. 5.8 (c) and (e)). The 22.4 wt% ZrO_2 (5.5–6.5 nm), an optimum loading, was inserted into SBA-15 by the wet impregnation method, which has a higher capacity for monolayer coverage of TPA. The crystallite size of the material calculated from TEM shows that for moderate loading (15 wt.%) of TPA, nanosized (3–4 nm) material was formed after wet impregnation over 22.4 wt.% ZrO_2/SBA-15 calcined at 1123 K.

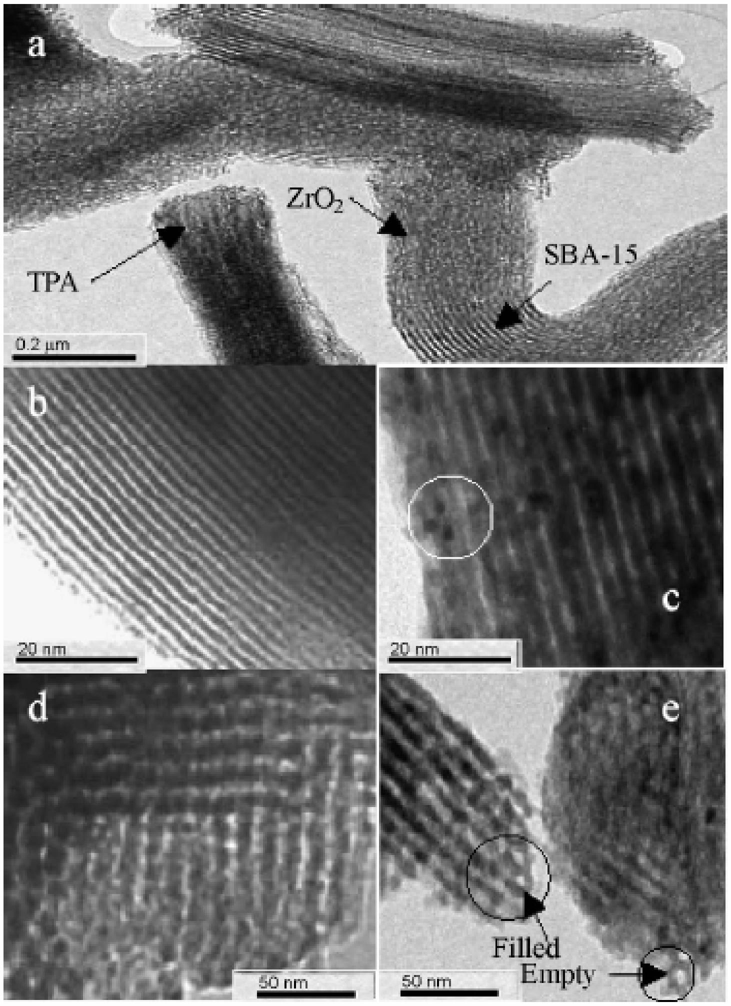

Fig. 5.8: *TEM images of (a) 15 wt.% TPA/22.4 wt.% ZrO_2/SBA-15 calcined at 1123 K, with the beam perpendicular to the pore direction of (b) SBA-15, (c) 15 wt.% TPA/22.4 wt.% ZrO_2/SBA-15 and with the beam parallel to the pore direction of (d) SBA-15, (e) 15 wt.% TPA/22.4 wt.% ZrO_2/SBA-15 calcined at 1123 K.*

5.2.7. FT-IR spectroscopy

Pure silica exhibited IR bands at 1100 and 806 cm^{-1} and a weak shoulder band at 974 cm^{-1} related to surface OH groups. Pure TPA showed characteristic peaks at 1079 cm^{-1} (P–O), 983 cm^{-1} (W=O_t), 893 cm^{-1} (W–O_c–W), and 810 cm^{-1} (W–O_e–W) [30], as shown in Figs. 5.9 (a) and (b). The spectra of ZrO_2 exhibited a wide band at 400–700 cm^{-1} extending up to 1150 cm^{-1} [27]. The spectra of different (%) loading of TPA over

ZrO_2/SBA-15 are shown in Fig. 5.9 (a). For the TPA/ZrO_2/SBA-15 samples, two bands of TPA appeared around 983 and 888 cm^{-1}, with the bands around 1079 and 810 cm^{-1} overlapping with the strong bands of SiO_2. The sample with the highest TPA loading (90 wt.%) showed characteristic bands of TPA but excluding a band at 983 cm^{-1} (W=O_t) due to decomposition of TPA intoWO_3 crystallites. Low TPA loading samples showed bands with lower intensity than bulk TPA spectra, due to masking of bands by wide bands of support.

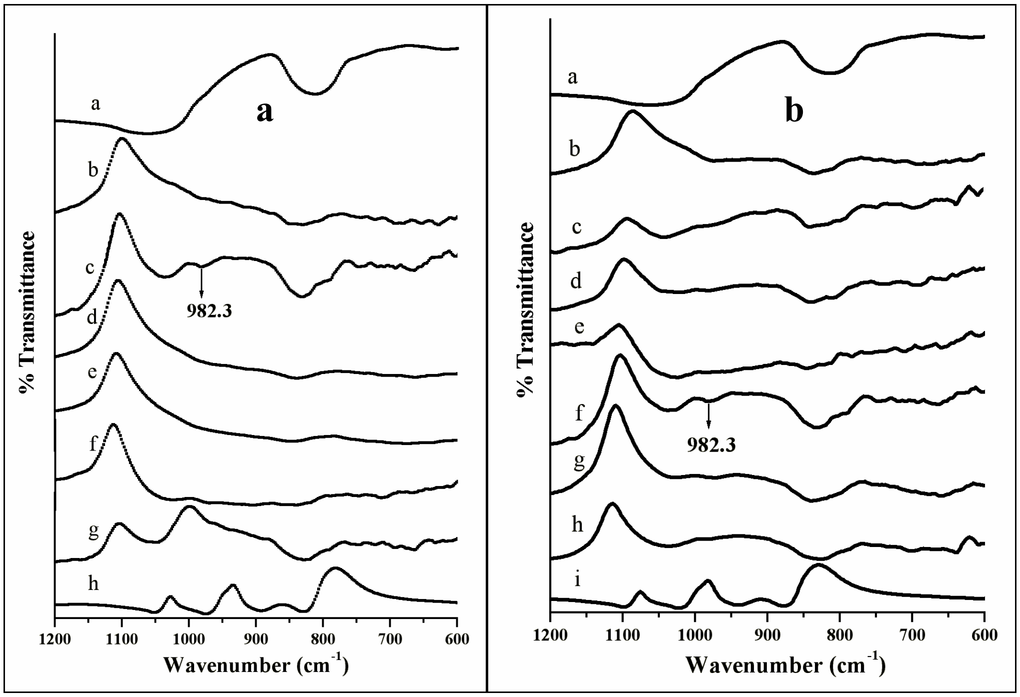

Fig. 5.9: *(a) FTIR spectra: a, pure silica, TPA/22.4 wt.% ZrO_2/SBA-15 with: b, 5; c, 15; d, 30; e, 50; f, 70; g, 90 wt.% TPA loading calcined at 1123 K; and h, pure TPA. (b) FTIR spectra: a, pure silica, 15 wt.% TPA/22.4 wt.% ZrO_2/SBA-15 calcined at b, 773; c, 923; d, 1023; e, 1123; f, 1173; g, 1223; h, 1273 K; and, i, pure TPA.*

5.2.8. UV-Vis. spectroscopy

The UV–Vis. spectra of HPA showed a band at 265 nm for TPA and 275 nm for $ZrOCl_2 \cdot 8H_2O$, in accordance with previous reports [27,28]. TPA-modified samples (i.e., 15 wt.% TPA/22.4 wt.% ZrO_2/MS) showed characteristic TPA bands at 263–265 nm (Fig. 5.10) in all of the spectra, which can be assigned to the oxygen–metal charge-transfer band of the tungstophosphate anion $[PW_{12}O_{40}]^{3-}$. However, the 22.4 wt.% ZrO_2/SBA-15 showed a band at 275.67 nm, which falls in the nanoparticle region of ZrO_2 as reported previously

[28,29]. TPA-modified samples showed only one band, because of the ZrO_2 band overlaps with strong band of TPA (Fig. 5.10).

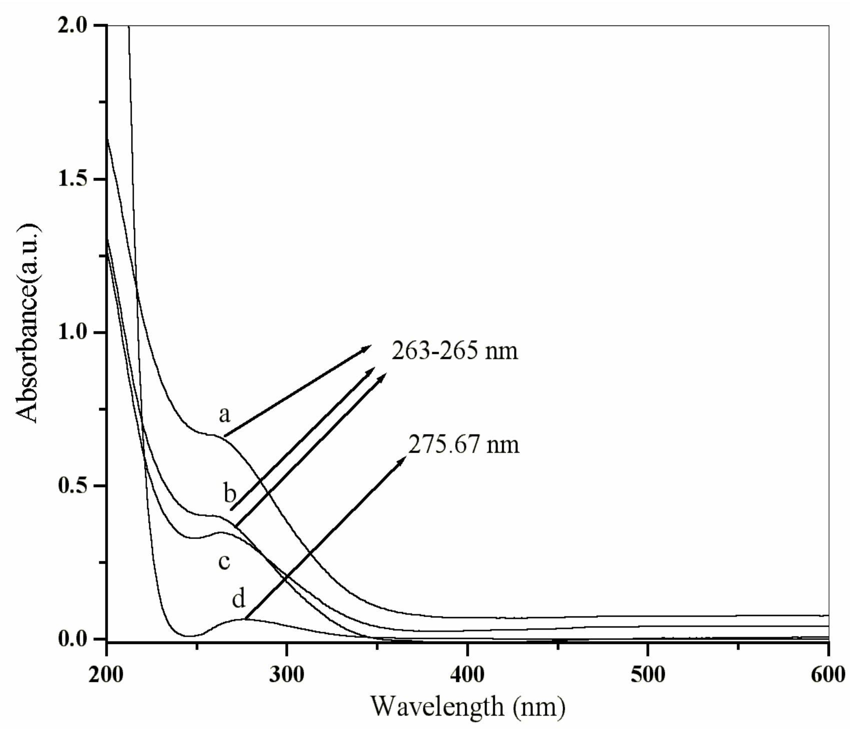

Fig. 5.10: *UV–Vis. spectra of (a) 15 wt.% TPA/22.4 wt.% ZrO_2/SBA-15, (b) 15 wt.% TPA/22.4 wt.% ZrO_2/MCM-41, (c) 15 wt.% TPA/22.4 wt.% ZrO_2/MCM-48, and (d) 22.4 wt.% ZrO_2/SBA-15 calcined at 1123 K.*

5.2.9. NMR spectroscopy

The ^{31}P CP-MAS NMR spectra of the supported TPA/ZrO_2 over SBA-15 with different TPA loadings (i.e., 5, 15, 30, and 50 wt.% TPA) are shown in Fig. 5.11 (a), and that of 70 and 90 wt.% TPA/22.4 wt.% ZrO_2/SBA-15 with 3.36 wt.% TPA/SBA-15 and 15 wt.% TPA/ZrO_2, all calcined at 1123 K, are shown in Fig. 5.11 (b).

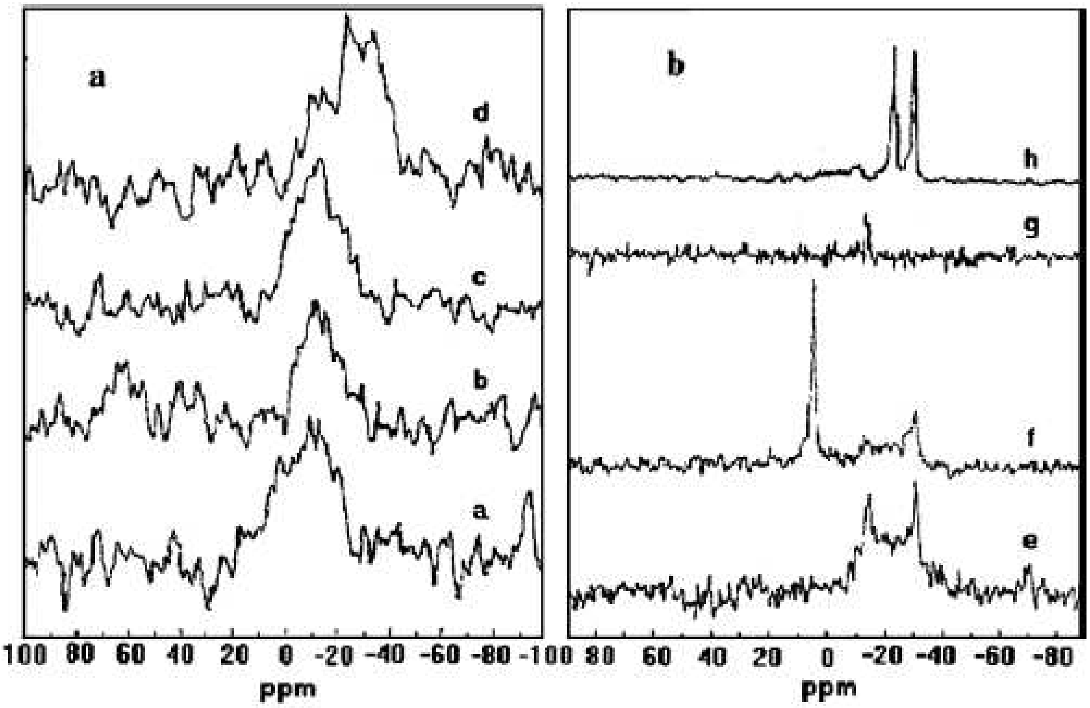

Fig. 5.11: *^{31}P CP-MAS NMR spectra of TPA/22.4 wt.% ZrO_2/SBA-15 with: a, 5; b, 15; c, 30; d, 50; e, 70; f, 90 wt.% TPA loading with: g, 3.36 wt.% TPA/SBA-15 and h, 15 wt.% TPA/ZrO_2 calcined at 1123 K.*

According to literature reports, in bulk TPA, ^{31}P NMR spectra exhibit an intense and sharp line at $\delta = -12$ ppm, showing intact Keggin units [2]. At TPA loading up to 30 wt.%, a peak around −12 to −13 ppm was observed. Further increases in loading above 50 wt.% produced a small extra peak at −24 ppm, which may be due to partially decomposed TPA with shifts in the original peak. When loading is increased above 70 wt.% produced an extra peak around −30 ppm, attributed to the presence of phosphorous in the decomposition product [3]. In 3.36 wt.% TPA/SBA-15, a small peak around −13 ppm was seen, whereas there was complete decomposition of Keggin structures (peak at −30 ppm) in neat 15 wt.% TPA/ZrO_2 calcined at 1123 K. An inspection of the chemical shifts *(δ)* shows their dependence on the TPA loading (%), type of support, and temperature treatment. TPA derivative species that may give rise to such chemical shifts could be due to partially fragmented Keggin units and also to the strong interaction of TPA with surface ≡Zr–OH groups. The broad line at −12 ppm is probably related to species formed by linking the Keggin units to the ZrO_2 support. Indeed, the first part of the interaction between TPA and ZrO_2 is a protonation of surface hydroxyl groups of ZrO_2, leading to

$(\equiv Zr–OH_2)^{n+}[H_{3-n}W_{12}PO_{40}]^{n-3}$ species [3]. After heating, water is removed, leading to a direct linkage between the polyanion (which has probably retained a structure like that of the Keggin ion) and the support. Because our system deals with high temperatures (1123 K), extensive dehydroxylation of TPA is possible to yield the aforementioned species. When the polyanion decomposes, a new signal appears at −30 ppm. Because the support is heterogeneous, a distribution of surface species obtained. TPA/ZrO_2 dispersed uniformly in the SBA-15 channels, instead of producing sharp peaks like bulk TPA, line broadening was observed in our system. As per shown in Fig. 5.12 (a), after modification of SBA-15 with 15 wt.% TPA/22.4 wt.% ZrO_2, ^{29}Si MAS NMR showed two peaks, at −110 ppm and −112 ppm, corresponding to Q^4, which could be due to the consumption of some silanols during the modification process which is reported previously [4,5]. While, ^{29}Si MAS NMR spectra for calcined MCM-41 mesostructures assembled from sodium silicate shows Q^4 Si-resonances at -108 ppm [6].

Fig 5.12 (b) shows ^{1}H MAS NMR spectra of neat TPA, along with different (%) loading of TPA over 22.4 wt.%ZrO_2/SBA-15 calcined at 1123 K. For bulk TPA treated under vacuum, chemical shift values as high as 9.3 ppm (with respect to TMS) were observed which is reported earlier [7]. Acidity of different HPAs has already been investigated by ^{1}H MAS-NMR [8, 9]. ^{1}H MAS-NMR spectra studies also indicate a chemical interaction of $H_3 [PW_{12}O_{40}]$ with the support and the formation of a new type of proton sites on the silica surface. Brønsted acid sites in solid acids can be characterized by ^{1}H MAS-NMR spectroscopy. The basic idea is that a more acidic proton has less electron in its vicinity, therefore is less shielded and, subsequently, its NMR chemical shift δ_H, will be more positive (lower-field shift) [10]. However, other contributions, such as hydrogen bonding, may also influence δ_H values, which may make its relationship with acidity strength ambiguous [11,12]. The chemical shift of ^{1}H can be considered as an indicator of the acidity of a proton. Since all our samples corresponded to the same Keggin anion to which the proton is attached and the Keggin anion remained stable during thermal treatments, the evolution of the proton resonance peak as a function of the degree of dehydration was therefore a reasonable indicator of the strength of the proton acidity. This assignment is different to that proposed by Misono [13] who attributed a peak at ca. 9 ppm observed after evacuation of the HPA at 473 K to the acidic 'free' proton and, surprisingly, reported the same ^1H chemical shift for both $H_3PW_{12}O_{40}.0H_2O$ and $H_3PW_{12}O_{40}.2.2H_2O$ samples.

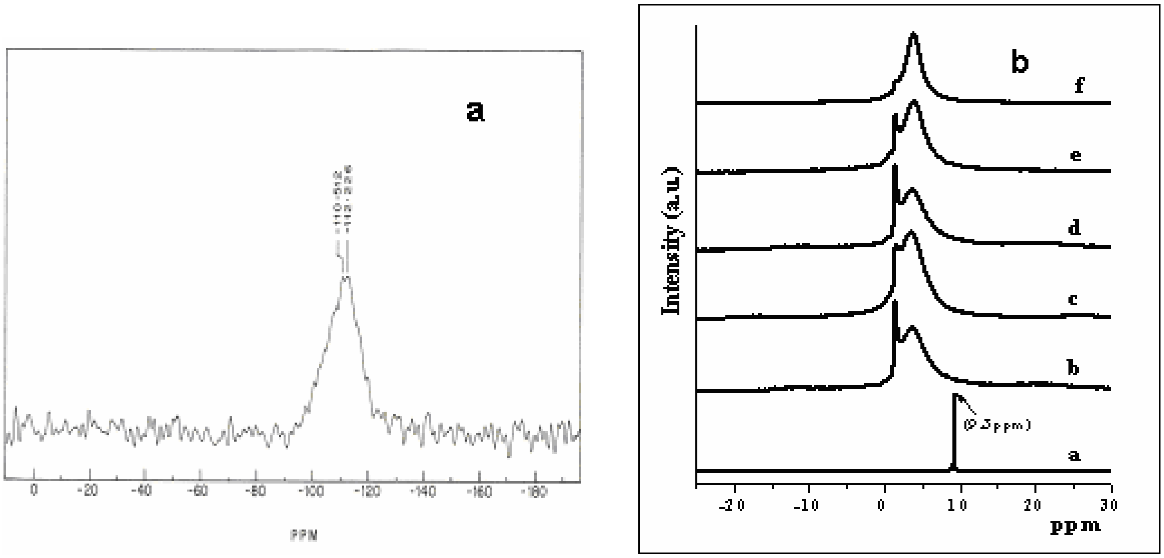

Fig. 5.12: *(a) ^{29}Si MAS NMR spectra of 15 wt.%TPA/22.4 wt.% ZrO_2/SBA-15 calcined at 1123 K.*
(b) ^1H MAS NMR spectra of (a) Neat TPA, (b) 5, (c) 15, (d) 30, (e) 50 wt.%TPA/22.4 wt.% ZrO_2/SBA-15 calcined at 1123 K and (f) 15 wt.%TPA/22.4 wt.%ZrO_2/MCM-41 calcined at 1123 K.

All spectra of supported TPA display similar feature with essentially two components, a sharp one at 1.5 ppm, which can be attributed to isolated silanol groups as, explained above and a broad one from 2 to 5 ppm, which could be, attributed to hydrogen-bonded hydroxyl groups. The peak at ca. 9 ppm which is attributed to protons in anhydrous TPA is not observed even for the highest TPA loading (50 wt.%) and whatever the dehydroxylation temperature. This observation is very important as the high acidity of HPA is related to this proton. We can then conclude from these data that the supported HPA is less acidic than the pure one, which is known in the literature [14]. These results are in agreement with other methods such as microcalorimetry [15, 16]. As per literature, the resonance around 2-5 ppm corresponding to hydrogen bonded silanol groups may be of silica support [17]. This may be the reason for getting a broad resonance around 2-5 ppm by merging of two peaks from TPA and from silica support. The ^1H MAS NMR spectra of calcined MCM-41consist of signals in the chemical shift range 1.3–2.2 ppm which are typical for silanol groups in inorganic solids [18, 19]. The unsymmetric shape of these signals is a hint for the presence of different types of silanol groups, such as isolated and geminal SiOH groups and internal silanol groups [20]. But, in case of MCM-41 support we observed only one peak i.e. around 3.8 ppm, may be due to unavailability of isolated silanol groups from silica support.

5.2.10. FT-RS

FT-Raman spectra of 22.4 wt.%ZrO_2/SBA-15 sample with and without TPA calcined at 1123 K are presented in Fig. 5.13. Distinctly, the intensity of the bands around 1009, 992 cm^{-1} and a weak peak around 905 cm^{-1} assigned to pure TPA [21,22]. The bands assigned to TPA are clearly seen in Fig. 5.13 for 15 wt.%TPA/22.4 wt.%ZrO_2/SBA-15 sample. The broadness and minor shift in the bands could be due to the formation of the species formed by linking the Keggin units to the ZrO_2 support. The Raman bands of ZrO_2 below 700 cm^{-1} interfere with the tungstate species, while above 700 $cm^{-1}$is free from characteristic bands of ZrO_2.

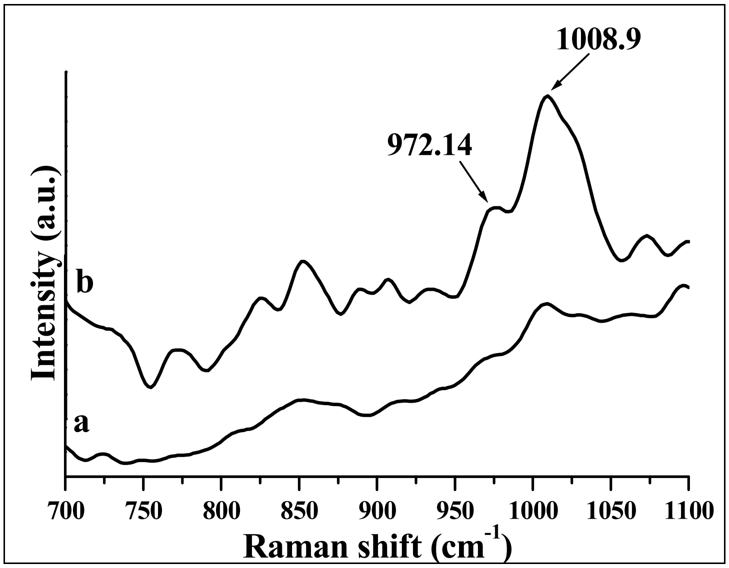

Fig. 5.13: *FT-Raman spectra of a) 22.4 wt.%ZrO_2/SBA-15 and b) 15 wt.%TPA/ 22.4 wt.%ZrO_2/SBA-15 calcined at 1123 K.*

5.2.11. XPS

In order to study the surface stability of TPA on ZrO_2/SBA-15 systems, we carried out XPS analysis. XPS analysis has been used to investigate the interaction between the guest (ZrO_2) and the host (SBA-15) and was found that ZrO_2 was more likely to interact with SBA-15 by hydrogen bonds involving Si-O-H groups of the SBA-15 with zirconium atoms in ZrO_2. Due to such interaction at monolayer coverage of TPA, free hydrogen is available from SBA-15 support. While below and above 22.4 wt.%ZrO_2 loading, this interaction was not that predominant due to less ZrO_2 content and also due to multilayer formation in both the supports. The results of XPS analyses for 22.4 wt.%ZrO_2/SBA-15 are shown without and with TPA calcined at 1123 K.

Table 5.2. XPS binding energies (eV) and FWHM (eV) values of the catalysts

Sample	O 1s		Zr $3d_{5/2}$		Si 2p		W $4f_{7/2}$		P 2p	
	BE	FWHM	BE	FWHM	BE	FWHM	BE	FWHM	BE	FWHM
A	531.2	2.7	183.5	4.7	102.3	2.8	-	-	-	-
B	531.2	3.4	183.5	8.9	102.8	2.9	35.9 (38.0)	3.5	134.0	6.9

Where, (A) = 22.4 wt.%ZrO_2/SBA-15 and (B) = 15 wt.%TPA/22.4wt.%ZrO_2/SBA-15

The binding energies and FWHM values of various core levels (Si 2p, O 1s, Zr $3d_{5/2}$, W $4f_{7/2}$, P 2p) of this mesoporous materials are summarized in Table 5.2. The spin-orbit split doublet of tungsten, W $4f_{7/2}$ and W $4f_{5/2}$ with full width at half maximum is obtained at 3.5 eV and are located at 35.9 and 38.2 eV, respectively. The observed binding energy value of W ($4f_{7/2}$) is 35.9 eV, a characteristic of W^{6+} indicating that it contain W-O bonding [23]. Fig. 5.14 (A) shows the contribution of the O^{2-} 1s at 531.2 eV, which is related to an O-H bonding. This indicates that the compound is hydrated. Si 2p binding energy (Fig. 5.14 (B)) values of silica support i.e. SBA-15 and modified SBA-15 with TPA/ZrO_2 are the same around 102-103 eV [24]. The same Si 2p FWHM values for samples 22.4 wt.%ZrO_2/SBA-15 i.e. without and with TPA shows that impregnation doesn't affect the silica support i.e. SBA-15 as seen in Table 5.2. In Fig. 5.14 (C), 22.4 wt.%ZrO_2/SBA-15 catalyst without and with 15 wt.%TPA shows similar Zr $3d_{5/2}$ binding energy values around 183.5 eV. Table 5.2 shows the binding enery values and FWHM values, which shows almost the same FWHM values even after TPA loading. The binding energy of the Zr $3d_{5/2}$ band in the case of modified ZrO_2 samples was found to be higher than that of the pure ZrO_2 (182.5 + 0.1 eV). This shift towards higher side could be attributed to an atomic dispersion of ZrO_2 on the other support oxides and/or the change in the coordination number of zirconium by the formation of a Zr-O-Support bond as per evidenced in literature [25,26]. The phosphorous signal P^{5+} 2p at 134.4 eV could be associated with a compound that contains P-O bonding as shown in Fig. 5.14 (D). However, high FWHM values are observed due to peak-broadening possibility and i.e. due to differential charging of the sample caused by mesoporous silica support.

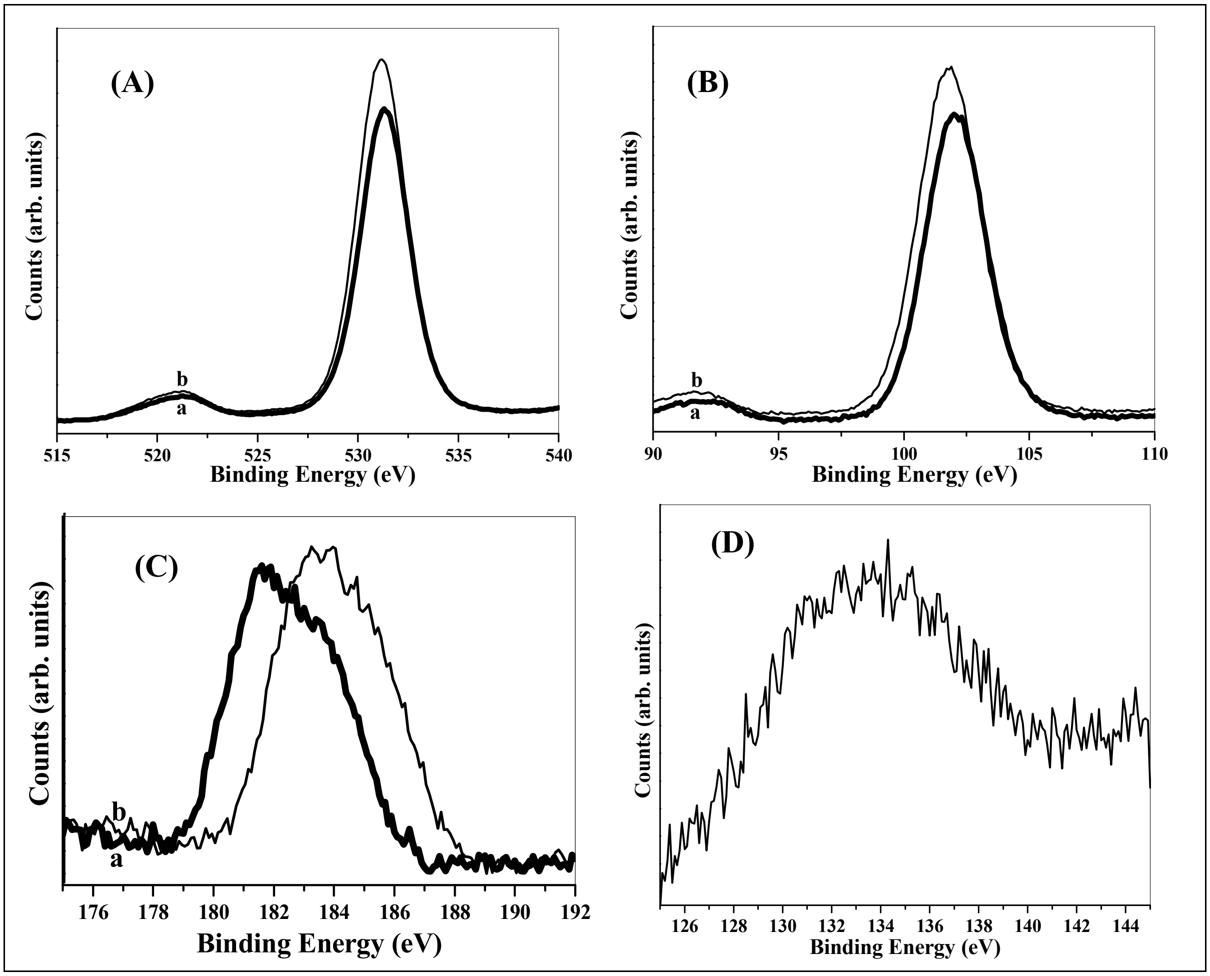

Fig.5.14: *XPS spectra of (A) O (1s) spectra of a) 22.4 wt.%*ZrO_2*/SBA-15 and b) 15 wt.%TPA/22.4 wt.%*ZrO_2*/SBA-15, (B) Si (2p) spectra of a) 22.4 wt.%*ZrO_2*/SBA-15 and b) 15 wt.%TPA/22.4 wt.%*ZrO_2*/SBA-15, (C) Zr (*$3d_{5/2}$*) spectra of a) 22.4 wt.%*ZrO_2*/SBA-15 and b) 15 wt.%TPA/22.4 wt.%*ZrO_2*/SBA-15 and (D) P (2p) spectra of a) 22.4 wt.%*ZrO_2*/SBA-15 and b) 15 wt.%TPA/22.4 wt.%*ZrO_2*/SBA-15 calcined at 1123 K.*

5.2.12. TG-DTG

TG-DTG spectra of all the samples dried at 100°C are shown in Fig. 5.15. Under similar measurement conditions, TG-DTG analysis of pure TPA hydrate showed three stages of weight loss (endothermic effect) [32]. The first weight loss, around 3–6%, occurred from room temperature to 125°C, due to the loss of physisorbed water. The second one, from 130–305°C, accounted for the loss of crystallization water, and the third, in the range of 370–550°C, was due to the loss of 1.5 H_2O molecules originating from all acidic protons. The total weight loss of the sample corresponded to 21 H_2O per Keggin unit. Furthermore, it showed a break at 350°C, due to the decomposition of HPA [21]. The TGA behavior was similar in all of the TPA/ZrO_2-supported samples, showing the first weight loss of about 3% in all TPA/ZrO_2 supported over SBA-15 samples, corresponding to physisorbed water. But the MCM-41 and MCM-48 supports showed heavy weight loss, corresponding to physisorbed water, compared with the SBA-15-supported samples. But none of the supported samples showed an appreciable change in weight loss until 900°C, indicating increasing stability of TPA. The neat 15 wt.% TPA/ZrO_2 sample exhibited weight loss corresponding to physisorbed water along with another weight loss around 450–600°C that may be due to a phase transition from tetragonal to monoclinic.

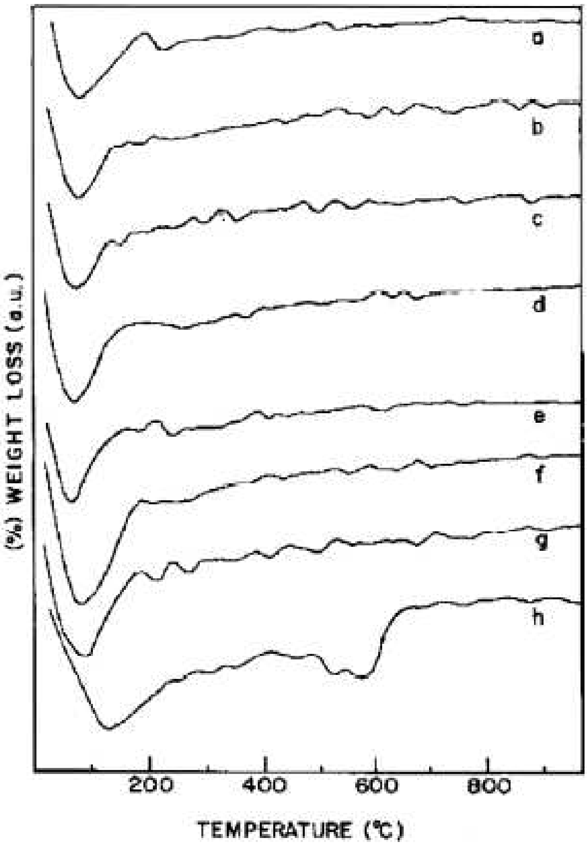

Fig. 5.15: *TG-DTG curves of (a) 22.4 wt.% ZrO_2/SBA-15, TPA/22.4 wt.% ZrO_2/SBA-15 with (b) 5, (c) 15, (d) 30, (e) 50 wt.% TPA loading with (f) 15 wt.% TPA/22.4 wt.% ZrO_2/MCM-41, (g) 15 wt.% TPA/22.4 wt.% ZrO_2/MCM-48, and (h) 15 wt.% TPA/ZrO_2 calcined at 1123 K.*

5.2.13. TPD of NH_3

NH_3-TPD was performed to determine the amount and the total acidity in the catalysts. TPD profiles of the catalysts with different (%) TPA loadings in TPA/ZrO_2/SBA-15 calcined at 1123 K are shown in Fig. 5.16 (a), and the profiles of TPA/ZrO_2 supported on various silica supports, unsupported TPA/ZrO_2, 22.4

wt%ZrO_2/SBA-15, and TPA supported on SBA-15, all calcined at 1123 K, are shown in Fig. 5.16 (b).

The total acidities of 15 wt.% TPA/22.4 wt.% ZrO_2/SBA-15 calcined at different temperatures are given in Table 5.1. Results from Fig. 5.16 (a) suggest that at TPA loading up to 50 wt.%, the samples showed a broad desorption band centered around 523 K, implying medium acidity. Further increases in TPA loading [Fig. 5.16 (a)] produced decreased acidity, which incidentally have lower surface areas. These results indicate that TPA/ZrO_2 dispersed uniformly over SBA-15. According to area under the peak, the supported TPA/ZrO_2 samples showed more acid sites than unsupported TPA/ZrO_2 or 3.36 wt.% TPA/SBA-15. Loading of TPA over 22.4 wt.%ZrO_2/SBA-15 [Fig. 5.16 (b)] produced increased acidity and thereby increased catalytic activity in benzylation reaction (Table 5.1). All samples showed a broad TPD profile, indicating that the surface acid strength was widely distributed. From these data, it is evident that an initial increase in total acidity up to 15 wt.% TPA loading is followed by a decrease in total acidity with further increases in TPA loading. It can be concluded that for low TPA loading, the Keggin unit of HPA retains its structure and acidity, but for higher loading (i.e., above 15 wt.% TPA), it decomposes at least partially into its oxides. The highest acidity corresponds to monolayer coverage of TPA (i.e., 15 wt.% TPA/22.4 wt.% ZrO_2/SBA-15 calcined at 1123 K), where the Keggin-like structure is intact, as supported by ^{31}P CP-MAS NMR and XRD. Table 5.1 indicates that the total acidity increases up to 1123 K but that further increases in calcinations temperature lead to decreased acidity and also decreased catalytic activity, which is due to decomposition of TPA intoWO_3 crystallites. Total acidity of the 15 wt.%TPA with different wt.% of ZrO_2 over SBA-15 calcined at 1123 K is shown in Table 5.1. Similarly, with increasing ZrO_2 loading till 22.4 wt.%, 15 wt.%TPA/ZrO_2/SBA-15 catalyst calcined at 1123 K shows increase in acidity and thereby catalytic activity.

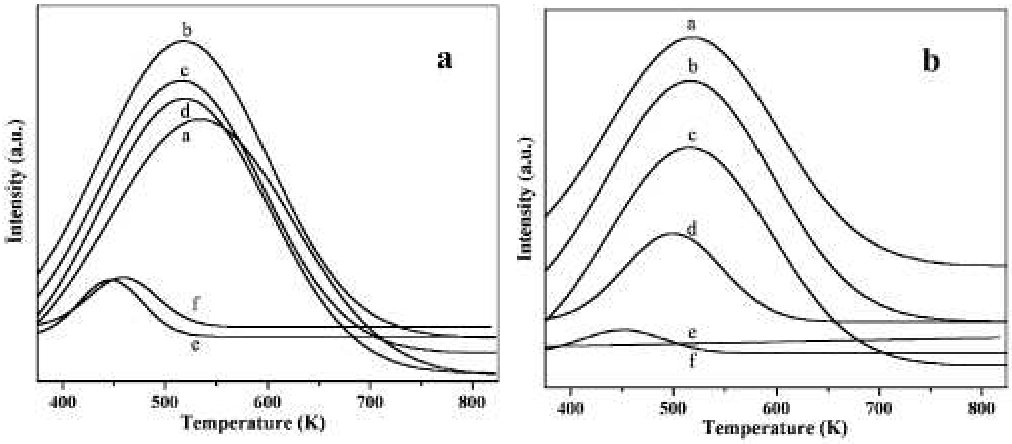

Fig. 5.16: *(a) NH_3-TPD profiles: TPA/22.4 wt.% ZrO_2/SBA-15 with a, 5; b, 15; c, 30; d, 50; e, 70; f, 90 wt.% TPA loading and (b) 15 wt.% TPA/22.4 wt.% ZrO_2 supported over a, SBA-15; b, MCM-41; c, MCM-48; d, 22.4 wt% ZrO_2/SBA-15; e, 3.36 wt% TPA/SBA-15; f, neat 15 wt% TPA/ZrO_2 calcined at 1123 K.*

5.2.14. FT-IR Pyridine adsorption

The Brønsted/Lewis (B/L) site ratio was calculated from the IR absorbance intensities [31] of bands at 1539 (B) and 1442 (L) cm^{-1} as per shown in Fig. 5.17, for different catalysts along with different (%) loadings of TPA, and were compared with catalytic activity in phenol benzylation with different calcination temperatures for 15 wt.% TPA/22.4 wt.% ZrO_2/SBA-15; the results are given in Table 5.1. It was found that the B/L ratio increased with increased TPA loading up to 15 wt.%, but then decreased with further increases in TPA loading. Thus the sample with 15 wt.% TPA/22.4 wt.%ZrO_2/SBA-15 had the highest acidity, due to the monolayer coverage of TPA on ZrO_2 finely dispersed in SBA-15 channels. But on further increases in TPA loading, the B/L ratio decreased, and hence the catalytic activity also decreased. The decrease in B/L ratio and activity was well explained earlier in Chapter 4, section 4.2.9, page no. 85.

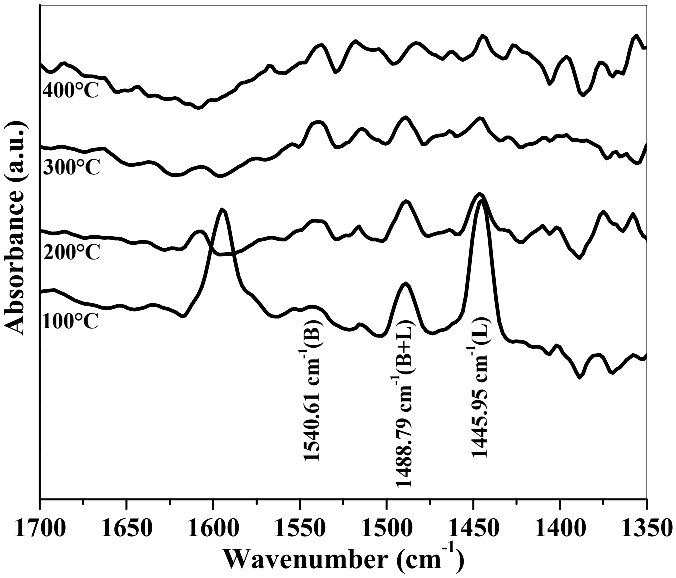

Fig. 5.17: *FT-IR Pyridine adsorption isotherms of 15 wt.%TPA/22.4 wt.%ZrO_2/SBA-15 calcined at 1123 K.*

5.3. BENZYLATION OF PHENOL BY BA

5.3.1. Introduction

Alkylation of phenol with different alcohols is an industrially important reaction in production of various products [33, 34]. Benzylation of phenol by BA to BP is an important reaction, and BPs are useful raw materials for producing antioxidants and plastic, rubber, and petroleum products [35]. The present work deals with the role of mesoporous support and how its properties influence over the catalytic activity of neat TPA/ZrO_2 in an acid-catalyzed benzylation as a test reaction. Our findings demonstrate that TPA/ZrO_2 dispersed uniformly in nanosized channels of SBA-15 and provided strong acidity and catalytic activity compared with neat TPA/ZrO_2 catalyst in benzylation of phenol.

5.3.2. Results and discussion

The liquid phase benzylation of phenol with BA was carried out using TPA/ZrO_2 formed in SBA-15 channels as a catalyst; the reaction is as shown in the scheme 5.1.

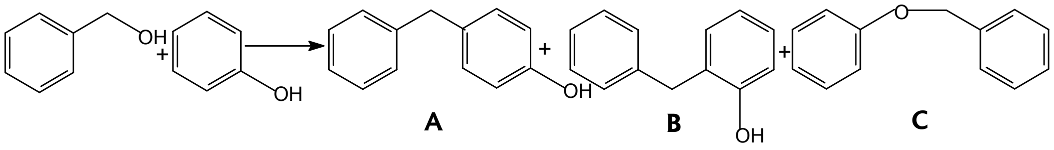

Scheme 1.

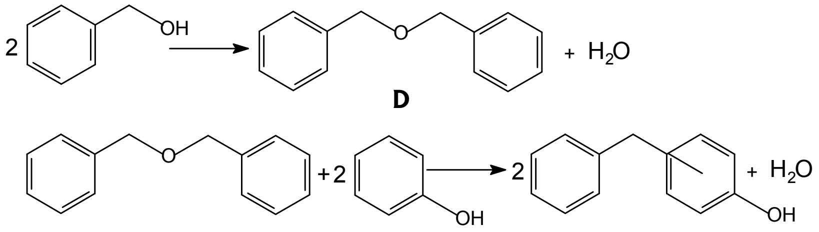

Scheme 2.

Scheme 5.1: *Benzylation of phenol with BA giving products as A (p-BP), B (o-BP), C (PBE) and D (DBE).*

Data on the catalytic performance of various (%) TPA-loaded catalysts calcined at 1123 K, and activity of 15 wt.% TPA/22.4 wt.% ZrO_2/SBA-15 calcined at different temperatures are presented in Table 5.1.

5.3.2.1. Comparison of catalytic activities of different catalysts

Benzylation of phenol with 15 wt.% TPA/22.4 wt.%ZrO_2/SBA-15 calcined at 1123 K catalysts under selected reaction conditions (363 K, 3 h, 150 mg catalyst, phenol/BA molar ratio 6) gave 77% (A + B) (i.e., mono-BP as the main product), 20% (C), and 3% (D).

The 15 wt.% TPA/22.4 wt.%ZrO_2/SBA-15 calcined at 1123 K gave the highest conversion of BA (56%) under selected reaction conditions (Table 5.1). The effect of TPA loading, ZrO_2 loading and calcination temperature on BA conversion data is presented in Table 5.1. Combining these findings with the results of FTIR pyridine adsorption data reveal that the B/L ratio of the catalysts increased up to 15% TPA loading and that 15 wt.% TPA/22.4 wt.%ZrO_2/SBA-15 calcined at 1123 K had the highest B/L ratio and gave the highest catalytic activity in benzylation of phenol under reaction conditions. In this catalytic system, ZrO_2 loaded on mesoporous silica support (i.e., 22.4 wt.% ZrO_2/SBA-15 calcined at 1123 K) showed some catalytic activity, whereas ZrO_2 loaded on 15 wt.% TPA showed a two-fold increase in catalytic activity (Table 5.1). The interaction between the

TPA and ZrO_2 is responsible for the high acidity and for high catalytic acitivity as discussed earlier in Chapter 4, section 4.2.9, page no. 85.

TPA species would exert an electron-withdrawing effect on surface Zr^{4+} cations, making them to behave as strong Lewis acid sites. But this phenomena occurred at temperatures up to 673 K. Accordingly, the strongly acidic properties of TPA/ZrO_2 could be attributed to electron-withdrawing effects similar to those ascribed to Zr bonded sulfate groups [36,37]. Above 673 K, all dehydrated ZrO_2 reacted with TPA. In this catalytic system, the fact that TPA remained amorphous at temperatures up to 923 K suggests strong interactions between HPA and ZrO_2 at the structural level. But crystallite size measurements (Table 5.1) showed that the presence of TPA inhibited crystal growth of the catalyst material; this behavior is very common in mixed materials containing a crystalline and an amorphous phase together. The crystalline material is usually surrounded by an amorphous phase layer, which acts as a physical barrier to hinder the sintering process and inhibit crystallite growth [37, 38]. Keeping in mind all of these findings, we hypothesize that at calcinations above 923 K, the interaction between TPA and ZrO_2 may weaken to monolayer coverage (15 wt.% and 1123 K), making TPA protons free for reactions to proceed and thereby increasing Brønsted acidity and total acidity (from the increase in Lewis acidity due to ZrO_2). With further increases in calcinations temperature above 1123 K, possibly due to multilayer formation, bulk properties of TPA will be more predominant, causing destruction of TPA to yield WO_3 crystallites, as was partially proved by NMR. Besides sulfate ions, tungstate and molybdate oxoanions also produce strong acidic sites when deposited on hydroxylated ZrO_2 [39].

The 15 wt.% TPA/22.4 wt.%ZrO_2 modified SBA-15 catalyst showed higher catalytic activity than the 15 wt.% TPA/ 22.4 wt.%ZrO_2 modified MCM-41 and MCM-48 catalysts calcined at 1123 K.We hypothesize that large TPA clusters (~12 Å) can readily clog the pores during solution impregnation when support pore sizes are smaller, as in the case of MCM-41 (30.5 Å) and MCM-48 (26.1 Å). But when the ZrO_2 along with TPA was dispersed in the mesoporous channels of supports at high temperature calcination, the acidity of the catalysts was altered, becoming higher with SBA-15. In contrast, TPA/ZrO_2 is likely have a better chance to uniformly coat the pores when the support pore size is sufficiently large, as in the case of SBA-15 (73.3 Å) compared with MCM-41 and MCM-

48. However, the neat 15 wt.% TPA/ZrO_2 calcined at 1123 K showed poor catalytic activity with conversion of BA (5%), at least 10 times less than that of the modified 15 wt.% TPA/22.4 wt.%ZrO_2/SBA-15 calcined at 1123 K under the same reaction conditions. This enhanced activity could be due to more accessible protons when 15 wt.% TPA/ZrO_2 is supported on large surface area and the larger pore diameters of the SBA-15 mesoporous silica material. Hence the above catalyst was used in catalytic studies to assess activity in the test reaction.

5.3.2.2. Effect of TPA loading and calcination temperature

The effect of TPA loading and calcination temperature as a function of product selectivities are presented in Fig.5.18 (A) and Fig.5.18 (B), respectively for benzylation of phenol. Fifteen wt.%TPA/22.4 wt.%ZrO_2/SBA-15 calcined at 1123 K gave the highest conversion of BA (56 %) under the optimized reaction conditions (Table 5.1). Combining with the results of FT-IR pyridine adsorption data, it was found that B/L ratio of the catalysts increases up to 15 wt.% TPA loading and 15 wt.%TPA/22.4 wt.%ZrO_2/SBA-15 calcined at 1123 K has the highest B/L ratio and gave the highest catalytic activity in phenol benzylation under optimized reaction conditions. However, the neat 15 wt.%TPA/ZrO_2 calcined at 1123K showed poor catalytic activity with conversion of BA (5 %), which is at least ten times less than the modified 15 wt.%TPA/22.4 wt. %ZrO_2/SBA-15 calcined at 1123 K catalyst under the same reaction conditions.

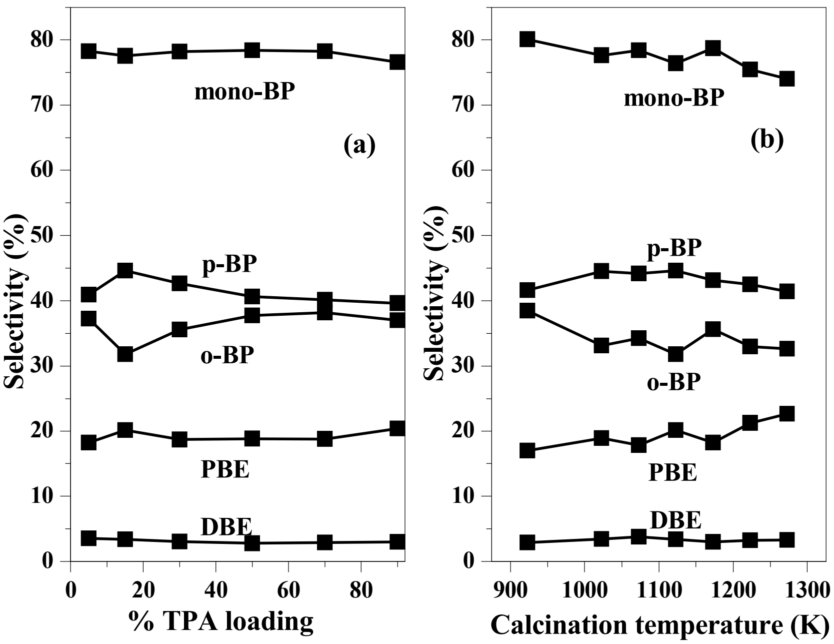

Fig. 5.18: (A) Effect of TPA loading and (B) calcination temperature on phenol benzylation. (Reaction conditions: phenol, 2.52 g (0.026 mol); BA, 0.48 g (0.0044 mol); catalyst weight, 150 mg; phenol/BA (mol ratio), 6:1; temperature, 363 K; time, 3 h.

5.3.2.3. Effect of reaction parameters

The effect of catalyst concentration on BA conversion was studied by varying catalyst from 1 to 10 wt.% of the total weight of the reaction mixture and the results are shown in Fig. 5.19 (a). It is seen that BA conversion increases from 4.6 to 84.7% with increase in catalyst concentration up to 10 wt.%, while the selectivity for mono-BP was unchanged.

We studied the effect of the phenol/BA molar ratio from 2 to 10 by keeping the total weight of the reaction mixture constant under optimized reaction conditions and the results are shown in Fig.5.19 (b). As the molar ratio increases from 2 to 10, the BA conversion increased from 23.9 to 75.7 %. The selectivity for mono-BP increases with increase in molar ratio, while selectivity for DBE decreased. From the results it is seen that the selectivity for *para*–BP is more than *ortho*–BP with 15 wt.%TPA/22.4 wt.%ZrO_2/SBA-15 catalyst.

The 15 wt.%TPA/22.4 wt.%ZrO_2/SBA-15 catalyst was used to study the effect of temperature in the range 343-383 K on the conversion and product selectivities [Fig. 5.20 (a) and Table 5.3]. With increasing temperature, BA conversion increased up to 73%, whereas selectivity for mono-BP increased and that of PBE decreased.

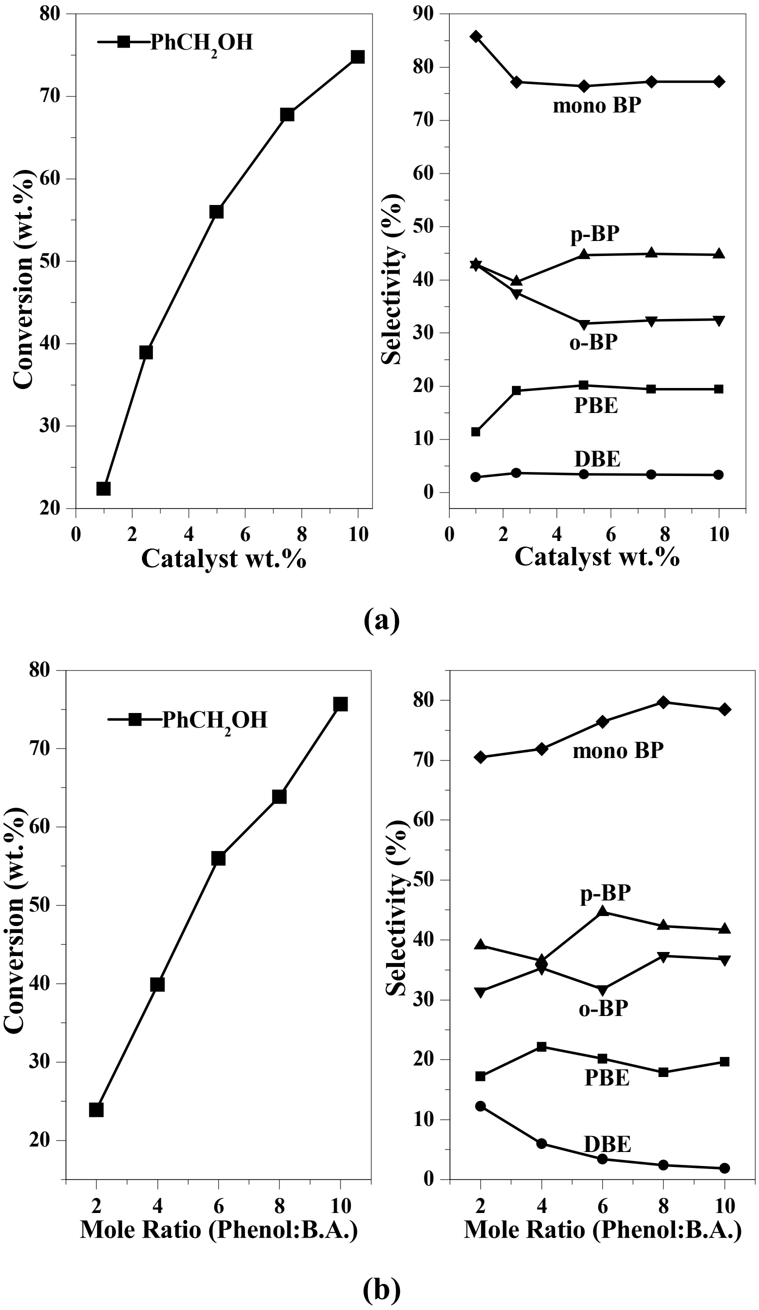

Fig. 5.19: *(a) Effect of catalyst concentration on phenol benzylation. (Reaction conditions: phenol, 2.52 g (0.026 mol); BA, 0.48 g (0.0044 mol); phenol/BA (mol ratio), 6:1; temperature, 363 K; time, 3 h.*

(b) Effect of Phenol: BA molar ratio on phenol benzylation. (Reaction conditions: phenol, 2.52 g (0.026 mol); BA, 0.48 g (0.0044 mol); catalyst weight, 150 mg; temperature, 363 K; time, 3 h.

Table 5.3: Study of effects of reaction temperature on conversion of BA

Catalyst	Conversion BA. (%)	Ist order Rate constant	Product selectivity (%)*	
			mono-BP	PBE
Temperature				
343	25	0.09	75	22
353	34	0.14	75	22
363	56	0.27	77	20
373	67	0.37	78	19
383	73	0.44	80	17
Regeneration of catalyst				
Fresh	56	-	77	20
Ist	56	-	77	20
IInd	55	-	77	20

*Reaction conditions: Phenol=2.52 g (0.026 mole), $PhCH_2OH$ (BA)=0.48 g (0.0044 mole), catalyst=0.15 g, temp. = 363 K, time=3 h. *DBE = 3% in all the cases.*

Benzylation of phenol by BA was carried out with catalyst, 0.15 g (3 wt.% of total reaction mixture), phenol/BA molar ratio 6 at 363 K for 7 h to investigate the effect of BA conversion and product selectivity as functions of time as per shown in Fig. 5.20 (b). With increase in time, BA conversion increased to a maximum of 85% after 7 h with 78% selectivity for mono-BP, 19% for PBE and the remainder for DBE.

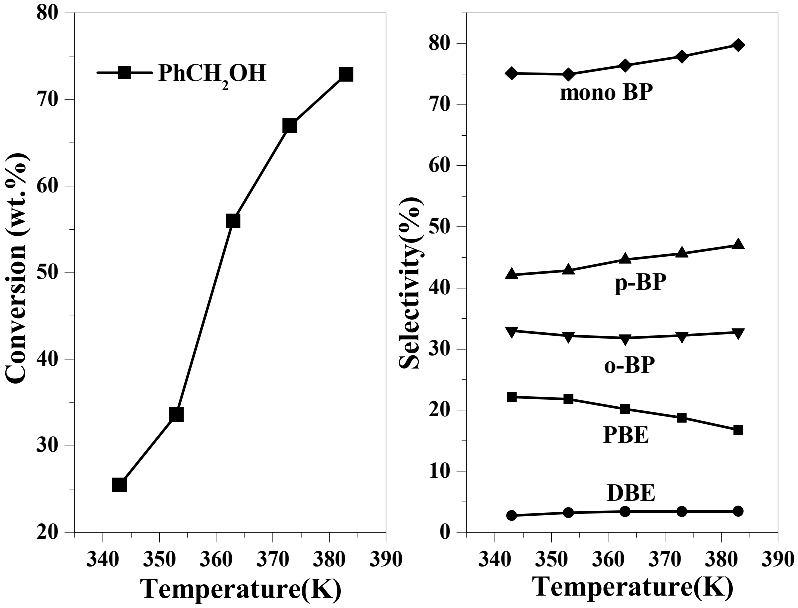

(a)

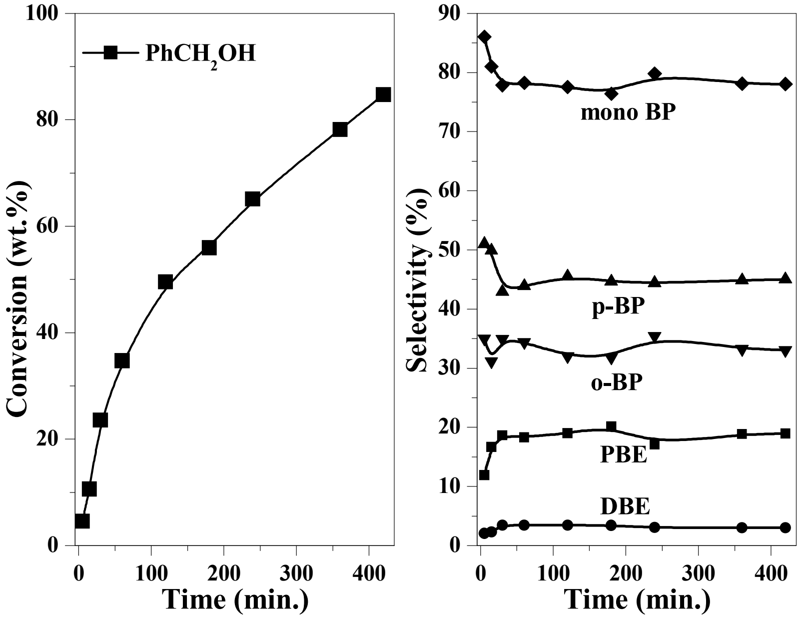

(b)

Fig. 5.20: *(a) Effect of reaction temperature on phenol benzylation. (Reaction conditions: phenol, 2.52 g (0.026 mol); BA, 0.48 g (0.0044 mol); catalyst weight, 150 mg; phenol/BA (mol ratio), 6:1; time, 3 h.*

(b)Effect of time on stream on BA conversion and product selectivity. (Reaction conditions: phenol, 2.52 g (0.026 mol); BA, 0.48 g (0.0044 mol); catalyst weight, 150 mg; phenol/BA (mol ratio), 6:1; temperature, 363 K; time, 3 h).

5.3.2.4. Kinetic study

Two reaction schemes have been proposed for phenol benzylation with BA (Scheme 5.1) [40]. The first scheme involves the direct formation of BP by alkylation of phenol with BA, whereas the second scheme involves a two-step process in which PBE is formed and then subsequently converted to BP. BA gave PBE as the product in a parallel reaction. With increasing temperature, PBE decreased, possibly due to internal transformation of O– and C–, an alkylated product. BP is a primary product, and PBE is a primary and/or secondary product that transforms during reaction to BP; such rearrangement occurs on heating or contact with an acid catalyst.

Because benzylation of phenol by BA involves two consecutive steps to form BP (Scheme 5.1), the standard equations for a first order series reaction, $C_A/C_{A0} = e^{-k_1 t}$, were used to determine the rate constant, where C_A and C_{A0} are the concentration of BA at initial time and at time t, respectively. The rate constants calculated at different temperatures are presented in Table 5.3. It is seen that k_1 increased with increasing temperature. The activation energy for benzylation of phenol was calculated from the Arrhenius graph and was found to be 10.38 kcal/mol.

5.3.3. Conclusions

The results presented in this work demonstrate that TPA/ZrO_2 dispersed uniformly inside the mesopores of SBA-15 formed nanocomposite material at a calcination temperature of 1123 K. The formation of nanosized (3–4 nm) TPA/ZrO_2 was found to depend on (%) TPA loading, monolayer coverage on ZrO_2, geometry, the nature of mesoporous supports, and calcinations temperature. Among mesoporous silica supports, SBA-15 was found to be better and provided higher thermal stability and catalytic activity than MCM-41 and MCM-48 in benzylation reactions. The mesoporous material has an advantage in the formation of nanosized and catalytically active TPA/ZrO_2 by stabilizing ZrO_2 in tetragonal phase at 1123 K, which provided higher catalytic activity than the neat TPA/ZrO_2 in benzylation reactions. The higher stability and catalytic activity can be achieved by incorporating TPA/ZrO_2 in supports like SBA-15 to get enhanced catalytic activity (ten-fold higher) than the corresponding neat TPA/ZrO_2 catalyst.

5.4. ACETYLATION OF VERATROLE WITH Ac_2O

5.4.1. Introduction

The use of solid acid catalysts such as zeolites, clays, mesoporous silica in acetylation of aromatic compounds like anisole, thioanisole, veratrole, isobutyl benzene and 2-MN have been reported in the literature [41-50]. The first industrial application of a zeolite-promoted acylation for the production of an aromatic ketone was reported by researchers at Rhone-Poulenc [42]. The acetylation of anisole to 4-methoxy acetophenone which is an intermediate for paracetamol drug, was performed over zeolites [51-53], Nafion-H on silica [54,55], and microencapsulated scandium (III) triflate in combination with nitromethane/lithium perchlorate [56]. The acetylation of isobutylbenzene over beta zeolite to produce 4-isobutyl acetophenone, as an intermediate for ibuprofen has been reported by Davis and coworkers [43]. Sulfur containing aromatic ketones such as 4-methylthio acetopheone produced by acetylation of thioanisole are potential intermediates for the synthesis of useful drugs as vioxx (refecoxib, for treating an arthritis) [57 -60]. Acylation of 2-MN was studied with various zeolites and clays [27] and found that the beta zeolite is found superior to others. Further, the acylation was studied with beta zeolite by several authors, but the conversions and selectivities towards 6-acyl-2-MN, a desired regiomer is poor to moderate. The migration of the acyl group from the 1-position to the 6-position [61] and protiodeacylation [62] of the acyl group at the 1-position may eventually result in the formation of the thermodynamically most stable 6-acylated product as an intermediate for a widely used anti-inflammatory drug – naproxen [63,64]**.** Such a reaction has been carried out over various acidic zeolites, HY, HBEA and HZSM12 [21,24,65,66], MCM-41 molecular sieves [67], clays [27] and sulphated ZrO_2 [68]. In particular, C-acylation of aromatic ethers has been successfully carried out over various solid catalysts, including clays [27] and large pore zeolites, such as HY and HBEA [22]; an extent to an industrial scale of the use of the latter for the synthesis of 4-methoxyacetophenone and 3’,4’-dimethoxyacetophenone has been recently patented [69,70].

Acetoveratrone (3’, 4’-dimethoxyacetophenone) is produced from veratrole using mineral acid catalysts and used in the synthesis of papaverine (1-(3,4-dimethoxybenzyl)-6,7-dimethoxyisoquinoline), an opium-alkaloid antispasmodic. Acetoveratrone is also synthesized by using hafnium (IV) triflate [71], scandium triflate [72] and hafnium triflate as catalysts in presence of lithium per chlorate nitromethane system [73] and carboxylic acid or trisubstituted silyl carboxylates in presence of trifluoromethyl benzoic acid anhydride [74]. Zeolite HY was found to be more active than Hß [75-78] in the above reaction. Cation-exchanged clays were also tested for this reaction [27]. HPA supported over hexagonal mesoporous silica (HMS) in presence of 1,2-dichloroethane as a solvent is used for the synthesis of acetoveratrone [79]. This catalyst system is already reported TPA/ZrO_2/MCM-41 for acetylation of veratrole in solvent free conditions [80]. The effect of ZrO_2 and SBA-15 together is expected to provide higher thermal stability for TPA by stabilizing the tetragonal phase of ZrO_2 in combination with SBA-15 at high calcination temperature. The present work reports with the resultant composite material an improved catalytic activity for acetylation of veratrole, anisole, thioanisole, isobutyl benzene and 2-MN.

5.4.2. Results and discussion

Acetylation of veratrole with Ac_2O catalyzed by 15 wt.%TPA/22.4 wt.%ZrO_2/SBA-15 under selected reaction conditions gave (A) acetoveratrone (3’, 4’-dimethoxyacetophenone) via electrophilic substitution of H_3CCO^+ to aromatic ring as shown in the Scheme 5.2.

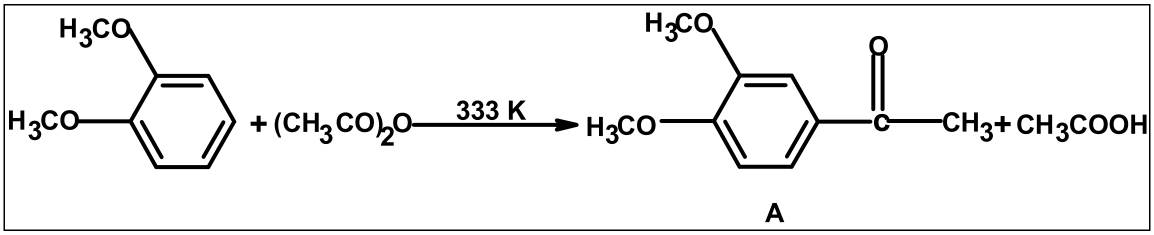

Scheme 5.2: *Acetylation of veratrole with Ac_2O.*

5.4.2.1. Comparison of catalytic activities of different catalysts

The catalytic activities of different catalysts such as H-beta, H-Y, H-Mordenite, H-ZSM-5 and Zn (II)-exchanged clay catalysts alongwith 22.4 wt.%ZrO_2/MCM-41 (with and without 15 wt.%TPA), 22.4 wt.%ZrO_2/MCM-48 (with and without 15 wt.%TPA) catalysts were evaluated in the acetylation of veratrole with Ac_2O under identical reaction conditions for comparison with the catalytic activity of 22.4 wt.%ZrO_2/SBA-15 (with and without 15 wt.%TPA) catalyst calcined at 1123 K (Table 5.4).

Table 5.4: Activities of different catalysts, recyclability and leaching study

Catalyst	S_{BET} (m)	Acidity (mmol g^{-1})	Ac_2O (% Conv.)
Comparison of different catalysts			
H-ß (30)	540	0.94	52.8
H-Y (13.5)	530	2.25	63.4
H-Mordenite (20)	490	0.72	12.3
H-ZSM-5 (60)	364	0.82	9.3
Zn (II)-exchanged clay	-	0.67	19.8
22.4 wt.% ZrO_2/SBA-15	426	0.24	36.9
15 wt.%TPA/22.4 wt.%ZrO_2/SBA-15	372	0.42	72.9
22.4 wt.%ZrO_2/MCM-41	589.8	0.24	9.3
15 wt.%TPA/22.4 wt.%ZrO_2/MCM-41	516.1	0.33	24.9
22.4 wt.%ZrO_2/MCM-48	612.3	0.10	6.0
15 wt.%TPA/22.4 wt.%ZrO_2/MCM-48	540.5	0.25	15.4
15 wt.%TPA/ZrO_2	11	0.02	10.9
3.36 wt.%TPA/SBA-15	341	0.29	30.3
Recyclability of the catalyst			
15 wt.%TPA/22.4 wt.%ZrO_2/SBA-15 (I^{st})	ne	ne	72.6
15 wt.%TPA/22.4 wt.%ZrO_2/SBA-15 (II^{nd})	ne	ne	72.0
Leaching study			
Filtrate *	-	-	59.7

Reaction conditions: temperature = 333 K, veratrole/Ac_2O molar ratio = 5, catalyst wt.=0.09g (3wt.% of total reaction mixture), time = 2 h.

**After 1 h the catalyst was removed and reaction was carried out for further 1h with the filtrate.*

ne = not evaluated.

It is seen from the results that neat 15 wt.% TPA/ZrO_2 gave the lowest conversion, which is due to its low surface area. It is also observed that 3.36 wt.% TPA/SBA-15 calcined at 1123 K shows very less catalytic activity in the reaction, since it has no acidity required for acid catalyzed reactions. Among the zeolite catalysts, H-Y is more active than others due to its highest acidity with large pores gave higher conversion of Ac_2O followed by H-beta (strong and medium acid sites). Similarly, lower activity of H-ZSM-5 might be explained on the basis of its smaller pore size compared with the larger size of the products attributed to diffusional limitations. While, H-Mordenites has one-dimensional pore with elliptical channels, 6.5 X 7.0 also has the low activity. In the present catalyst system, ZrO_2 alone loaded on mesoporous silica support i.e. 22.4 wt.%ZrO_2/SBA-15 calcined at 1123 K shows some catalytic activity, while after loading 15 wt.%TPA over it shows two-fold increase in catalytic activity (Table 5.4). So here is the specific role of the composite materials and the effect of ZrO_2 on the acidity function of TPA, which enhances the catalytic activity. Therefore, we have chosen 15wt.% TPA/22.4 wt.%ZrO_2/SBA-15 calcined at 1123 K as the catalyst for further investigations on its catalytic performance in the veratrole acetylation with Ac_2O.

5.4.2.2. Effect of TPA loading, calcination temperature and ZrO_2 loading

Veratrole acetylation was conducted using different TPA (5-70 wt.%) loaded catalysts to know the effect on the conversion of Ac_2O and the results are shown in Fig 5.21 (a). The discussion is same as previously mentioned. It is seen that conversion of Ac_2O increases with increase in TPA loading upto 15 wt.% and on further increase in loading of TPA there is decrease in Ac_2O conversion. The decrease in its activity at higher TPA loading is due to the formation of WO_3 crystallites due to decomposition of HPA's (XRD Fig. 5.2 (a)). As shown in Fig. 5.21 (a), 15 wt.% catalyst is more acidic than others hence, it gave highest Ac_2O conversion (72.9 %) with 100 % selectivity for acetoveratrone (3', 4'-dimethoxyacetophenone) as unique product under the selected reaction conditions.

Veratrole acetylation by Ac_2O was conducted for knowing the effect of calcination temperature on 15 wt.%TPA/22.4 wt.%ZrO_2/SBA-15 catalyst and the results are shown in Fig. 5.21 (b). There is an increase in Ac_2O conversion upto 1123 K calcinations temperature but on further increase, Ac_2O conversion decreased.

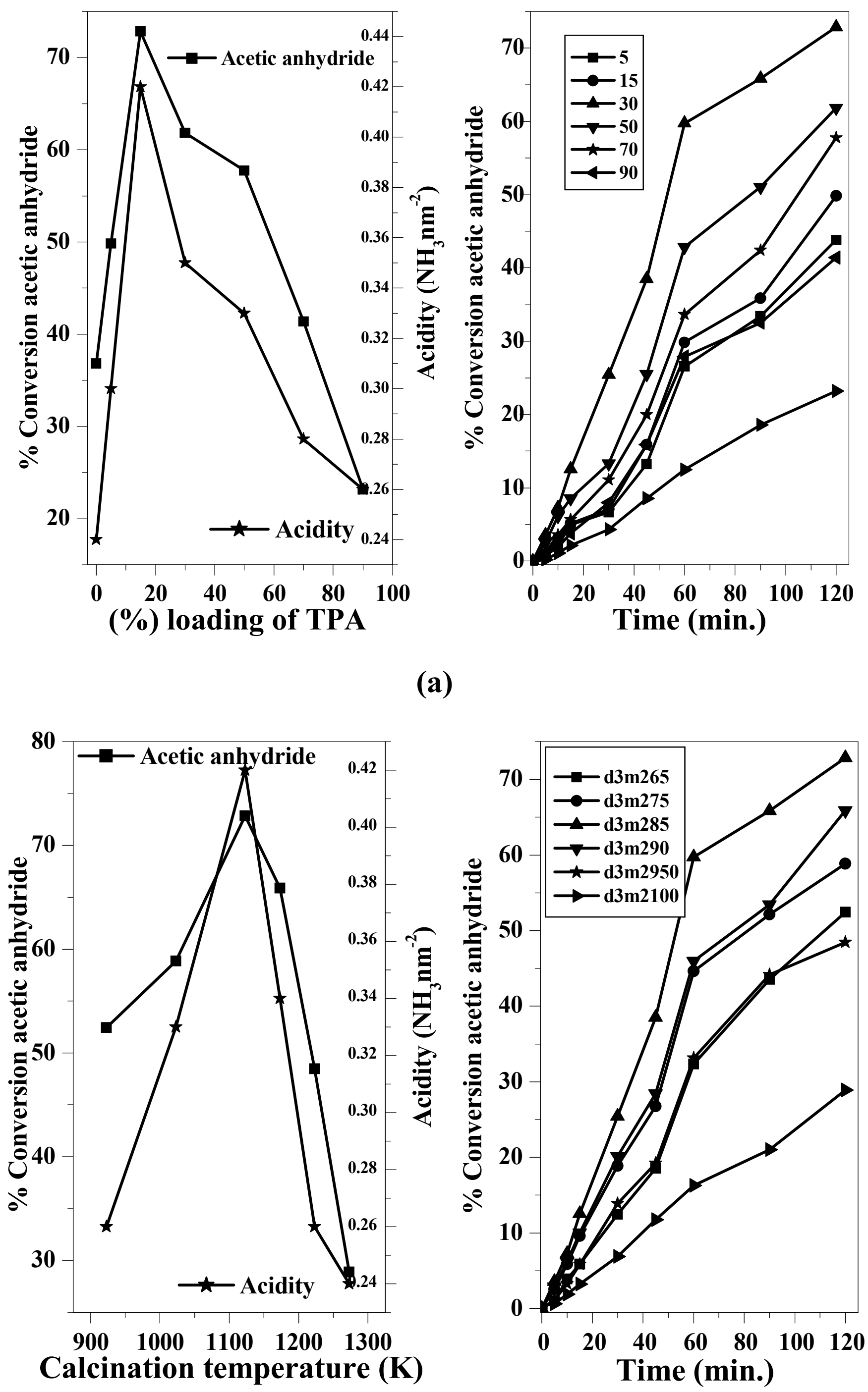

(a)

(b)

Fig. 5.21: *(a) Effect of TPA loading and acidity on Ac$_2$O conversion and time on stream study. (Reaction conditions: temperature = 333 K, veratrole/ Ac$_2$O (molar ratio) = 5, catalyst weight = 0.09 g (3 wt.% of total reaction mixture), time = 2h).*
(b) Effect of calcination temperature and acidity on Ac$_2$O conversion and time on stream study. (Reaction conditions: temperature = 333 K, veratrole/ Ac$_2$O (molar ratio) = 5, catalyst weight = 0.09 g (3 wt.% of total reaction mixture), time = 2h).

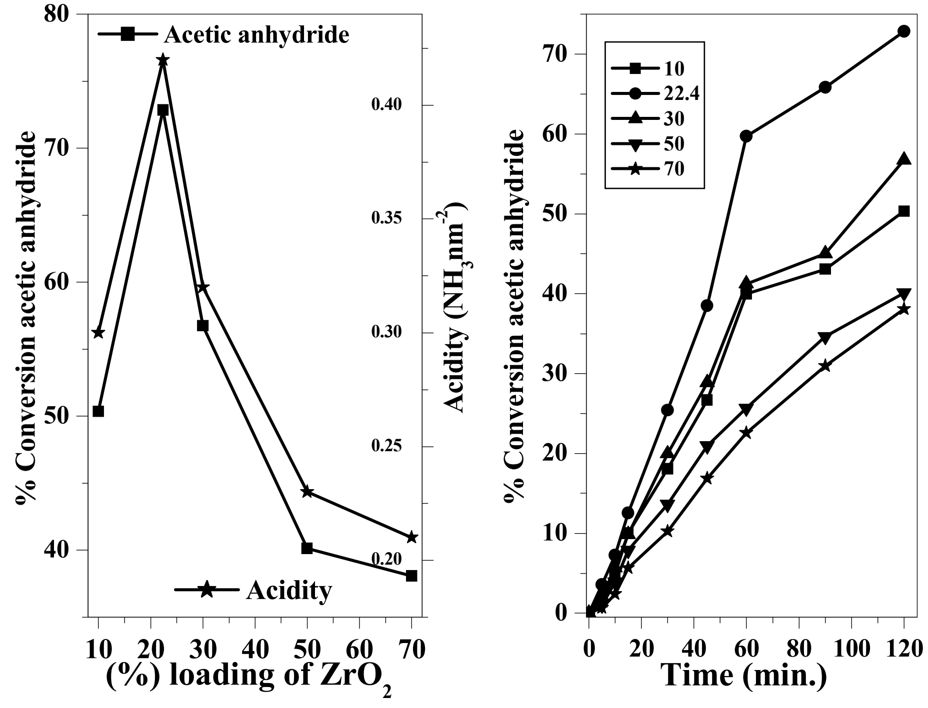

Fig. 5.22: *Effect of ZrO_2 loading and acidity on Ac_2O conversion and time on stream study. (Reaction conditions: temperature = 333 K, veratrole/ Ac_2O (molar ratio) = 5, catalyst weight = 0.09 g (3 wt.% of total reaction mixture), time = 2h).*

This observation is supported by the fact that 15 wt.%TPA/22.4 wt.%ZrO_2/SBA-15 calcined at 1123 K has the maximum concentration of acid sites, where TPA forms a monolayer coverage over the support. Hence, catalyst calcined at 1123 K was chosen for further study. In order to study the effect of ZrO_2 loading over SBA-15 with 15 wt.%TPA catalyst calcined at 1123 K, veratrole acetylation by Ac_2O was conducted under selected reaction conditions. As shown in Fig. 5.22, there is an increase in Ac_2O conversion upto 22.4 wt.% ZrO_2 loading and on further increase in loading Ac_2O conversion decreased. This could be due to the formation of monolayer coverage of 22.4 wt.% of ZrO_2 over SBA-15 giving rise to maximum total acidity. While on further increase in ZrO_2 loading it shows the formation of monoclinic phase of ZrO_2 alongwith tetragonal phase and thereby decreasing the conversion of Ac_2O in veratrole acetylation.

The amount and the total acidity of the catalysts were determined from TPD of ammonia. Then it was correlated with catalytic activities of 22.4 wt.%ZrO_2/SBA-15 with different (%) TPA loadings as shown in Fig. 5.21 (a), 15 wt.%TPA/22.4 wt.%ZrO_2/SBA-

15 calcined at different calcination temperatures as shown in Fig. 5.21 (b) and 15 wt.%TPA/wt.% ZrO_2/SBA-15 with different (%) ZrO_2 loading as per shown in (Fig 5.22). It shows that total acidity of TPA/22.4 wt.%ZrO_2/SBA-15 calcined at 1123 K catalyst increases till 15 wt.% and then on further increasing TPA loading it shows decrease so as to catalytic activity. It can be concluded as till 15 wt.%TPA, the Keggin unit of HPA retains its structure and acidity. Total acidity data of the catalyst 15 wt.%TPA/22.4 wt.%ZrO_2/SBA-15 at different calcination temperatures were plotted along with catalytic activity. It shows that till 1123 K, total acidity increases and on further increase in calcination temperature shows decrease in acidity and also decrease in catalytic activity, which is due to decomposition of TPA into WO_3 crystallites. Similarly, with increasing ZrO_2 loading till 22.4 wt.% catalyst 15 wt.%TPA/ZrO_2/SBA-15 calcined at 1123 K shows increase in acidity and thereby catalytic activity. The highest acidity corresponds to monolayer coverage of TPA (i.e. 15 wt.%TPA/22.4 wt.%ZrO_2/SBA-15 calcined at 1123 K), where the Keggin–like structure is intact, as supported by ^{31}P CP-MAS NMR and XRD. The total acidities of 22.4 wt.%ZrO_2 and 15 wt.%TPA/22.4 wt.%ZrO_2 supported on various silica supports, unsupported TPA/ZrO_2 and TPA supported on SBA-15, all calcined at 1123 K, are given in Table 5.4. Among all of them, 15 wt.% TPA/22.4 wt.%ZrO_2/SBA-15 calcined at 1123 K shows the highest acidity corresponds to monolayer coverage of TPA, where the Keggin –like structure is intact, as supported by ^{31}P CP-MAS NMR, FT-Raman and XPS. These results indicate that TPA/ZrO_2 dispersed more uniformly over large surface area and large pore volume SBA-15 as compared with other supports.

5.4.2.3. Effect of reaction parameters

From Fig. 5.23 (a) shows that with increase in catalyst concentration from 1-5 wt.% of total reaction mixture (3 g), by keeping constant molar ratio of veratrole: Ac_2O as 5, 333 K and 2 h, it shows increase in Ac_2O conversion from 28.8 % to 82.1 % with 100 % selectivity for acetoveratrone as a monoacetylated product. The effect of veratrole to Ac_2O molar ratio on the conversion of veratrole and time on stream study for different molar ratios are presented in Fig. 5.23 (b). The mole ratio of veratrole to Ac_2O was varied from 1 to 9, by keeping other conditions the same. As veratrole: Ac_2O molar ratio is increased from 1 to 9, conversion of Ac_2O increased from 36.2 to 81.7 % with 100 % selectivity for a monoacetylated product.

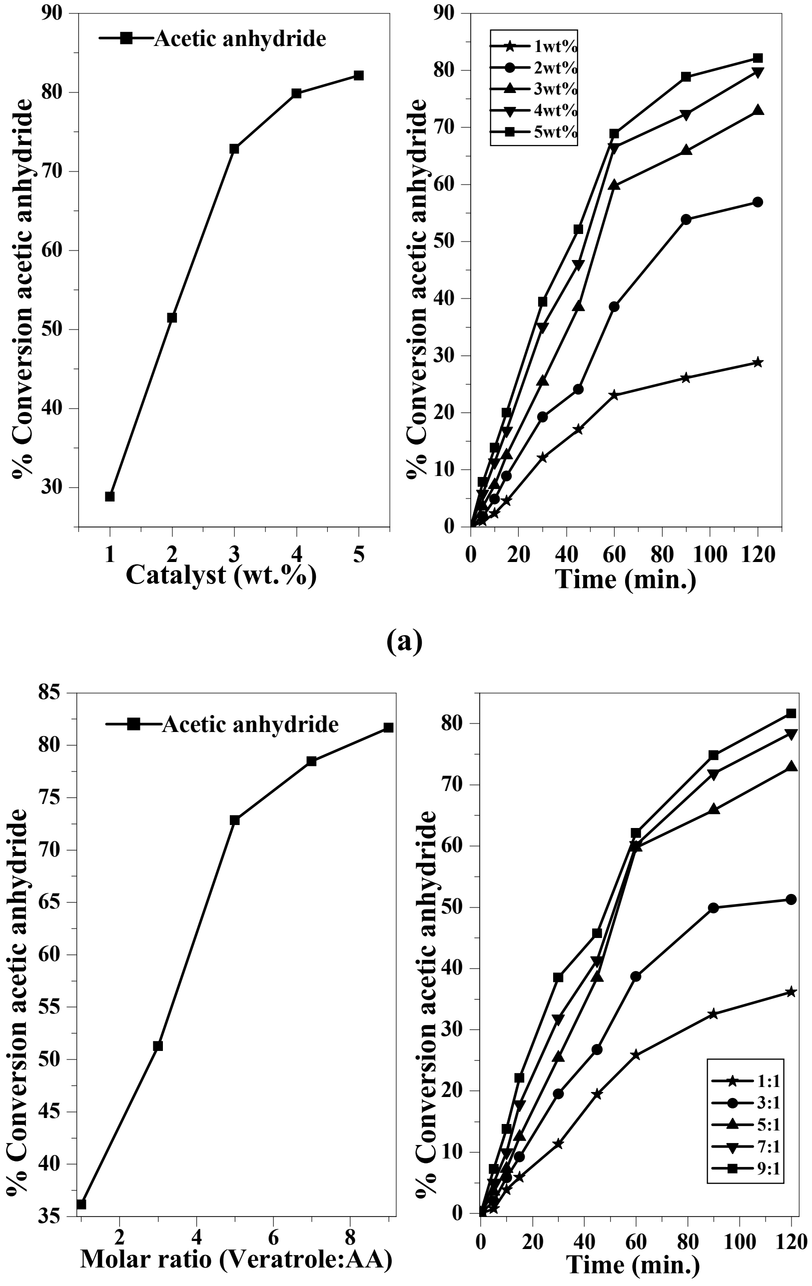

(a)

(b)

Fig. 5.23: *(a) Effect of catalyst weight on Ac_2O conversion and time on stream study. (Reaction conditions: temperature = 333 K, veratrole/ Ac_2O (molar ratio) = 5, time = 2h). (b) Effect of molar ratio on Ac_2O conversion and time on stream study. (Reaction conditions: temperature = 333 K, catalyst weight = 0.09 g (3 wt.% of total reaction mixture), time = 2h).*

The acetylation of veratrole with Ac_2O was carried out in the temperature range 313-353 K, to know the effect of temperature on the conversion of Ac_2O. It is seen from Fig. 5.24 that the conversion of Ac_2O increases from 46.1 % to 83.1 % with increase in temperature from 313 to 353 K.

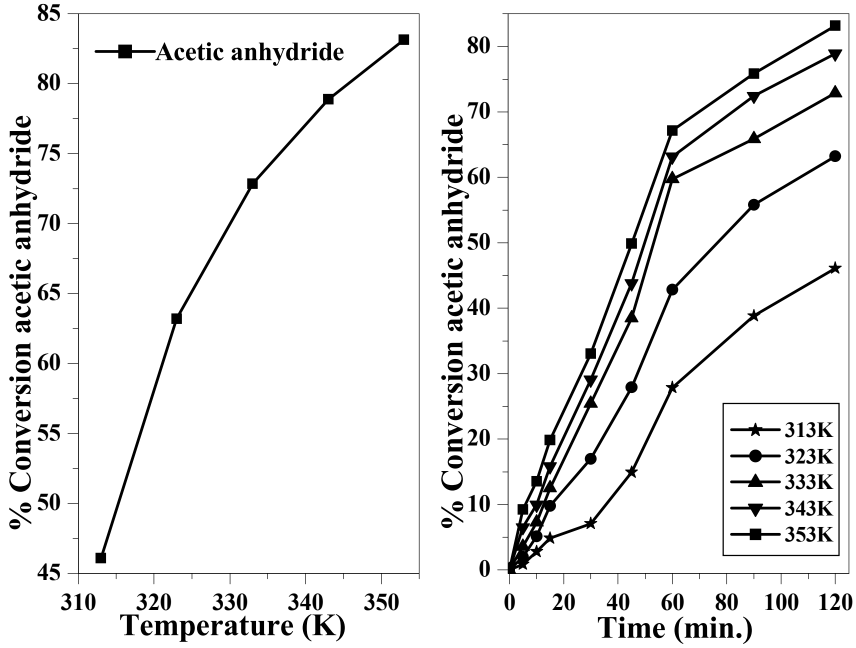

Fig. 5.24: *Effect of temperature on Ac_2O conversion and time on stream study. (Reaction conditions: veratrole/ Ac_2O (molar ratio) = 5, catalyst weight = 0.09 g (3 wt.% of total reaction mixture), time = 2h).*

5.4.2.4. Acetylation of different aromatic substrates with Ac_2O

15 wt.%TPA/22.4 wt.%ZrO_2/SBA-15 calcined at 1123 K with an Ac_2O was employed to acylate the aromatic hydrocarbons. The data for the catalytic efficiencies along with reaction conditions are listed in Table 5.5 under mentioned reaction conditions in Table 5.5.

Anisole acylation gave 97.9 % p-methoxyacetopheone (A) and remaining is o-methoxyacetopheone (B) (Scheme- 5.3) with 60 % of Ac_2O conversion. For acetylation of thioanisole 15 wt.%TPA/22.4 wt.%ZrO_2/SBA-15 calcined at 1123 K was employed under mentioned reaction conditions in Table 5.5 with an Ac_2O. It is giving 99.6 % p-(methylthio acetopheone) (A) and remaining is o- (methylthio acetopheone) (B) (Scheme-5.3) isomer with 35.8 % of Ac_2O conversion. The acetylation of isobutyl benzene was carried out with Ac_2O giving rise to 30 % Ac_2O conversion with 100% product selectivity for 4-isobutylacetophenone (A) (Scheme-5.4) as shown in Table 5.5. The acetylation of 2-MN with Ac_2O under different solvents are presented in Table 5.5. Product formation can be attributed to the strong support interaction to enable the formation of carbocation, an essential requirement for Friedel-Crafts electrophilic acylation of aromatic ethers. Acetylation reaction with different solvents are presented in Table 5.5. Solvent effect on the conversions is visible, affording higher conversion with nitrobenzene.

Table 5.5: Acetylation of aromatic substrates with Ac_2O

Substrate	Mole ratio	Temp.	Catalyst wt.%	Time (h)	% Ac_2O Conversion
Veratrole	5:1	60	0.09	2	72.9
Anisole	10:1	90	0.15	3	60.9
Thioanisole	10:1	90	0.15	3	35.8
Isobutyl benzene	10:1	100	0.15	5	30.0
2-MN (Nitrobenzene)*	2:1	100	0.15	8	61.2
2-MN (Chlorobenzene)*	2:1	100	0.15	8	50.3
2-MN (1,2-DCB)*	2:1	100	0.15	8	56.7
2-MN (Benzene)*	2:1	100	0.15	8	39.1

** Solvent amount = 20 ml.*

Reaction conditions: Catalyst = 15 wt.%TPA/22.4 wt.%ZrO_2/SBA-15 calcined at 1123 K.

The selectivity of the products, 1-acyl-2-MN (A) formed remains identical, close to 97% and remaining 3% of 6-acyl-2-MN (B), which is as shown in Scheme-5.5 irrespective of the solvents employed, which is in contrast to the classical homogeneous acylation reaction. In the classical acylation reaction conducted with anhydrous aluminium chloride employed in more than stoichiometric quantities, the solvent plays a major role in the isomer distribution, depending on the ability of the solvent to form the complex with acylating agent [61]. Acylation occurs at 1-position predominantly in carbon disulphide, and at 6-position in nitrobenzene. Isomeric ratio varies with different transition metal chlorides in stoichiometric amounts correlated to their acid strength. Insufficient acid strength in the present catalytic reaction due to the use of small amounts of solid acids precludes formation of other isomers accentuated by protiodeacetylation at moderate temperatures instead favours exclusive formation of 1-acetyl derivative. The acylation of 2-MN has been extensively studied as a test reaction for zeolites, USY, and ZSM-12 [81] and has recently been used with MCM-41 catalysts [82]. Acetylation with Ac_2O occurs at the 1-position yielding the kinetically favored 1-acetyl-2-MN. Although Friedel–Crafts acylation is usually irreversible, the main product 1-acetyl-2-MN can undergo protiodeacylation [62] and reacylation then yields the thermodynamically more stable 2-acetyl-6-Methoxynaphthalene (2-Ac-6-MN), which is also produced by migration of the acetyl group [61].

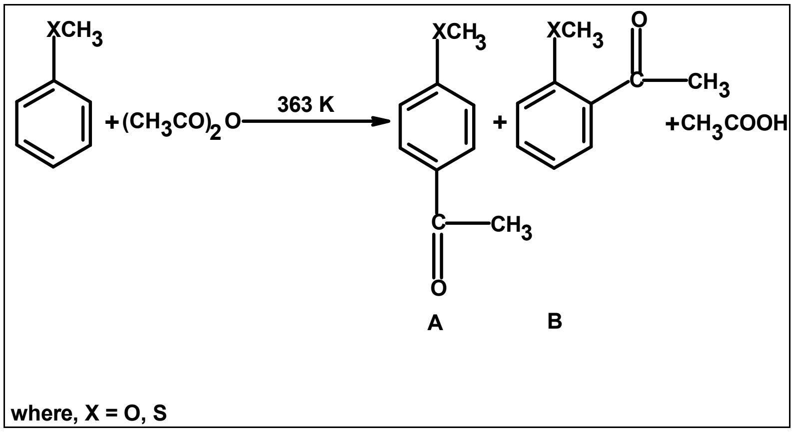

Scheme 5.3: *Acetylation of anisole or thioanisole with Ac_2O.*

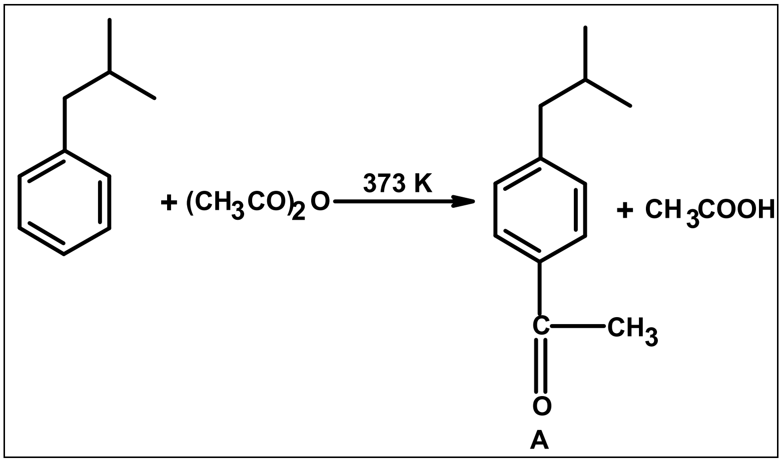

Scheme 5.4: *Acetylation of isobutyl benzene with Ac_2O.*

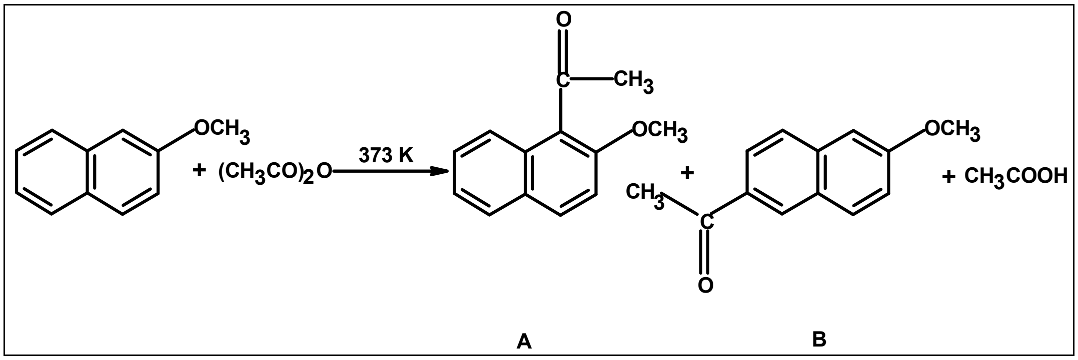

Scheme 5.5: *Acetylation of 2-MN with Ac_2O.*

5.4.2.5. Kinetic study

The maximum conversion of Ac_2O (72.9 %) was obtained at 333 K, by keeping veratrole: Ac_2O molar ratio as 5 with catalyst amount as 3 wt.% of total reaction mixture. At one particular temperature, first-order rate constants were calculated for 1 h of reaction time, and then the constant values of 'k_1' showed that the acetylation of veratrole is a first-order reaction. The standard equations for a first order series reaction $C_A/C_{Ao} = e^{-k_1 t}$ has been used for the determination of rate constant, where C_A and C_{Ao} are the concentration of Ac_2O at initial time and at time t, respectively. Activation energy evaluated from graph of –ln rate Vs 1/T was found to be 5.79 kcal mol^{-1}.

5.4.3. Conclusions

The results presented in this work again demonstrate that TPA/ZrO_2 dispersed uniformly inside the mesopores of SBA-15 formed nano-sized (3-4 nm) composite material at a calcination temperature of 1123 K. The 15 wt.% TPA/22.4 wt.%ZrO_2/SBA-15 catalyst calcined at 1123 K was found to be the most active catalyst in all the acetylation reactions studies under selected liquid phase conditions under N_2 atmosphere and shows greater catalytic activity (6-7 fold higher) than with the corresponding neat TPA/ZrO_2 catalyst. The higher activity of the catalyst in acetylation reaction is because of uniform dispersion of TPA/ZrO_2 over large surface area and large pore volume SBA-15 as compared with other supports. The performance of HPA supported on ZrO_2 embedded inside the mesoporous silica support like SBA-15 catalyst was found to depend on catalyst pretreatment conditions such as effect of loadings of TPA, ZrO_2 and calcination temperatures and most importantly on the nature and the characterstics of the mesoporous support.

5.5. REFERENCES

1. D. Zhao, J. Feng, Q. Huo, N. Melosh, G. H. Fredrickson, B. F. Chmelka, G. D. Stucky, Science, 279 (1998) 548.
2. M. Misono, Chem. Commun., (2001) 1141.
3. E. Lopez-Salinas, J. G. Hernandez-Corez, I. Schifter, E. Torres-Garcia, J. Navarrete, A. Gutierrez-Carillo, T. Lopez, P. P. Lottici, D. Bersani, Appl. Catal. A: General, 193 (2000) 215.
4. M. W. McKittrick, C. W. Jones, Chem. Mater., 15 (2003) 1132.
5. A. S. Maria Chong, X. S. Zhao, A. T. Kwtedji, S. Z. Qiao, Micropor. Mesopor. Mater., 72 (2004) 33.
6. T. R. Pauly, V. Petkov, Y. Liu, Simon J. L. Billinge, T. J. Pinnavaia, J. Am. Chem. Soc., 124 (1) (2002) 99.
7. P. A. Jalil , N. Tabet , M. Faiz, N. M. Hamdan, Z. Hussain, Appl. Catal.A: General, 257 (2004) 1.
8. E. Brunner, Catal. Today, 38 (1997) 361.
9. T. Baba, Y. Hasada, M. Nomura, Y. I. Ohno, Y. Ono, J. Mol. Catal. A: Chem., 114 (1996) 247.
10. N. Essayem, Y. Y. Tong, H. Jobic, J. C. Vedrine, Appl. Catal. A: General, 194 – 195 (2000) 109.
11. V. M. Mastikhin, I. L. Mudrakovsky, A. V. Nosov, Prog. NMR Spectrosc., 23 (1991) 259.
12. M. Hunger, Catal. Rev.- Sci. Eng., 39 (4) (1997) 345.
13. S. Uchida, K. Inumaru, J. M. Dereppe, M. Misono, Chem. Lett., 643 (1998).
14. A. Thomas, C. Dablemont, J.-M. Basset, F. Lefebvre, C. R. Chimie, 8 (2005) 1969.
15. E. F. Kozhevnikova, I. V. Kozhevnikov, J. Catal., 224 (2004) 164.
16. J. A. Dias, E. Caliman, S. C. L. Dias, M. Paulo, A. T. C. P. de Souza, Catal. Today, 85 (2003) 39.
17. N. Millot, C. S. Santini, F. Lefebvre, C. R. Chimie, 7 (2004) 725.
18. M. Hunger, Solid State Nucl. Magn. Reson., 6 (1996).
19. M. Hunger, S. Ernst, S. Steuernagel, J. Weitkamp, Micropor. Mater., 6 (1996) 349.

20. M. Hunger, U. Schenk, M. Breuninger, R. Gla¨ser, J. Weitkamp, Micropor. Mesopor. Mater., 27 (1999) 261.
21. T. Okuhara, N. Mizuno, M. Misono, Adv. Catal., 41 (1996) 113.
22. Y. Nakano, T. Iizuka, H. Hattori, K. Tanabe, J. Catal., 57 (1978) 1.
23. Y. Saito, P. N. Cook, H. Niiyama, E. Echigoya, J. Catal., 95 (1985) 49.
24. K. Tanabe, M. Misono, Y. Ono, H. Hattori, Stud. Surf. Sci. Catal., 51 (1989) 169.
25. T. Jin, T. Yamaguchi, K. Tanabe, J. Phys. Chem., 90 (1986) 4794.
26. K. Tanabe, H. Hattori, T. Yamaguchi, Crit. Rev. Surf. Chem., 1 (1990) 1.
27. L. Pizzio, P. Vázquez, C. Cáceres, M. Blanco, Catal. Lett., 4 (2001) 77.
28. A. V. Emeline, G. V. Kataeva, A. S. Litke, A. V. Rudakova, V. K. Ryabchuk, N. Serpone, Langmuir, 14 (1998) 5011.
29. J. Joo, T. Yu, Y. W. Kim, H. M. Park, F. Wu, J. Z. Zhang, T. Hyeon, J. Am. Chem. Soc., 125 (2003) 6553.
30. W. Kuang, A. Rives, M. Fournier, R. Hubaut, Appl. Catal. A: General, 250 (2003) 221.
31. B. H. Davis, R. A. Keogh, S. Alerasool, D. J. Zalewski, D. E. Day, P. K. Doolin, J. Catal., 183 (1999) 45.
32. I. V. Kozhevnikov, ‘Catalysis by Polyoxometalates, Catalysts for Fine Chemical Synthesis’, vol. 2, Wiley, 2002, p. 15.
33. H.-W. Voges, in: B. Elvers, S. Hawkins, G. Schulz (Eds.), Ullmann’s Encyclopedia of Industrial Chemistry, vol. 19, VCH, Weimheim, Germany, 1991, p. 328.
34. B. M. Devassy, G. V. Shanbhag, F. Lefebvre, W. Böhringer, J. Fletcher, S. B. Halligudi, J. Mol. Catal. A: Chem., 230 (2005) 113.
35. T. Matsuura, Y. Ohkatsu, Polym. Degrad. Stab., 70 (2000) 59.
36. C. J. Norman, P. A. Goulding, P. J. Moles, Stud. Surf. Sci. Catal., 90 (1994) 269.
37. D. H. Aguilar, L. C. Torres-Gonzalez, L. M. Torres-Martinez, T. Lopez, P. Quintana, J. Solid State Chem., 158 (2001) 349.
38. E. Torres-Garcia, G. Rosas, J. A. Ascencio, E. Haro-Poniatowski, R. Perez, Appl. Phys. A, 79 (2004) 401.
39. K. Arata, Adv. Catal., 37 (1990) 165.

40. A. B. Deshpande, A. R. Bajpai, S. D. Samant, Appl. Catal. A: General, 209 (2001) 229.
41. E. G. Derouane, C. J. Dillon, D. Bethell, S. B. D. Hamid, J. Catal., 187 (1999) 209.
42. M. Spagnol, L. Gilbert, R. Jacquot, H. Guillot, P. J. Triel, A. M. LeGovic, 'Book of Abstracts of 4th International Symposium on Heterogeneous Catalysts and Fine Chemicals', Basel, Switzerland, 1996.
43. D. P. Sawant, S. B. Halligudi, Cata. Commun., 5 (2004) 659.
44. P. Andy, J. Gracia-Martinez, G. Lee, H. Gonzalez, C. W. Jones, M. E. Davis, J. Catal., 215 (2000) 192.
45. K. Gaare, D. Akporiaye, J. Mol. Catal. A: Chem., 109 (1996) 177.
46. E. Fromentin, J.-M. Coustard, M. Guisnet, J. Mol. Catal. A: Chem., 159 (2000) 377.
47. P. Botella, A. Corma, G. Sastre, J. Catal., 197 (2001) 81.
48. P. Moreau, A. Finiels, P. Meric, J. Mol. Catal. A: Chem., 154 (2000) 185.
49. M. Spagnol, L. Gilbert, H. Guillot, J. P. Triel, PCT Int. Patent WO 97/48665 (1997).
50. S. D. Kim, K. H. Lee, J. S. Lee, Y. J. Kim, K. E. Yoon, J. Mol. Catal. A: Chem., 152 (2000) 33.
51. A. Corma, M. J. Climent, H. Garcia, J. Primo, Appl. Catal. A: General, 49 (1989) 109.
52. D. Rohan, C. Canaff, E. Fromentin, M. Guisnet, J. Catal., 177 (1998) 296.
53. B. M. Choudary, M. Sateesh, M. L. Kantam, K. V. R. Prasad, Appl. Catal. A: General, 171 (1998) 155.
54. A. Heidekum, M. A. Harmer, W. F. Hoelderich, J. Catal., 188 (1999) 230.
55. Y. Izumi, M. Ogawa, W. Nohara, K. Urabe, Chem. Lett., (1992) 1987.
56. S. Kobayashi, S. Nagayama, J. Am. Chem. Soc., 120 (1998) 2985.
57. H. G. Franck, J. W. Stadelhofer, Industrial Aromatic Chemistry, Springer, New York, 1988, p. 324.
58. M. Aslam, K. G. Davenport, R. R. Graham, US Patent 4,794,205 (1988).
59. C. G. Overberger, A. Lebovits, J. Am. Chem. Soc., 74 (1956) 4792.
60. J. R. Zoeller Jr., C. E. Sumner, J. Org. Chem., 55 (1990) 319.

61. P. H. Gore, in: ‘G.A. Olah (Ed.), Friedel-Crafts and Related Reactions’, vol. III, Wiley, New York, 1964, p. 64, 72.
62. J. Al-Ka'bi, J. A. Farooqui, P. H. Gore, A. M. G. Nassar, E. F. Saad, E. L. Short, D. N. Waters, J. Chem. Soc. Perkin Trans. II (1988) 943.
63. K. T. Wan, M. E. Davis, J. Catal., 152 (1994) 25.
64. M. E. Davis, Micropor. Mesopor. Mater., 21 (1998) 173.
65. H. K. Heinichen, W. Hölderich, J. Catal., 185 (1999) 408.
66. A. Berrhegis, P. Ayrault, E. Fromentin, M. Guisnet, Catal. Lett., 68 (2000) 121.
67. H. Hitz, R. Prins, J. Catal., 168 (1997) 194.
68. G. D. Yadav, M. S. Krishnan, Chem. Eng. Sci., 54 (1999) 4189.
69. M. Spagnol, L. Gilbert, E. Benazzi, C. Marcilly, Patent PCT Int. Appl. WO 96,35,655 (1996).
70. M. Spagnol, L. Gilbert, E. Benazzi, C. Marcilly, Patent PCT Int. Appl. WO 96,35,656 (1996).
71. A. Kawada, S. Mitamura, S. Kobayashi, Syn. Lett.,7 (1994) 545.
72. I. Hachiya, M. Moriwaki, S. Kobayashi, Tet. Lett., 36 (1995) 409.
73. I. Hachiya, M. Moriwaki, S. Kobayashi, Bull. Chem. Soc. Jpn., 68 (1995) 2053.
74. K. Suzuki, M. Mukoyama, Jpn. Pat. , 06 145 092, 1994.
75. M. Spagnol, L. Gilbert, D. Alby, Ind. Chem. Libr., 8 (1996) 29.
76. T. Raja, A. P. Singh, A. V. Ramaswamy, A. Finiels, P. Moreau, Appl. Catal. A: General, 211 (2001) 31.
77. C. Guignard, V. Pédron, F. Richard, R. Jacquat, M. Spagnol, J.M. Coustard, G. Pérot, Appl. Catal. A: General, 234 (2002) 79.
78. P. Moreau, A. Finiels, P. Meric, J. Mol. Catal. A: Chem., 154 (2000) 185.
79. G. D. Yadav, H. Manyar, Micropor. Mesopor. Mater., 63 (2003) 85.
80. D. P. Sawant , Vinu A., F. Lefebvre, S. B. Halligudi, J. Mol. Catal. A: Chem., (Accepted).
81. G. Harvey, G. Mäder, Collect. Czech. Chem. Commun.,57 (1992) 862.
82. E. A. Gunnewegh, S. S.Gopie, H.van Bekkum, J. Mol. Catal. A: Chem., 106 (1996) 151.

CHAPTER – 5

ZIRCONIA SUPPORTED TPA IN SBA-15

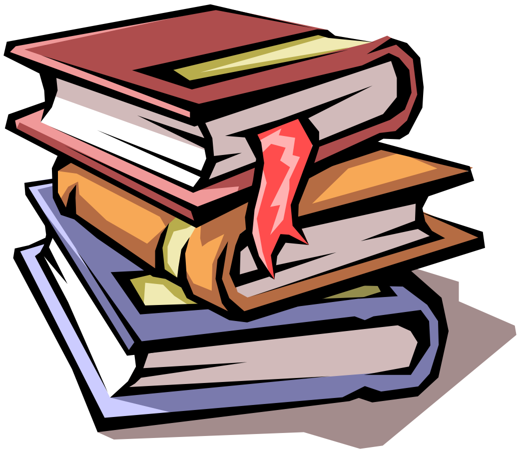

5. ZIRCONIA SUPPORTED TPA IN SBA-15

5.1. INTRODUCTION

This section presents the characterization of TPA over ZrO_2 dispersed uniformly in mesoporous silica (MS) channels of MCM-41, MCM-48 and SBA-15. Catalysts with different TPA loadings (5 to 90 wt.%) on 22.4 wt.%ZrO_2/MCM-41 and 15 wt.%TPA on different ZrO_2 loadings (10-70 wt.%)/MCM-41 were prepared and calcined at 1123 K. Also, 15 wt.%TPA/22.4 wt.%ZrO_2/ SBA-15 catalysts calcined in the range 923 to 1273 K were prepared. These catalysts were screened for their catalytic activities in the liquid phase benzylation of phenol with BA and acetylation of veratrole and other aromatic substates with Ac_2O.

5.2. CHARACTERIZATION-RESULTS AND DISCUSSION

5.2.1. Elemental analysis

The ratio of P: W (1: 12) in 15 wt.%TPA/22.4 wt.%ZrO_2/MCM-41 corresponding to a Keggin unit was estimated by XRF analysis as (1: 12.13) and by ICP-OES analysis as (1:12.07).

5.2.2. XRD

The X-ray powder diffraction patterns of the catalysts with different (%) TPA loadings calcined at 1123 K are shown in Fig. 5.1 (a), and those of 15 wt.% TPA/22.4 wt.% ZrO_2/SBA-15 calcined at different calcination temperatures are shown in Fig. 5.1 (b). The small angle XRD patterns of TPA/ZrO_2 modified samples were typical of hexagonally ordered mesoporous materials, with one sharp peak indexed as (100) and two smaller peaks indexed as (110) and (200), typical of hexagonal (*p6mm*) of parent SBA-15.

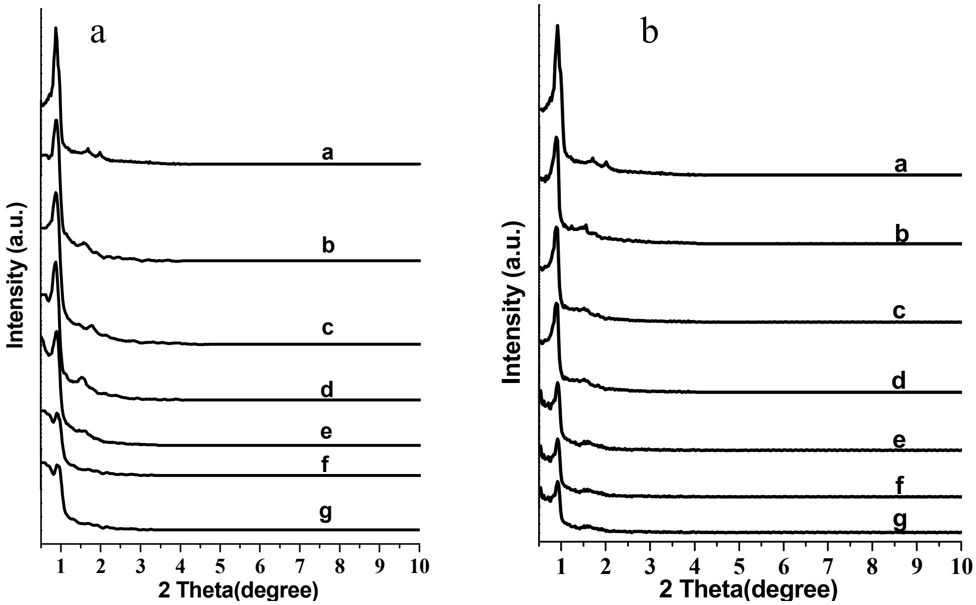

Fig. 5.1: *(a) Low angle XRD: a, SBA-15, TPA/22.4 wt% ZrO_2/SBA-15 with: b, 5; c, 15; d, 30; e, 50; f, 70; and g, 90 wt% TPA loading and calcined at 1123 K, including insight wide-angle XRD, respectively. (b) Low angle XRD: a, SBA-15, 15 wt% TPA/22.4 wt% ZrO_2/SBA-15 calcined at: b, 923; c, 1023; d, 1123; e, 1173; f, 1223; and g, 1273 K; including insight wide-angle XRD, respectively.*

Fig. 5.1 (a) shows that the mesoporous structure remained intact up to 50 wt.% TPA loading and after this it started loosing mesoporosity. In addition, the 15 wt.% TPA-loaded sample showed intact mesoporosity even after calcination up to 1273 K. Further the added TPA stabilized the tetragonal phase of ZrO_2. Such stabilization of the phase composition desired for specific applications in the presence of other mesoporous oxides prevented the particles from growing larger than the pore sizes. XRD patterns displayed three well-defined peaks characteristic of tetragonal ZrO_2; these can be indexed as (111), (202), and (131). Fig.5.2 (a) shows the wide-angle XRD patterns of the catalysts with different (%) TPA loadings calcined at 1123 K, wherein XRD patterns of pure TPA is compared with all modified samples. Wide-angle XRD patterns show three well-defined peaks characteristics of tetragonal ZrO_2 (t-ZrO_2) i.e. $2\theta \sim 30$, 50 and 60° phase, which could be indexed as (111), (202) and (131). Wide-angle XRD of TPA over 22.4 wt.% ZrO_2/SBA-15 shows monolayer coverage up to 15 wt.% loading and above this, it started decomposing into WO_3 ($2\theta \sim 23.12$, 23.59, and 24.38°) crystalline peaks as seen in Fig. 5.2(a). Similarly, 15 wt.% TPA/22.4 wt.% ZrO_2/SBA-15 showed monolayer coverage up to 1123 K calcination temperature. However, above 1123 K, it showed decomposition of TPA into WO_3 crystallites [Fig. 5.2 (b)]. As for bulk ZrO_2, crystallization of the amorphous phase to the metastable tetragonal phase typically occurred in the range 673–773 K, but after impregnating over SBA-15, the stabilization of transition of phases shifted to 923 K.

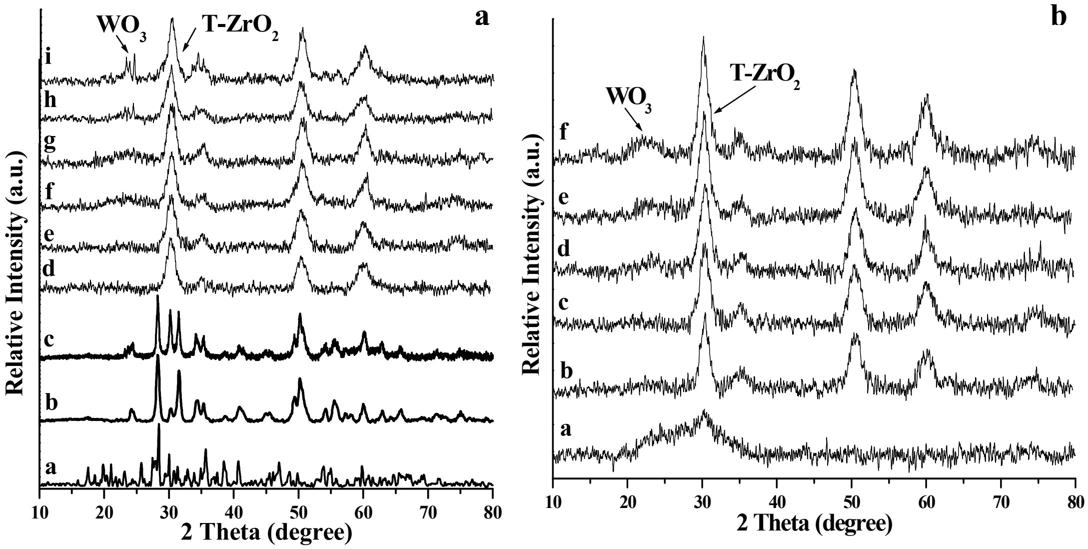

Fig. 5.2: *XRD patterns of (a) a) neat TPA, b) ZrO_2, c) 15 wt.%TPA/ZrO_2, d) 5, e) 15, f) 30, g) 50, h) 70 and i) 90 wt.% catalysts calcined at 1123 K and (b) 15 wt.% catalyst calcined at a) 923, b) 1023, c) 1123, d) 1173, e) 1223, and f) 1273 K.*

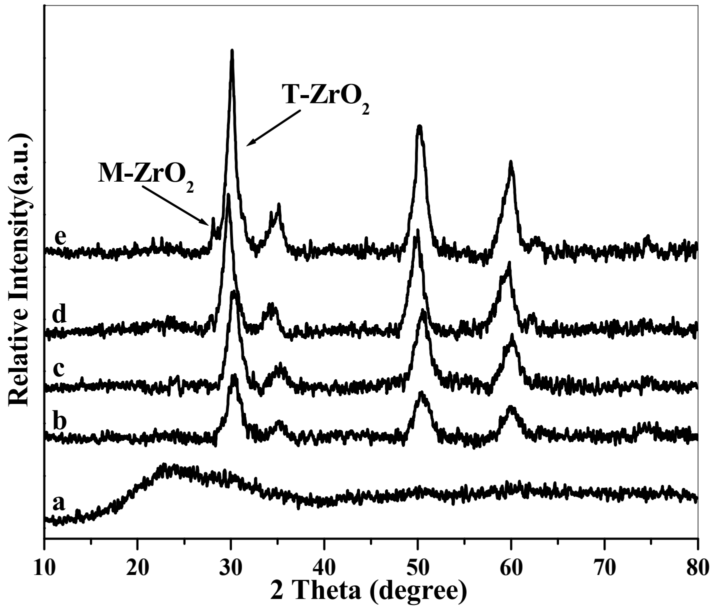

Fig. 5.3: *XRD patterns of 15 wt.% TPA over a) 10, b) 22.4, c) 30, d) 50, and e) 70 wt.% ZrO_2/SBA-15 catalysts calcined at 1123 K.*

The XRD patterns of 15 wt.%TPA/ 22.4 wt.%ZrO_2/SBA-15 with different ZrO_2 (%) loading over SBA-15 shows that, monoclinic ZrO_2 (m-ZrO_2, 2θ ~ 28°) phase also appeared when the ZrO_2/SBA-15 wt. ratio was higher than 0.5.

5.2.3. Sorption study

The textural properties of plain and modified SBA-15 with different loadings of TPA (wt.%)/22.4 wt.% ZrO_2 are presented in Table 5.1. It is seen that the surface area, pore size, and pore volume of modified SBA-15 decreased when compared with parent SBA-15. This indicates that TPA/ZrO_2 was well dispersed inside the pores of mesoporous channels. The adsorption isotherms and BJH pore size distributions of 15 wt.% TPA/22.4 wt.% ZrO_2/SBA-15 and parent SBA-15 are shown in Fig. 5.4.

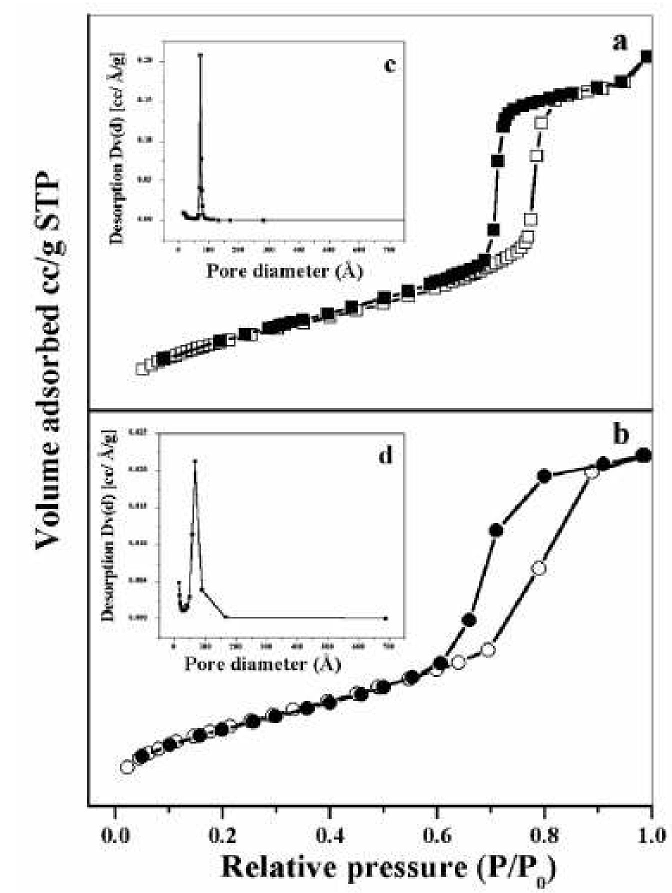

Fig. 5.4: *Nitrogen adsorption isotherms with insight figure of (pore size distribution) of (a) calcined SBA-15 (c) and (b) 15 wt.% TPA/22.4 wt.% ZrO_2/SBA-15 (d) calcined at 1123 K.*

It is seen from Fig. 5.4 that the mesostructure was retained after loading of 15 wt.% TPA/22.4 wt.% ZrO_2 into SBA-15 even after calcination up to 1123 K. However, the surface area of the samples up to 50 wt.% TPA loading were still >300 m^2 g^{-1}, and pore volume was in the range of 0.53– 0.63 cm^3 g^{-1} (Table 5.1), which are sufficient for catalytic functions. Though the surface areas of modified MCM-41 and MCM-48 were greater than those of corresponding modified SBA-15 samples, their catalytic activities were lower compared with those of 15 wt.% TPA/22.4 wt.% ZrO_2/SBA-15 (Table 5.1) due to narrow pore diameters. Also, the surface area and pore size of 15 wt.% TPA/22.4 wt.% ZrO_2/SBA-15 decreased with increasing calcinations temperature (Table 5.1). The neat 15 wt.% TPA/ZrO_2 calcined at 1123 K had low surface area due to sintering of ZrO_2 support, resulting in the formation of larger particles and low acidity due to the decomposition of TPA into WO$_3$ and other corresponding oxides.

Table 5.1: Physicochemical properties of the catalysts and their catalytic activities

Sample	Surface area (m^{2}g^{-1})	Pore volume (cm^{3}g^{-1})	Pore diameter (Å)	Total Acidity (mmolg^{-1})	B/L	BA Conv., (%)
SBA-15	929	1.36	73.3	-	-	-
MCM-41	1155	0.88	30.5	-	-	-
MCM-48	1096	0.71	26.1	-	-	-
22.4% ZrO$_2$/SBA-15	426	0.69	71.3	0.30	0.92	27
3.36%TPA/SBA-15	341	0.60	70.4	0.29	0.88	21
5%TPA/ZrO$_2$/SBA-15	398	0.63	67.9	0.30	1.01	29
15%TPA/ZrO$_2$/SBA-15	372	0.59	67.7	0.42	1.45	56
30%TPA/ZrO$_2$/SBA-15	329	0.57	67.4	0.35	1.16	43
50%TPA/ZrO$_2$/SBA-15	328	0.53	67.0	0.33	1.12	31
70%TPA/ZrO$_2$/SBA-15	199	0.33	66.7	0.28	0.85	21
90%TPA/ZrO$_2$/SBA-15	199	0.31	66.0	0.26	0.58	15
15%TPA/22.4%ZrO$_2$/ MCM-41	516	0.28	19.7	0.33	0.21	44
15%TPA/22.4%ZrO$_2$/ MCM-48	540	0.34	17.2	0.25	0.17	10
15%TPA/ZrO$_2$ (Neat)	11	-	-	0.02	1.09	5
Effect of calcinations temperature (K) on 15 wt.% TPA/22.4 wt.%ZrO$_2$/SBA-15						
923	481	0.63	68.4	0.26	0.58	15
1023	410	0.61	68.1	0.33	1.12	32
1123	372	0.59	67.7	0.42	1.45	56
1173	326	0.47	67.3	0.34	1.19	38
1223	249	0.42	66.8	0.26	0.69	29
1273	212	0.33	66.1	0.24	0.42	13
Effect of ZrO$_2$(%) loading on 15 wt.%TPA/wt.%ZrO$_2$/SBA-15 calcined at 1123 K						
10	416.8	0.67	68.6	0.30	0.92	30
30	297.3	0.48	67.1	0.32	1.15	33
50	190.9	0.34	66.6	0.23	1.09	24
70	167.9	0.25	66.0	0.21	0.76	14

All catalysts were calcined at 1123 K except entries 1, 2 and 3. Entries from 6–11 were with 22.4% ZrO$_2$. Entry 1, crystal size (by TEM) = 7.1 nm; entry 4, ZrO$_2$ phase (tetragonal), crystal size (by TEM) = 5.5–6.5 nm and (by XRD) = 6.1 nm; entry 7, ZrO$_2$ phase (tetragonal), crystal size (by TEM) = 3–4 nm and (by XRD) = 3.4 nm.

Reaction Conditions: phenol, 2.52 g (0.026 mol); PhCH$_2$OH, 0.48 g (0.0044 mol); catalyst, 0.15 g; temperature 363 K; time, 3 h.

The nitrogen adsorption-desorption isotherms and pore size distribution at 77 K shown in Fig. 5.5 are of type IV for SBA-15 and for different TPA (%) loadings over 22.4 wt.%ZrO_2/SBA-15 calcined at 1123 K.

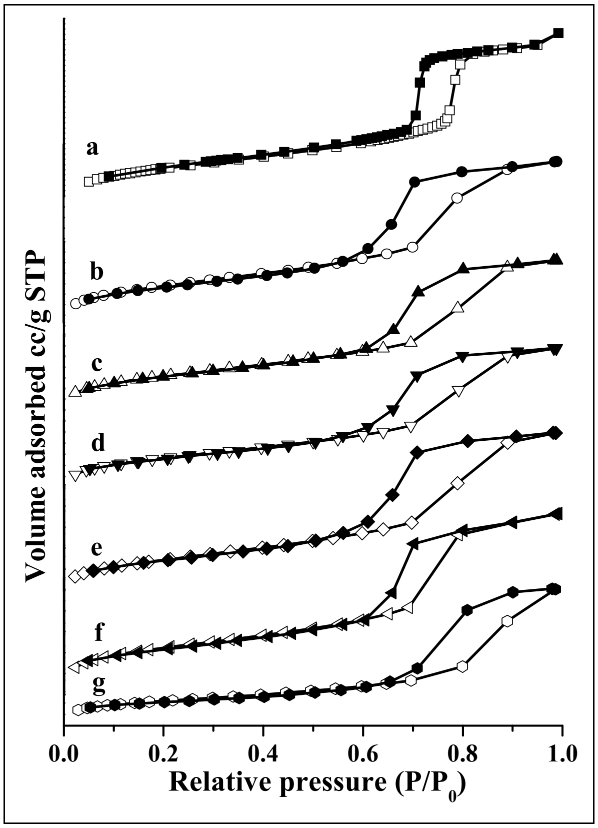

Fig. 5.5: *BET isotherm a) SBA-15, b) 5, c) 15, d) 30, e) 50, f) 70 and g) 90wt.%TPA/22.4 wt.%*ZrO_2*/SBA-15 calcined at 1123 K.*

A well-defined step associated with the filling of the mesopores due to capillary condensation occurs approximately at P/P_0 = 0.54 to 0.59-1.00 for 5-90 wt.% of TPA over 22.4 wt.%ZrO_2/SBA-15 catalyst calcined at 1123 K and at P/P_0 = 0.69-1.00 in SBA-15. These phenomena can be attributed to the encapsulation of TPA inside the channels of SBA-15, and furthermore, the higher loading above 50 wt.% lead to a partial blocking of the pores. The textural properties of 22.4 wt.%ZrO_2/SBA-15 with different (%) TPA loadings, 15 wt.%TPA/22.4 wt.%ZrO_2/SBA-15 calcined at different calcination temperatures and 15 wt.%TPA/wt.%ZrO_2/SBA-15 with different (%) ZrO_2 loadings are presented in Table 5.1. It is seen that the surface area, pore size and pore volume of modified SBA-15 decreased as compared with parent SBA-15. As TPA/ZrO_2 was well dispersed inside the pores of mesoporous channels so with increase in TPA and ZrO_2 loadings catalysts shows decrease in surface area, pore volume and pore diameter. Similarly, in case of 15 wt.%TPA/22.4 wt.%ZrO_2/SBA-15 surface area and pore size decreases with increase in calcination temperature.

5.2.4. AFM

The agglomerate-like morphology of the layer was studied by atomic force microscopy (AFM) method. The reactive particles of zirconium oxide formed are of 5.5-6.5 nm size, while size of TPA is about 3-4.5 nm and this combination of sizes appears to prevent a dense uniform packing of the particles.

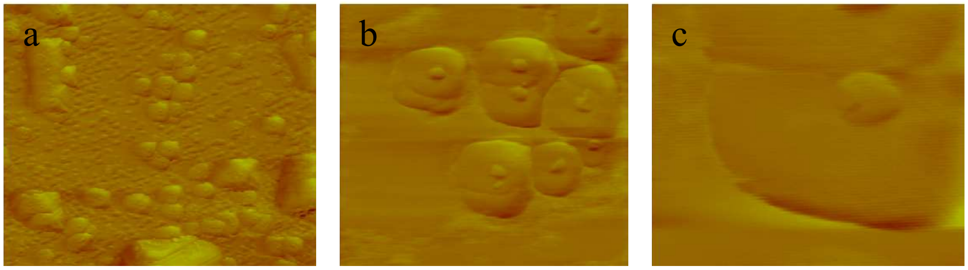

Fig. 5.6: AFM contact mode friction images of 15 wt.%TPA/22.4wt.%ZrO_2/SBA-15 on mica surface a) 5μm x 5μm, b) 1μm x 1μm, c) 266 nm x 266 nm.

5.2.5. SEM

The morphology of the supported and unsupported SBA-15 catalyst is shown in Fig. 5.7. The micromorphology of the supported catalyst remained the same, which was wheat-like even after modification of SBA-15 [1].

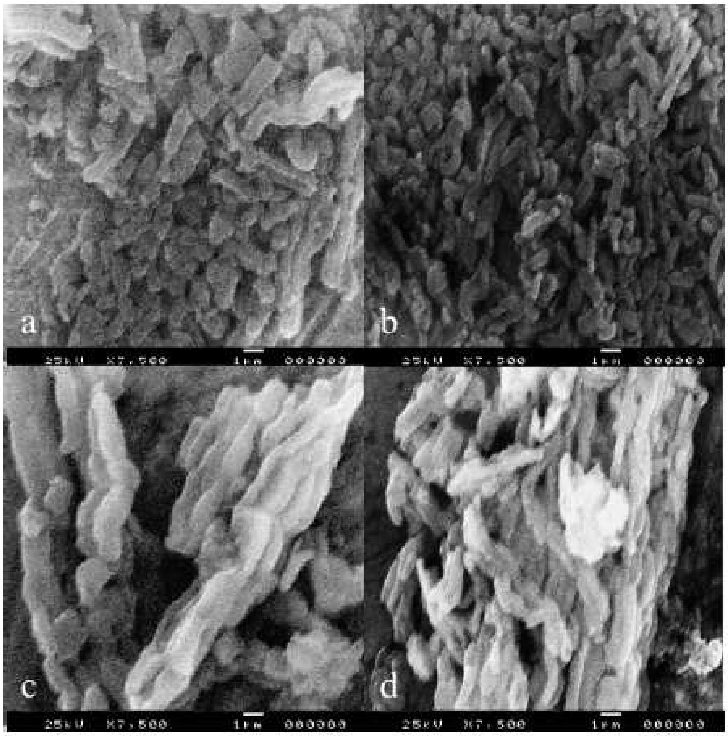

Fig. 5.7: *Scanning electron micrograph of (a) calcined SBA-15 at 813 K, and (b) SBA-15, (c) 22.4 wt.% ZrO_2/SBA-15, (d) 15 wt.% TPA/22.4 wt.% ZrO_2/SBA-15 calcined at 1123K.*

5.2.6. TEM

TEM measurements were carried out to study the morphology of the parent SBA-15 and TPA/22.4 wt.% ZrO_2 modified SBA-15 samples. TEM images of 15 wt.% TPA/22.4 wt.% ZrO_2/SBA-15 show the retention of the periodic structure of SBA-15 precursor even after calcining at 1123 K. TEM images of 15 wt.% TPA/22.4 wt.% ZrO_2/SBA-15 [Figs. 5.8 (a–d)] confirm that the hexagonally arranged mesopores of SBA-15 are retained and TPA/ZrO_2 mainly dispersed inside the pores. Fig. 5.8(a) clearly shows the uniform dispersion of TPA/ZrO_2 inside the SBA-15 channels. Figs. 5.8(b) and (d) show the periodic structure of SBA-15 precursor in different beam directions with pore size of 7.1 nm. After supporting SBA-15 with 15 wt.% TPA/22.4 wt.% ZrO_2, small particles of TPA/ZrO_2 formed inside nanochannels of SBA-15 (Figs. 5.8 (c) and (e)). The 22.4 wt% ZrO_2 (5.5–6.5 nm), an optimum loading, was inserted into SBA-15 by the wet impregnation method, which has a higher capacity for monolayer coverage of TPA. The crystallite size of the material calculated from TEM shows that for moderate loading (15 wt.%) of TPA, nanosized (3–4 nm) material was formed after wet impregnation over 22.4 wt.% ZrO_2/SBA-15 calcined at 1123 K.

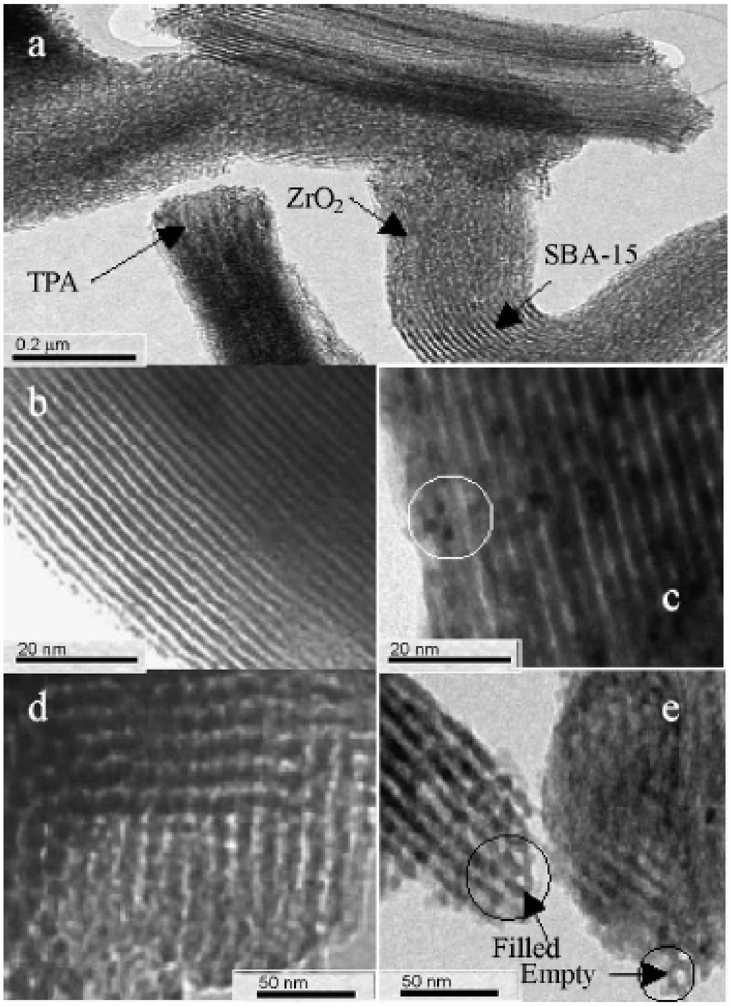

Fig. 5.8: *TEM images of (a) 15 wt.% TPA/22.4 wt.%* ZrO_2*/SBA-15 calcined at 1123 K, with the beam perpendicular to the pore direction of (b) SBA-15, (c) 15 wt.% TPA/22.4 wt.%* ZrO_2*/SBA-15 and with the beam parallel to the pore direction of (d) SBA-15, (e) 15 wt.% TPA/22.4 wt.%* ZrO_2*/SBA-15 calcined at 1123 K.*

5.2.7. FT-IR spectroscopy

Pure silica exhibited IR bands at 1100 and 806 cm^{-1} and a weak shoulder band at 974 cm^{-1} related to surface OH groups. Pure TPA showed characteristic peaks at 1079 cm^{-1} (P–O), 983 cm^{-1} ($W=O_t$), 893 cm^{-1} ($W–O_c–W$), and 810 cm^{-1} ($W–O_e–W$) [30], as shown in Figs. 5.9 (a) and (b). The spectra of ZrO_2 exhibited a wide band at 400–700 cm^{-1} extending up to 1150 cm^{-1} [27]. The spectra of different (%) loading of TPA over

ZrO_2/SBA-15 are shown in Fig. 5.9 (a). For the TPA/ZrO_2/SBA-15 samples, two bands of TPA appeared around 983 and 888 cm^{-1}, with the bands around 1079 and 810 cm^{-1} overlapping with the strong bands of SiO_2. The sample with the highest TPA loading (90 wt.%) showed characteristic bands of TPA but excluding a band at 983 cm^{-1} (W=O_t) due to decomposition of TPA intoWO_3 crystallites. Low TPA loading samples showed bands with lower intensity than bulk TPA spectra, due to masking of bands by wide bands of support.

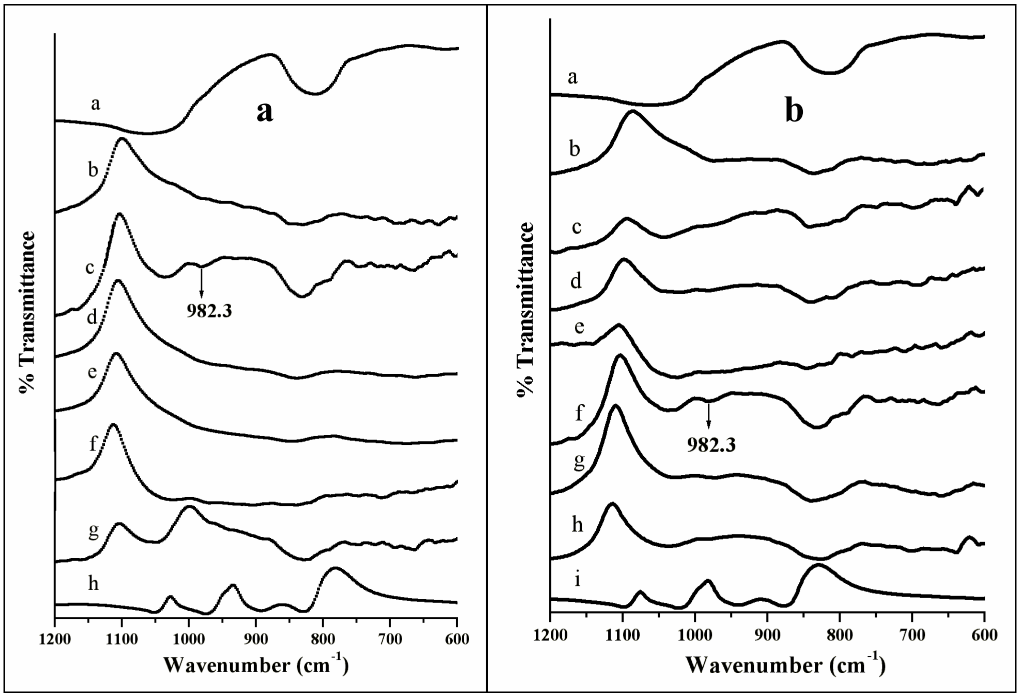

Fig. 5.9: *(a) FTIR spectra: a, pure silica, TPA/22.4 wt.% ZrO_2/SBA-15 with: b, 5; c, 15; d, 30; e, 50; f, 70; g, 90 wt.% TPA loading calcined at 1123 K; and h, pure TPA. (b) FTIR spectra: a, pure silica, 15 wt.% TPA/22.4 wt.% ZrO_2/SBA-15 calcined at b, 773; c, 923; d, 1023; e, 1123; f, 1173; g, 1223; h, 1273 K; and, i, pure TPA.*

5.2.8. UV-Vis. spectroscopy

The UV–Vis. spectra of HPA showed a band at 265 nm for TPA and 275 nm for $ZrOCl_2 \cdot 8H_2O$, in accordance with previous reports [27,28]. TPA-modified samples (i.e., 15 wt.% TPA/22.4 wt.% ZrO_2/MS) showed characteristic TPA bands at 263–265 nm (Fig. 5.10) in all of the spectra, which can be assigned to the oxygen–metal charge-transfer band of the tungstophosphate anion $[PW_{12}O_{40}]^{3-}$. However, the 22.4 wt.% ZrO_2/SBA-15 showed a band at 275.67 nm, which falls in the nanoparticle region of ZrO_2 as reported previously

[28,29]. TPA-modified samples showed only one band, because of the ZrO_2 band overlaps with strong band of TPA (Fig. 5.10).

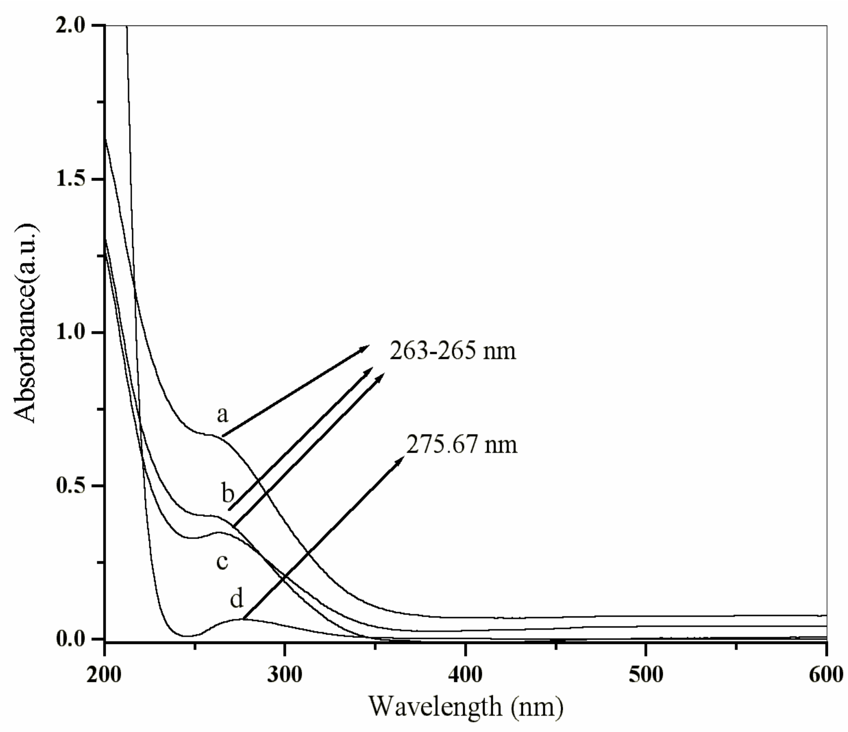

Fig. 5.10: *UV–Vis. spectra of (a) 15 wt.% TPA/22.4 wt.% ZrO_2/SBA-15, (b) 15 wt.% TPA/22.4 wt.% ZrO_2/MCM-41, (c) 15 wt.% TPA/22.4 wt.% ZrO_2/MCM-48, and (d) 22.4 wt.% ZrO_2/SBA-15 calcined at 1123 K.*

5.2.9. NMR spectroscopy

The ^{31}P CP-MAS NMR spectra of the supported TPA/ZrO_2 over SBA-15 with different TPA loadings (i.e., 5, 15, 30, and 50 wt.% TPA) are shown in Fig. 5.11 (a), and that of 70 and 90 wt.% TPA/22.4 wt.% ZrO_2/SBA-15 with 3.36 wt.% TPA/SBA-15 and 15 wt.% TPA/ZrO_2, all calcined at 1123 K, are shown in Fig. 5.11 (b).

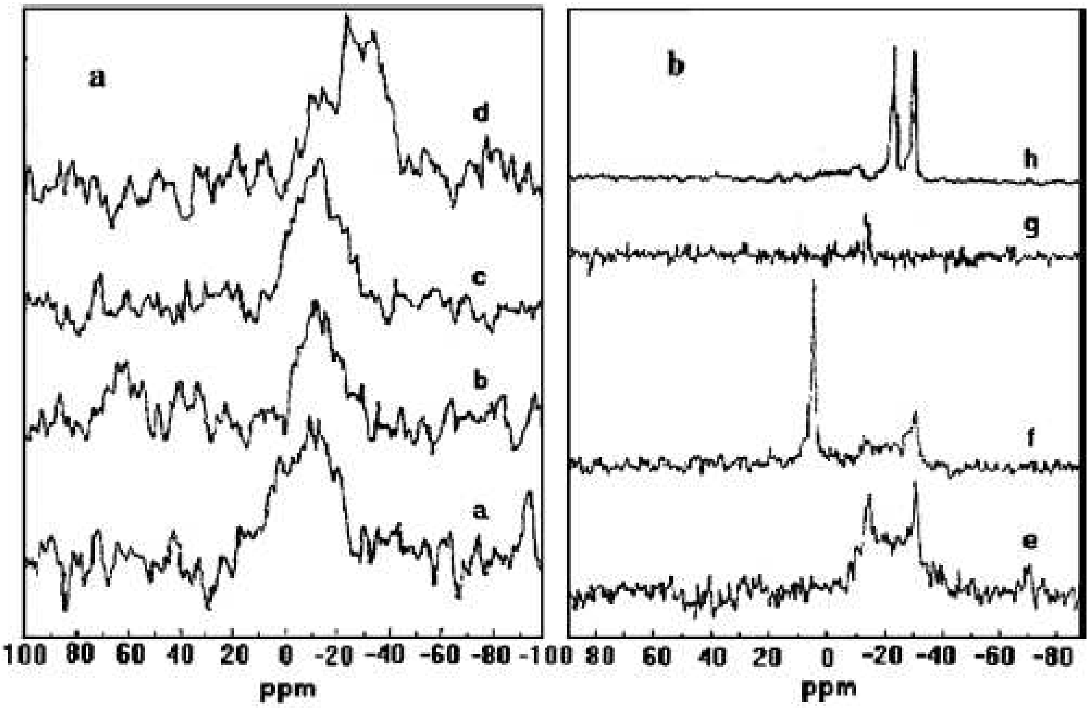

Fig. 5.11: *^{31}P CP-MAS NMR spectra of TPA/22.4 wt.% ZrO_2/SBA-15 with: a, 5; b, 15; c, 30; d, 50; e, 70; f, 90 wt.% TPA loading with: g, 3.36 wt.% TPA/SBA-15 and h, 15 wt.% TPA/ZrO_2 calcined at 1123 K.*

According to literature reports, in bulk TPA, ^{31}P NMR spectra exhibit an intense and sharp line at $\delta = -12$ ppm, showing intact Keggin units [2]. At TPA loading up to 30 wt.%, a peak around −12 to −13 ppm was observed. Further increases in loading above 50 wt.% produced a small extra peak at −24 ppm, which may be due to partially decomposed TPA with shifts in the original peak. When loading is increased above 70 wt.% produced an extra peak around −30 ppm, attributed to the presence of phosphorous in the decomposition product [3]. In 3.36 wt.% TPA/SBA-15, a small peak around −13 ppm was seen, whereas there was complete decomposition of Keggin structures (peak at −30 ppm) in neat 15 wt.% TPA/ZrO_2 calcined at 1123 K. An inspection of the chemical shifts *(δ)* shows their dependence on the TPA loading (%), type of support, and temperature treatment. TPA derivative species that may give rise to such chemical shifts could be due to partially fragmented Keggin units and also to the strong interaction of TPA with surface ≡Zr–OH groups. The broad line at −12 ppm is probably related to species formed by linking the Keggin units to the ZrO_2 support. Indeed, the first part of the interaction between TPA and ZrO_2 is a protonation of surface hydroxyl groups of ZrO_2, leading to

$(\equiv Zr–OH_2)^{n+}[H_{3-n}W_{12}PO_{40}]^{n-3}$ species [3]. After heating, water is removed, leading to a direct linkage between the polyanion (which has probably retained a structure like that of the Keggin ion) and the support. Because our system deals with high temperatures (1123 K), extensive dehydroxylation of TPA is possible to yield the aforementioned species. When the polyanion decomposes, a new signal appears at −30 ppm. Because the support is heterogeneous, a distribution of surface species obtained. TPA/ZrO_2 dispersed uniformly in the SBA-15 channels, instead of producing sharp peaks like bulk TPA, line broadening was observed in our system. As per shown in Fig. 5.12 (a), after modification of SBA-15 with 15 wt.% TPA/22.4 wt.% ZrO_2, ^{29}Si MAS NMR showed two peaks, at −110 ppm and −112 ppm, corresponding to Q^4, which could be due to the consumption of some silanols during the modification process which is reported previously [4,5]. While, ^{29}Si MAS NMR spectra for calcined MCM-41 mesostructures assembled from sodium silicate shows Q^4 Si-resonances at -108 ppm [6].

Fig 5.12 (b) shows ^1H MAS NMR spectra of neat TPA, along with different (%) loading of TPA over 22.4 wt.%ZrO_2/SBA-15 calcined at 1123 K. For bulk TPA treated under vacuum, chemical shift values as high as 9.3 ppm (with respect to TMS) were observed which is reported earlier [7]. Acidity of different HPAs has already been investigated by ^1H MAS-NMR [8, 9]. ^1H MAS-NMR spectra studies also indicate a chemical interaction of $H_3\,[PW_{12}O_{40}]$ with the support and the formation of a new type of proton sites on the silica surface. Brønsted acid sites in solid acids can be characterized by ^1H MAS-NMR spectroscopy. The basic idea is that a more acidic proton has less electron in its vicinity, therefore is less shielded and, subsequently, its NMR chemical shift δ_H, will be more positive (lower-field shift) [10]. However, other contributions, such as hydrogen bonding, may also influence δ_H values, which may make its relationship with acidity strength ambiguous [11,12]. The chemical shift of ^1H can be considered as an indicator of the acidity of a proton. Since all our samples corresponded to the same Keggin anion to which the proton is attached and the Keggin anion remained stable during thermal treatments, the evolution of the proton resonance peak as a function of the degree of dehydration was therefore a reasonable indicator of the strength of the proton acidity. This assignment is different to that proposed by Misono [13] who attributed a peak at ca. 9 ppm observed after evacuation of the HPA at 473 K to the acidic 'free' proton and, surprisingly, reported the same ^{1}H chemical shift for both $H_3PW_{12}O_{40}.0H_2O$ and $H_3PW_{12}O_{40}.2.2H_2O$ samples.

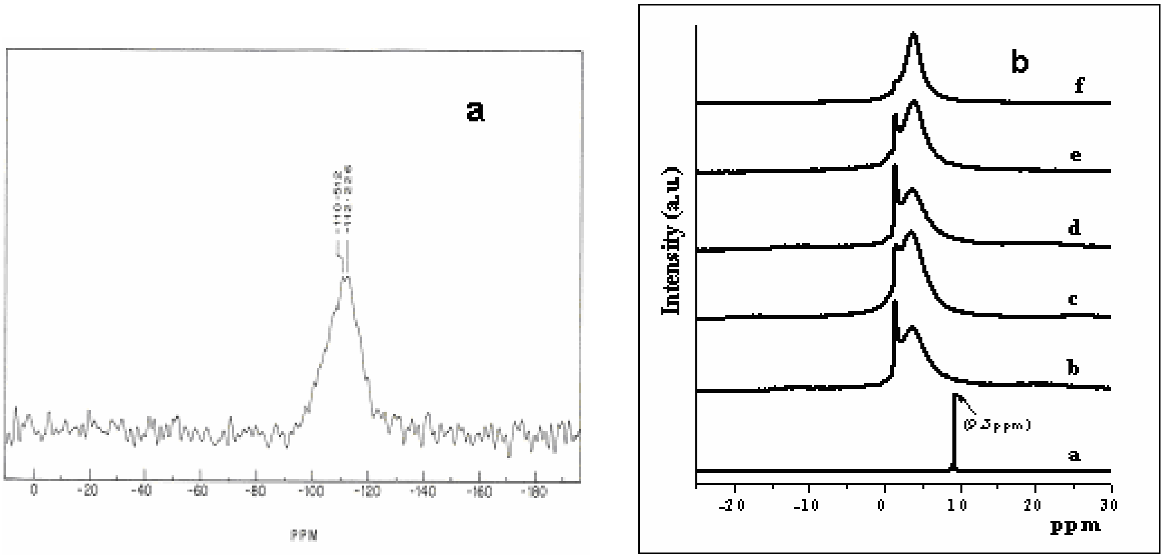

Fig. 5.12: *(a) ^{29}Si MAS NMR spectra of 15 wt.%TPA/22.4 wt.% ZrO$_2$/SBA-15 calcined at 1123 K.*
(b) ^{1}H MAS NMR spectra of (a) Neat TPA, (b) 5, (c) 15, (d) 30, (e) 50 wt.%TPA/22.4 wt.% ZrO$_2$/SBA-15 calcined at 1123 K and (f) 15 wt.%TPA/22.4 wt.%ZrO$_2$/MCM-41 calcined at 1123 K.

All spectra of supported TPA display similar feature with essentially two components, a sharp one at 1.5 ppm, which can be attributed to isolated silanol groups as, explained above and a broad one from 2 to 5 ppm, which could be, attributed to hydrogen-bonded hydroxyl groups. The peak at ca. 9 ppm which is attributed to protons in anhydrous TPA is not observed even for the highest TPA loading (50 wt.%) and whatever the dehydroxylation temperature. This observation is very important as the high acidity of HPA is related to this proton. We can then conclude from these data that the supported HPA is less acidic than the pure one, which is known in the literature [14]. These results are in agreement with other methods such as microcalorimetry [15, 16]. As per literature, the resonance around 2-5 ppm corresponding to hydrogen bonded silanol groups may be of silica support [17]. This may be the reason for getting a broad resonance around 2-5 ppm by merging of two peaks from TPA and from silica support. The ^{1}H MAS NMR spectra of calcined MCM-41consist of signals in the chemical shift range 1.3–2.2 ppm which are typical for silanol groups in inorganic solids [18, 19]. The unsymmetric shape of these signals is a hint for the presence of different types of silanol groups, such as isolated and geminal SiOH groups and internal silanol groups [20]. But, in case of MCM-41 support we observed only one peak i.e. around 3.8 ppm, may be due to unavailability of isolated silanol groups from silica support.

5.2.10. FT-RS

FT-Raman spectra of 22.4 wt.%ZrO_2/SBA-15 sample with and without TPA calcined at 1123 K are presented in Fig. 5.13. Distinctly, the intensity of the bands around 1009, 992 cm^{-1} and a weak peak around 905 cm^{-1} assigned to pure TPA [21,22]. The bands assigned to TPA are clearly seen in Fig. 5.13 for 15 wt.%TPA/22.4 wt.%ZrO_2/SBA-15 sample. The broadness and minor shift in the bands could be due to the formation of the species formed by linking the Keggin units to the ZrO_2 support. The Raman bands of ZrO_2 below 700 cm^{-1} interfere with the tungstate species, while above 700 $cm^{-1}$is free from characteristic bands of ZrO_2.

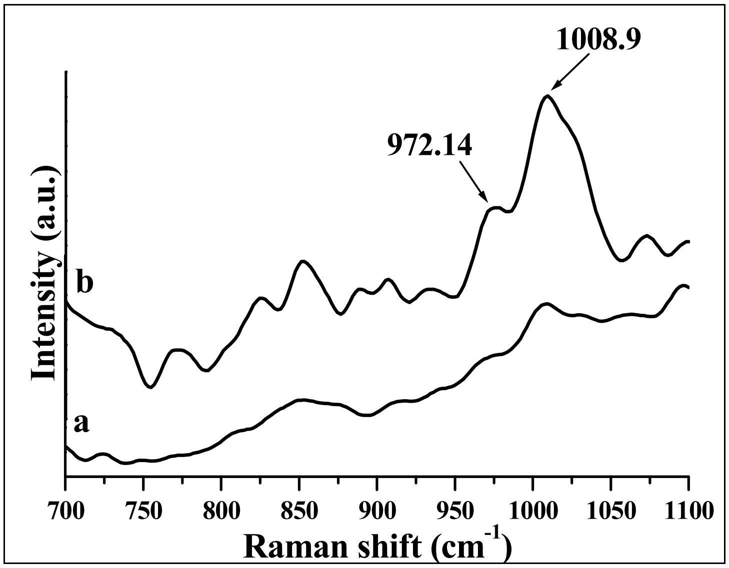

Fig. 5.13: *FT-Raman spectra of a) 22.4 wt.%ZrO_2/SBA-15 and b) 15 wt.%TPA/ 22.4 wt.%ZrO_2/SBA-15 calcined at 1123 K.*

5.2.11. XPS

In order to study the surface stability of TPA on ZrO_2/SBA-15 systems, we carried out XPS analysis. XPS analysis has been used to investigate the interaction between the guest (ZrO_2) and the host (SBA-15) and was found that ZrO_2 was more likely to interact with SBA-15 by hydrogen bonds involving Si-O-H groups of the SBA-15 with zirconium atoms in ZrO_2. Due to such interaction at monolayer coverage of TPA, free hydrogen is available from SBA-15 support. While below and above 22.4 wt.%ZrO_2 loading, this interaction was not that predominant due to less ZrO_2 content and also due to multilayer formation in both the supports. The results of XPS analyses for 22.4 wt.%ZrO_2/SBA-15 are shown without and with TPA calcined at 1123 K.

Table 5.2. XPS binding energies (eV) and FWHM (eV) values of the catalysts

Sample	O 1s		Zr $3d_{5/2}$		Si 2p		W $4f_{7/2}$		P 2p	
	BE	FWHM	BE	FWHM	BE	FWHM	BE	FWHM	BE	FWHM
A	531.2	2.7	183.5	4.7	102.3	2.8	-	-	-	-
B	531.2	3.4	183.5	8.9	102.8	2.9	35.9 (38.0)	3.5	134.0	6.9

Where, (A) = 22.4 wt.%ZrO_2/SBA-15 and (B) = 15 wt.%TPA/22.4wt.%ZrO_2/SBA-15

The binding energies and FWHM values of various core levels (Si 2p, O 1s, Zr $3d_{5/2}$, W $4f_{7/2}$, P 2p) of this mesoporous materials are summarized in Table 5.2. The spin-orbit split doublet of tungsten, W $4f_{7/2}$ and W $4f_{5/2}$ with full width at half maximum is obtained at 3.5 eV and are located at 35.9 and 38.2 eV, respectively. The observed binding energy value of W ($4f_{7/2}$) is 35.9 eV, a characteristic of W^{6+} indicating that it contain W-O bonding [23]. Fig. 5.14 (A) shows the contribution of the O^{2-} 1s at 531.2 eV, which is related to an O-H bonding. This indicates that the compound is hydrated. Si 2p binding energy (Fig. 5.14 (B)) values of silica support i.e. SBA-15 and modified SBA-15 with TPA/ZrO_2 are the same around 102-103 eV [24]. The same Si 2p FWHM values for samples 22.4 wt.%ZrO_2/SBA-15 i.e. without and with TPA shows that impregnation doesn't affect the silica support i.e. SBA-15 as seen in Table 5.2. In Fig. 5.14 (C), 22.4 wt.%ZrO_2/SBA-15 catalyst without and with 15 wt.%TPA shows similar Zr $3d_{5/2}$ binding energy values around 183.5 eV. Table 5.2 shows the binding enery values and FWHM values, which shows almost the same FWHM values even after TPA loading. The binding energy of the Zr $3d_{5/2}$ band in the case of modified ZrO_2 samples was found to be higher than that of the pure ZrO_2 (182.5 + 0.1 eV). This shift towards higher side could be attributed to an atomic dispersion of ZrO_2 on the other support oxides and/or the change in the coordination number of zirconium by the formation of a Zr-O-Support bond as per evidenced in literature [25,26]. The phosphorous signal P^{5+} 2p at 134.4 eV could be associated with a compound that contains P-O bonding as shown in Fig. 5.14 (D). However, high FWHM values are observed due to peak-broadening possibility and i.e. due to differential charging of the sample caused by mesoporous silica support.

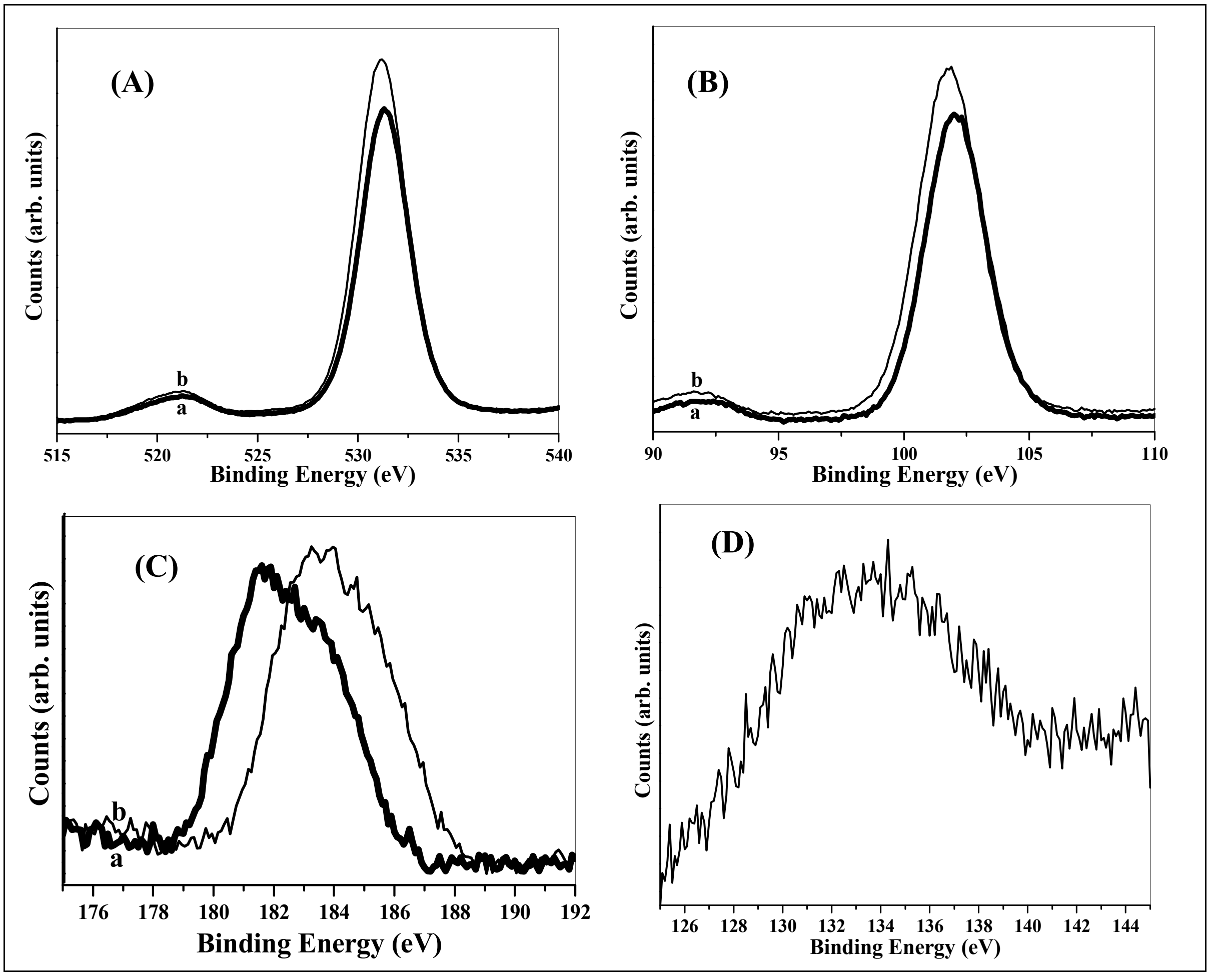

Fig.5.14: *XPS spectra of (A) O (1s) spectra of a) 22.4 wt.%ZrO_2/SBA-15 and b) 15 wt.%TPA/22.4 wt.%ZrO_2/SBA-15, (B) Si (2p) spectra of a) 22.4 wt.%ZrO_2/SBA-15 and b) 15 wt.%TPA/22.4 wt.%ZrO_2/SBA-15, (C) Zr ($3d_{5/2}$) spectra of a) 22.4 wt.%ZrO_2/SBA-15 and b) 15 wt.%TPA/22.4 wt.%ZrO_2/SBA-15 and (D) P (2p) spectra of a) 22.4 wt.%ZrO_2/SBA-15 and b) 15 wt.%TPA/22.4 wt.%ZrO_2/SBA-15 calcined at 1123 K.*

5.2.12. TG-DTG

TG-DTG spectra of all the samples dried at 100°C are shown in Fig. 5.15. Under similar measurement conditions, TG-DTG analysis of pure TPA hydrate showed three stages of weight loss (endothermic effect) [32]. The first weight loss, around 3–6%, occurred from room temperature to 125°C, due to the loss of physisorbed water. The second one, from 130–305°C, accounted for the loss of crystallization water, and the third, in the range of 370–550°C, was due to the loss of 1.5 H_2O molecules originating from all acidic protons. The total weight loss of the sample corresponded to 21 H_2O per Keggin unit. Furthermore, it showed a break at 350°C, due to the decomposition of HPA [21]. The TGA behavior was similar in all of the TPA/ZrO_2-supported samples, showing the first weight loss of about 3% in all TPA/ZrO_2 supported over SBA-15 samples, corresponding to physisorbed water. But the MCM-41 and MCM-48 supports showed heavy weight loss, corresponding to physisorbed water, compared with the SBA-15-supported samples. But none of the supported samples showed an appreciable change in weight loss until 900°C, indicating increasing stability of TPA. The neat 15 wt.% TPA/ZrO_2 sample exhibited weight loss corresponding to physisorbed water along with another weight loss around 450–600°C that may be due to a phase transition from tetragonal to monoclinic.

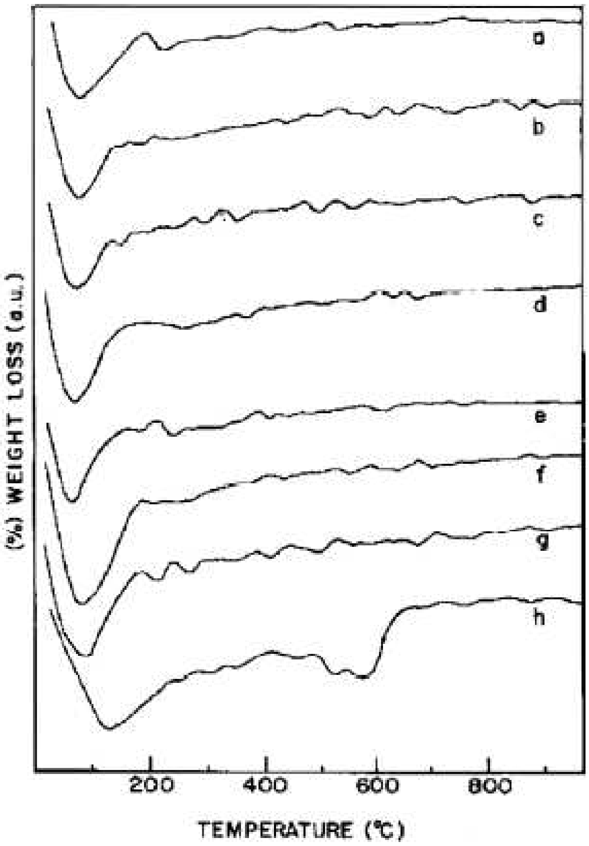

Fig. 5.15: *TG-DTG curves of (a) 22.4 wt.% ZrO_2/SBA-15, TPA/22.4 wt.% ZrO_2/SBA-15 with (b) 5, (c) 15, (d) 30, (e) 50 wt.% TPA loading with (f) 15 wt.% TPA/22.4 wt.% ZrO_2/MCM-41, (g) 15 wt.% TPA/22.4 wt.% ZrO_2/MCM-48, and (h) 15 wt.% TPA/ZrO_2 calcined at 1123 K.*

5.2.13. TPD of NH_3

NH_3-TPD was performed to determine the amount and the total acidity in the catalysts. TPD profiles of the catalysts with different (%) TPA loadings in TPA/ZrO_2/SBA-15 calcined at 1123 K are shown in Fig. 5.16 (a), and the profiles of TPA/ZrO_2 supported on various silica supports, unsupported TPA/ZrO_2, 22.4

wt%ZrO_2/SBA-15, and TPA supported on SBA-15, all calcined at 1123 K, are shown in Fig. 5.16 (b).

The total acidities of 15 wt.% TPA/22.4 wt.% ZrO_2/SBA-15 calcined at different temperatures are given in Table 5.1. Results from Fig. 5.16 (a) suggest that at TPA loading up to 50 wt.%, the samples showed a broad desorption band centered around 523 K, implying medium acidity. Further increases in TPA loading [Fig. 5.16 (a)] produced decreased acidity, which incidentally have lower surface areas. These results indicate that TPA/ZrO_2 dispersed uniformly over SBA-15. According to area under the peak, the supported TPA/ZrO_2 samples showed more acid sites than unsupported TPA/ZrO_2 or 3.36 wt.% TPA/SBA-15. Loading of TPA over 22.4 wt.%ZrO_2/SBA-15 [Fig. 5.16 (b)] produced increased acidity and thereby increased catalytic activity in benzylation reaction (Table 5.1). All samples showed a broad TPD profile, indicating that the surface acid strength was widely distributed. From these data, it is evident that an initial increase in total acidity up to 15 wt.% TPA loading is followed by a decrease in total acidity with further increases in TPA loading. It can be concluded that for low TPA loading, the Keggin unit of HPA retains its structure and acidity, but for higher loading (i.e., above 15 wt.% TPA), it decomposes at least partially into its oxides. The highest acidity corresponds to monolayer coverage of TPA (i.e., 15 wt.% TPA/22.4 wt.% ZrO_2/SBA-15 calcined at 1123 K), where the Keggin-like structure is intact, as supported by ^{31}P CP-MAS NMR and XRD. Table 5.1 indicates that the total acidity increases up to 1123 K but that further increases in calcinations temperature lead to decreased acidity and also decreased catalytic activity, which is due to decomposition of TPA intoWO_3 crystallites. Total acidity of the 15 wt.%TPA with different wt.% of ZrO_2 over SBA-15 calcined at 1123 K is shown in Table 5.1. Similarly, with increasing ZrO_2 loading till 22.4 wt.%, 15 wt.%TPA/ZrO_2/SBA-15 catalyst calcined at 1123 K shows increase in acidity and thereby catalytic activity.

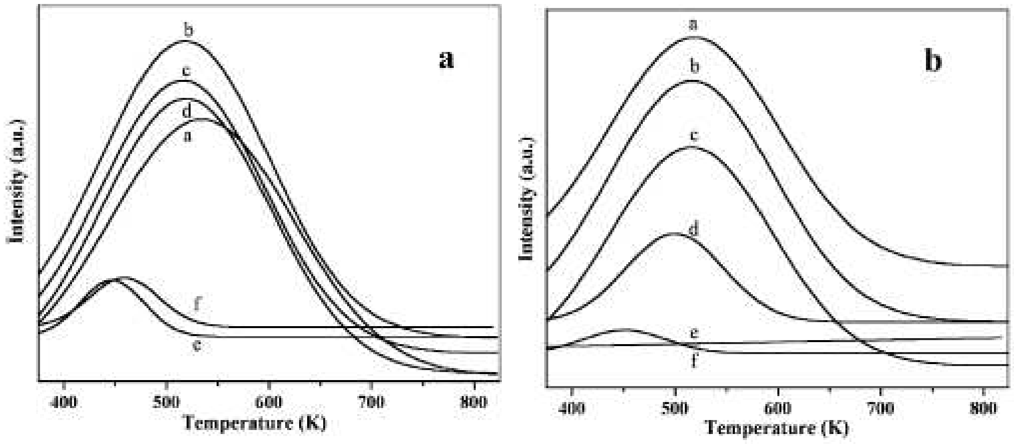

Fig. 5.16: *(a) NH_3-TPD profiles: TPA/22.4 wt.% ZrO_2/SBA-15 with a, 5; b, 15; c, 30; d, 50; e, 70; f, 90 wt.% TPA loading and (b) 15 wt.% TPA/22.4 wt.% ZrO_2 supported over a, SBA-15; b, MCM-41; c, MCM-48; d, 22.4 wt% ZrO_2/SBA-15; e, 3.36 wt% TPA/SBA-15; f, neat 15 wt% TPA/ZrO_2 calcined at 1123 K.*

5.2.14. FT-IR Pyridine adsorption

The Brønsted/Lewis (B/L) site ratio was calculated from the IR absorbance intensities [31] of bands at 1539 (B) and 1442 (L) cm^{-1} as per shown in Fig. 5.17, for different catalysts along with different (%) loadings of TPA, and were compared with catalytic activity in phenol benzylation with different calcination temperatures for 15 wt.% TPA/22.4 wt.% ZrO_2/SBA-15; the results are given in Table 5.1. It was found that the B/L ratio increased with increased TPA loading up to 15 wt.%, but then decreased with further increases in TPA loading. Thus the sample with 15 wt.% TPA/22.4 wt.%ZrO_2/SBA-15 had the highest acidity, due to the monolayer coverage of TPA on ZrO_2 finely dispersed in SBA-15 channels. But on further increases in TPA loading, the B/L ratio decreased, and hence the catalytic activity also decreased. The decrease in B/L ratio and activity was well explained earlier in Chapter 4, section 4.2.9, page no. 85.

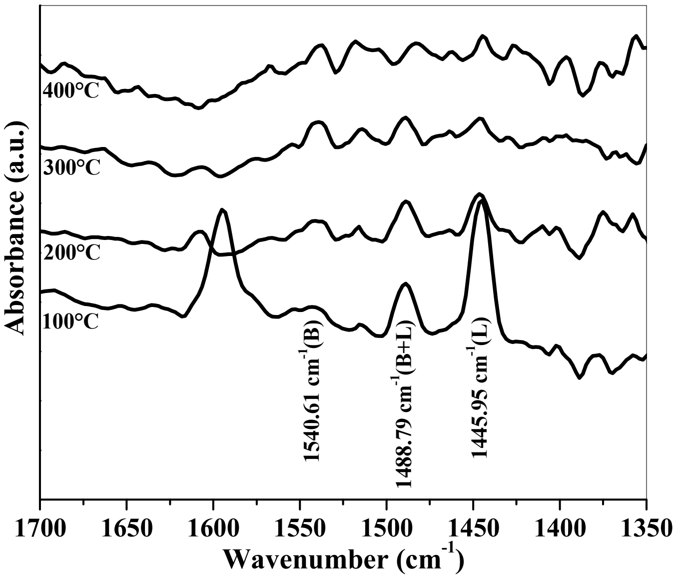

Fig. 5.17: *FT-IR Pyridine adsorption isotherms of 15 wt.%TPA/22.4 wt.%ZrO_2/SBA-15 calcined at 1123 K.*

5.3. BENZYLATION OF PHENOL BY BA

5.3.1. Introduction

Alkylation of phenol with different alcohols is an industrially important reaction in production of various products [33, 34]. Benzylation of phenol by BA to BP is an important reaction, and BPs are useful raw materials for producing antioxidants and plastic, rubber, and petroleum products [35]. The present work deals with the role of mesoporous support and how its properties influence over the catalytic activity of neat TPA/ZrO_2 in an acid-catalyzed benzylation as a test reaction. Our findings demonstrate that TPA/ZrO_2 dispersed uniformly in nanosized channels of SBA-15 and provided strong acidity and catalytic activity compared with neat TPA/ZrO_2 catalyst in benzylation of phenol.

5.3.2. Results and discussion

The liquid phase benzylation of phenol with BA was carried out using TPA/ZrO_2 formed in SBA-15 channels as a catalyst; the reaction is as shown in the scheme 5.1.

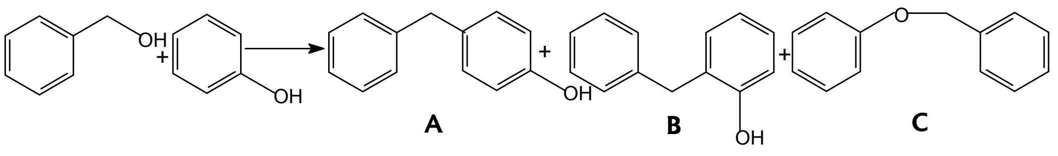

Scheme 1.

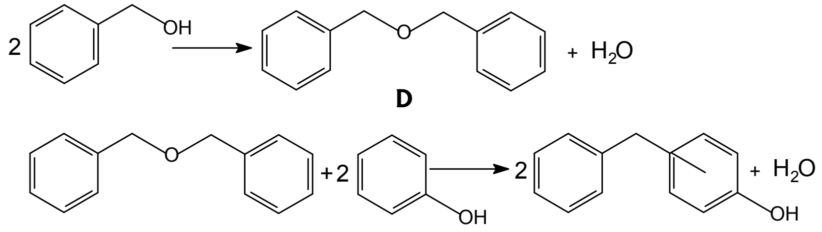

Scheme 2.

Scheme 5.1: *Benzylation of phenol with BA giving products as A (p-BP), B (o-BP), C (PBE) and D (DBE).*

Data on the catalytic performance of various (%) TPA-loaded catalysts calcined at 1123 K, and activity of 15 wt.% TPA/22.4 wt.% ZrO_2/SBA-15 calcined at different temperatures are presented in Table 5.1.

5.3.2.1. Comparison of catalytic activities of different catalysts

Benzylation of phenol with 15 wt.% TPA/22.4 wt.%ZrO_2/SBA-15 calcined at 1123 K catalysts under selected reaction conditions (363 K, 3 h, 150 mg catalyst, phenol/BA molar ratio 6) gave 77% (A + B) (i.e., mono-BP as the main product), 20% (C), and 3% (D).

The 15 wt.% TPA/22.4 wt.%ZrO_2/SBA-15 calcined at 1123 K gave the highest conversion of BA (56%) under selected reaction conditions (Table 5.1). The effect of TPA loading, ZrO_2 loading and calcination temperature on BA conversion data is presented in Table 5.1. Combining these findings with the results of FTIR pyridine adsorption data reveal that the B/L ratio of the catalysts increased up to 15% TPA loading and that 15 wt.% TPA/22.4 wt.%ZrO_2/SBA-15 calcined at 1123 K had the highest B/L ratio and gave the highest catalytic activity in benzylation of phenol under reaction conditions. In this catalytic system, ZrO_2 loaded on mesoporous silica support (i.e., 22.4 wt.% ZrO_2/SBA-15 calcined at 1123 K) showed some catalytic activity, whereas ZrO_2 loaded on 15 wt.% TPA showed a two-fold increase in catalytic activity (Table 5.1). The interaction between the

TPA and ZrO_2 is responsible for the high acidity and for high catalytic acitivity as discussed earlier in Chapter 4, section 4.2.9, page no. 85.

TPA species would exert an electron-withdrawing effect on surface Zr^{4+} cations, making them to behave as strong Lewis acid sites. But this phenomena occurred at temperatures up to 673 K. Accordingly, the strongly acidic properties of TPA/ZrO_2 could be attributed to electron-withdrawing effects similar to those ascribed to Zr bonded sulfate groups [36,37]. Above 673 K, all dehydrated ZrO_2 reacted with TPA. In this catalytic system, the fact that TPA remained amorphous at temperatures up to 923 K suggests strong interactions between HPA and ZrO_2 at the structural level. But crystallite size measurements (Table 5.1) showed that the presence of TPA inhibited crystal growth of the catalyst material; this behavior is very common in mixed materials containing a crystalline and an amorphous phase together. The crystalline material is usually surrounded by an amorphous phase layer, which acts as a physical barrier to hinder the sintering process and inhibit crystallite growth [37, 38]. Keeping in mind all of these findings, we hypothesize that at calcinations above 923 K, the interaction between TPA and ZrO_2 may weaken to monolayer coverage (15 wt.% and 1123 K), making TPA protons free for reactions to proceed and thereby increasing Brønsted acidity and total acidity (from the increase in Lewis acidity due to ZrO_2). With further increases in calcinations temperature above 1123 K, possibly due to multilayer formation, bulk properties of TPA will be more predominant, causing destruction of TPA to yield WO_3 crystallites, as was partially proved by NMR. Besides sulfate ions, tungstate and molybdate oxoanions also produce strong acidic sites when deposited on hydroxylated ZrO_2 [39].

The 15 wt.% TPA/22.4 wt.%ZrO_2 modified SBA-15 catalyst showed higher catalytic activity than the 15 wt.% TPA/ 22.4 wt.%ZrO_2 modified MCM-41 and MCM-48 catalysts calcined at 1123 K.We hypothesize that large TPA clusters (~12 Å) can readily clog the pores during solution impregnation when support pore sizes are smaller, as in the case of MCM-41 (30.5 Å) and MCM-48 (26.1 Å). But when the ZrO_2 along with TPA was dispersed in the mesoporous channels of supports at high temperature calcination, the acidity of the catalysts was altered, becoming higher with SBA-15. In contrast, TPA/ZrO_2 is likely have a better chance to uniformly coat the pores when the support pore size is sufficiently large, as in the case of SBA-15 (73.3 Å) compared with MCM-41 and MCM-

48. However, the neat 15 wt.% TPA/ZrO_2 calcined at 1123 K showed poor catalytic activity with conversion of BA (5%), at least 10 times less than that of the modified 15 wt.% TPA/22.4 wt.%ZrO_2/SBA-15 calcined at 1123 K under the same reaction conditions. This enhanced activity could be due to more accessible protons when 15 wt.% TPA/ZrO_2 is supported on large surface area and the larger pore diameters of the SBA-15 mesoporous silica material. Hence the above catalyst was used in catalytic studies to assess activity in the test reaction.

5.3.2.2. Effect of TPA loading and calcination temperature

The effect of TPA loading and calcination temperature as a function of product selectivities are presented in Fig.5.18 (A) and Fig.5.18 (B), respectively for benzylation of phenol. Fifteen wt.%TPA/22.4 wt.%ZrO_2/SBA-15 calcined at 1123 K gave the highest conversion of BA (56 %) under the optimized reaction conditions (Table 5.1). Combining with the results of FT-IR pyridine adsorption data, it was found that B/L ratio of the catalysts increases up to 15 wt.% TPA loading and 15 wt.%TPA/22.4 wt.%ZrO_2/SBA-15 calcined at 1123 K has the highest B/L ratio and gave the highest catalytic activity in phenol benzylation under optimized reaction conditions. However, the neat 15 wt.%TPA/ZrO_2 calcined at 1123K showed poor catalytic activity with conversion of BA (5 %), which is at least ten times less than the modified 15 wt.%TPA/22.4 wt. %ZrO_2/SBA-15 calcined at 1123 K catalyst under the same reaction conditions.

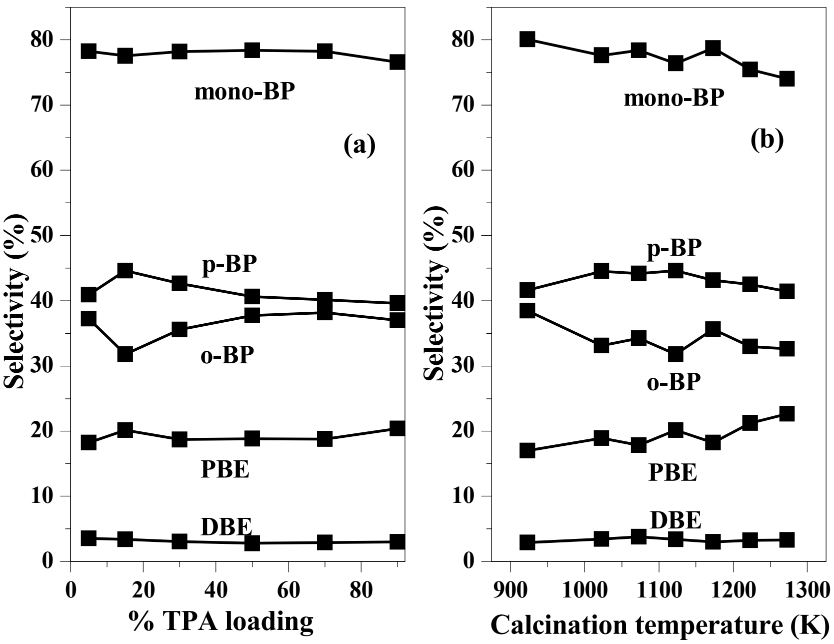

Fig. 5.18: (A) Effect of TPA loading and (B) calcination temperature on phenol benzylation. (Reaction conditions: phenol, 2.52 g (0.026 mol); BA, 0.48 g (0.0044 mol); catalyst weight, 150 mg; phenol/BA (mol ratio), 6:1; temperature, 363 K; time, 3 h.

5.3.2.3. Effect of reaction parameters

The effect of catalyst concentration on BA conversion was studied by varying catalyst from 1 to 10 wt.% of the total weight of the reaction mixture and the results are shown in Fig. 5.19 (a). It is seen that BA conversion increases from 4.6 to 84.7% with increase in catalyst concentration up to 10 wt.%, while the selectivity for mono-BP was unchanged.

We studied the effect of the phenol/BA molar ratio from 2 to 10 by keeping the total weight of the reaction mixture constant under optimized reaction conditions and the results are shown in Fig.5.19 (b). As the molar ratio increases from 2 to 10, the BA conversion increased from 23.9 to 75.7 %. The selectivity for mono-BP increases with increase in molar ratio, while selectivity for DBE decreased. From the results it is seen that the selectivity for *para*–BP is more than *ortho*–BP with 15 wt.%TPA/22.4 wt.%ZrO_2/SBA-15 catalyst.

The 15 wt.%TPA/22.4 wt.%ZrO_2/SBA-15 catalyst was used to study the effect of temperature in the range 343-383 K on the conversion and product selectivities [Fig. 5.20 (a) and Table 5.3]. With increasing temperature, BA conversion increased up to 73%, whereas selectivity for mono-BP increased and that of PBE decreased.

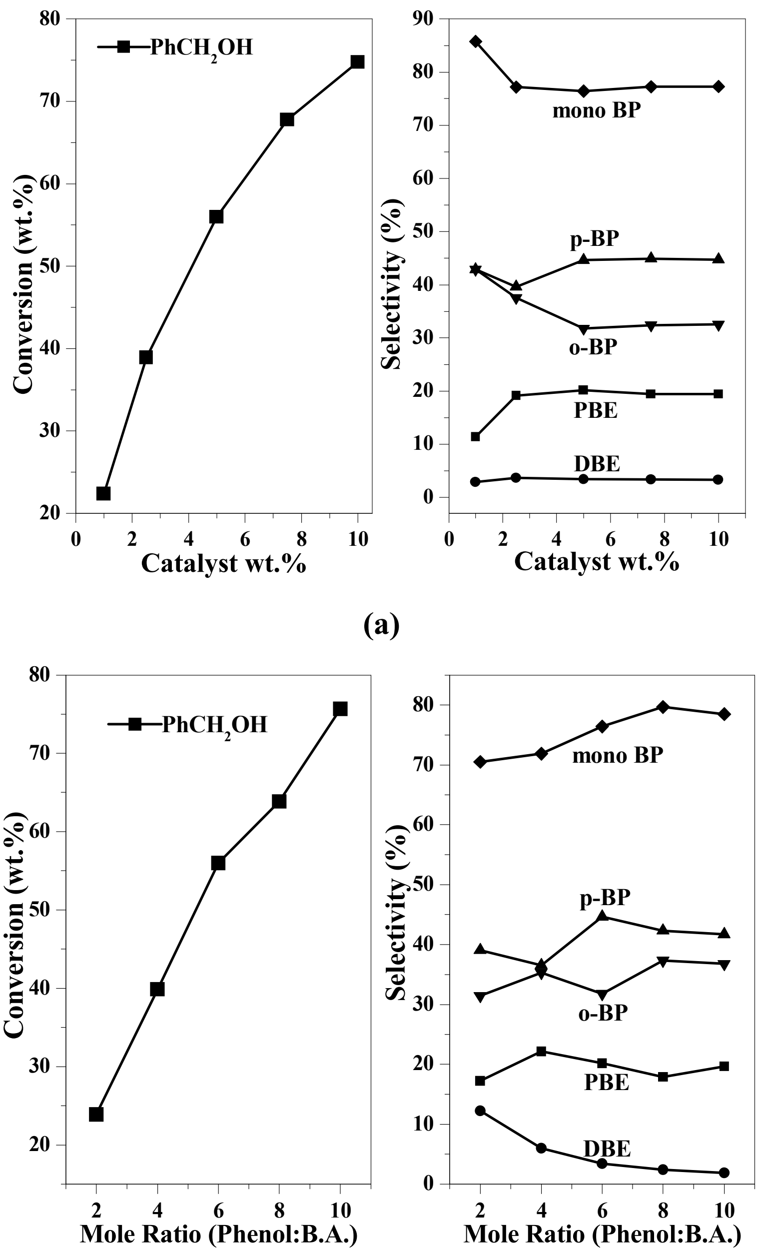

Fig. 5.19: *(a) Effect of catalyst concentration on phenol benzylation. (Reaction conditions: phenol, 2.52 g (0.026 mol); BA, 0.48 g (0.0044 mol); phenol/BA (mol ratio), 6:1; temperature, 363 K; time, 3 h.*

(b) Effect of Phenol: BA molar ratio on phenol benzylation. (Reaction conditions: phenol, 2.52 g (0.026 mol); BA, 0.48 g (0.0044 mol); catalyst weight, 150 mg; temperature, 363 K; time, 3 h.

Table 5.3: Study of effects of reaction temperature on conversion of BA

Catalyst	Conversion BA. (%)	Ist order Rate constant	Product selectivity (%)*	
			mono-BP	PBE
Temperature				
343	25	0.09	75	22
353	34	0.14	75	22
363	56	0.27	77	20
373	67	0.37	78	19
383	73	0.44	80	17
Regeneration of catalyst				
Fresh	56	-	77	20
Ist	56	-	77	20
IInd	55	-	77	20

*Reaction conditions: Phenol=2.52 g (0.026 mole), $PhCH_2OH$ (BA)=0.48 g (0.0044 mole), catalyst=0.15 g, temp. = 363 K, time=3 h. *DBE = 3% in all the cases.*

Benzylation of phenol by BA was carried out with catalyst, 0.15 g (3 wt.% of total reaction mixture), phenol/BA molar ratio 6 at 363 K for 7 h to investigate the effect of BA conversion and product selectivity as functions of time as per shown in Fig. 5.20 (b). With increase in time, BA conversion increased to a maximum of 85% after 7 h with 78% selectivity for mono-BP, 19% for PBE and the remainder for DBE.

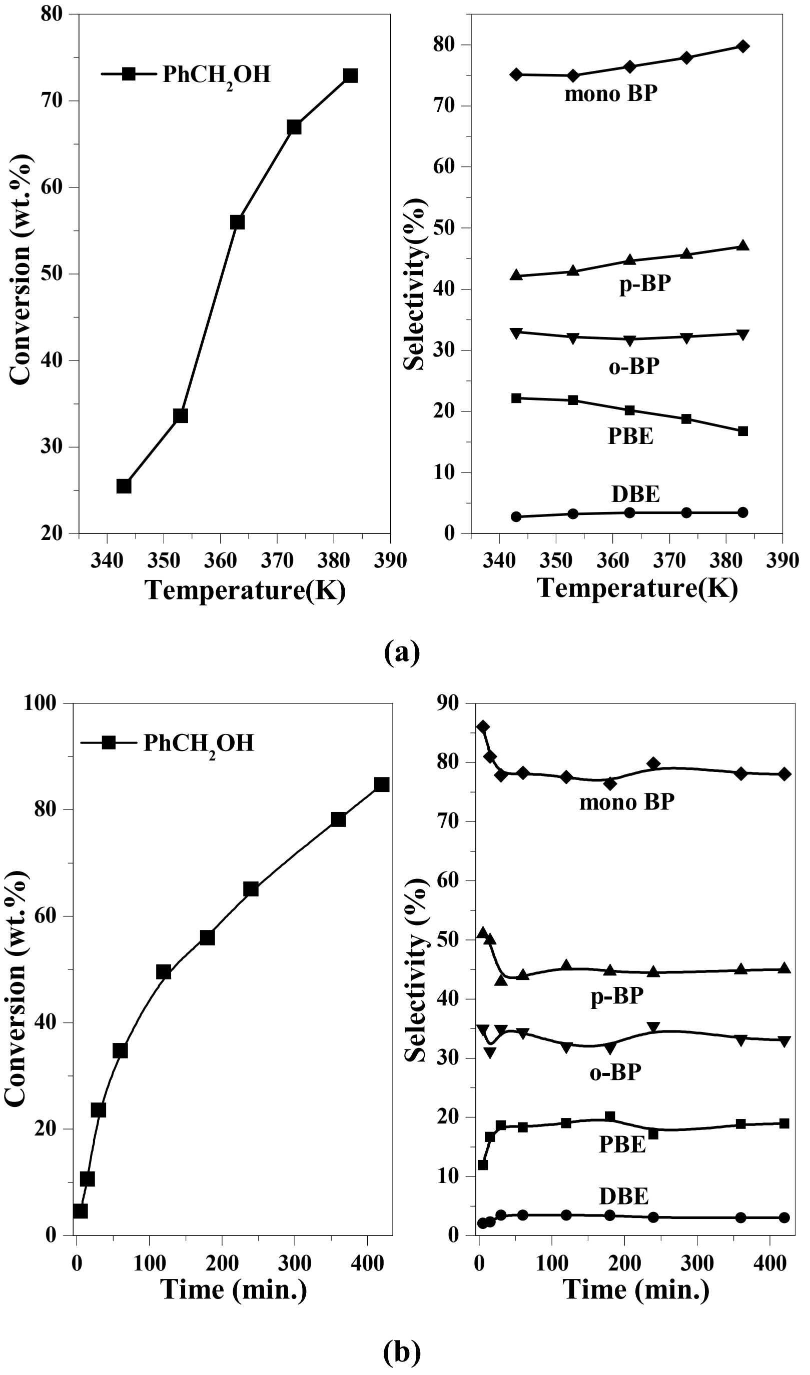

Fig. 5.20: *(a) Effect of reaction temperature on phenol benzylation. (Reaction conditions: phenol, 2.52 g (0.026 mol); BA, 0.48 g (0.0044 mol); catalyst weight, 150 mg; phenol/BA (mol ratio), 6:1; time, 3 h.*

(b)Effect of time on stream on BA conversion and product selectivity. (Reaction conditions: phenol, 2.52 g (0.026 mol); BA, 0.48 g (0.0044 mol); catalyst weight, 150 mg; phenol/BA (mol ratio), 6:1; temperature, 363 K; time, 3 h).

5.3.2.4. Kinetic study

Two reaction schemes have been proposed for phenol benzylation with BA (Scheme 5.1) [40]. The first scheme involves the direct formation of BP by alkylation of phenol with BA, whereas the second scheme involves a two-step process in which PBE is formed and then subsequently converted to BP. BA gave PBE as the product in a parallel reaction. With increasing temperature, PBE decreased, possibly due to internal transformation of O– and C–, an alkylated product. BP is a primary product, and PBE is a primary and/or secondary product that transforms during reaction to BP; such rearrangement occurs on heating or contact with an acid catalyst.

Because benzylation of phenol by BA involves two consecutive steps to form BP (Scheme 5.1), the standard equations for a first order series reaction, $C_A/C_{A0} = e^{-k_1 t}$, were used to determine the rate constant, where C_A and C_{A0} are the concentration of BA at initial time and at time *t,* respectively. The rate constants calculated at different temperatures are presented in Table 5.3. It is seen that k_1 increased with increasing temperature. The activation energy for benzylation of phenol was calculated from the Arrhenius graph and was found to be 10.38 kcal⁄mol.

5.3.3. Conclusions

The results presented in this work demonstrate that TPA/ZrO_2 dispersed uniformly inside the mesopores of SBA-15 formed nanocomposite material at a calcination temperature of 1123 K. The formation of nanosized (3–4 nm) TPA/ZrO_2 was found to depend on (%) TPA loading, monolayer coverage on ZrO_2, geometry, the nature of mesoporous supports, and calcinations temperature. Among mesoporous silica supports, SBA-15 was found to be better and provided higher thermal stability and catalytic activity than MCM-41 and MCM-48 in benzylation reactions. The mesoporous material has an advantage in the formation of nanosized and catalytically active TPA/ZrO_2 by stabilizing ZrO_2 in tetragonal phase at 1123 K, which provided higher catalytic activity than the neat TPA/ZrO_2 in benzylation reactions. The higher stability and catalytic activity can be achieved by incorporating TPA/ZrO_2 in supports like SBA-15 to get enhanced catalytic activity (ten-fold higher) than the corresponding neat TPA/ZrO_2 catalyst.

5.4. ACETYLATION OF VERATROLE WITH Ac_2O

5.4.1. Introduction

The use of solid acid catalysts such as zeolites, clays, mesoporous silica in acetylation of aromatic compounds like anisole, thioanisole, veratrole, isobutyl benzene and 2-MN have been reported in the literature [41-50]. The first industrial application of a zeolite-promoted acylation for the production of an aromatic ketone was reported by researchers at Rhone-Poulenc [42]. The acetylation of anisole to 4-methoxy acetophenone which is an intermediate for paracetamol drug, was performed over zeolites [51-53], Nafion-H on silica [54,55], and microencapsulated scandium (III) triflate in combination with nitromethane/lithium perchlorate [56]. The acetylation of isobutylbenzene over beta zeolite to produce 4-isobutyl acetophenone, as an intermediate for ibuprofen has been reported by Davis and coworkers [43]. Sulfur containing aromatic ketones such as 4-methylthio acetopheone produced by acetylation of thioanisole are potential intermediates for the synthesis of useful drugs as vioxx (refecoxib, for treating an arthritis) [57 -60]. Acylation of 2-MN was studied with various zeolites and clays [27] and found that the beta zeolite is found superior to others. Further, the acylation was studied with beta zeolite by several authors, but the conversions and selectivities towards 6-acyl-2-MN, a desired regiomer is poor to moderate. The migration of the acyl group from the 1-position to the 6-position [61] and protiodeacylation [62] of the acyl group at the 1-position may eventually result in the formation of the thermodynamically most stable 6-acylated product as an intermediate for a widely used anti-inflammatory drug – naproxen [63,64]**.** Such a reaction has been carried out over various acidic zeolites, HY, HBEA and HZSM12 [21,24,65,66], MCM-41 molecular sieves [67], clays [27] and sulphated ZrO_2 [68]. In particular, C-acylation of aromatic ethers has been successfully carried out over various solid catalysts, including clays [27] and large pore zeolites, such as HY and HBEA [22]; an extent to an industrial scale of the use of the latter for the synthesis of 4-methoxyacetophenone and 3’,4’-dimethoxyacetophenone has been recently patented [69,70].

Acetoveratrone (3’, 4’-dimethoxyacetophenone) is produced from veratrole using mineral acid catalysts and used in the synthesis of papaverine (1-(3,4-dimethoxybenzyl)-6,7-dimethoxyisoquinoline), an opium-alkaloid antispasmodic. Acetoveratrone is also synthesized by using hafnium (IV) triflate [71], scandium triflate [72] and hafnium triflate as catalysts in presence of lithium per chlorate nitromethane system [73] and carboxylic acid or trisubstituted silyl carboxylates in presence of trifluoromethyl benzoic acid anhydride [74]. Zeolite HY was found to be more active than Hß [75-78] in the above reaction. Cation-exchanged clays were also tested for this reaction [27]. HPA supported over hexagonal mesoporous silica (HMS) in presence of 1,2-dichloroethane as a solvent is used for the synthesis of acetoveratrone [79]. This catalyst system is already reported TPA/ZrO_2/MCM-41 for acetylation of veratrole in solvent free conditions [80]. The effect of ZrO_2 and SBA-15 together is expected to provide higher thermal stability for TPA by stabilizing the tetragonal phase of ZrO_2 in combination with SBA-15 at high calcination temperature. The present work reports with the resultant composite material an improved catalytic activity for acetylation of veratrole, anisole, thioanisole, isobutyl benzene and 2-MN.

5.4.2. Results and discussion

Acetylation of veratrole with Ac_2O catalyzed by 15 wt.%TPA/22.4 wt.%ZrO_2/SBA-15 under selected reaction conditions gave (A) acetoveratrone (3’, 4’-dimethoxyacetophenone) via electrophilic substitution of H_3CCO^+ to aromatic ring as shown in the Scheme 5.2.

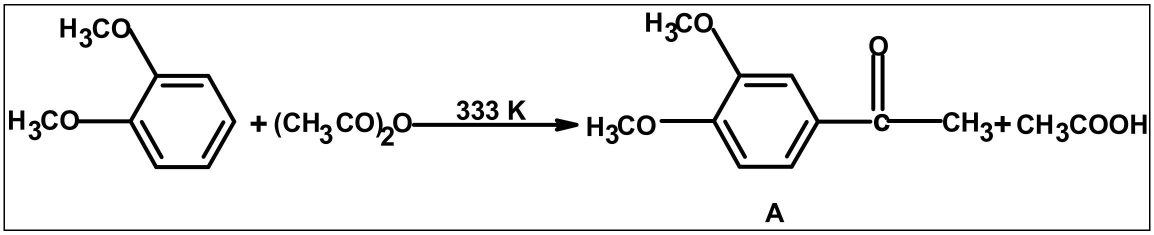

Scheme 5.2: *Acetylation of veratrole with Ac_2O.*

5.4.2.1. Comparison of catalytic activities of different catalysts

The catalytic activities of different catalysts such as H-beta, H-Y, H-Mordenite, H-ZSM-5 and Zn (II)-exchanged clay catalysts alongwith 22.4 wt.%ZrO_2/MCM-41 (with and without 15 wt.%TPA), 22.4 wt.%ZrO_2/MCM-48 (with and without 15 wt.%TPA) catalysts were evaluated in the acetylation of veratrole with Ac_2O under identical reaction conditions for comparison with the catalytic activity of 22.4 wt.%ZrO_2/SBA-15 (with and without 15 wt.%TPA) catalyst calcined at 1123 K (Table 5.4).

Table 5.4: Activities of different catalysts, recyclability and leaching study

Catalyst	S_{BET} (m)	Acidity (mmol g^{-1})	Ac_2O (% Conv.)
Comparison of different catalysts			
H-ß (30)	540	0.94	52.8
H-Y (13.5)	530	2.25	63.4
H-Mordenite (20)	490	0.72	12.3
H-ZSM-5 (60)	364	0.82	9.3
Zn (II)-exchanged clay	-	0.67	19.8
22.4 wt.% ZrO_2/SBA-15	426	0.24	36.9
15 wt.%TPA/22.4 wt.%ZrO_2/SBA-15	372	0.42	72.9
22.4 wt.%ZrO_2/MCM-41	589.8	0.24	9.3
15 wt.%TPA/22.4 wt.%ZrO_2/MCM-41	516.1	0.33	24.9
22.4 wt.%ZrO_2/MCM-48	612.3	0.10	6.0
15 wt.%TPA/22.4 wt.%ZrO_2/MCM-48	540.5	0.25	15.4
15 wt.%TPA/ZrO_2	11	0.02	10.9
3.36 wt.%TPA/SBA-15	341	0.29	30.3
Recyclability of the catalyst			
15 wt.%TPA/22.4 wt.%ZrO_2/SBA-15 (I^{st})	ne	ne	72.6
15 wt.%TPA/22.4 wt.%ZrO_2/SBA-15 (II^{nd})	ne	ne	72.0
Leaching study			
Filtrate *	-	-	59.7

Reaction conditions: temperature = 333 K, veratrole/Ac_2O molar ratio = 5, catalyst wt.=0.09g (3wt.% of total reaction mixture), time = 2 h.
**After 1 h the catalyst was removed and reaction was carried out for further 1h with the filtrate.*
ne = not evaluated.

It is seen from the results that neat 15 wt.% TPA/ZrO_2 gave the lowest conversion, which is due to its low surface area. It is also observed that 3.36 wt.% TPA/SBA-15 calcined at 1123 K shows very less catalytic activity in the reaction, since it has no acidity required for acid catalyzed reactions. Among the zeolite catalysts, H-Y is more active than others due to its highest acidity with large pores gave higher conversion of Ac_2O followed by H-beta (strong and medium acid sites). Similarly, lower activity of H-ZSM-5 might be explained on the basis of its smaller pore size compared with the larger size of the products attributed to diffusional limitations. While, H-Mordenites has one-dimensional pore with elliptical channels, 6.5 X 7.0 also has the low activity. In the present catalyst system, ZrO_2 alone loaded on mesoporous silica support i.e. 22.4 wt.%ZrO_2/SBA-15 calcined at 1123 K shows some catalytic activity, while after loading 15 wt.%TPA over it shows two-fold increase in catalytic activity (Table 5.4). So here is the specific role of the composite materials and the effect of ZrO_2 on the acidity function of TPA, which enhances the catalytic activity. Therefore, we have chosen 15wt.% TPA/22.4 wt.%ZrO_2/SBA-15 calcined at 1123 K as the catalyst for further investigations on its catalytic performance in the veratrole acetylation with Ac_2O.

5.4.2.2. Effect of TPA loading, calcination temperature and ZrO_2 loading

Veratrole acetylation was conducted using different TPA (5-70 wt.%) loaded catalysts to know the effect on the conversion of Ac_2O and the results are shown in Fig 5.21 (a). The discussion is same as previously mentioned. It is seen that conversion of Ac_2O increases with increase in TPA loading upto 15 wt.% and on further increase in loading of TPA there is decrease in Ac_2O conversion. The decrease in its activity at higher TPA loading is due to the formation of WO_3 crystallites due to decomposition of HPA's (XRD Fig. 5.2 (a)). As shown in Fig. 5.21 (a), 15 wt.% catalyst is more acidic than others hence, it gave highest Ac_2O conversion (72.9 %) with 100 % selectivity for acetoveratrone (3', 4'-dimethoxyacetophenone) as unique product under the selected reaction conditions.

Veratrole acetylation by Ac_2O was conducted for knowing the effect of calcination temperature on 15 wt.%TPA/22.4 wt.%ZrO_2/SBA-15 catalyst and the results are shown in Fig. 5.21 (b). There is an increase in Ac_2O conversion upto 1123 K calcinations temperature but on further increase, Ac_2O conversion decreased.

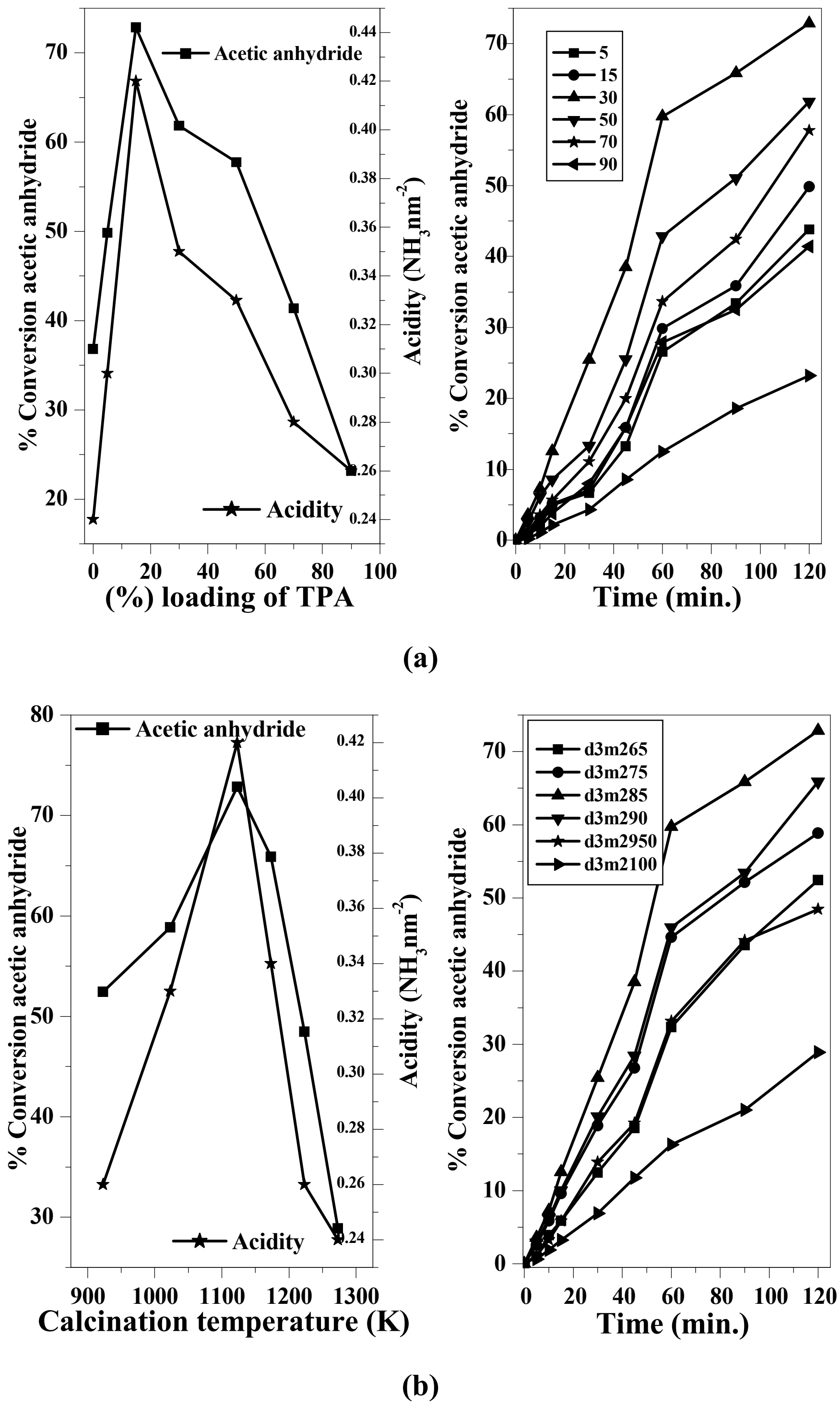

Fig. 5.21: *(a) Effect of TPA loading and acidity on Ac_2O conversion and time on stream study. (Reaction conditions: temperature = 333 K, veratrole/ Ac_2O (molar ratio) = 5, catalyst weight = 0.09 g (3 wt.% of total reaction mixture), time = 2h).*
(b) Effect of calcination temperature and acidity on Ac_2O conversion and time on stream study. (Reaction conditions: temperature = 333 K, veratrole/ Ac_2O (molar ratio) = 5, catalyst weight = 0.09 g (3 wt.% of total reaction mixture), time = 2h).

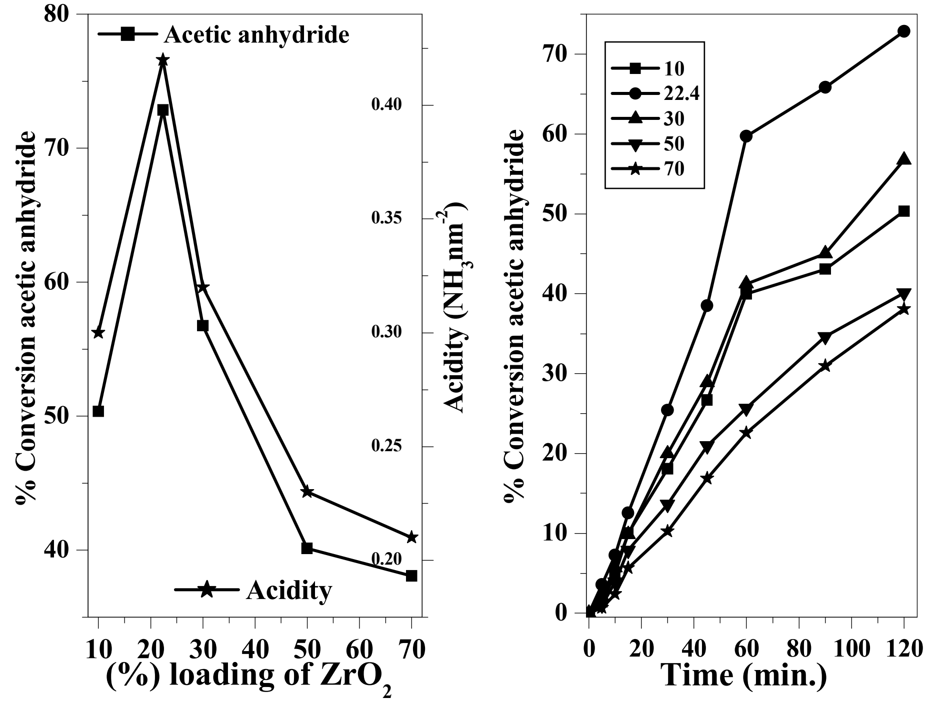

Fig. 5.22: *Effect of ZrO_2 loading and acidity on Ac_2O conversion and time on stream study. (Reaction conditions: temperature = 333 K, veratrole/ Ac_2O (molar ratio) = 5, catalyst weight = 0.09 g (3 wt.% of total reaction mixture), time = 2h).*

This observation is supported by the fact that 15 wt.%TPA/22.4 wt.%ZrO_2/SBA-15 calcined at 1123 K has the maximum concentration of acid sites, where TPA forms a monolayer coverage over the support. Hence, catalyst calcined at 1123 K was chosen for further study. In order to study the effect of ZrO_2 loading over SBA-15 with 15 wt.%TPA catalyst calcined at 1123 K, veratrole acetylation by Ac_2O was conducted under selected reaction conditions. As shown in Fig. 5.22, there is an increase in Ac_2O conversion upto 22.4 wt.% ZrO_2 loading and on further increase in loading Ac_2O conversion decreased. This could be due to the formation of monolayer coverage of 22.4 wt.% of ZrO_2 over SBA-15 giving rise to maximum total acidity. While on further increase in ZrO_2 loading it shows the formation of monoclinic phase of ZrO_2 alongwith tetragonal phase and thereby decreasing the conversion of Ac_2O in veratrole acetylation.

The amount and the total acidity of the catalysts were determined from TPD of ammonia. Then it was correlated with catalytic activities of 22.4 wt.%ZrO_2/SBA-15 with different (%) TPA loadings as shown in Fig. 5.21 (a), 15 wt.%TPA/22.4 wt.%ZrO_2/SBA-

15 calcined at different calcination temperatures as shown in Fig. 5.21 (b) and 15 wt.%TPA/wt.% ZrO_2/SBA-15 with different (%) ZrO_2 loading as per shown in (Fig 5.22). It shows that total acidity of TPA/22.4 wt.%ZrO_2/SBA-15 calcined at 1123 K catalyst increases till 15 wt.% and then on further increasing TPA loading it shows decrease so as to catalytic activity. It can be concluded as till 15 wt.%TPA, the Keggin unit of HPA retains its structure and acidity. Total acidity data of the catalyst 15 wt.%TPA/22.4 wt.%ZrO_2/SBA-15 at different calcination temperatures were plotted along with catalytic activity. It shows that till 1123 K, total acidity increases and on further increase in calcination temperature shows decrease in acidity and also decrease in catalytic activity, which is due to decomposition of TPA into WO_3 crystallites. Similarly, with increasing ZrO_2 loading till 22.4 wt.% catalyst 15 wt.%TPA/ZrO_2/SBA-15 calcined at 1123 K shows increase in acidity and thereby catalytic activity. The highest acidity corresponds to monolayer coverage of TPA (i.e. 15 wt.%TPA/22.4 wt.%ZrO_2/SBA-15 calcined at 1123 K), where the Keggin–like structure is intact, as supported by ^{31}P CP-MAS NMR and XRD. The total acidities of 22.4 wt.%ZrO_2 and 15 wt.%TPA/22.4 wt.%ZrO_2 supported on various silica supports, unsupported TPA/ZrO_2 and TPA supported on SBA-15, all calcined at 1123 K, are given in Table 5.4. Among all of them, 15 wt.% TPA/22.4 wt.%ZrO_2/SBA-15 calcined at 1123 K shows the highest acidity corresponds to monolayer coverage of TPA, where the Keggin –like structure is intact, as supported by ^{31}P CP-MAS NMR, FT-Raman and XPS. These results indicate that TPA/ZrO_2 dispersed more uniformly over large surface area and large pore volume SBA-15 as compared with other supports.

5.4.2.3. Effect of reaction parameters

From Fig. 5.23 (a) shows that with increase in catalyst concentration from 1-5 wt.% of total reaction mixture (3 g), by keeping constant molar ratio of veratrole: Ac_2O as 5, 333 K and 2 h, it shows increase in Ac_2O conversion from 28.8 % to 82.1 % with 100 % selectivity for acetoveratrone as a monoacetylated product. The effect of veratrole to Ac_2O molar ratio on the conversion of veratrole and time on stream study for different molar ratios are presented in Fig. 5.23 (b). The mole ratio of veratrole to Ac_2O was varied from 1 to 9, by keeping other conditions the same. As veratrole: Ac_2O molar ratio is increased from 1 to 9, conversion of Ac_2O increased from 36.2 to 81.7 % with 100 % selectivity for a monoacetylated product.

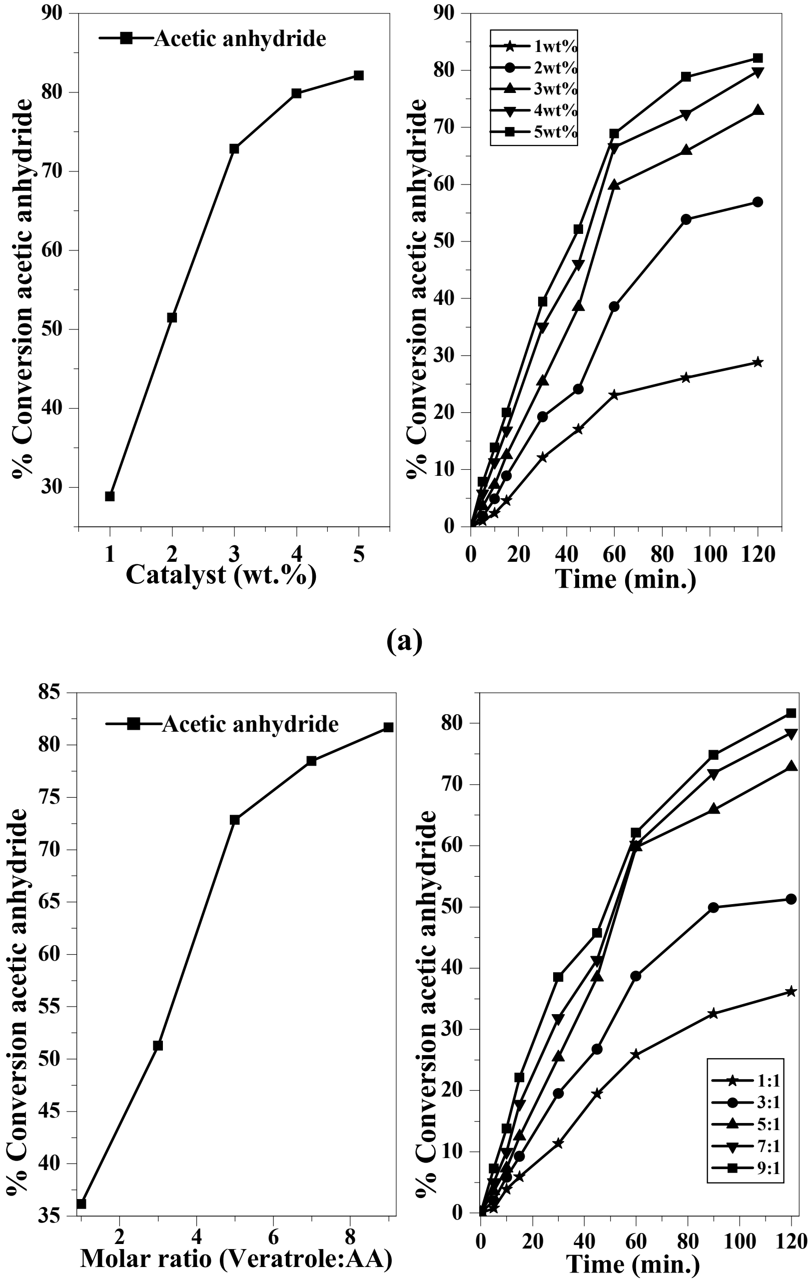

(a)

(b)

Fig. 5.23: *(a) Effect of catalyst weight on Ac_2O conversion and time on stream study. (Reaction conditions: temperature = 333 K, veratrole/ Ac_2O (molar ratio) = 5, time = 2h). (b) Effect of molar ratio on Ac_2O conversion and time on stream study. (Reaction conditions: temperature = 333 K, catalyst weight = 0.09 g (3 wt.% of total reaction mixture), time = 2h).*

The acetylation of veratrole with Ac_2O was carried out in the temperature range 313-353 K, to know the effect of temperature on the conversion of Ac_2O. It is seen from Fig. 5.24 that the conversion of Ac_2O increases from 46.1 % to 83.1 % with increase in temperature from 313 to 353 K.

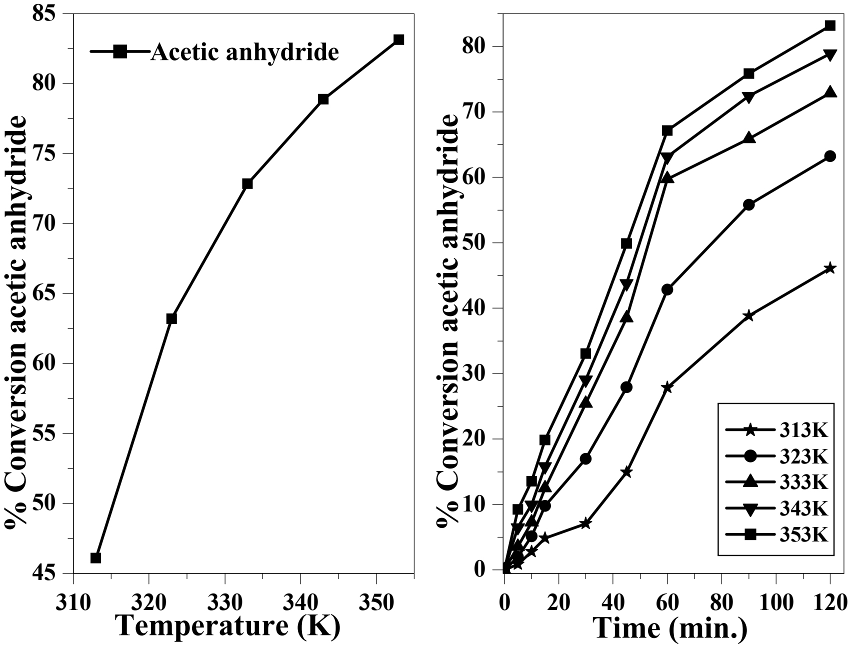

Fig. 5.24: *Effect of temperature on Ac_2O conversion and time on stream study. (Reaction conditions: veratrole/ Ac_2O (molar ratio) = 5, catalyst weight = 0.09 g (3 wt.% of total reaction mixture), time = 2h).*

5.4.2.4. Acetylation of different aromatic substrates with Ac_2O

15 wt.%TPA/22.4 wt.%ZrO_2/SBA-15 calcined at 1123 K with an Ac_2O was employed to acylate the aromatic hydrocarbons. The data for the catalytic efficiencies along with reaction conditions are listed in Table 5.5 under mentioned reaction conditions in Table 5.5.

Anisole acylation gave 97.9 % p-methoxyacetopheone (A) and remaining is o-methoxyacetopheone (B) (Scheme- 5.3) with 60 % of Ac_2O conversion. For acetylation of thioanisole 15 wt.%TPA/22.4 wt.%ZrO_2/SBA-15 calcined at 1123 K was employed under mentioned reaction conditions in Table 5.5 with an Ac_2O. It is giving 99.6 % p-(methylthio acetopheone) (A) and remaining is o- (methylthio acetopheone) (B) (Scheme-5.3) isomer with 35.8 % of Ac_2O conversion. The acetylation of isobutyl benzene was carried out with Ac_2O giving rise to 30 % Ac_2O conversion with 100% product selectivity for 4-isobutylacetophenone (A) (Scheme-5.4) as shown in Table 5.5. The acetylation of 2-MN with Ac_2O under different solvents are presented in Table 5.5. Product formation can be attributed to the strong support interaction to enable the formation of carbocation, an essential requirement for Friedel-Crafts electrophilic acylation of aromatic ethers. Acetylation reaction with different solvents are presented in Table 5.5. Solvent effect on the conversions is visible, affording higher conversion with nitrobenzene.

Table 5.5: Acetylation of aromatic substrates with Ac_2O

Substrate	Mole ratio	Temp.	Catalyst wt.%	Time (h)	% Ac_2O Conversion
Veratrole	5:1	60	0.09	2	72.9
Anisole	10:1	90	0.15	3	60.9
Thioanisole	10:1	90	0.15	3	35.8
Isobutyl benzene	10:1	100	0.15	5	30.0
2-MN (Nitrobenzene)*	2:1	100	0.15	8	61.2
2-MN (Chlorobenzene)*	2:1	100	0.15	8	50.3
2-MN (1,2-DCB)*	2:1	100	0.15	8	56.7
2-MN (Benzene)*	2:1	100	0.15	8	39.1

** Solvent amount = 20 ml.*

Reaction conditions: Catalyst = 15 wt.%TPA/22.4 wt.%ZrO_2/SBA-15 calcined at 1123 K.

The selectivity of the products, 1-acyl-2-MN (A) formed remains identical, close to 97% and remaining 3% of 6-acyl-2-MN (B), which is as shown in Scheme-5.5 irrespective of the solvents employed, which is in contrast to the classical homogeneous acylation reaction. In the classical acylation reaction conducted with anhydrous aluminium chloride employed in more than stoichiometric quantities, the solvent plays a major role in the isomer distribution, depending on the ability of the solvent to form the complex with acylating agent [61]. Acylation occurs at 1-position predominantly in carbon disulphide, and at 6-position in nitrobenzene. Isomeric ratio varies with different transition metal chlorides in stoichiometric amounts correlated to their acid strength. Insufficient acid strength in the present catalytic reaction due to the use of small amounts of solid acids precludes formation of other isomers accentuated by protiodeacetylation at moderate temperatures instead favours exclusive formation of 1-acetyl derivative. The acylation of 2-MN has been extensively studied as a test reaction for zeolites, USY, and ZSM-12 [81] and has recently been used with MCM-41 catalysts [82]. Acetylation with Ac_2O occurs at the 1-position yielding the kinetically favored 1-acetyl-2-MN. Although Friedel–Crafts acylation is usually irreversible, the main product 1-acetyl-2-MN can undergo protiodeacylation [62] and reacylation then yields the thermodynamically more stable 2-acetyl-6-Methoxynaphthalene (2-Ac-6-MN), which is also produced by migration of the acetyl group [61].

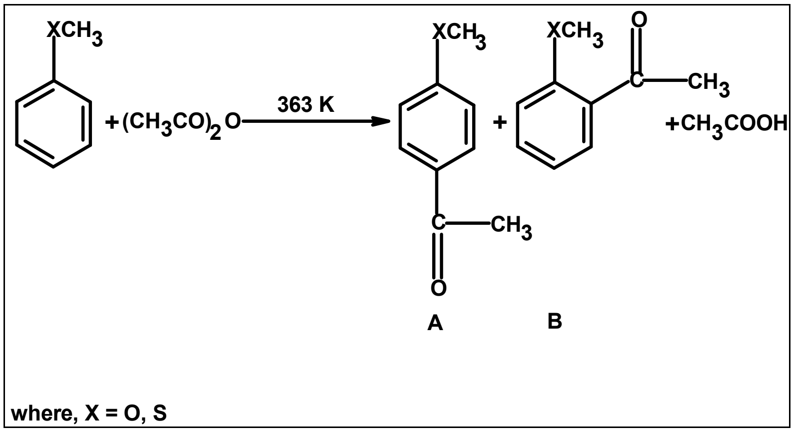

Scheme 5.3: *Acetylation of anisole or thioanisole with Ac_2O.*

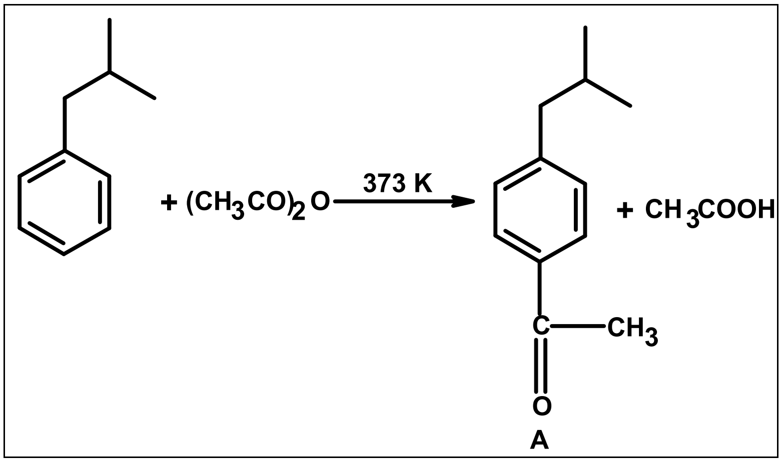

Scheme 5.4: *Acetylation of isobutyl benzene with Ac_2O.*

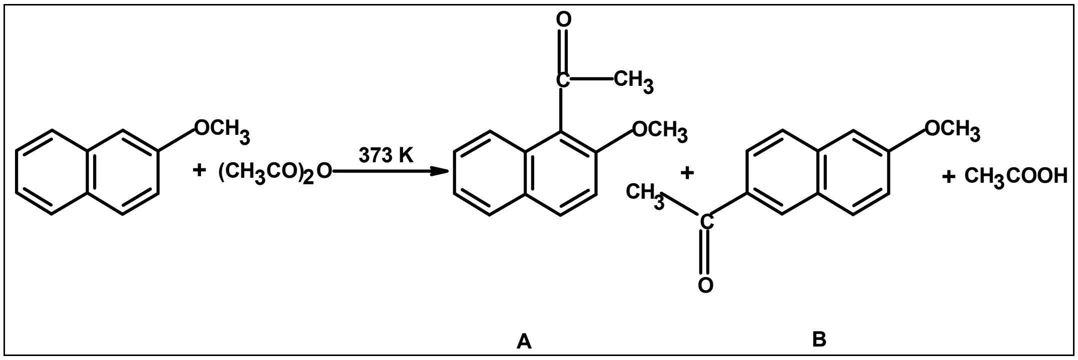

Scheme 5.5: *Acetylation of 2-MN with Ac_2O.*

5.4.2.5. Kinetic study

The maximum conversion of Ac_2O (72.9 %) was obtained at 333 K, by keeping veratrole: Ac_2O molar ratio as 5 with catalyst amount as 3 wt.% of total reaction mixture. At one particular temperature, first-order rate constants were calculated for 1 h of reaction time, and then the constant values of 'k_1' showed that the acetylation of veratrole is a first-order reaction. The standard equations for a first order series reaction $C_A/C_{Ao} = e^{-k_1 t}$ has been used for the determination of rate constant, where C_A and C_{Ao} are the concentration of Ac_2O at initial time and at time t, respectively. Activation energy evaluated from graph of –ln rate Vs 1/T was found to be 5.79 kcal mol^{-1}.

5.4.3. Conclusions

The results presented in this work again demonstrate that TPA/ZrO_2 dispersed uniformly inside the mesopores of SBA-15 formed nano-sized (3-4 nm) composite material at a calcination temperature of 1123 K. The 15 wt.% TPA/22.4 wt.%ZrO_2/SBA-15 catalyst calcined at 1123 K was found to be the most active catalyst in all the acetylation reactions studies under selected liquid phase conditions under N_2 atmosphere and shows greater catalytic activity (6-7 fold higher) than with the corresponding neat TPA/ZrO_2 catalyst. The higher activity of the catalyst in acetylation reaction is because of uniform dispersion of TPA/ZrO_2 over large surface area and large pore volume SBA-15 as compared with other supports. The performance of HPA supported on ZrO_2 embedded inside the mesoporous silica support like SBA-15 catalyst was found to depend on catalyst pretreatment conditions such as effect of loadings of TPA, ZrO_2 and calcination temperatures and most importantly on the nature and the characterstics of the mesoporous support.

5.5. REFERENCES

1. D. Zhao, J. Feng, Q. Huo, N. Melosh, G. H. Fredrickson, B. F. Chmelka, G. D. Stucky, Science, 279 (1998) 548.
2. M. Misono, Chem. Commun., (2001) 1141.
3. E. Lopez-Salinas, J. G. Hernandez-Corez, I. Schifter, E. Torres-Garcia, J. Navarrete, A. Gutierrez-Carillo, T. Lopez, P. P. Lottici, D. Bersani, Appl. Catal. A: General, 193 (2000) 215.
4. M. W. McKittrick, C. W. Jones, Chem. Mater., 15 (2003) 1132.
5. A. S. Maria Chong, X. S. Zhao, A. T. Kwtedji, S. Z. Qiao, Micropor. Mesopor. Mater., 72 (2004) 33.
6. T. R. Pauly, V. Petkov, Y. Liu, Simon J. L. Billinge, T. J. Pinnavaia, J. Am. Chem. Soc., 124 (1) (2002) 99.
7. P. A. Jalil , N. Tabet , M. Faiz, N. M. Hamdan, Z. Hussain, Appl. Catal.A: General, 257 (2004) 1.
8. E. Brunner, Catal. Today, 38 (1997) 361.
9. T. Baba, Y. Hasada, M. Nomura, Y. I. Ohno, Y. Ono, J. Mol. Catal. A: Chem., 114 (1996) 247.
10. N. Essayem, Y. Y. Tong, H. Jobic, J. C. Vedrine, Appl. Catal. A: General, 194 – 195 (2000) 109.
11. V. M. Mastikhin, I. L. Mudrakovsky, A. V. Nosov, Prog. NMR Spectrosc., 23 (1991) 259.
12. M. Hunger, Catal. Rev.- Sci. Eng., 39 (4) (1997) 345.
13. S. Uchida, K. Inumaru, J. M. Dereppe, M. Misono, Chem. Lett., 643 (1998).
14. A. Thomas, C. Dablemont, J.-M. Basset, F. Lefebvre, C. R. Chimie, 8 (2005) 1969.
15. E. F. Kozhevnikova, I. V. Kozhevnikov, J. Catal., 224 (2004) 164.
16. J. A. Dias, E. Caliman, S. C. L. Dias, M. Paulo, A. T. C. P. de Souza, Catal. Today, 85 (2003) 39.
17. N. Millot, C. S. Santini, F. Lefebvre, C. R. Chimie, 7 (2004) 725.
18. M. Hunger, Solid State Nucl. Magn. Reson., 6 (1996).
19. M. Hunger, S. Ernst, S. Steuernagel, J. Weitkamp, Micropor. Mater., 6 (1996) 349.

20. M. Hunger, U. Schenk, M. Breuninger, R. Gla¨ser, J. Weitkamp, Micropor. Mesopor. Mater., 27 (1999) 261.
21. T. Okuhara, N. Mizuno, M. Misono, Adv. Catal., 41 (1996) 113.
22. Y. Nakano, T. Iizuka, H. Hattori, K. Tanabe, J. Catal., 57 (1978) 1.
23. Y. Saito, P. N. Cook, H. Niiyama, E. Echigoya, J. Catal., 95 (1985) 49.
24. K. Tanabe, M. Misono, Y. Ono, H. Hattori, Stud. Surf. Sci. Catal., 51 (1989) 169.
25. T. Jin, T. Yamaguchi, K. Tanabe, J. Phys. Chem., 90 (1986) 4794.
26. K. Tanabe, H. Hattori, T. Yamaguchi, Crit. Rev. Surf. Chem., 1 (1990) 1.
27. L. Pizzio, P. Vázquez, C. Cáceres, M. Blanco, Catal. Lett., 4 (2001) 77.
28. A. V. Emeline, G. V. Kataeva, A. S. Litke, A. V. Rudakova, V. K. Ryabchuk, N. Serpone, Langmuir, 14 (1998) 5011.
29. J. Joo, T. Yu, Y. W. Kim, H. M. Park, F. Wu, J. Z. Zhang, T. Hyeon, J. Am. Chem. Soc., 125 (2003) 6553.
30. W. Kuang, A. Rives, M. Fournier, R. Hubaut, Appl. Catal. A: General, 250 (2003) 221.
31. B. H. Davis, R. A. Keogh, S. Alerasool, D. J. Zalewski, D. E. Day, P. K. Doolin, J. Catal., 183 (1999) 45.
32. I. V. Kozhevnikov, 'Catalysis by Polyoxometalates, Catalysts for Fine Chemical Synthesis', vol. 2, Wiley, 2002, p. 15.
33. H.-W. Voges, in: B. Elvers, S. Hawkins, G. Schulz (Eds.), Ullmann's Encyclopedia of Industrial Chemistry, vol. 19, VCH, Weimheim, Germany, 1991, p. 328.
34. B. M. Devassy, G. V. Shanbhag, F. Lefebvre, W. Böhringer, J. Fletcher, S. B. Halligudi, J. Mol. Catal. A: Chem., 230 (2005) 113.
35. T. Matsuura, Y. Ohkatsu, Polym. Degrad. Stab., 70 (2000) 59.
36. C. J. Norman, P. A. Goulding, P. J. Moles, Stud. Surf. Sci. Catal., 90 (1994) 269.
37. D. H. Aguilar, L. C. Torres-Gonzalez, L. M. Torres-Martinez, T. Lopez, P. Quintana, J. Solid State Chem., 158 (2001) 349.
38. E. Torres-Garcia, G. Rosas, J. A. Ascencio, E. Haro-Poniatowski, R. Perez, Appl. Phys. A, 79 (2004) 401.
39. K. Arata, Adv. Catal., 37 (1990) 165.

40. A. B. Deshpande, A. R. Bajpai, S. D. Samant, Appl. Catal. A: General, 209 (2001) 229.
41. E. G. Derouane, C. J. Dillon, D. Bethell, S. B. D. Hamid, J. Catal., 187 (1999) 209.
42. M. Spagnol, L. Gilbert, R. Jacquot, H. Guillot, P. J. Triel, A. M. LeGovic, 'Book of Abstracts of 4th International Symposium on Heterogeneous Catalysts and Fine Chemicals', Basel, Switzerland, 1996.
43. D. P. Sawant, S. B. Halligudi, Cata. Commun., 5 (2004) 659.
44. P. Andy, J. Gracia-Martinez, G. Lee, H. Gonzalez, C. W. Jones, M. E. Davis, J. Catal., 215 (2000) 192.
45. K. Gaare, D. Akporiaye, J. Mol. Catal. A: Chem., 109 (1996) 177.
46. E. Fromentin, J.-M. Coustard, M. Guisnet, J. Mol. Catal. A: Chem., 159 (2000) 377.
47. P. Botella, A. Corma, G. Sastre, J. Catal., 197 (2001) 81.
48. P. Moreau, A. Finiels, P. Meric, J. Mol. Catal. A: Chem., 154 (2000) 185.
49. M. Spagnol, L. Gilbert, H. Guillot, J. P. Triel, PCT Int. Patent WO 97/48665 (1997).
50. S. D. Kim, K. H. Lee, J. S. Lee, Y. J. Kim, K. E. Yoon, J. Mol. Catal. A: Chem., 152 (2000) 33.
51. A. Corma, M. J. Climent, H. Garcia, J. Primo, Appl. Catal. A: General, 49 (1989) 109.
52. D. Rohan, C. Canaff, E. Fromentin, M. Guisnet, J. Catal., 177 (1998) 296.
53. B. M. Choudary, M. Sateesh, M. L. Kantam, K. V. R. Prasad, Appl. Catal. A: General, 171 (1998) 155.
54. A. Heidekum, M. A. Harmer, W. F. Hoelderich, J. Catal., 188 (1999) 230.
55. Y. Izumi, M. Ogawa, W. Nohara, K. Urabe, Chem. Lett., (1992) 1987.
56. S. Kobayashi, S. Nagayama, J. Am. Chem. Soc., 120 (1998) 2985.
57. H. G. Franck, J. W. Stadelhofer, Industrial Aromatic Chemistry, Springer, New York, 1988, p. 324.
58. M. Aslam, K. G. Davenport, R. R. Graham, US Patent 4,794,205 (1988).
59. C. G. Overberger, A. Lebovits, J. Am. Chem. Soc., 74 (1956) 4792.
60. J. R. Zoeller Jr., C. E. Sumner, J. Org. Chem., 55 (1990) 319.

61. P. H. Gore, in: ‘G.A. Olah (Ed.), Friedel-Crafts and Related Reactions’, vol. III, Wiley, New York, 1964, p. 64, 72.
62. J. Al-Ka'bi, J. A. Farooqui, P. H. Gore, A. M. G. Nassar, E. F. Saad, E. L. Short, D. N. Waters, J. Chem. Soc. Perkin Trans. II (1988) 943.
63. K. T. Wan, M. E. Davis, J. Catal., 152 (1994) 25.
64. M. E. Davis, Micropor. Mesopor. Mater., 21 (1998) 173.
65. H. K. Heinichen, W. Hölderich, J. Catal., 185 (1999) 408.
66. A. Berrhegis, P. Ayrault, E. Fromentin, M. Guisnet, Catal. Lett., 68 (2000) 121.
67. H. Hitz, R. Prins, J. Catal., 168 (1997) 194.
68. G. D. Yadav, M. S. Krishnan, Chem. Eng. Sci., 54 (1999) 4189.
69. M. Spagnol, L. Gilbert, E. Benazzi, C. Marcilly, Patent PCT Int. Appl. WO 96,35,655 (1996).
70. M. Spagnol, L. Gilbert, E. Benazzi, C. Marcilly, Patent PCT Int. Appl. WO 96,35,656 (1996).
71. A. Kawada, S. Mitamura, S. Kobayashi, Syn. Lett.,7 (1994) 545.
72. I. Hachiya, M. Moriwaki, S. Kobayashi, Tet. Lett., 36 (1995) 409.
73. I. Hachiya, M. Moriwaki, S. Kobayashi, Bull. Chem. Soc. Jpn., 68 (1995) 2053.
74. K. Suzuki, M. Mukoyama, Jpn. Pat. , 06 145 092, 1994.
75. M. Spagnol, L. Gilbert, D. Alby, Ind. Chem. Libr., 8 (1996) 29.
76. T. Raja, A. P. Singh, A. V. Ramaswamy, A. Finiels, P. Moreau, Appl. Catal. A: General, 211 (2001) 31.
77. C. Guignard, V. Pédron, F. Richard, R. Jacquat, M. Spagnol, J.M. Coustard, G. Pérot, Appl. Catal. A: General, 234 (2002) 79.
78. P. Moreau, A. Finiels, P. Meric, J. Mol. Catal. A: Chem., 154 (2000) 185.
79. G. D. Yadav, H. Manyar, Micropor. Mesopor. Mater., 63 (2003) 85.
80. D. P. Sawant , Vinu A., F. Lefebvre, S. B. Halligudi, J. Mol. Catal. A: Chem., (Accepted).
81. G. Harvey, G. Mäder, Collect. Czech. Chem. Commun.,57 (1992) 862.
82. E. A. Gunnewegh, S. S.Gopie, H.van Bekkum, J. Mol. Catal. A: Chem., 106 (1996) 151.

CHAPTER – 6

ZIRCONIA SUPPORTED STA IN MESOPOROUS SILICA

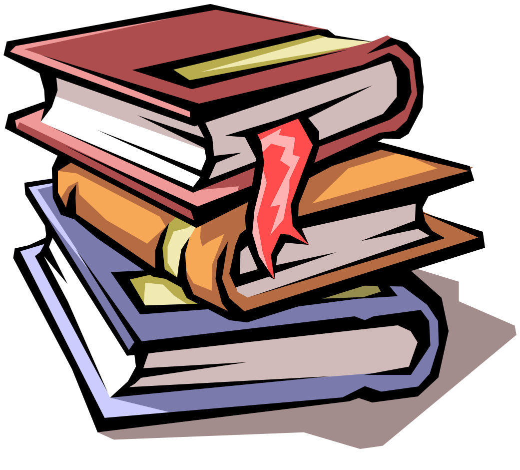

6. ZIRCONIA SUPPORTED STA IN MESOPOROUS SILICA

6.1. INTRODUCTION

This chapter presents the characterization of STA over ZrO_2 dispersed uniformly in mesoporous silica (MS) channels of MCM-41, MCM-48 and SBA-15. Catalysts with different STA loadings (5 to 90 wt.%) on 22.4 wt.%ZrO_2/MCM-41 and 15 wt.%STA on different ZrO_2 loadings (10-70 wt.%)/MCM-41 were prepared and calcined at 1123 K. Also, 15 wt.%STA/22.4 wt.%ZrO_2/ SBA-15 catalysts calcined in the range 923 to 1273 K were prepared. These catalyst systems were screened for their catalytic activities in the liquid phase esterification of alcohols with carboxylic acids.

6.2. CHARACTERIZATION-RESULTS AND DISCUSSION

6.2.1. Elemental analysis

The ratio of Si: W (1: 12) in 15 wt.%STA/22.4 wt.%ZrO_2/SBA-15 corresponding to a single Keggin unit was estimated by XRF and ICP-OES analysis which were (1: 12.13) and (1:12.07), respectively.

6.2.2. XRD

Fig. 6.1 shows the wide-angle XRD patterns of pure ZrO_2, 15 wt.%STA/ZrO2, 3.36 wt.%STA/SBA-15, 22.4 wt.%ZrO_2/SBA-15 and pure STA calcined at 1123 K. As shown in Fig. 6.1(a), only ZrO_2 calcined at 1123 K shows both tetragonal and monoclinic phases. While 15 wt.%STA/ZrO_2 calcined at 1123 K shows monoclinic and tetragonal phases of ZrO_2 and WO_3 crystallites due to decomposition of STA. While 3.36 wt.%STA/SBA-15 shows amorphous phase and 22.4 wt.%ZrO_2/SBA-15 shows only broad tetragonal phase of ZrO_2.

The small angle X-ray powder diffraction patterns of the catalysts with different (%) STA loadings calcined at 1123 K are shown in Fig. 6.2 (a), and those of 15 wt.% STA/22.4 wt% ZrO_2/SBA-15 calcined at different calcination temperatures are shown in Fig. 6.3 (a). The wide-angle XRD patterns with different (%) STA loadings calcined at 1123 K shows only tetragonal phase of ZrO_2 till 15 wt.%STA i.e. up to a monolayer coverage. But beyond monolayer coverage, it starts showing WO_3 crystallites due to partial decomposition of STA [Fig.6.2 (b)]. Similarly, 15 wt.%STA/22.4 wt.%ZrO_2/SBA-15 catalysts shows a tetragonal phase along with WO_3 crystallites only after calcination beyond 1123 K [Fig. 6.3 (b)]. Fig. 6.4 represents the XRD patterns of the catalysts with 15 wt.% STA/ different loadings of ZrO_2 /SBA-15 calcined at 1123 K. The explanation is similar as per described earlier in Chapter 5, section 5.5.2., page no. 102.

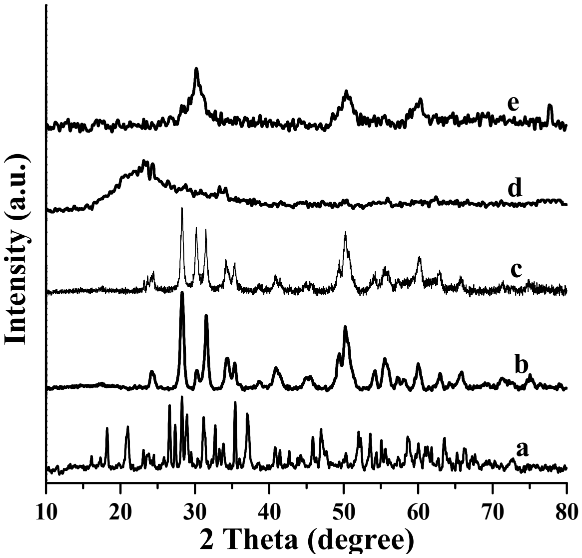

Fig. 6.1: *Wide-angle XRD patterns for a) pure STA, and b) pure ZrO_2, c) 15wt.%STA/ZrO_2, d) 3.36 wt.%STA/SBA-15, e) 22.4 wt.% ZrO_2/SBA-15 calcined at 1123 K.*

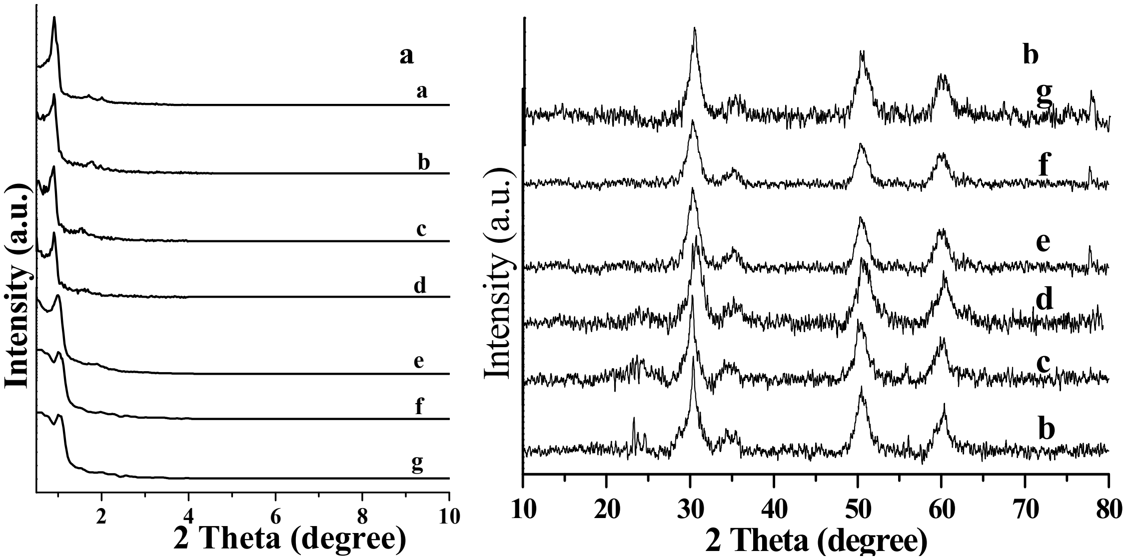

Fig. 6.2: *Low angle XRD (a) (%) loading a) SBA-15, STA/22.4 wt.%ZrO_2/SBA-15 with b) 5,c) 15,d) 30,e) 50,f) 70 and g) 90 wt.%STA loadings and calcined at 1123 K, including (b) wide-angle xrd, respectively.*

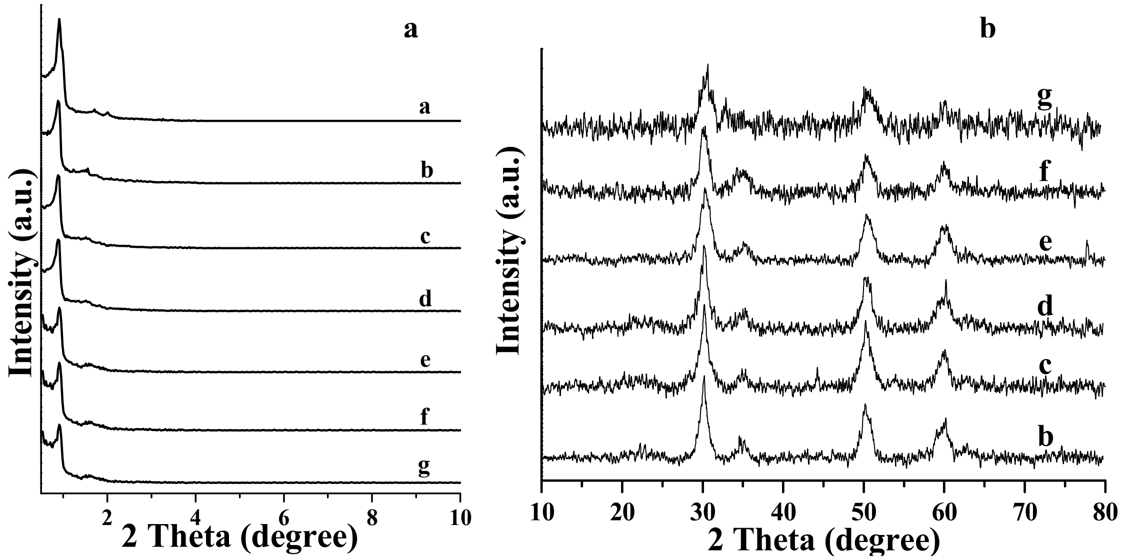

Fig. 6.3: *Low angle XRD (a) calcination temperature a) SBA-15, 15 wt.%STA/22.4 wt.%ZrO$_2$/SBA-15 calcined at b) 923,c) 1023,d) 1123,e) 1173,f) 1223 and g) 1273 K, including (b) wide-angle xrd, respectively.*

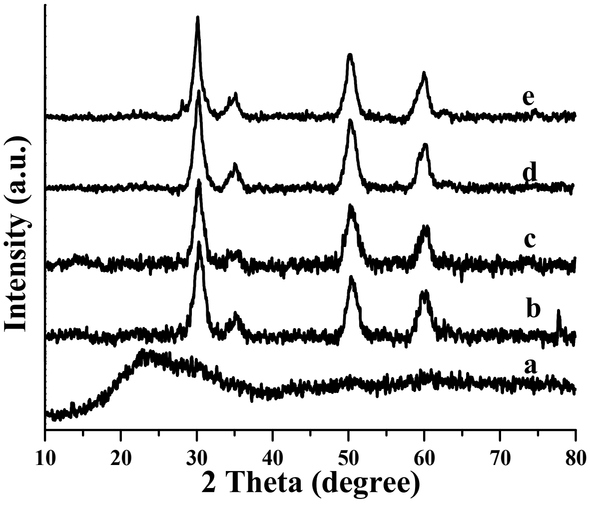

Fig. 6.4: *Wide-angle XRD pattern for 15 wt.%STA with a) 10, b) 22.4, c) 30, d) 50 and e) 70 wt.% ZrO$_2$/SBA-15 calcined at 1123 K.*

6.2.3. Sorption study

The textural properties of modified SBA-15 with different loadings of STA (wt.%)/22.4 wt% ZrO$_2$, 15 wt.%STA/wt.%ZrO$_2$/SBA-15 with different (%) ZrO$_2$ loadings and 15 wt.%STA/22.4 wt.%ZrO$_2$/SBA-15 calcined at different calcination temperatures are presented in Table 6.1.

Table 6.1. Physicochemical properties of the catalysts and their catalytic activities

Sample	Surface area (m^2g^{-1})	Pore volume (cm^3g^{-1})	Pore diameter (Å)	Total Acidity ($mmolg^{-1}$)	Rate constant x $10^{-5}(s^{-1})$	IAA Conv., (%)
5 wt.%STA/ZrO_2/ SBA-15	396	0.63	65.7	0.29	2.91	27
15 wt.%STA/ZrO_2/ SBA-15	372	0.61	65.3	0.40	6.42	50
30 wt.%STA/ZrO_2/ SBA-15	334	0.58	65.1	0.35	4.89	41
50 wt.%STA/ZrO_2/ SBA-15	333	0.54	64.7	0.30	3.30	30
70 wt.%STA/ZrO_2/ SBA-15	200	0.34	64.4	0.27	2.07	20
90 wt.%STA/ZrO_2/ SBA-15	200	0.31	63.7	0.22	1.39	14
STA/10 wt.%ZrO_2/ SBA-15	415	0.66	67.6	0.32	3.57	32
STA/30 wt.%ZrO_2/ SBA-15	296	0.46	64.2	0.33	3.85	34
STA/50 wt.%ZrO_2/ SBA-15	188	0.32	65.6	0.20	1.50	15
STA/70 wt.%ZrO_2/ SBA-15	166	0.24	65.3	0.10	0.77	8
Effect of calcination temperature (K) on 15 wt.%STA/22.4 wt.%ZrO_2/SBA-15						
873	484	0.67	69.8	-	nil	0
923	472	0.64	67.0	0.25	1.39	14
1023	412	0.62	66.7	0.31	3.44	31
1173	325	0.48	64.9	0.34	4.23	28
1223	250	0.43	64.4	0.30	3.04	12
1273	210	0.32	63.7	0.12	1.18	12

Entries from 1-6 were with 22.4 wt.%ZrO_2 , 7-10 were with 15 wt.% STA and all these catalysts were calcined at 1123 K.

Reaction conditions: IAA = 1.27 g (0.014 mole), AA = 1.73 g (0.028 mole), catalyst = 0.15 g, Temp. = 373 K, Time = 3 h.

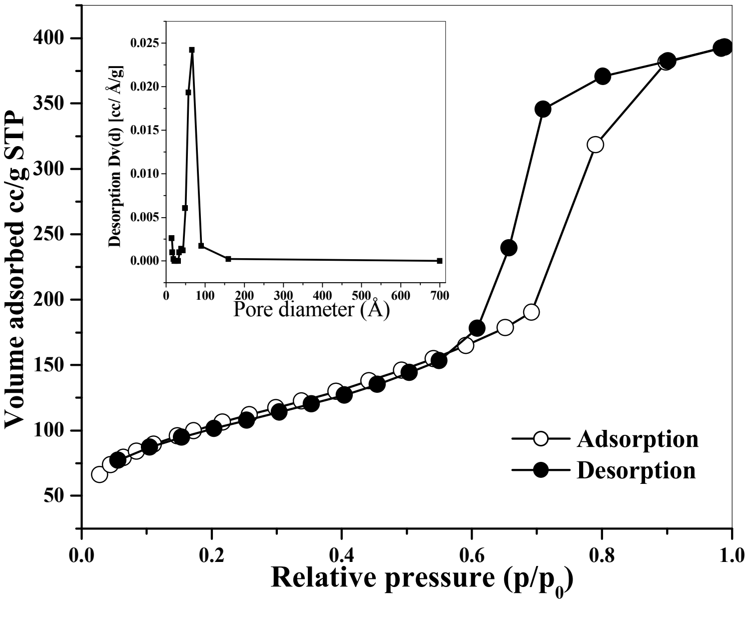

Fig. 6.5: *(a) Nitrogen adsorption isotherms with (b) inset figure of (pore size distribution) of 15 wt.%STA/22.4 wt.%ZrO_2/SBA-15 calcined at 1123 K.*

The adsorption isotherms and BJH pore size distributions of 15 wt.% STA/22.4 wt.% ZrO_2/SBA-15 are shown in Fig. 6.5, which are of type IV. Figure 6.5 shows that the mesostructure was retained after loading of 15 wt.% STA/22.4 wt.%ZrO_2 into SBA-15 and up to a calcination temperature of 1123 K. Though the surface areas of modified MCM-41 and MCM-48 were greater than those of the corresponding modified SBA-15 samples, their catalytic activities were lower compared to 15 wt.% STA/22.4 wt.% ZrO_2/SBA-15 (Table 6.2). This was attributed to blocking of the mesoporous channels of MCM-41 and MCM-48 due to narrow pore diameters. The observation are similar as per described earlier in Chapter 5, section 5.2.3, page no. 101.

Table 6.2: Esterification of IAA with AA: A comparison between different catalysts

Sample	S.A. (m^2g^{-1})	P.V. (cm^3g^{-1})	P.D. (Å)	Total Acidity ($mmolg^{-1}$)	B(L)	B/L	IAA ,%Conv. (TOF) x 10^{-1} (s^{-1})*	Rate Constant x 10^{-5}(s^{-1})	IAA Conv., (%)
SBA-15	929	1.36	73.3	-	-	-	-	-	-
MCM-41	1155	0.88	30.5	-	-	-	-	-	-
MCM-48	1096	0.71	26.1	-	-	-	-	-	-
22.4 wt.% ZrO_2/SBA-15	426	0.69	71.3	0.30	0.055(0.059)	0.92	-	2.54	24
22.4 wt.%ZrO_2/MCM-41	589	0.38	27.7	0.24	0.039(0.163)	0.24	-	0.88	9.1
22.4 wt.%ZrO_2/MCM-48	612	0.62	24.8	0.10	0.021(0.21)	0.10	-	0.53	5.6
15 wt.%STA/ZrO_2/SBA-15	372	0.61	65.3	0.40	0.099(0.070)	1.42	0.95	6.42	50
15 wt.%STA/ZrO_2/MCM-41	510	0.27	18.5	0.31	0.049(0.245)	0.20	0.34	1.84	18
15 wt.%STA/ZrO_2/MCM-48	541	0.21	16.9	0.22	0.049	0.16	0.21	1.08	11
3.36 wt.%STA/SBA-15	340	0.59	69.9	0.27	0.030	0.85	0.36	1.95	19
15 wt.%STA/ZrO_2 (Neat)	3	-	-	0.02	0.020	1.00	0.03	0.57	6

All catalysts were calcined at 1123 K except entry No 1,2,3.

**TOF is calculated by considering three protons per Keggin unit (mol. $mol^{-1}H^{+}.s^{-1}$)*

Entry 1. Crystal size/nm (by TEM) = 7.1; Entry 4. ZrO_2 phase (tetragonal) Crystal size /nm (by TEM) = 5.5-6.5 and (by XRD) = 6.1 Entry 7. ZrO_2 phase (tetragonal) Crystal size /nm (by TEM) = 4-5 and (by XRD) = 4.6

Reaction conditions: IAA = 1.27 g (0.014 mole), AA =1.73 g (0.028 mole), catalyst = 0.15 g, Temp. = 373 K, Time = 3 h.

6.2.4. SEM

The micromorphology of the supported catalyst i.e. 15 wt.%STA/22.4 wt.%ZrO_2 /SBA-15 calcined at 1123 K [Fig. 6.6] remained the same, which was wheat-like even after modification of SBA-15 [1].

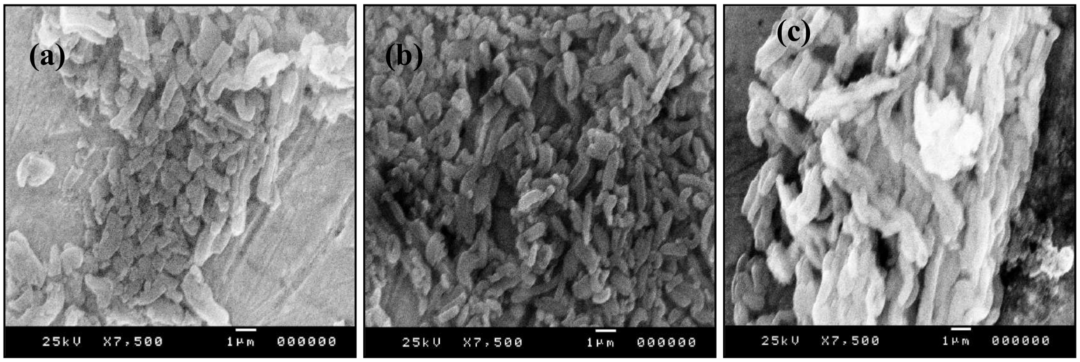

Fig. 6.6: *Scanning electron micrograph of a) SBA-15 calcined at 813 K, b) SBA-15 calcined at 1123 K and c) 15 wt.%STA/22.4 wt.%ZrO_2/SBA-15 calcined at 1123 K.*

6.2.5. TEM

TEM measurements were carried out to study the morphology of the parent SBA-15 and STA/22.4 wt.% ZrO_2 modified SBA-15 samples. TEM images of 15 wt.% STA/22.4 wt.% ZrO_2/SBA-15 show the retention of the periodic structure of SBA-15 precursor even after calcining at 1123 K.

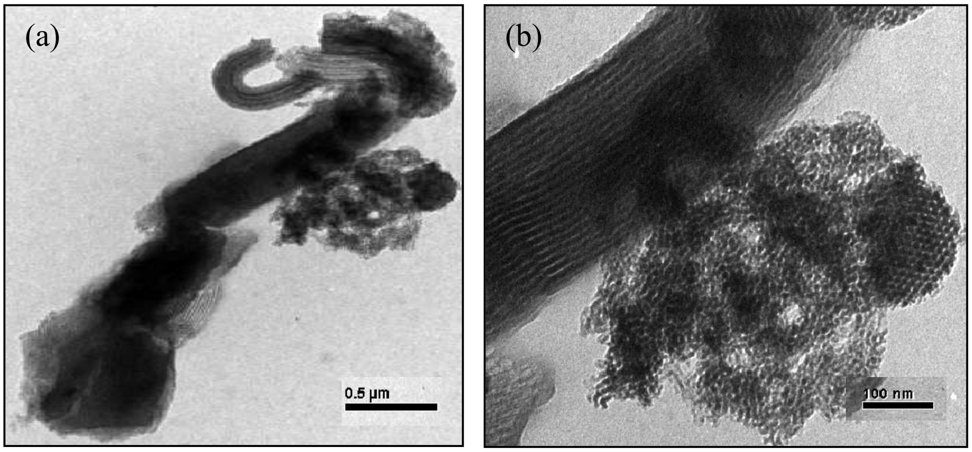

Fig. 6.7: *TEM image of 15 wt.%STA/22.4 wt.%ZrO_2/SBA-15 calcined at 1123 K, with the beam perpendicular to the pore direction and with the beam parallel to the pore direction at different magnification (a) 0.5 µm and (b) 100 nm.*

TEM images of 15 wt.% TPA/22.4 wt.% ZrO_2/SBA-15 [Figs. 6.7 (a, b)] confirm that the hexagonally arranged mesopores of SBA-15 were retained and STA/ZrO_2 mainly dispersed inside the pores. Fig. 6.7 clearly shows the uniform dispersion of TPA/ZrO_2 inside the SBA-15 channels. As per given in literature [2] it shows the periodic structure of SBA-15 precursor in different beam directions with pore size of 7.1 nm. After supporting SBA-15 with 15 wt.% STA/22.4 wt.% ZrO_2, small particles of STA/ZrO_2 formed inside nanochannels of SBA-15 (Figs. 6.7 (a) and (b)). The 22.4 wt% ZrO_2 (5.5–6.5 nm), an optimum loading, was inserted into SBA-15 by the wet impregnation method, which has a higher capacity for monolayer coverage of STA. The crystallite size of the material calculated from TEM shows that for moderate loading (15 wt.%) of STA, nanosized (4–5 nm) material was formed after wet impregnation over 22.4 wt.% ZrO_2/SBA-15 calcined at 1123 K.

6.2.6. FT-IR spectroscopy

FT-IR spectra of bulk STA shows bands at 1020, 982, 926, 882, 778, and 541 cm^{-1} [Fig. 6.8 (a), (b) and 5.13], which are the same as those reported for the acid $H_4SiW_{12}O_{40}$ [3]. The first band is not assigned, while the others correspond to the stretching vibrations $W–O_d$, $Si–O_a$, $W–O_b–W$, and $W–O_c–W$ and to the bending vibrations $O_a–Si–O_a$ and W–O–W, respectively. The subscripts indicate oxygen bridging the W and the heteroatom (a), corner-sharing oxygen (b), and edge-sharing oxygen (c) belonging to octahedra WO_6 and terminal oxygen (d). According to Kozhevnikov [4], the decomposition temperature of STA was 698 K. Pure silica exhibited IR bands at 1100 and 806 cm^{-1} and a weak shoulder band at 974 cm^{-1} related to surface OH groups.

The spectra of ZrO_2 exhibited a wide band at 400–700 cm^{-1} extending up to 1150 cm^{-1} [5]. The spectra of different (%) loading of STA over ZrO_2/SBA-15 are shown in Fig. 6.8 (a) while for different calcinations temperature and different ZrO2 loading (%) are shown in Fig. 6.8 (b) and 6.9, respectively. For the STA/ZrO_2/SBA-15 samples, two bands of STA appeared around 982 and 882 cm^{-1}, with the bands around 1079 and 810 cm^{-1} overlapping with the strong bands of SiO_2. The sample with the highest STA loading (90 wt.%) showed characteristic bands of STA but excluding a band at 983 cm^{-1} ($W=O_t$) due to decomposition of STA intoWO_3 crystallites. Low STA loading samples showed bands with lower intensity than bulk TPA spectra, due to masking of bands by wide bands of support.

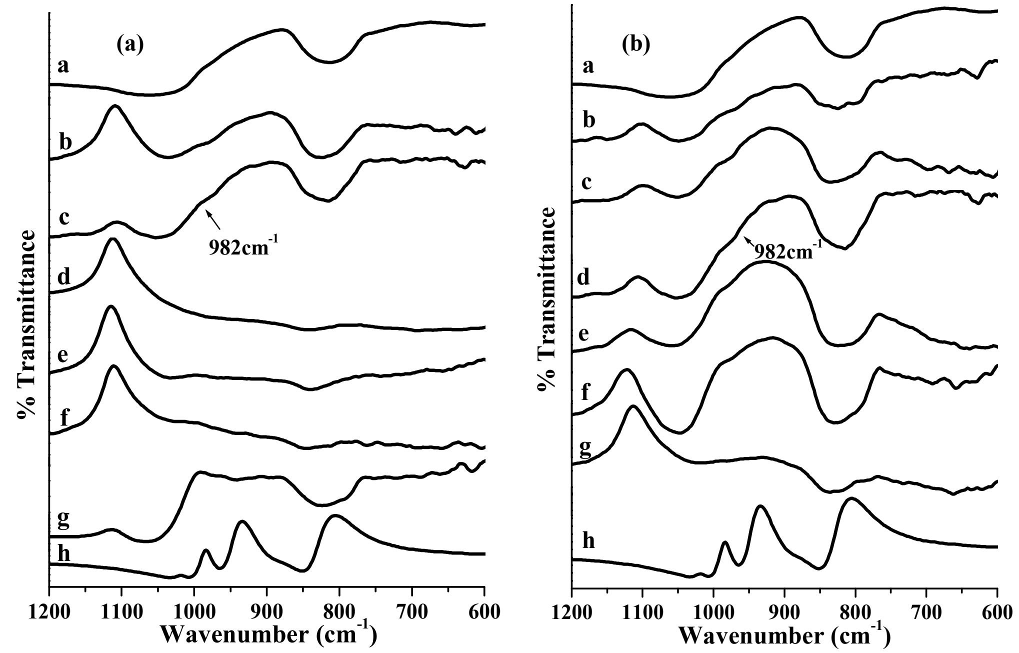

Fig. 6.8: *(a) FT-IR spectra: a) pure silica, STA/22.4 wt.%ZrO$_2$/SBA-15 with b) 5, c) 15,d) 30, e) 50, f) 70, g) 90 wt.%STA loading calcined at 1123 K and h) pure STA. (b) FT-IR spectra: a) pure silica, 15 wt.%STA/22.4 wt.%ZrO$_2$/SBA-15 calcined at b) 773, c) 923, d) 1023, e) 1123, f) 1173, g) 1223, h) 1273 K and i) pure STA.*

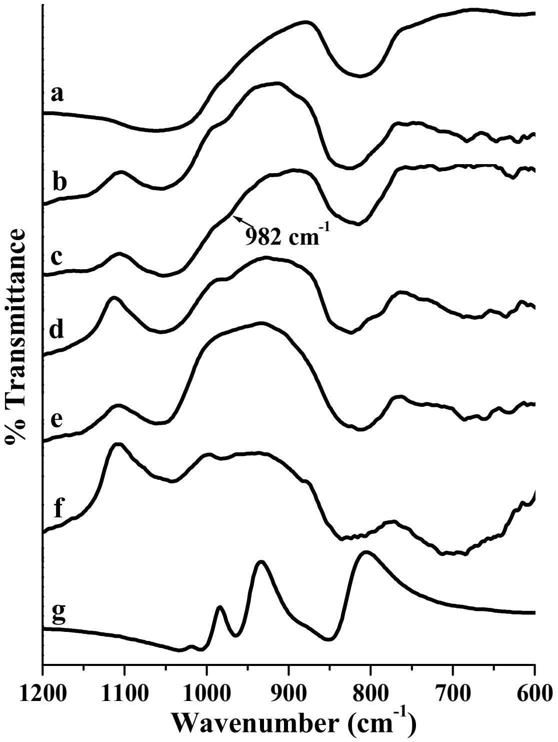

Fig. 6.9: *FT-IR spectra: a) pure silica, 15 wt.%STA/ wt.%ZrO$_2$/SBA-15 with b) 10, c) 22.4,d) 30, e) 50, f) 70 wt.%ZrO$_2$ loading calcined at 1123 K.*

6.2.7. UV-Vis. spectroscopy

The UV–Vis. spectra of parent STA for $[SiW_{12}O_{40}]^{4-}$ showed a band at 264-265 nm [6, 7], which corresponds to the characteristic oxygen to metal charge transfer band. Also, $ZrOCl_2 \cdot 8H_2O$ salt shows a band at 275 nm in accordance with previous reports [5, 8]. However, the 22.4 wt% ZrO_2/SBA-15 showed a band at 275.67 nm, which falls in the nanoparticle region of ZrO_2 as reported previously [5, 9]. While, the UV-Visible spectra of 15 wt.%STA/22.4 wt.%ZrO_2 modified different silica supports like MCM-41, MCM-48 and SBA-15 shows absorption bands in the range of 262-264 nm as shown in Fig. 6.10.

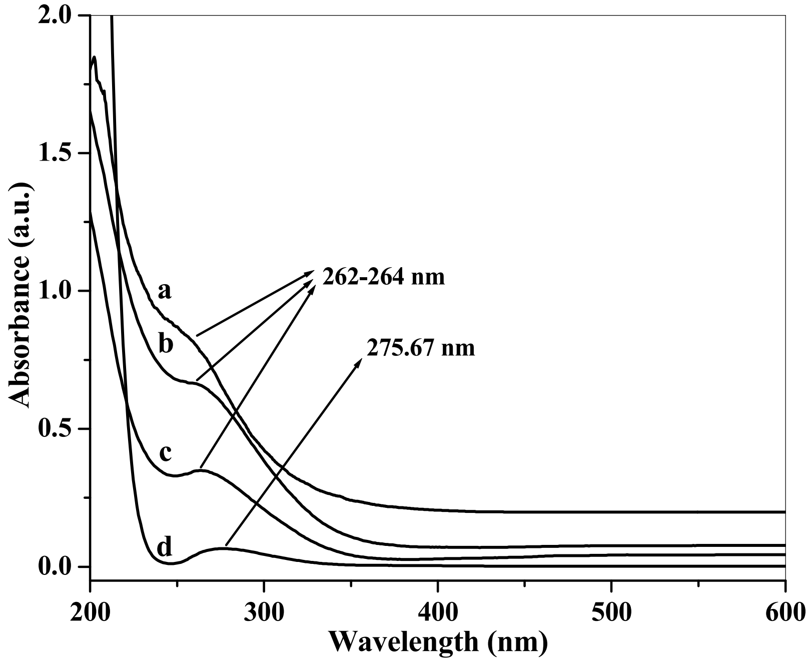

Fig. 6.10: *UV-Vis. spectra of a) 15 wt.%STA/22.4 wt.%ZrO_2/SBA-15, b) 15 wt.%STA/22.4 wt.%ZrO_2/MCM-41, c) 15 wt.%STA/22.4 wt.%ZrO_2/MCM-48 and d) 22.4 wt.%ZrO_2/SBA-15 calcined at 1123 K.*

6.2.8. NMR spectroscopy

^{29}Si MAS NMR spectrum of SBA-15 shows the peaks at -100 ppm and -110 ppm due to $SiO_3(OH)$ and SiO_4 components, respectively [1]. While ^{29}Si MAS NMR spectra of modified SBA-15 with 15 wt.%STA/22.4 wt.%ZrO_2 is shown in Fig. 6.11 (a). The broadness of the ^{29}Si signals has been attributed to the large distribution of the T–O–T angle [10]. The broad high field resonance at -110 ppm are due to the Si $(OSi)_4$ environment (Q^4). While other resonance at –100 ppm corresponding to $SiOH(OSi)_3$ environment (Q^3) species respectively. The Q^3 sites probably result from two structure units including Si $(OSi)_3(OH)$ and Si $(OSi)_3(OAl)$, and the Q_2 sites stem from either Si $(OSi)_2(OH)_2$ or Si $(OSi)_2(OAl)(OH)$ [11].

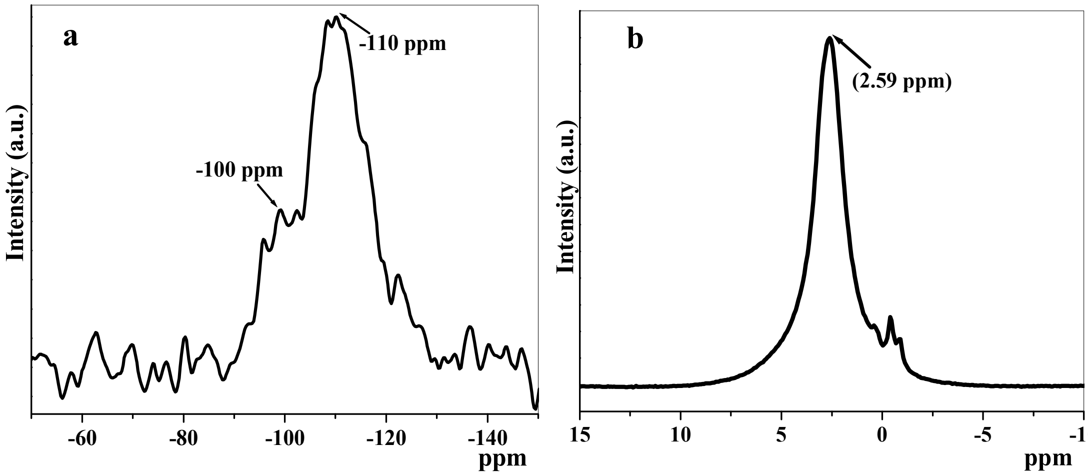

Fig. 6.11: *(a) ^{29}Si MAS NMR spectra and (b) ^{1}H MAS NMR spectra of 15 wt.%STA/22.4 wt.%ZrO_2/SBA-15 calcined at 1123 K.*

In case of neat STA, the anhydrous polyacid is obtained after treatment at room temperature, as evidenced by the ^{1}H signal at ca. 9 ppm, which can be attributed to strong acid sites. The signal of the protons remains until 673 K and disappears only at 773 K. This shows that this polyanion is stable in its protonated form at a higher temperature compared to TPA [12]. For 15 wt.%STA/22.4 wt.%ZrO_2/SBA-15 calcined at 1123 K catalysts, the behavior is very different. The spectra shows clearly the broad resonance around 2.6 ppm corresponding to hydrogen bonded silanol groups may be of silica support [Fig. 6.11 (b)]. Due to low loading of STA w.r.t. silica support, peak at 8-9 ppm corresponding to acidic protons of STA are not seen.

6.2.9. FT-RS

Pure STA shows a sharp band at 998 cm^{-1} with a distinct shoulder at 974 cm^{-1} which are assigned to ν (W=O) symmetric and asymmetric stretching modes, respectively. FT-RS of 22.4wt.%ZrO_2/SBA-15 sample with and without STA calcined at 1123 K are presented in Fig. 6.12. Another broad band at 893 cm^{-1} is attributed to the ν (W-O-W) asymmetric stretching mode [13-15]. The positions in the spectrum of pure STA characteristic for $H_4SiW_{12}O_{40}.xH_2O$ are 1019(w), 981(s), 927(vs), 880(m), 785(vs), 555(sh), 542(m), 476(w). The bands assigned to STA are clearly seen in Fig. 6.12 for 15 wt.%STA/22.4 wt.%ZrO_2/SBA-15 sample. The broadning and minor shifts in the bands could be due to the formation of the species formed by linking the Keggin units to the ZrO_2 support. The raman bands of ZrO_2 below 700 cm^{-1} interfere with the tungstate species, while above 700 cm^{-1} is free from characteristic bands of ZrO_2.

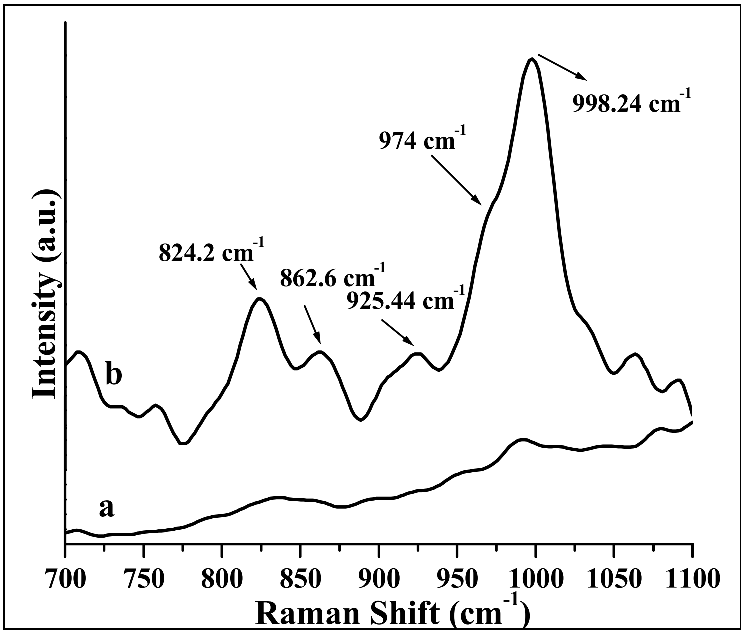

Fig. 6.12: *FT-Raman of a) 22.4 wt.%ZrO_2/SBA-15 and b) 15 wt.%STA/22.4 wt.%ZrO_2/SBA-15 calcined at 1123 K.*

6.2.10. XPS

The results of XPS analyses for 22.4 wt.%ZrO_2/SBA-15 are shown without and with STA calcined at 1123 K in Fig. 6.13. The binding energies and FWHM values of various core levels (Si 2p, O 1s, Zr $3d_{5/2}$, W $4f_{7/2}$) of the catalysts materials are summarized in Table 6.3.

Table 6.3: XPS binding energies (eV) and FWHM (eV) values of the catalysts

Sample	O 1s		Zr $3d_{5/2}$		Si 2p		W $4f_{7/2}$	
	BE	FWHM	BE	FWHM	BE	FWHM	BE	FWHM
22.4wt.%ZrO_2/SBA-15	531.8	3.22	183.8	4.8	102.7	3.4	-	-
15wt.%STA/ 22.4wt.%ZrO_2/SBA-15	531.8	3.53	183.8	4.5	102.9	3.8	35.6	3.4

The W (4f) spectra of 15 wt.%STA/22.4 wt.%ZrO_2/SBA-15 shows the spin-orbit split doublet of tungsten, W $4f_{7/2}$ and W $4f_{5/2}$ with full width at half maximum is obtained at 3.4 eV and are located at 35.6 and 37.9 eV, respectively. The observed B.E value of W ($4f_{7/2}$) is 35.6 eV, a characteristic of W^{6+} indicating that it contains W-O bonding [16]. This strongly suggests that there is only one covalent state of tungsten atoms in 22.4 wt.% ZrO_2/SBA-15 doped with silicic HPAs. The observed B.E. value is in accordance with the literature data 35.6 eV for Rh_2WO_6 [17], 35.40 eV for $NiWO_4$ [18] and 35.30 eV for H_2WO_4 [19]. Undoubtedly, there is always W^{6+} indicating that W-O bonding [16] is present in the catalysts samples. The other observations regarding O (1s), Si (2p) and Zr (3d 5/2) are similar as per described earlier in Chapter 5, section 5.2.11., page no.113.

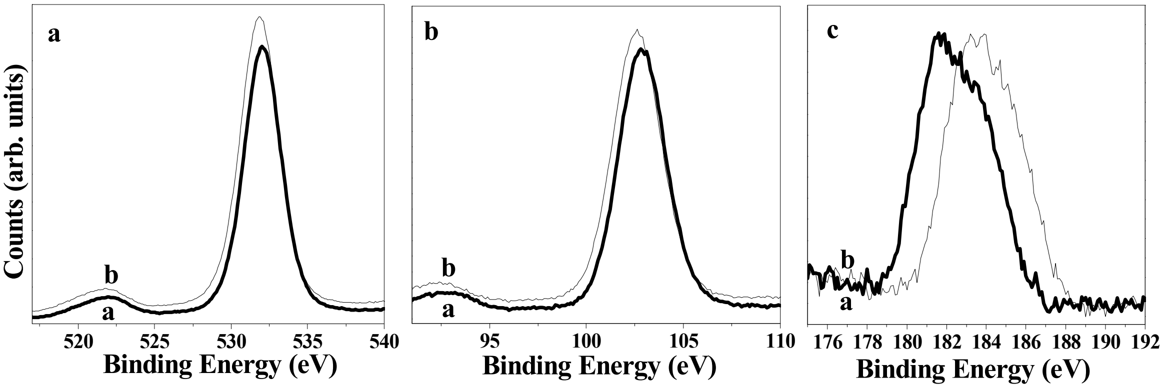

Fig. 6.13: *XPS spectra of: (a) O (1s) spectra of a) 22.4 wt.%ZrO_2/SBA-15 and b) 15 wt.%TPA/22.4 wt.%ZrO_2/SBA-15, (b) Si (2p) spectra of a) 22.4 wt.%ZrO_2/SBA-15 and b) 15 wt.%TPA/22.4 wt.%ZrO_2/SBA-15, (c) Zr ($3d_{5/2}$) spectra of a) 22.4 wt.%ZrO_2/SBA-15 and b) 15 wt.%TPA/22.4 wt.%ZrO_2/SBA-15 calcined at 1123 K.*

6.2.11. TG-DTA

TGA and DTA spectra of all the samples dried at 120°C are shown in Fig. 6.14. Under similar measurement conditions, TG-DTG analysis of pure STA hydrate showed three stages of weight loss (endothermic effect). The first weight loss, around 3–6%, occurred from room temperature to 125°C, due to the loss of physisorbed water. The second one, from 130–305°C, accounted for the loss of crystallization water, and the third, in the range of 370–550°C, was due to the loss of 1.5 H_2O molecules originating from all acidic protons. The total weight loss of the sample corresponded to 21 H_2O per Keggin unit [20]. Furthermore, it showed a break at 350°C, due to the decomposition of HPA. The DTA shows an exothermic peak at 607 °C due to the complete decomposition of the Keggin structure to form a mixture of oxides followed by its crystallization. The DTA of pure STA and zirconium oxyhydroxide (not shown) showed exothermic peaks at 548 and

452°C, due to the decomposition of STA to its constituent oxides [21] and the crystallization of zirconium oxyhydroxide to ZrO_2.

The TGA behavior was similar in all of the STA/ZrO_2-supported samples, showing the first weight loss of about 3 wt.% in all STA/ZrO_2 supported over SBA-15 samples, corresponding to physisorbed water. But none of the supported samples showed an appreciable change in weight loss until 900°C, indicating increasing stability of STA. The neat 15 wt.% STA/ZrO_2 sample exhibited weight loss corresponding to physisorbed water along with another weight loss around 450–600°C that may be due to a phase transition from tetragonal to monoclinic. The TGA behavior of all of the STA/ZrO_2/SBA-15 samples were almost similar, but differed in DTA behavior from 15 wt.%STA/ZrO_2 [Fig. 6.14 (d)]. The DTA of the 15 wt.%STA/ZrO_2 sample shows a broad exothermic peak from 273 to 360°C with a peak maximum at 305°C, assigned to the formation of Zr–O–W bonds between STA's terminal W=O oxygen atoms and surface $\equiv Zr^+$ species or to the formation of water by the reaction of STA protons with ≡ZrOH hydroxyl groups [5,22,23]. While other samples were showing similar DTA behavior, when SBA-15 was used as an additional support.

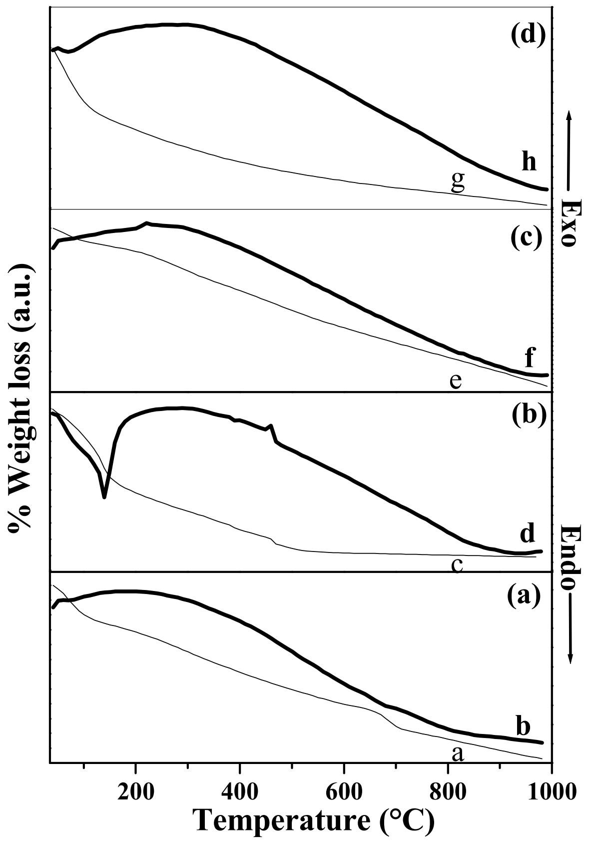

Fig. 6.14: *TGA curves of the catalysts a) 22.4 wt.%ZrO_2/SBA-15, c) 15 wt.%STA/ZrO_2, e) 15 wt.% STA/SBA-15, g) 15 wt.%STA/22.4 Wt.%ZrO_2/SBA-15 and DTA curves of the catalysts b) 22.4 wt.%ZrO_2/SBA-15 d) 15 wt.%STA/ZrO_2, f) 15 wt.% STA/SBA-15, h) 15 wt.%STA/22.4 Wt.%ZrO_2/SBA-15 (all dried at 120°C).*

6.2.12. TPD of NH_3

The NH_3-TPD profile for the catalyst 22.4 wt.%ZrO_2/SBA-15 without and with 15 wt.%STA, along with the deconvolution of catalyst with optimum STA loading i.e. 15 wt.%STA/22.4 wt.%ZrO_2/SBA-15 and an optimum calcination temperature i.e. 1123 K are shown in Fig. 6.15 (a) and 6.15 (b), respectively. The catalyst showed a broad TPD profile, revealing that the surface acid strength was widely distributed. The total acidity in terms of amounts of NH_3 in mmol g^{-1} for the catalysts with different STA loadings, different calcination temperatures and different ZrO_2 loadings are presented in Table 6.1. The comparison of the strength of different catalysts in terms of the total acidity were presented in Table 6.2 and 6.4. All the observations regarding TPA loading, calcination temperature and ZrO_2 loading were similar as per discussed in Chapter 5, section no. 5.2.13., page no. 116.

The highest acidity corresponds to a monolayer coverage of STA (15wt.% STA/22.4 wt% ZrO_2/SBA-15 calcined at 1123 K), where the Keggin-like structure is intact, as supported by FT-IR, FT-RS, XRD, XPS and UV-Vis. spectroscopic techniques. According to area under the peak, the loading of STA over 22.4 wt.% ZrO_2/SBA-15 [Fig. 6.15 (a)] shows more acid sites as compared with 22.4 wt.% ZrO_2/SBA-15 catalyst. The desorption peaks were deconvoluted using Gaussian function with temperature as variant [24]. The first peak, around 440-450 K, referred to as (type i), which is attributed to weak (structural) Lewis acid sites. The other observations regarding Brønsted and Lewis acidity were similar to as explained earlier in Chapter 4, section 4.2.9., page no.85 and Chapter no. 5, section 5.3.2.1., page no. 120.

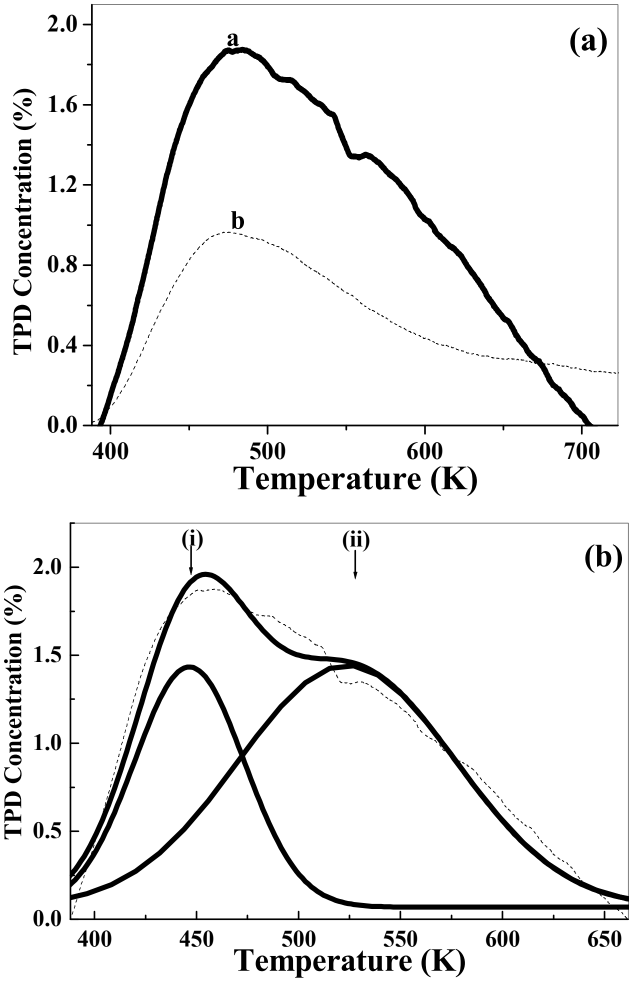

Fig. 6.15: *NH_3-TPD profiles of (a) 22.4 wt.%ZrO_2/SBA-15 a) with 15 wt.% STA and b) without STA and (b) Deconvolution of curve of 15 wt.%STA/22.4 wt.%ZrO_2/SBA-15, all calcined at 1123 K.*

6.2.13. FT-IR Pyridine adsorption

The B/L ratio was calculated from the IR absorbance intensities [25] by FT-IR pyridine adsorption spectra of catalysts with different STA loadings calcined at 1123 K, 15 wt.%STA/22.4 wt.%ZrO_2/SBA-15 catalysts calcined at different temperatures and 15 wt.%STA/ wt.%ZrO_2/SBA-15 with different wt.% of ZrO_2 are shown in Fig. 6.16 (a), (b) and (c), respectively. The corresponding B/L ratios for different catalysts were compared with catalytic activity in IAA esterification with AA; the results are given in Table 6.2.

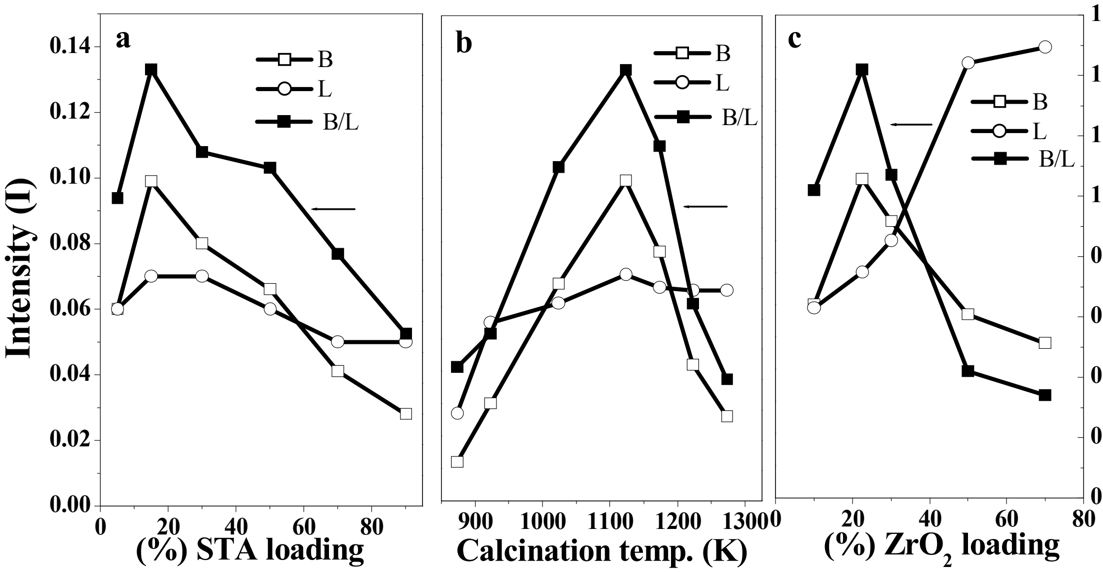

Fig. 6.16: *(a) Effect of STA loading on B acidity, L acidity and B/L ratio of wt.% STA/22.4 wt.%ZrO_2/SBA-15 catalysts calcined at 1123 K, (b) Effect of calcination temperature on B acidity, L acidity and B/L ratio of 15 wt.%STA/22.4 wt.%ZrO_2/SBA-15, (c) Effect of ZrO_2 loading on B acidity, L acidity and B/L ratio of 15 wt.%STA/ wt.%ZrO_2/SBA-15 catalysts calcined at 1123 K. (Reaction conditions: Temperature = 373 K, AA/IAA (molar ratio) = 2, Catalyst weight = 0.15 g (5 wt.% of total reaction mixture) and Time = 3h).*

It was found that the B/L ratio increased with increased STA loading up to 15 wt.%, but then decreased with further increases in STA loading [Fig. 6.16 (a)]. At low loading, the catalyst showed mainly Lewis acidity; with an increase in loading Lewis acidity decreased, whereas Brønsted acidity increased and reached a maximum at 15 wt.% STA loading. An increase in STA loading above 15 wt.% decreased the Brønsted acidity. The decrease in acidity above 15 wt.% could be due to the formation of crystalline WO_3, which prevents the accessibility of pyridine to the active sites. At low calcination temperature (823 K), the catalyst 15 wt.%STA/22.4 wt.%ZrO_2/SBA-15 showed mainly

Lewis acidity with very low Brønsted acidity that increases with calcination temperature up to 1123 K [Fig. 6.16 (b)]. Also, in case of (%) ZrO_2 loading, with increase in ZrO_2 (%) loading Lewis acidity increased, while Brønsted acidity decreased [Fig. 6.16 (c)]. But at 22.4 wt.%ZrO_2 loading (at monolayer coverage), it shows highest Brønsted acidity. It has been reported that pure STA shows mainly Brønsted type acidity. The support zirconium oxyhydroxide is shown to be amphoteric in character. The interaction of zirconium oxyhydroxide with HPA neutralizes the Brønsted acid sites of HPA and from $(Zr(OH_2)_n{}^{+})(H_{3-n}W_{12}O_{40})$ like species [22]. The higher Lewis acidity at lower calcination temperature shows that the Lewis acidity mainly originates from the support itself. At higher calcination temperature, dehydration/ dehydroxylation occurs and the interaction of HPA with the support increases and STA anchored to ZrO_2 through Zr-O-W bond, and during this process, new Brønsted acid sites are generated. Formation of such Brønsted acid sites are also observed in ZrO_2-supported isopolytungstate catalysts. The other observations are similar to as per described in an earlier Chapter 4, section 4.2.9, page no. 85 and Chapter 5, section 5.3.2.1, page no. 120.

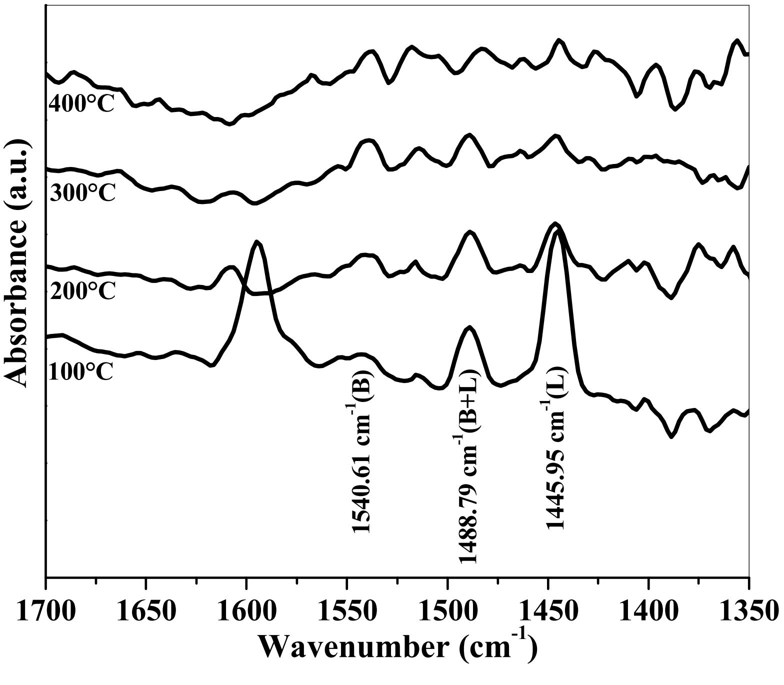

Fig. 6.17: *FT-IR pyridine adsorption spectra of 15 wt.%STA/22.4 wt.%ZrO_2/SBA-15 calcined at 1123 K.*

6.3. ESTERIFICATION OF ALCOHOLS WITH CARBOXYLIC ACIDS

6.3.1. Introduction

A wide category of organic compounds ranging from aliphatic to aromatic esters, are generally used as plasticizers, solvents, perfumery, flavor chemicals, and also as precursors for a gamut of pharmaceuticals, agrochemicals and other fine chemicals [26]. The major product of esterification of an IAA with AA i.e. isoamyl esters (especially isoamyl acetate) are flavour esters of commercial importance in the food industry (74,000 kg/year) because of their strong banana flavour [27, 28]. Esterification of alcohols by carboxylic acids is one of the most important reactions in organic synthesis [29]. The esterification of IAA and AA in gaseous phase was studied using TPA supported on different carriers, silica materials, carbon and alumina [30]. Also, Mesoporous silica Al-MCM-41 also used for the esterification of an IAA with an AA under vapour phase reaction conditions [31]. Also, kinetic study of immobilized lipase catalyzing the synthesis of isoamyl acetate by transesterification in n-hexane solvent [32]. Esterification reactions have been extensively studied in the presence of Keggin and Well-Dawson HPAs as homogeneous catalysts. [33-35]. HPA is more active and selective catalyst than H_2SO_4 and TsOH for the homogeneous alcoholysis of epoxides under mild conditions [34]. Maksimov and Kozhevnikov [36] showed that in the homogeneous reaction, Keggin acids such as $H_3 [PW_{12}O_{40}]$ and $H_4 [SiW_{12}O_{40}]$ are 2-4 times more active than the conventional catalysts per unit proton site. Active carbon strongly adsorbs a certain amount of HPA and carbon-supported acid catalysts thus obtained catalyze, liquid-phase esterification and related reactions in polar media [34]. Izumi et al. [37] showed that the insoluble salt $Cs_{2.5}H_{0.5}[PW_{12}O_{40}]$ is an active solid-acid catalyst for esterification and hydrolysis. Bulk and supported HPAs are active catalysts for the esterification of AA with ethanol [34]. In order to perform a new contribution to the field of ecofriendly acid-catalyzed reactions, the present work deals with the esterification of IAA with AA using ZrO_2 supported STA in mesoporous silica.

6.3.2. Results and discussion

The liquid phase esterification of IAA with AA was carried out using 15 wt.%STA/22.4wt.%ZrO_2/SBA-15 calcined at 1123 K. Scheme 6.1 (A) and (B) shows the schematic representation of the esterification of an IAA with AA. Scheme 6.1 (A) shows the general mechanism for an esterification reaction while the proposed mechanism is shown in (B). In the first step, AA accepts a proton from the strong acid and in the second step, the IAA molecule attacks the protonated carbonyl group to give a tetrahedral intermediate. In the next step, a proton is lost at one oxygen atom and gained at another to form another intermediate, which further loses a molecule of water that gives a protonated ester. In the final step, a proton is transferred to a water molecule (acts as a base) to give the ester, isoamyl acetate. All these steps are reversible.

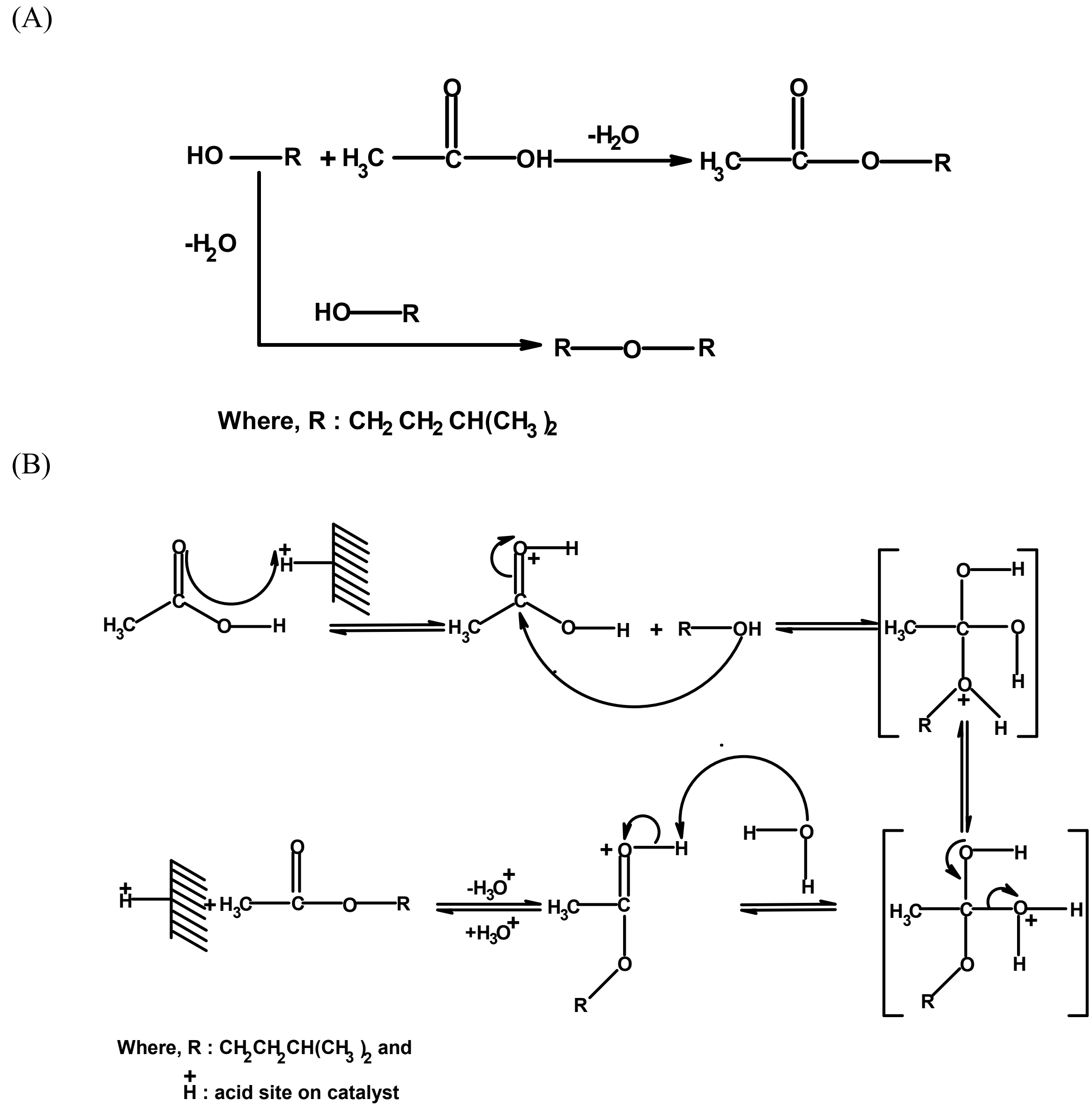

Scheme 6.1: *Esterification of IAA with AA.*

6.3.2.1. Comparison of catalytic activities of different catalysts

Data on the catalytic performance of various catalysts (%) STA-loaded, (%) ZrO_2-loaded catalysts calcined at 1123 K, along with and the reaction conditions of esterification of an IAA with AA and the data on the catalytic activity of 15 wt.% STA/22.4 wt.% ZrO_2/SBA-15 calcined at different temperatures are presented in Table 6.1. Esterification of IAA with 15 wt.% STA/22.4 wt.% ZrO_2/SBA-15 calcined at 1123 K catalyst under selected reaction conditions (373 K, 3h, 150 mg catalyst, AA/IAA molar ratio 2:1) gave

100 % isoamyl acetate as the only product at 50% IAA conversion. Turn over frequencies (mol. mol$^{-1}{}_{H}{}^{+}$.s^{-1}) (by considering three protons per Keggin unit) and rate constants (s^{-1}, by considering esterification of IAA as a pseudo-first order reaction) for 15 wt.% STA/22.4 wt.% ZrO_2/SBA-15 calcined at 1123 K evaluated are 0.0095 (mol. mol^{-1}H^{+}.s^{-1}) and 6.42 x 10^{-5} s^{-1}, respectively (Table 6.2).

It is seen from the results that 15 wt.%STA/ZrO_2 calcined at 1123 K gave the lowest conversion which is at least 8 times less as compared to 15 wt.%STA/22.4wt.%ZrO_2/SBA-15 calcined at 1123 K. under the same reaction conditions. The enhancement in activity of 15 wt.%STA/22.4wt.%ZrO_2/SBA-15 calcined at 1123 K is attributed due to more accessible protons resulting when 15 wt.%STA/ZrO_2 is supported on large surface area and bigger pore diameter like SBA-15 mesoporous silica material. It is also observed that 3.36 wt.% STA/SBA-15 and 22.4 wt.%ZrO_2/SBA-15 calcined at 1123 K shows very less catalytic activities in the reaction, since these have no required acidity for acid catalyzed reactions. In the present catalyst system, ZrO_2 alone loaded on mesoporous silica support i.e. 22.4 wt.%ZrO_2/SBA-15 calcined at 1123 K shows some catalytic activity, while after loading 15 wt.%STA over it shows two-fold increase in catalytic activity (Table 6.2). So here is the specific role of the composite materials and the effect of ZrO_2 on the acidity function of STA, which enhances the catalytic activity. Therefore, we have chosen 15 wt.%STA/22.4 wt.%ZrO_2/SBA-15 calcined at 1123 K as the catalyst for further investigations on its catalytic performance in an esterification of an IAA with AA. We hypothesize that large-sized STA clusters (~12 Å) can readily clog the pores during solution impregnation when support pore sizes are smaller as in the case of MCM-41 (30.5 Å) and MCM-48 (26.1 Å), respectively. In contrast, STA/ZrO_2 is likely have a better chance to uniformly coat the pores when the support pore size is sufficiently large as in the case of SBA-15 (73.3 Å) as compared to MCM-41 and MCM-48. Hence, 15 wt.%STA/22.4 wt.%ZrO_2 modified SBA-15 shows highest catalytic activity as compared to 15 wt.%STA/22.4 wt.%ZrO_2 modified MCM-41 and MCM-48 catalysts calcined at 1123 K. However, when the ZrO_2 along with STA is dispersed in the mesoporous channels of supports at high temperature calcination, wherein the acidity of the catalysts is altered, which is higher with SBA-15.

Table 6.4. A catalyst comparison study in an esterification of IAA

Sample (Si/Al ratio)	Surface area (m^2g^{-1})	Total Acidity ($mmolg^{-1}$)	(%) Conv. IAA (TOF) x 10^{-1} (s^{-1})*	Rate constant x 10^{-5}(s^{-1})	IAA Conv., (%)
15 wt.%STA/ZrO_2/ SBA-15	372	0.40	0.95	6.42	50
H-ß (30)	540	0.94	0.04	6.61	51
H-Y (13.5)	530	2.25	0.017	5.20	43
H-Mordenite (20)	490	0.72	0.016	3.17	29
H-ZSM-5 (60)	364	0.82	0.036	3.57	22
TPA/MS	ne	ne	ne	3.17	29
TPA/MS-F	ne	ne	ne	3.85	34
Regeneration of catalyst					
Ist cycle	-	-	0.95	6.42	50
IInd cycle	-	-	0.95	6.42	50

**TOF is calculated by considering three protons per Keggin unit (mol. mol^{-1}H^{+}.s^{-1}) ne=not evaluated. (Reaction conditions: IAA=1.27g (0.014 mole), AA = 1.73 g (0.028 mole), Catalyst =0.15 g, Temp. = 373 K, Time = 3 h.*

The catalytic activities of different catalysts such as H-beta, H-Y, H-ZSM-5, H-Mordenite, TPA/MS, TPA/MS-F and 15 wt.% STA/22.4 wt.% ZrO_2/SBA-15 calcined at 1123 K tested in the esterification of an IAA with AA under identical reaction conditions are summarized in Table 6.4. Among the zeolite catalysts, H-beta is more active than others due to its strong and medium acid sites followed by H-Y (highest acidity with large pores). Similarly, poorest activity of H-ZSM-5 might be explained on the basis of its smaller pore size compared with the larger size of the products. While, H-Mordenites has one-dimensional pore with elliptical channels, 6.5 X 7.0 also has the low activity. TPA/MS-F shows higher catalytic activity as compared with TPA/MS catalyst and thereby shows higher rate constant. Therefore, we considered 15 wt.% STA/22.4 wt.% ZrO_2/SBA-15 calcined at 1123 K as the catalyst for further investigations on its catalytic performance in the esterification of an IAA with AA.

6.3.2.2. Effect of STA loading, ZrO_2 loading and calcination temperature

The 15 wt.% STA/22.4 wt.% ZrO_2/SBA-15 calcined at 1123 K gave the highest conversion of IAA (50 %) under selected reaction conditions (Table 6.1). The effect of (%) STA loading, calcination temperature and (%) ZrO_2 loading on IAA conversion obtained are presented in Table 6.1. Combining these findings with the result of FTIR pyridine adsorption data (Fig. 6.15) revealed that the B/L ratio of the catalysts increased up to 15 % STA loading and that 15 wt.% STA/22.4 wt.% ZrO_2/SBA-15 calcined at 1123 K had the highest B/L ratio and gave the highest catalytic activity in esterification of IAA under similar reaction conditions. Turnover frequency decreased with increase in (%) STA loading from 5 to 90 wt.% (Fig. 6.18 (a). The effect of calcination temperature on 15 wt.%STA/22.4 wt.%ZrO_2/SBA-15 catalyst in its performance in esterification of IAA by AA is shown in Fig. 6.18 (b). There is an increase in IAA conversion upto 1123 K calcination temperature but on further increase, IAA conversion decreased.

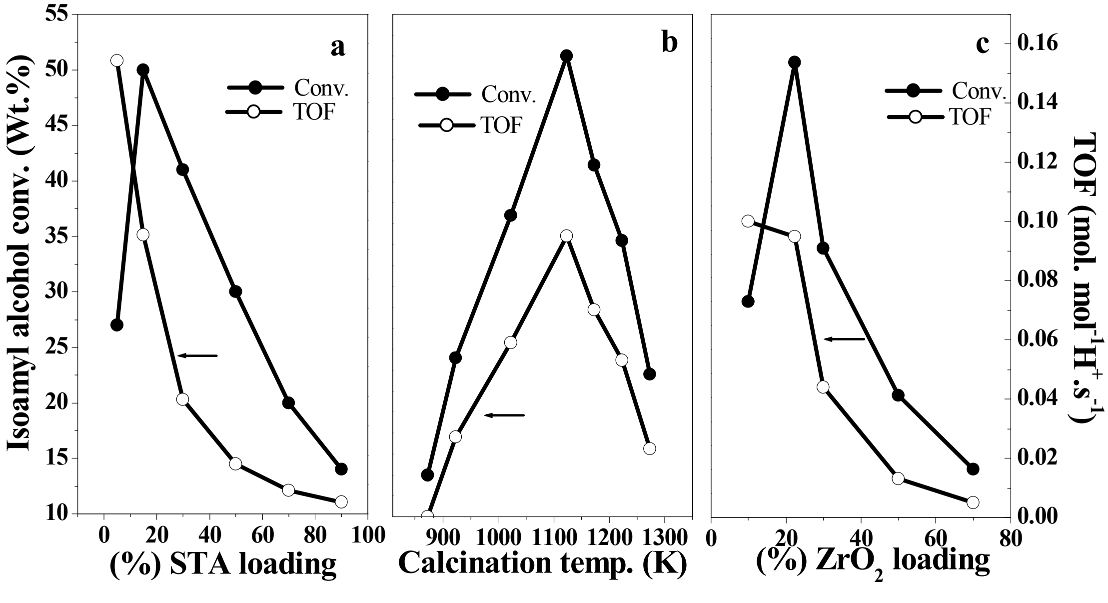

Fig. 6.18: *(a) Effect of STA loading on IAA conversion and TOF over wt.% STA/22.4 wt.%ZrO_2/SBA-15 catalysts calcined at 1123 K. (Reaction conditions: temperature = 373 K, AA/IAA (molar ratio) = 2, catalyst weight = 0.15 g (5 wt.% of total reaction mixture), time = 3h).*

(b) Effect of calcination temperature on IAA conversion and TOF over 15 wt.%STA/22.4 wt.%ZrO_2/SBA-15. (Reaction conditions: temperature = 373 K, AA/IAA (molar ratio) = 2, catalyst weight = 0.15 g (5 wt.% of total reaction mixture), time = 3h).

(c) Effect of ZrO_2 loading on IAA conversion and TOF over 15 wt.%STA/ wt.%ZrO_2/SBA-15 catalysts calcined at 1123 K. (Reaction conditions: temperature = 373 K, AA/IAA (molar ratio) = 2, catalyst weight = 0.15 g (5 wt.% of total reaction mixture), time = 3h).

This is because 15 wt.%STA/22.4 wt.%ZrO_2/SBA-15 calcined at 1123 K has the maximum concentration of acid sites, where STA forms a monolayer coverage over the support. In order to study the effect of ZrO_2 loading over SBA-15 with 15 wt.%STA catalyst calcined at 1123 K, IAA esterification with AA was conducted under selected reaction conditions. As shown in Fig. 6.18 (c), there is an increase in IAA conversion upto 22.4 wt.% ZrO_2 loading and on further increase in loading IAA conversion decreased.

6.3.2.3. Effect of reaction parameters

The effect of catalyst concentration on IAA conversion was studied by varying catalyst from 1 to 10 wt.% of the total weight of the reaction mixture and the results are shown in Fig. 6.19 (a). It shows that IAA conversion increases from 16.4 to 70.1 % with increase in catalyst concentration up to 10 wt.%, while the selectivity for isoamyl acetate was unchanged.

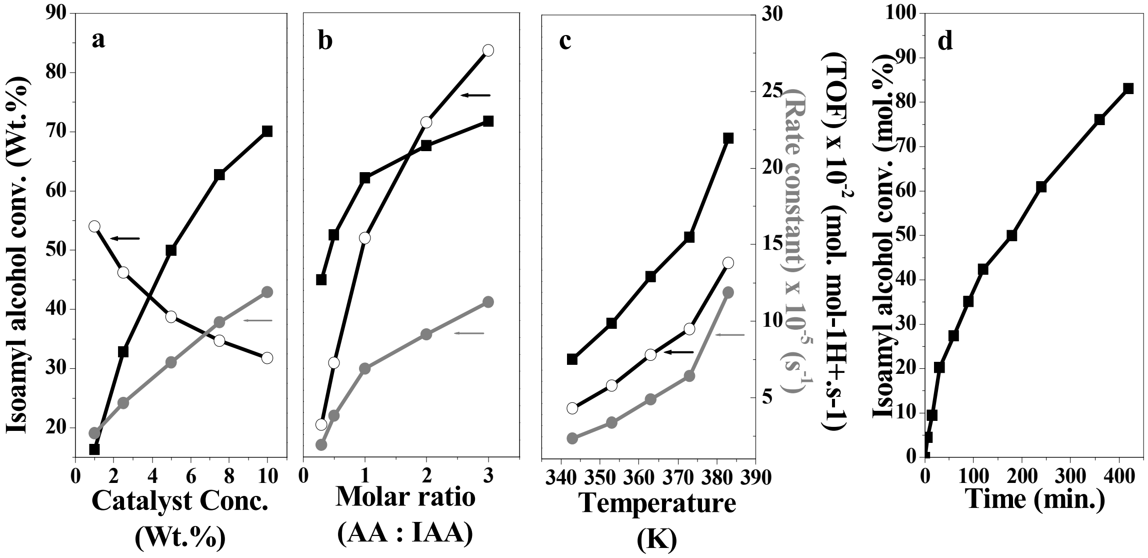

Fig. 6.19: *(a) Effect of Catalyst concentration on IAA conversion, TOF and Rate constant over 15 wt.%STA/22.4 wt.%ZrO_2/SBA-15 calcined at 1123 K. (Reaction conditions: temperature = 373 K, AA/IAA (molar ratio) = 2, time = 3h).*

(b) Effect of molar ratio on IAA conversion, TOF and Rate constant over 15 wt.%STA/22.4 wt.%ZrO_2/SBA-15 calcined at 1123 K. (Reaction conditions: temperature = 373 K, catalyst weight = 0.15 g (5 wt.% of total reaction mixture), time = 3h).

(c) Effect of temperature on IAA conversion, TOF and Rate constant over15 wt.%STA/22.4 wt.%ZrO_2/SBA-15 calcined at 1123 K. (Reaction conditions: AA/IAA (molar ratio) = 2, catalyst weight = 0.15 g (5 wt.% of total reaction mixture), time = 3h).

(d) Time on stream study over 15 wt.%STA/22.4 wt.%ZrO_2/SBA-15 catalyst system calcined at 1123 K. (Reaction conditions: AA/IAA (molar ratio) = 2, catalyst weight = 0.15 g (5 wt.% of total reaction mixture), time = 3h).

The higher the catalyst loading, the faster the rate at which reaction equilibrium was reached because of the increase in the total number of available active catalytic sites for the reaction.

The molar ratio of AA to IAA was varied from 3:1 to 2:1 to1: 1 to 1:2 to 1:3 at a temperature of 373 K and 5% (w/w) catalyst loading. The results are shown in Fig. 6.19 (b). Esterification of IAA with AA is an equilibrium-limited chemical reaction and because the position of equilibrium controls the amount of ester formed, the use of an excess of AA increases the conversion of IAA. The equilibrium conversion of AA increased from 39.9 % to 75.6 % when the mole ratio varied from 1:3 to 3.1, respectively.

For calculating the activation energy for this reaction, the study on the effect of temperature is very important for a heterogeneously catalyzed reaction. The effect of temperature on conversion and product selectivities was studied in the range of 343-383 K and the results are shown in Fig. 6.19 (c). It is seen that with increase in temperature, IAA conversion increases up to 72.3 %, while selectivities for isoamyl acetate was remain unchanged.

Esterification of IAA was carried out with catalyst, 0.150 g (5 wt.% of total reaction mixture), AA/IAA molar ratio 2 at 373 K for 3 h to see the effect IAA conversion and products selectivity as a function of time [Fig. 6.19 (d)]. Under the optimized reaction conditions of 373 K, 3 h, catalyst, 150 mg (5 wt.% of total reaction mixture) and AA/IAA molar ratio 2, the esterification of IAA with AA performed for 7 h and the results are shown in Fig. 6.19 (d). With increase in time, conversion of IAA increases to maximum of 83.12 % with selectivity for isoamyl acetate (100 %).

6.3.2.4. Esterification of different alcohols with different acids

The results of esterification of different alcohols with AA, propionic acid and acrylic acid using 15 wt.%STA/22.4 wt.%ZrO_2/SBA-15 calcined at 1123 K under solvent-free conditions are presented in Table 6.5.Except BA, all other reactions shows100 % product selectivity with variety of conversions for all the reactants were observed in a period of 3 h. For complete conversion, the reaction had to be carried out for longer time.

Table 6.5: Results of esterification of different alcohols and acids

Alcohol	Conv. (%)	Ester	Uses	Fragrance
Benzyl alcohol*	59	Benzyl acetate	In perfume formulation and as a solvent	Peach
Isoamyl alcohol	49	Isoamyl acetate	Flavour esters in the food industry	Banana
Tert- amyl alcohol	20	Tert-amyl acetate	In perfume formulation and as a solvent	Banana
Dodecyl alcohol	57	Dodecyl acetate	Dodecyl acetate is the first repellent allomone	Characteristic odor
1-Octanol	37	Octyl acetate	Flavorings	Orange, Jasmine
Methanol	6	Methyl acetate	Solvent in lacquers and paint removers and to make pharmaceuticals	Sweet
Ethanol	46	Ethyl acetate	Solvent in lacquers and paint removers and in pharmaceuticals	Fruity
Isobutanol	35	Isobutyl acetate	Lacquers	Polish remover
Ethanol	12	Ethyl propionate	Solvent, flavoring agent and fragrance.	Pear
Isobutanol	14	Isobutyl propionate	Solvent or lacquer thinner, in perfumes and flavors	Rum
Isoamyl alcohol	34	Isoamyl propionate	Flavorings	Pineapple, apricot
Benzyl alcohol	36	Benzyl propionate	An additives in tobacco products, alcoholic lotion, anti perspirant, deo-stick, detergent perborate, detergent TAED, fabric softener, shampoo and soap.	Sweet, Apple, Banana, Jam,
Methanol	48	Methyl acrylate	Ingredients in paints, coatings, textiles, adhesives and in polymer industry.	Sharp fruity
Ethanol	52	Ethyl acrylate	Ingredients in paints, coatings, textiles, adhesives, and used in making acrylic resins.	Sharp Ethereal rum
Isoamyl alcohol	60	Isoamyl acrylate	Manufacturing polymers and as a feedstock for synthesis	Sharp fruity

*Entries from 1-8 with HOAc, 9-12 with PrOAc and 13-15 with ArOAc, Except *(96.1 % Benzyl acetate and 3.9 % DBE), all other entries from 2-15 shows 100% selectivity for respective products. (Reaction conditions: IAA=1.27 g (0.014 mole), AA=1.73 g (0.028 mole), catalyst=15 wt.%STA/22.4 wt.%ZrO_2/SBA-15 (0.15 g), temp. = 373 K, time=3h).*

6.3.2.5. Kinetic study

The standard equation for a first order series reaction, $C_A/C_{A0} = e^{-k_1 t}$, were used to determine the rate constant, where C_A and C_{A0} are the concentration of IAA at initial time and at time *t,* respectively. At one particular temperature, first-order rate constants were calculated at different reaction time and then the constant values of 'k_1' showed that the esterification of IAA is a first-order reaction. Energy of activation of the reaction was evaluated graphically. The activation energy (E_a) was obtained from a plot of $-\ln k_1$ against 1/T. A linear plot with negative slope equivalent to (E_a/R), which gave an activation energy of 9.96 k cal mol^{-1}.

6.3.3. Conclusions

The results presented in this work demonstrate that STA/ZrO_2 dispersed uniformly inside the mesopores of SBA-15 formed nanocomposite material at a calcination temperature of 1123 K. The formation of nanosized (4-5 nm) STA/ZrO_2 was found to depend on (%) STA loading, monolayer coverage on ZrO_2, geometry, the nature of mesoporous supports, and calcinations temperature. Among mesoporous silica supports, SBA-15 was found to be better and provided higher thermal stability and catalytic activity than MCM-41 and MCM-48 in an esterification reaction. The mesoporous material has an advantage in the formation of nanosized and catalytically active STA/ZrO_2 by stabilizing ZrO_2 in tetragonal phase at 1123 K, which provided higher catalytic activity than the neat STA/ZrO_2 in an esterification reaction. The higher stability and catalytic activity can be achieved by incorporating STA/ZrO_2 in supports like SBA-15 to get enhanced catalytic activity (eight-fold higher) than the corresponding neat STA/ZrO_2 catalyst.

6.4. REFERENCES

1. D. Zhao, J. Feng, Q. Huo, N. Melosh, G. H. Fredrickson, B. F. Chmelka, G. D. Stucky, Science, 279 (1998) 548.
2. D. P. Sawant, A. Vinu, N. E. Jacob, F. Lefebvre, S.B. Halligudi, J. Catal., 235 (2005) 341.
3. J. Joo, T. Yu, Y. W. Kim, H. M. Park, F. Wu, J. Z. Zhang, T. Hyeon, J. Am. Chem. Soc., 125 (2003) 6553.
4. I. V. Kozhevnikov, Catal. Rev. Sci. Eng., 37(2) (1995) 311.
5. L. Pizzio, P. Vázquez, C. Cáceres, M. Blanco, Catal. Lett., 4 (2001) 77.
6. D. A. Stephenson, N. J. Binkowski, J. Non Cryst. Solids, 22 (1976) 399.
7. L. R.´ Pizzio, C. V. Ca´ceres, M. N. Blanco, Journal of colloid and interface science, 190 (1997) 318.
8. S. Shanmugam, B. Viswanathan, T. K. Varadarajan, Journal of Membrane Science, (2005) (article in press).
9. A. V. Emeline, G. V. Kataeva, A. S. Litke, A. V. Rudakova, V. K. Ryabchuk, N. Serpone, Langmuir, 14 (1998) 5011.
10. N. Chino, T. Okubo, Micropor. Mesopor. Mater., 87 (2005) 15.
11. K. Miyazawa, S. Inagaki, Chem. Commun., (2000) 2121.
12. W. Hu, Q. Luo, Y. Su, L. Chen, Y. Yue, C. Ye, F. Deng, Micropor. Mesopor. Mater., (2006) 22 (article in press).
13. A. Thomas, C. Dablemont, J.-M. Basset, F. Lefebvre, C. R. Chimie, 8 (2005) 1969.
14. C. Rocchiccioli-Deltcheff, M. Fournier, R. Franck, R. Thouvenot, Inorg. Chem., 22 (1983) 207.
15. C. M. Teague, X. Li, M. E. Biggin, L. Lee, J. Kim, A. A. Gewirth, J. Phys. Chem. B, 108 (2004) 1974.
16. G. Zukowska, J. R. Stevens, K. R. Jeffrey, Electrochimica Acta, 48 (2003) 2157.
17. H. Chermette, G. Hollinger, P. Pertosa, Chem. Phys. Lett., 86 (1982) 170.
18. V. I. Nefedov, M. N. Firsov, I. S. Shaplygin, J. Electron Spectrosc. Relat. Phenom., 26 (1982) 65.
19. K. T. Ng, D. M. Hercules, J. Phys. Chem., 80 (1976) 2095.
20. T. Okuhara, N. Mizuno, M. Misono, Adv. Catal., 41 (1996) 113.

21. I. V. Kozhevnikov, ‘Catalysis by Polyoxometalates, Catalysts for Fine Chemical Synthesis’, vol. 2, Wiley, New York, 2002, p. 15.
22. E. Lopez-Salinas, J. G. Hermandez-Cortez, I. Schifter, E. Torres-Garcia, J. Navarrete, A. Gutierrez-Carrillo, T. Lopez, P. P. Lottici, D. Bersani, Appl. Catal. A:General, 193 (2000) 215.
23. J. B. Moffat, ‘Catalysis by Acids and Bases’, Elsevier, Amsterdam, 1985, p. 157.
24. A. Sakthivel, S. K. Badamali, P. Selvam, Micropor. Mesopor. Mater., 39 (2000) 457.
25. B. H. Davis, R. A. Keogh, S. Alerasool, D. J. Zalewski, D. E. Day, P. K. Doolin, J. Catal., 183 (1999) 45.
26. A. Zaidi, J. L. Gainer, G. Carta, Biotechnol. Bioeng., 48 (1995) 601.
27. G. Langrand, C. Triantaphylides, J. Baratti, Biotechnol Lett., 12(8) (1988) 549.
28. F. W. Welsh, W. D. Muray, R. E. Williams, Crit Rev Biotechnol., 9(2) (1989) 105.
29. R. C. Larock, Comprehensive Organic Transformations, second ed., VCH, New York, 1999.
30. L. R. Pizzio, P. G. Vázquez, C. V. Cáceres, M. N. Blanco, Appl. Catal. A: General, 256 (2003) 125-139.
31. A. Palani, A. Pandurangan, J. Mol. Cata. A: Chem., 226 (2004) 129-134.
32. M. Rizzi, P. Stylos, A. Riek , M. Reuss, Enzyme and Microbial Technology 14 (1992) 709-714.
33. I. V. Kozhevnikov, Chem. Rev., 98 (1998) 171
34. Y. Izumi, K. Urabe, M. Onaka, Zeolite, Clay and Heteropoly Acid in Organic Reactions; Kodansha/VCH: Tokyo, 1992;p.99-161
35. C. Hu, Hashimoto, T. Okuhara, M. Misono, J.Catal. , 143 (1993) 437.
36. G. M. Maksimov, I. V. Kozhevnikov, React. Kinet. Catal. Lett., 39 (1989) 317.
37. Y. Izumi, M. Ono, M. Ogawa, K. Urabe, Chem.Lett. (1993) 825.

CHAPTER – 7

SUMMARY AND CONCLUSIONS

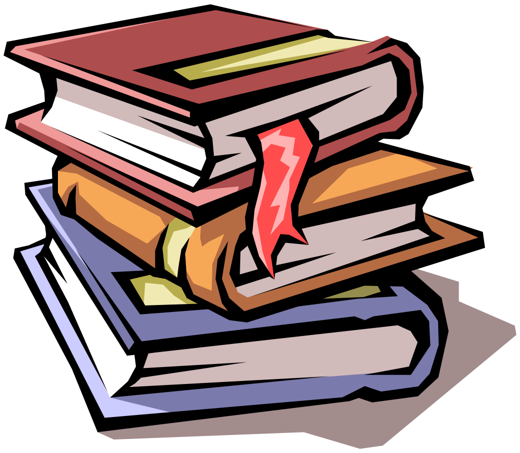

7.1. SUMMARY AND CONCLUSIONS

In this thesis, the synthesis, characterization and catalytic properties of TPA and STA supported on ZrO_2 and mesoporous supports like MCM-41, MCM-48 and SBA-15 have been investigated. The immobilization was achieved by wet-impregenation technique. The structure and the integrity of the catalyst were investigated using different techniques like ICP-OES, EDX, XRF, XRD, surface area with N_2 adsorption – desorption BET isotherm, SEM, AFM, TEM, ^{31}P, ^{1}H, ^{29}Si MAS NMR spectroscopy, UV-Vis., FT-IR, FT-Raman, XPS, TG-DTA, Temperature programmed reaction techniques and FT-IR pyridine adsorption. The integrity of Keggin-like structure HPAs over ZrO_2/MS after calcinations at higher temperature were established mainly by NMR and FT-RS. The XRD patterns of the catalysts showed that the added HPAs stabilized tetragonal form of ZrO_2. When the loading exceeds 15 wt.%, WO_3 crystallizes (as excess HPA does not interact with ZrO_2). TPD of NH_3 showed that the density of acid sites increased with HPA loading till 15 wt.% and decreased with further increase in loading. The higher acidity was due to a monolayer coverage of HPA. It was also observed that upto the calcination temperature 1023 K, the acidity increased and further at higher temperatures, it decreased due to the decomposition of HPA.

When HPAs were dispersed on mesoporous supports, it was observed that the thermal stability of the active components increased to 1123 K. From the sorption study, it concluded that HPA/ZrO_2 was finely dispersed inside the channels of MCM-41, MCM-48 and SBA-15 supports. The results from TEM demonstrate that HPA/ZrO_2 dispersed uniformly inside the mesopores of SBA-15 formed nanocomposite material at a calcination temperature of 1123 K. The formation of nanosized (3-4 nm) TPA/ZrO_2 and (4-5 nm) STA/ZrO_2 was found to depend on (%) HPA loading, monolayer coverage on ZrO_2, geometry, the nature of mesoporous supports, and calcinations temperature. The intact Keggin-like structure of the material is confirmed mainly by NMR spectroscopy. It was found that upto 15 wt.% loading only one major peak was observed at –12.2 ppm (intact Keggin-like) but on increasing the HPA loading it showed two peaks at –12.2 ppm and –24.8 ppm indicating partial decomposition of HPA into WO_3 crystallites. Assuming that some TPA protons react with (OH) groups in hydrated ZrO_2, it would be reasonable to expect that some terminal W=O bonds of HPA might react with partially dehydroxylated

$(Zr\ (\text{-}O)_3)^+$ species to form anchored HPA species, e.g. the formation of Zr-O-W bonds. These HPA species would exert an electron withdrawing effect on surface Zr^{4+} cations, making them to behave as strong Lewis acid sites.

Keeping in view of all the above facts, we hypothesize that the interaction between HPA and ZrO_2 might be weakened till monolayer coverage (15 wt.% and 1123 K) so that HPA protons are free for reactions to proceed and thereby increasing Brønsted acidity and the total acidity (due to ZrO_2 Lewis acidity increases). XPS analysis was instrumental in proving the interaction between ZrO_2 and MS materials and was found that ZrO_2 interacts with mesoporous materials by hydrogen bond.

The activity of these supported catalysts were studied in different industrially important reactions vis. benzylation of DPO with BC, alkylation of benzene with 1-dd, alkylation of phenol by BA, acetylation of veratrole by Ac_2O and an esterifiaction of an IAA with AA. HPA/ZrO_2 gave better catalytic activity compared to neat as well as HPA/SiO_2 because of the lower acidity of the later, due to the decomposition of HPA at 1023 K. On comparing the activity of supported HPA with the zeolite catalyst like H-beta, H-Y etc. it was observed that zeolite gave lower activity due to pore size effect. HPA/ZrO_2/MS gave high substrate conversion compared to HPA/ZrO_2 due to increase in acidity caused by uniform dispersion on large surface area MS materials.

The results presented in the thesis have provided the definite and convincing evidence of the intact Keggin-like structure of HPA/ZrO_2 and also on MS supports. The enhanced thermal stability, acidity and catalytic activity of above catalyst systems were found to be advantageous and hold promise for application in chemical industry.

LIST OF PUBLICATIONS

1. Trissa Joseph, S.B. Halligudi, C. Satyanarayan, **Dhanashree P. Sawant**, S. Gopinathan, Journal of Molecular Catalysis A: Chemical 2966(2000) 1-11.
   ‘Oxidation by molecular oxygen using zeolite encapsulated Co (II) Saloph complexes.’

2. Trissa Joseph, **Dhanashree P. Sawant**, C.S. Gopinath, S.B. Halligudi, Bull.Catal.Soc.India (August 2000, 8-11).
   ‘Allylic oxidation of α-pinene to D-Verbenone catalyzed by zeolite encapsulated metal Schiff base complexes’.

3. Rajani Rajan, **Dhanashri P. Sawant**, N.K.Kala Raj, I.R.Unny, Sarada Gopinathan and C.Gopinathan, Indian Journal of Chemical Technology (Vol.7, November 2000,pp. 273-275).
   ‘Catalysis by heteropoly acids: Hydroxyacetophenones via phenyl acetate by vapour phase acetylation of phenol.’

4. Trissa Joseph, **Dhanashree P. Sawant**, C.S. Gopinath, S.B. Halligudi, Journal of Molecular Catalysis A: Chemical 184 (2002) 289-299.
   ‘Zeolite encapsulated ruthenium and cobalt schiff base complexes catalyzed allylic oxidation of ∝-pinene’.

5. Kala Nair, **Dhanashri P. Sawant**, G.V. Shanbhag, S.B. Halligudi, Catalysis Communication 5 (2004) 9–13.
   ‘Aerial oxidation of substituted aromatic hydrocarbons catalyzed by Co/Mn/Br in water-dioxane medium’.

6. **Dhanashri P. Sawant**, S.B. Halligudi, Catalysis Communication 5 (2004) 659–663.
   ‘Liquid phase acetylation of thioanisole with acetic anhydride to 4-(methylthio) acetophenone (4-MTAP) using H-beta catalyst’.

7. **Dhanashri P. Sawant**, Biju M. Devassy, S.B. Halligudi, Journal of Molecular Catalysis A: Chemical 217 (2004) 211–217.
   ‘Friedel–Crafts benzoylation of diphenyl oxide over zirconia supported 12-tungstophosphoric acid’.

8. **Dhanashri P. Sawant**, S.B. Halligudi, Journal of Molecular Catalysis A: Chemical 237 (2005) 137–145.
   ‘Alkylation of benzene with α-olefins over zirconia supported 12-silicotungstic acid’.

9. A. Vinu, **Dhanashri P. Sawant**, K. Ariga, M. Hartmann, S.B. Halligudi, Microporous and Mesoporous Materials 80 (2005) 195–203.

‘Benzylation of benzene and other aromatics by benzyl chloride over mesoporous AlSBA-15 catalysts’.

10. A. Vinu, **Dhanashri P. Sawant**, K. Ariga, K. Z. Hossain, S. B. Halligudi, M. Hartmann, and M. Nomura, Chemistry of Materials 17(21) (2005) 5339-5345.
    ‘Direct Synthesis of Well-Ordered and Unusually Reactive FeSBA-15 Mesoporous Molecular Sieves’.

11. **Dhanashri P. Sawant**, A. Vinu, Nalini E. Jacob , F. Lefebvre, S.B. Halligudi Journal of Catalysis 235 (2005) 341–352.
    ‘Formation of nanosized zirconia-supported 12-tungstophosphoric acid in mesoporous silica SBA-15: a stable and versatile solid acid catalyst for benzylation of phenol’.

12. S.A. Mirji, S.B. Halligudi , **Dhanashri P. Sawant**, Nalini E. Jacob , K.R. Patil , A.B. Gaikwad , S.D. Pradhan, Applied Surface Science xxx (2005) xxx–xxx (article in press).
    ‘Adsorption of octadecyltrichlorosilane on mesoporous SBA-15’.

13. B. Vijaya Kumar Naidu, S. D. Bhat, M. Sairam, A. C. Wali, **D. P. Sawant**, S. B. Halligudi, N. N. Mallikarjuna, T. M. Aminabhavi, Journal of Applied Polymer Science, 96 (2005) 1968-1978.
    ‘Comparison of the Pervaporation Separation of a Water–Acetonitrile Mixture with Zeolite-Filled Sodium Alginate and Poly(vinyl alcohol)–Polyaniline Semi Interpenetrating Polymer Network Membranes’.

14. S.A. Mirji, S.B. Halligudi, **Dhanashri P. Sawant**, K.R. Patil, A.B. Gaikwad, S.D. Pradhan, Colloids and Surfaces A: Physicochem. Eng. Aspects 272 (2006) 220–226.
    ‘Adsorption of toluene on Si (1 0 0)/SiO_2 substrate and mesoporous SBA-15’.

15. **Dhanashri P. Sawant**, Vinu A., F. Lefebvre, S. B. Halligudi, Journal of Molecular Catalysis A: Chemical (special edition), 2006 (accepted).
    ‘Tungstophosphoric acid supported over zirconia in mesoporous channels of MCM-41 as catalyst in veratrole acetylation’.

16. Trissa Joseph, G.V. Shanbhag, **D.P. Sawant**, S.B. Halligudi, Journal of Molecular Catalysis A: Chemical 250 (1-2) (2006) 210-217.
    ‘Chemoselective anti-Markovnikov hydroamination of α,β-ethylenic compounds with amines using montmorillonite clay’.

17. **Dhanashri P. Sawant**, M.Hartmann and S. B. Halligudi, Microporous and Mesoporous Materials, 2006 (communicated).
    ‘Effect of pretreatment conditions on the performance of nano-sized TPA/ZrO_2 dispersed inside SBA-15 channels in the acetylation of substituted aromatics with acetic anhydride’.

18. **Dhanashri P. Sawant,** M. Hartmann, S.P. Mirajkar, F. Lefebvre, and S. B. Halligudi , Journal of Catalysis ' 2006 (Communicated).
‘Supported Silicotungstic acid over zirconia inside mesochannels of SBA-15 for ecofriendly reaction’.

19. **Dhanashri P. Sawant**, Rajani Rajan, N.K.Kala Raj, I.R.Unny, Sarada Gopinathan and C.Gopinathan, Indian Journal of Chemical Technology (Communicated).
‘Metal catalyzed hydroxylation of phenol’.

Patent

1. A process for production of Hydroxyacetophenones. Indian Patent Ref. No. NCL-53/2000.